Galectin-3 as a regulator of γ-herpesvirus specific $CD8^+$ T cell immunity and the utility of single domain antibodies

A Dissertation

Presented by

Manpreet Kaur

for the degree of

Doctor of Philosophy

Department of Biological Sciences

Indian Institute of Science Education and Research (IISER) Mohali

Sector-81, Mohali-140306, Punjab, India

June 2019

Declaration

The work presented in this thesis has been carried out by me under the supervision of Dr. Sharvan Sehrawat at the Department of Biological Sciences, Indian Institute of Science Education and Research (IISER) Mohali.

The work has not been submitted in part or full for a degree, diploma, or a fellowship to any other university or institute.

Whenever contributions of others are involved, every effort is made to indicate this clearly, with due acknowledgement of collaborative research and discussions. This thesis is a bona fide record of original work done by me and all sources listed within have been detailed in the bibliography.

Date **Place** **Manpreet Kaur**

In my capacity as the supervisor of the candidate's thesis work, I certify that the above statements made by the candidate are ture to the best of my knowledge.

Dr. Sharvan Sehrawat

(Supervisor)

Dedicated to my parents

Acknowledgements

Last five years have been an adventurous journey during which I have experienced so many things. I have been blessed and feel privileged as I was the first student of Dr. Sharvan Sehrawat, so I got an opportunity to learn experiments directly from him. I am very grateful to him as he taught me how to critically analyze the results while being optimistic. I am sincerely thankful to my committee members, Professor Purnananda Guptasarma and Dr. Shravan Kumar Mishra for evaluating my research work from time to time.

I express my gratitude to all my lab members, Dr. Parveen, Dr. Nitin, Nirdosh, Dhaneshwar, Sramona, Dr. Prerna, Roman, Sudhakar, Ankit, Amal, Shubham, Aswathy, Sreenath, Param, Jasreen, Yashu, Divya, Inamur and Surbhi for providing the harmonious and healthy working environment. Especially I am thankful to Abhishek for his time and continuous support during the critical phase. My sincere gratitude to my friends Gayathri, Naimat, Kanchan and Muskan for giving their precious time during the entire journey at IISER Mohali. I am highly thankful to Sai, Nisha, Surbhi, Sayan and Jagadish from Dr Sabysachi Rakshit’s lab.

Finally, I express my deepest regards to my father, mother, and brother for being pillars of my strength. I am grateful to my father who taught me how to be perseverant and humble during tough times. He always says " Hard work is the key to success" so I have tried to apply this in completing my Ph.D.

Contents

Abstract

The study was planned to gain insights into the molecular mechanisms and pathways involved in differentiating $CD8^+$ T cells during γ-herpesvirus infection. These viruses are species-specific and hence are studied in a specific host. Murine herpesvirus 68 serve as one of the most accessible model system.

$CD8^+$ T cells are critically involved in controlling intracellular infections such as those caused by viruses. A comprehensive transcriptomic analysis of γ-herpesvirus (MHV68)-specific TCR transnuclear (TCR-TN) $CD8^+$ T cells, that were obtained somatic cell nuclear transfer (SCNT) approach, was performed. These cells are considered as physiologically relevant population because of their method of generation that requires no transgenesis. We observed differential expression of several thousand transcripts in γ-HV expanded $CD8^+$ T cells as compared to their naïve counterparts encompassing various pathways and forming different networks. Activated cells highly upregulated galectin-3, a member protein of galectin family. We therefore explored the role of galectin-3 in influencing anti-MHV68 immunity and demonstrated its recruitment intracellularly at immunological synapse (IS) during $CD8^+$ T cell activation. By virtue of its presence at the IS, galectin-3 constrained T cell activation, proliferation and functionality. The localization of galectin-3 to IS was evident both in the naïve and memory $CD8^+$ T cells responding through their TCRs or the coreceptors suggesting for its role as an intrinsic negative regulator. Accordingly, animals lacking galectin-3 signal because of gene knockout mounted a stronger MHV68-specific $CD8^+$ T cell response to the majority viral epitopes displayed by different MHC haplotypes. The enhanced effector $CD8^+$ T cell response led to a better viral control. This study therefore established galectin-3 as a potential intracellular target in γ-herpesvirus specific $CD8^+$ T cells whose function could be disrupted to enhance antiviral immunity.

Then we explored the possibility of using single domain antibodies (sdAbs) as intrabodies to disrupt galectin-3 interaction intracellularly. Intrabodies can be efficiently selected from phage display libraries of sdAbs. The genetic information encoded in differentiated camelid B cells is used to generate these libraries. We generated such a library that consisted of more than 20 million clones and biopanned sdAbs not only against galectin-3 but also against other antigens and some of these tcould have a translational value. The expression of such sdAbs was demonstrated intracellularly. Additionally, sdAbs against the components of snake venom were selected from the phage display libraries and their efficacy in neutralizing the toxicological effects was demonstrated using *in vitro* assays as well as *in vivo* zebrafish model. Our data showed that sdAbs can serve as a potent anti-toxin to manage envenoming by snake bites.

Synopsis

Introduction

T cells constitute an essential component of adaptive immune system and expand exponentially after recognizing the antigen. A timely and optimal activation of cytotoxic T lymphocytes requires the ligation of three signals: interaction between cognate peptide loaded onto MHC I with the specific TCR, binding of co-stimulatory pairs of molecules and the cytokine milieu (1). Activation of T cells leads to the downstream signalling events that result in their expansion and the production of proinflammatory cytokines. Various surface receptors (TCR, CD8/CD4, CD28, CD45, etc.) with their cytoplasmic domains participate in the formation of the immunological synapse and their expression as well as glycosylation pattern change depending on the differentiation stages of T cells (2). For example glycosylation of CD43 and CD45 changes during activation and differentiation process (3, 4). These heavily glycosylated molecules act as a target receptor for galectins. For example, galectin-1 binds to CD3, CD7, and CD45, galectin-3 binds to CD7, CD29, CD70 (5). Galectins are the animal lectins that have affinity for β-galactosides and such interactions are commonly mediated by their carbohydrate recognition domains (CRD). There are 15 members in galectin family and these are classified into three structural groups;– prototype have one CRD, tandem repeats contain members having more than one type of CRD and the third type have one CRD linked with non-lectin N terminal domain (6). The third type of galectins are also known as chimeric type lectins.

Galectins are expressed by various immune as well non-immune cells. Upon their synthesis in cytoplasm these molecules migrate to different regions within or outside the cells. During proliferation of cells, galectins move inside the nucleus or accumulate

around vacuoles during some bacterial infections (7). These molecules can also exit the cells following non-classical mechanisms and be present in the extracellular regions (8). Once galectins bind to their respective receptors on the activated T cells, a variety of cellular signalling events are induced to help decide cellular fate and functions. Galectins can also bind to surface glycans of microbes to modify the outcome of infection leading to either an enhancement or the reduction of cell susceptibility to infections (9, 10). Galectin-3 exhibits different functions depending on its location in the cell or the cell types involved (11, 12). In most cases, galectin-3 enhances the host-pathogen interaction and increases the infectivity. In different types of cancers, its expression is highly upregulated and by binding to different surface receptors on infiltrating immune cells, dampen their activity. Galectin-3 can exhibit either an anti- or pro-apoptotic activity in the cells involved and its localization critically help decide the fate. Of all the galectins, galectin-3 has been extensively studied because of its key roles in different diseases but how does it influence the outcome of infection and immunity caused by γ -herpesviruses (γ -HV) is not known. Therefore, the study was planned to investigate the role of galectin-3 in influencing anti-gamma-herpesvirus (γ -HV) CD8 T cell immunity.

Various strategies were used to modify the expression and interaction of galectin-3 with its counter receptors. One approach that has not yet been tested is the ability of intrabodies to disrupt intermolecular interactions with in the cells without its genetic ablation. The genetic depletion of molecules might be confounded with biasness in cellular response and such artefacts are unlikely to be observed with the use of intrabodies to disrupt intermolecular interactions. This necessitated the generation of phage display libraries of camelid single domain antibodies (sdAbs) that have deservedly gain the adjective of robust reagents and could function both intracellularly as well as

extracellularly. Such sdAbs bind to their counter structures with a pinpoint precision and exhibit high affinity.

Objectives

Considering the diverse activities performed during the course of investigation, the dissertation is divided to achieve the following objectives:

1 To investigate the role of galectin-3 in anti γ-herpes viral $CD8^+$ T cell immunity

2 To attempt to modify galectin-3 function intracellularly by using intrabodies selected from phage display libraries.

3 To select sdAbs against the components of snake venom as an overarching aim to harness the utility of sdAb phage display libraries.

Results

The results for Objective 1 (To investigate the role of galectin-3 in anti γ-herpes viral immunity):

γ-HVs are species-specific pathogens and therefore analysis of anti-γ-HV responses requires a natural host. Infection of mice with murine herpesvirus 68 (MHV68), is one of the more accessible model systems to study anti-γ-HV immunity and immunopathology (13–15). Various immune mediators induced in MHV68 infected mice display similarity to those induced during γ-HV infections in humans (16). In this study we used two different types of C57BL/6 mice strains to serve as the source of antigen-specific $CD8^+$ T cells. These include γ-HV specific $CD8^+$ T cell receptor transnuclear (TCR TN) mice which were generated previously (17) and one of the most commonly used mouse model, OT I TCR transgenic mice (18).

For activating and differentiating the latter population, we used viruses that encode for the specific epitope (SIINFEKL) to stimulate OT1 cells. The antigen-specific

$CD8^+$ T cells were transferred into congenic mice. Their activation and differentiation was analysed using high throughput transcriptomic approaches, functional immunological assays and knock out recipient or the donor animals. Furthermore, a gamut of *in vitro* assays were performed.

We first compared the RNA transcriptome and phenotypic profile of naïve ORF8 TN $CD8^+$ T cells with their activated counterparts in the acute stage of infection. At 6dpi, 30-40% of total $CD8^+$ T cells in spleen were ORF8 TN donor cells and such cells upregulated the expression of activation markers i.e. CD62L, TIM-3, PD1, CD44, CCR7, galectin-3, IFN-γ etc. These cells were sorted and their RNA was used for transcriptomic analyses by RNAseq. We observed that a majority of differentially expressed genes showed alterations by two folds but approximately 5% genes were expressed to a greater level in genes encoded different class of proteins.

Among the upregulated genes in MHV68 expanded $CD8^+$ T cells, only two members of galectins family were highly upregulated i.e. galectin-1 (up by 87-fold) and galectin-3 (up by 140-fold). Therefore, we focused to elucidate the role of galectin-3 in anti- γ -HV $CD8^+$ T cell immunity. We performed the kinetics of galectin-3 expression in stimulated $CD8^+$ T cells using *in vitro* assays wherein the cells were stimulated by *anti*-CD3 and *anti*-CD28 antibodies. We observed that 70% of total $CD8^+$ T cells upregulated galectin-3 after 70 hrs post activation and major proportion of galectin-3 was present intracellularly. In order to decipher its role, we used immunofluorescent microscopic analyses in specific TCR transgenic $CD8^+$ T cells (OT1 cells) stimulated cells and in so doing measured the formation of immune synapse. The cells were stimulated either with the cognate peptide (SIINFEKL) loaded APCs or cognate peptide-MHC I tetramer coated on magnetic beads to serve as artificial APCs. To mark the immune synapse formation,

galectin-3 localization with the adaptor molecules for TCR stimulation, ZAP70, was measured. We observed that galectin-3 co-localised with ZAP70 at the immunological synapse in cells stimulated recently or those re-stimulated using different approaches.

Long-term protective immunity to intracellular infections or vaccines is critically dependent on memory response. Therefore, we investigated whether or not galectin-3 is also involved in regulating the immune synapse formation by virtue of its localization at the proximal end during the activation of memory $CD8^+$ T cells. To this end we used two different viruses, one that causes an acute infection (Influenza A virus; WSN-SIIN) and another that causes a persistent infection (MHV68-SIIN). After re-stimulating the memory $CD8^+$ T cells generated by an acute and persistent infections, we observed similar results. Re-stimulation of MHV68-SIIN specific cells were done by pMHC I tetramers and for influenza (WSN SIIN) specific cells pMHC I tetramer coated magnetic beads were used.

We further demonstrated that galectin-3 expressed intracellularly in $CD8^+$ T cells and not the pool of galectin-3 present extracellularly interfered with the proliferation and cytokine production by virus-specific activated $CD8^+$ T cells to influence the viral control. To quench the extracellular galectin-3, experiments described earlier were performed but additionally either α-lactose or a neutralizing antibody against galectin-3 was added. We did not find significant difference in the recruitment of galectin-3 towards the immunological synapse in such assays. To further investigate the effect of intracellular versus extracellular galectin-3 on the proliferation of $CD8^+$ T cells, we incubated CFSE labelled $CD8^+$ T cells with or without *anti*-galectin-3 neutralizing antibody that is likely to block extracellular galectin-3. Then, we measured CFSE dilution and observed no significant difference between these two groups which confirmed no

extracellular role of galectin-3 in regulating the proliferation of activated $CD8^+$ T cells. Then we verified these results using galectin-3 knock out animals. After adoptive transfer of wild type γ-HV specific $CD8^+$ T cells into wild type (able to produce galectin-3) and galectin-3 KO animals. Upon infection of these recipient animals with MHV68 virus, we did not find any difference on the activation profile or the magnitude of virus-specific $CD8^+$ T cells between two groups.

References

1. Zinkernagel, R. M. 1996. Immunology taught by viruses. *Science (80-.).* 271: 173–178.

2. Van Leeuwen, J. E. M., and L. E. Samelson. 1999. T cell antigen-receptor signal transduction. *Curr. Opin. Immunol.* 11: 242–248.

3. Hernandez, J. D., J. Klein, S. J. Van Dyken, J. D. Marth, and L. G. Baum. 2007. T-cell activation results in microheterogeneous changes in glycosylation of CD45. *Int. Immunol.* 19: 847–856.

4. Clark, M. C., and L. G. Baum. 2012. T cells modulate glycans on CD43 and CD45 during development and activation, signal regulation, and survival. *Ann. N. Y. Acad. Sci.* 1253: 58–67.

5. Yang Ry, Hsu Dk, and Liu Ft. 1996. Expression of galectin-3 modulates T-cell growth and apoptosis. *Proc. Natl. Acad. Sci. U. S. A.* 93: 6737–6742.

6. Hirabayashi, J., and K. I. Kasai. 1993. The family of metazoan metal-independent β-galactoside-binding lectins: Structure, function and molecular evolution. *Glycobiology* 3: 297–304.

7. Inohara, H., S. Akahani, and A. Raz. 1998. Galectin-3 stimulates cell proliferation. *Exp. Cell Res.* 245: 294–302.

8. Metz, C., R. Döger, E. Riquelme, P. Cortés, C. Holmes, R. Shaughnessy, C. Oyanadel, C. Grabowski, A. González, and A. Soza. 2016. Galectin-8 promotes migration and proliferation and prevents apoptosis in U87 glioblastoma cells. *Biol. Res.* 49.

9. Woodward, A. M., J. Mauris, and P. Argueso. 2013. Binding of Transmembrane Mucins to Galectin-3 Limits Herpesvirus 1 Infection of Human Corneal Keratinocytes. *J. Virol.* 87: 5841–5847.

10. Takasaki, I., K. Taniguchi, F. Komatsu, A. Sasaki, T. Andoh, H. Nojima, K. Shiraki, D. K. Hsu, F. T. Liu, I. Kato, K. Hiraga, and Y. Kuraishi. 2012. Contribution of spinal galectin-3 to acute herpetic allodynia in mice. *Pain* 153: 585–592.

11. Zhao, Z., L. Liu, G. Tai, H. Cheng, Y. Guan, Y. Zhou, H. Xue, and Z. Zhang. 2017. The N-terminal tail coordinates with carbohydrate recognition domain to mediate galectin-3 induced apoptosis in T cells. *Oncotarget* 8.

12. Liu, F. T., R. J. Patterson, and J. L. Wang. 2002. Intracellular functions of galectins. *Biochim. Biophys. Acta - Gen. Subj.* 1572: 263–273.

13. Nash, A. A., and B. M. Dutia. 2008. Murine Gammaherpesvirus 68. In *Encyclopedia of Virology* Elsevier. 372–378.

14. Nash, A. A., B. M. Dutia, J. P. Stewart, and A. J. Davison. 2001. Natural history of murine gamma-herpesvirus infection. *Philos. Trans. R. Soc. Lond. B. Biol. Sci.* 356: 569–79.

15. Sehrawat, S., D. Kumar, and B. T. Rouse. 2018. Herpesviruses: Harmonious Pathogens but Relevant Cofactors in Other Diseases? *Front. Cell. Infect. Microbiol.* 8: 177.

16. Barton, E., P. Mandal, and S. H. Speck. 2011. Pathogenesis and Host Control of Gammaherpesviruses: Lessons from the Mouse. *Annu. Rev. Immunol.* 29: 351–397.

17. Sehrawat, S., O. Kirak, P.-A. Koenig, M. K. Isaacson, S. Marques, G. Bozkurt, J. P. Simas, R. Jaenisch, and H. L. Ploegh. 2012. CD8(+) T cells from mice transnuclear for a TCR that recognizes a single H-2K(b)-restricted MHV68 epitope derived from gB-ORF8 help control infection. *Cell Rep.* 1: 461–71.

18. Clarke, S. Rm. K., M. Barnden, C. Kurts, F. R. Carbone, J. F. Miller, and W. R. Heath. 2000. Characterization of the ovalbumin-specific TCR transgenic line OT-I: MHC elements for positive and negative selection. *Immunol. Cell Biol.* 78: 110–117.

19. Ahmed, S., A. Choudhary, J. Mahajan, J. Pal, A. Nadeem, and M. Ahmed. 2009. Emergency treatment of a snake bite: Pearls from literature. *J. Emergencies, Trauma Shock* 1: 97.

20. Alirol, E., S. K. Sharma, H. S. Bawaskar, U. Kuch, and F. Chappuis. 2010. Snake bite in south asia: A review. *PLoS Negl. Trop. Dis.* 4.

21. Calvete, J. J., R. A. Harrison, N. R. Casewell, S. C. Wagstaff, F. M. S. Bolton, L. Sanz, W. Wuster, D. A. N. Cook, D. Pla, and S. I. King. 2014. Medically important differences in snake venom composition are dictated by distinct postgenomic mechanisms. *Proc. Natl. Acad. Sci.* 111: 9205–9210.

22. Geneviève, L. D., N. Ray, F. Chappuis, G. Alcoba, M. R. Mondardini, I. Bolon, and R. Ruiz de Castañeda. 2018. Participatory approaches and open data on venomous snakes: A neglected opportunity in the global snakebite crisis? *PLoS Negl. Trop. Dis.* 12.

Abbreviations

PCR	Polymerase chain reaction
β2m	Beta 2 microglobulin
MHC I	Major histocompatibility complex I
CRD	Carbohydrate recognition domain
TLR's	Toll like receptors
shRNA	Short hairpin RNA
siRNA	Small interference RNA
CDR	Complementary determining regions
HCAb's	Heavy chain antibodies
FR	Framework region
VHH	Variable domain of heavy chain of heavy chain antibodies
VH	Variable domain of heavy chain of conventional antibodies
$C_H1/2$	Constant domain 1/2 of heavy chain
sdAbs	Single domain antibodies
RVV	Russell viper venom
PLA_2	Phospholipase A_2
T_m	Melting temperature
AVS	Anti-venom sera
PI	Propidium iodide

FBS	Fetal bovine serum
Fr	Fractions
MHV68	Murine herpesvirus 68
γ-HV	γ-Herpesvirus
WSN SIIN	Influenza virus expressing SIINFEKL epitope
HSV	Herpes simplex virus
TCR	T cell receptor
tg	Transgenic
TN	Transnuclear
WT	Wild type
OT I	Ovalbumin specific TCR transgenic $CD8_+$ T cells
Ori	Origin of replication
dNTP	Deoxyribonucleotide triphosphate
HF	High fidelity
Ni NTA	Nickel nitrilotriacetic acid
RT	Room temperature
PBMC	Peripheral blood mononuclear cell
Fab	Fragment antigen-binding
O/N	Overnight
IFNγ	Interferon gamma

TNFα	Tumor necrosis factor
LTR’s	Long terminal repeats
ICCS	Intracellular cytokine staining
ORF	Open reading frame
FACS	Fluorescence-activated cell sorting
KO	Knock out
RPKM	Reads per kilobase million
ELAND	Efficient Large6Scale Alignment of Nucleotide Databases
REFSEQ	Reference sequence database
PPI	Protein protein interaction
STRING	Search Tool for the Retrieval of Interacting Genes/Proteins
PCC	Pearson correlation coefficient
GM-CSF	Granulocyte-macrophage colony-stimulating factor
IL-2	Interleukin 2
Dpi	Days post infection
LN	Lymph node
BMDCs	Bone marrow derived dendritic cells
APCs	Antigen presenting cells
CFSE	Carboxyfluorescein succinimidyl ester
Ribo.	Ribosome

sh	shine dalgarno
CDS	Coding sequences
CD	Cluster of differentiation
MACS	Magnetic associated cell sorting
LCMV	Lymphocytic choriomeningitis
GO	Gene ontology
HIS	Hyper-immune serum
PIS	Per-immune serum
PFU	Plaque forming unit
Gal-3	Galectin-3

List of figures

List of tables

Chapter 1

Review of literature

Introduction

Galectins (galectins) bind to β-galactosides through their conserved carbohydrate binding domains (CRDs). The first ever galectin was described in the electric eels and was accordingly named as electroelectin (1). Galectins were named earlier as S type lectins due to the requirement of reducing conditions for their activity but some members discovered later did not follow this rule and therefore the term "galectin" was coined to name all the family members by Hirabayashi and Kasai in 1994 (2). Different galectins are named according to the sequence of their discovery. Currently 15 members are identified in the galectin family and are divided into three groups based on their structure (Fig no. 1) (3). The three groups are as follows:

- Prototype group members have only one CRD and exist either as a monomer or form homodimers via non-covalent interactions. Examples of prototype galectins include Galectin-1, 5, 7, 10 and 11.
- Tandem repeat type galectins have more than one CRD which are linked through the stretch of 5 to 50 amino acids and these CRDs can bind to different ligands. Examples of tandem repeat type galectins are galectin-2, 4, 6, 8, 9 and 12.
- Chimeric type galectins have only one CRD which is linked to a non-lectin domain. The only member of this group is galectin-3.

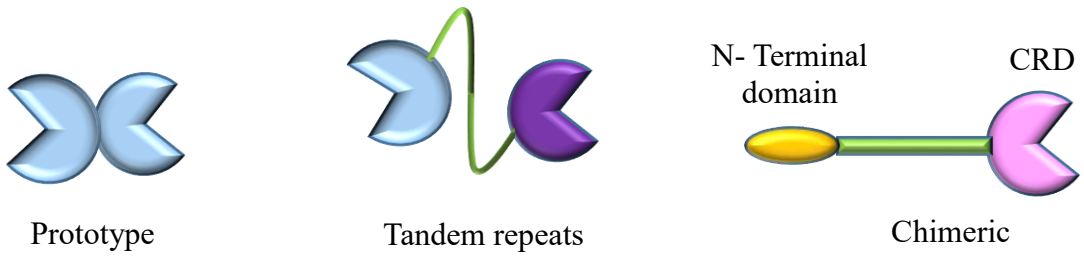

Figure no. 1.1. Structural features of different types of galectins.

The classification described is also applicable to non-mammalian galectins and many galectins are present in most invertebrates as well as vertebrate organisms. Two criteria are followed for classifying different galectins, i) the sequence similarity between their CRDs and ii) their capability to bind sugar molecules. Galectins tend to form oligomers in the absence of carbohydrates and such events are mediated by CRDs. The binding affinity of galectins increases with an increase in the numbers of carbohydrate moieties on ligands. Accordingly, galectins have lower affinity for monosaccharides than that for oligosaccharides (4). The structures of CRDs present in galectins, as analysed by X-ray crystallography revealed the existence of two sheets of β strands (5). Five β strands are present on the convex side and while six β strands on the concave side.

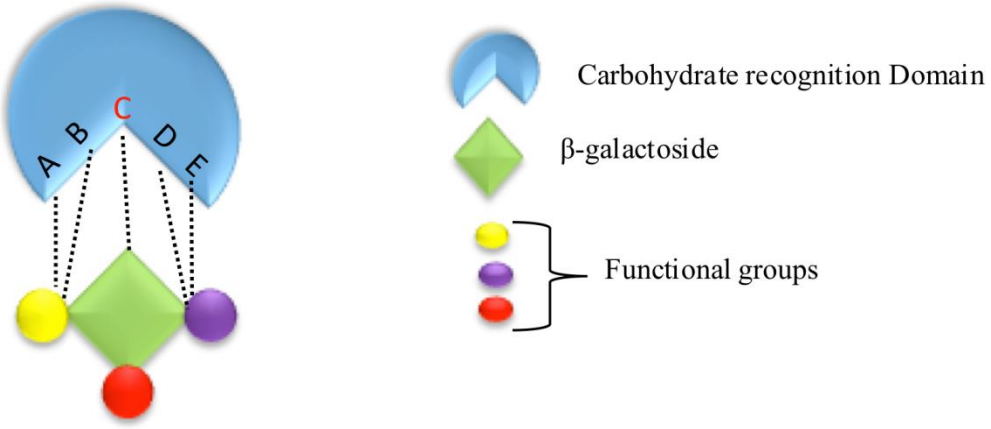

Figure no. 1.2. An arrangement of carbohydrate binding sites in the CRD of galectins.

The concave side provides the binding site for the sugar molecules and four such major subsites i.e. A to D and one minor subsite i.e. E are present (6). Figure no. 2 describes the arrangement of interacting sites in CRD of galectins. Subsite C has a highly conserved motif consisting of seven amino acids, sometimes called a glycotype. This is the actual binding site for β-glycosides. Of all the binding subsites in CRD, subsite D is less conserved and is least preferred by carbohydrates involved in the interactions. The overall strength of the ligand binding among different galectins is dictated by the interaction between the functional

moieties present at OH groups of galactosides and A, B, D and E subsites of CRDs. The N-terminal domain (NTD) of galectin-3 is rich in proline and glycine repeats and due to its homology to collagen exhibit susceptibility to collagenases (7). Galectins are expressed by different cells and are localized intracellularly in different compartments as well as present extracellularly at tissue sites. Galectin-1, 2, 3, 4, 7, 8, 9, 12 and HSPC159 are described in humans, rats, mice and other mammals but galectin-5 is reported only in rats (8). C-terminal CRD of galectin-5 and galectin-9 are homologous (9). Mouse galectin-6 contains two CRDs and these are identical to those present in galectin-4 (10). In humans, there is an additional homologous gene for galectin-9, which is also present on the same chromosome but it does not express well. They also do not have GRIFIN but additionally contain galectin-10, 13, PP13 and PPL13 (11). Galectin-1 and galectin-3 are expressed in embryonic stages while galectin-4 is expressed in the epithelial layers of gastrointestinal tract and galectin-7 in the epithelial layers of epidermis. Galectin-1, 3, 7, 10, 11 and 12 have been demonstrated to localize inside the nucleus, cytoplasm as well as in the extracellular spaces (12). Of all the members, galectin-3 is an extensively studied protein and is expressed in a wide variety of immune cells such as B cells, T cells, macrophages and dendritic cells (DCs) etc. Subsequently, the biosynthesis, localization and functions of galectin-3 are discussed.

Biosynthesis and transportation of galectins

Galectins are synthesised on free polysomes in the cytosol and are subsequently transported to different intracellular compartments or released in the extracellular spaces (13). As is the case with all other members, galectin-3 does not have signal peptide sequences and does not follow the classical secretory pathways (14). Galectin-3 first accumulates at the inner side of plasma membrane and is then released out of the cells by the process of exocytosis. During its transportation, the movement towards the plasma membrane serves as the rate limiting step and the process can be enhanced by its acylation as well as the presence of NTD (15,

16). Galectin-3 is also exported by exosomal pathways and is shown to interact with the components of endosomal sorting complexes required for transport 1 (ESCRT1) such as Alix-2 (ALG-2 interacting protein X), Tsg101 and Vps4a. P(S/T)AP motif at the N terminus of galectin-3 interacts with the ubiquitin E2 variant (UEV) domain of Tsg101 at its amino terminus. This interaction proceeds with the inward fission of plasma membrane of multivesicular bodies that leads to the delivery of galectin-3 into intraluminal vesicles (ILV's) (17, 18). These ILVs then fuse with the plasma membrane and facilitate the release of galectin-3 exosomes into the extracellular spaces. The exosomes are then mechanically burst open to release galectin-3 and this process could be enhanced by a low pH in the extracellular space (19). The exosomes containing galectin-3 could subsequently be endocytosed by other cells

Contrasting roles of galectin-3 in cell survival depending on its spatial localization

Given the ubiquitous expression of galectin-3 intracellularly in different subcellular organelles and compartments as well as its presence extracellularly, many investigators aimed at deciphering its functions (20, 21). The clear understanding on how the shuttling of galectin-3 from the cytoplasm to nucleus occurs after its biosynthesis and what biological functions it performs in one compartment versus the others are still lacking. A diffuse staining for galectin-1 and galectin-3 was shown in the nucleoplasm and nuclear bodies (22). The nuclear export signal (NES) and the nuclear localisation signal (NLS) present in the overlapping region between 240-258 amino acid stretch are present in the CRD of galectin-3. These sequences could regulate its movement between cytoplasm and the nucleus (23). The amino acid at position 247 (Leucine) and 249 (Isoleucine) were shown to be crucial for the nuclear export while IXTL sequences at 253-256 position were found essential for its nuclear localisation (24). The X-ray crystallography studies on CRD of galectin-3 revealed that it forms β sandwich structures having two antiparallel β-sheets connected with a α-helical

structure. Of the two amino acids at 247 and 249, one is present in the β strand and the other in the α-helix (25). These residues are usually buried but exposed upon the structural disruption of galectin-3 as could be achieved by insertional mutations or under specific physiological conditions such as the cell cycle stages. Thus, in quiescent 3T3 cells, galectin-3 is predominantly present in the cytoplasm. In its native conformation, the majority of galectin-3 is localised in the nucleus and the nuclear localisation pattern could be reversed when NLS is blocked by actinomycin D this leads to its accumulation in the cytoplasm. CRM1 receptor, an exportin 1, present in the nuclear membrane regulates the export of galectin-3 from the nucleus into the cytoplasm. CRM1 interacts with NES of galectin-3 and can be inhibited by the drug leptomycin leading a sequestration of galectin-3 in the nucleus. Nuclear localisation of galectin-3 could suggest for its role inside the nucleus (26, 27). Accordingly, galectin-3 as well as galectin-1 were shown to be involved in pre-mRNA splicing. A sugar treatment of nuclear extract causing the depletion of these galectins impaired an early splicing complex formation attesting to the role of galectin-3 in the spliceosome assembly. Both galectin-3 and galectin-1 were shown to bind to Gemin4, a component protein of the spliceosome complex that helped assemble snRNP and hnRNP's (28). Surprisingly, only the CRD of galectin-3 was found sufficient for the initiation of spliceosome formation and this was further enhanced by full length galectin-3 protein. However, the isolated NTD of galectin-3 exerted a dominant negative effect in the splicing process. The mechanisms involved in the observed anomalous behaviour are not known but could relate to the presence of inhibitory motifs. The post translation modifications such as the phosphorylation of galectin-3 vary depending on its localization and could critically influence its function (29). While the major proportion of galectin-3 exists in phosphorylated form, the nuclear galectin-3 is present in both the phosphorylated and non-phosphorylated forms. The phosphorylation at 6^{th} serine residue seems to be necessary for an anti-apoptotic

activity, a process independent of its binding to sugars (30, 31). The extracellular galectin-3 could bind to cell surface receptors as well as to soluble ligands having carbohydrate moieties (32). It can also interact with other proteins, an activity that occurs independent of its CRD (33, 34). Such interactions are known to occur with proteins having cysteine and histidine rich residues commonly known as Chrps and are predominantly observed in the cytoplasm (35). Many groups have focused to elucidate the cellular and extracellular roles of galectin-3 in diverse pathophysiological processes.

The role of galectin-3 during cellular processes

In the following section a brief summary highlighting the function of galectin-3 in cellular context is provided.

Cellular proliferation, cell growth and apoptosis

Galectin-3 expression is upregulated during proliferation of the cells (36). In quiescent stage, galectin-3 preferentially resides in the cytoplasm but its migration to the nucleus is evident in the proliferating cells. After achieving a certain level of expression, proliferating cells downregulate their galectin-3 by mechanisms such as its release out of the cells, degradation or the negative feedback loop (37). The kinetics of expression suggests that galectin-3 might halt various activities in the cell, as has been shown for T cells. Thus, galectin-3 is recruited to the immunological synapse to diminish T cell activation (38, 39). As the availability of nutrients become limited, cells maintain their numbers and homeostatic processes by decreasing the rate of metabolism. Accordingly, Jurkat cells transfected with galectin-3 followed by their nutrient deprivation grew normally as compared to non-transfected cells. Therefore, intracellular galectin-3 helps maintain the total number of cells either by enhancing their proliferation rate or by inhibiting their apoptosis (40). When the over expression of galectin-3 was counter balanced by anti-sense cDNA, the cell growth reached

to the levels similar to their non-transfected counterparts demonstrating the modulation of the cell growth by galectin-3 (41). Similar effects were observed in cancer cells. Thus, during metastasis, the cancerous cells are dislodged from the initial site of cancer development and migrate to different regions for generating new focal points for cancer formation. During this process, galectin-3 could play a critical role as it arrests the cell cycle in the late G1 phase and helps the cell survive until it invades a new site. Galectin-3 could indeed help cancer cells evading intrinsic pathways of apoptosis or blunting anti-tumor immunity either by inhibiting the appropriate activation of effector T cells or by neutralizing the activity of effector molecules (42). Therefore, galectin-3 is investigated as a front target for managing malignancies of various kinds (30).

All galectins are known to cause apoptosis but galectin-3 plays a dual role i.e. either pro- or anti-apoptotic, depending on the context, concentration and the location. It is reported that during oxidative stress, galectin-3 binds to synexin and is transported to mitochondria to interact with Bcl-2 through NWGR residues (43). This interaction regulates the release of cytochrome-c from mitochondria to cytoplasm and in so doing apoptosis is prevented (40). However, one of the pro-apoptotic proteins called nucling, down regulates the expression of galectin-3 both at the mRNA and protein levels to promote the release of cytochrome-C from mitochondria, a step critical for apoptosis. Therefore, the functions associated with galectin-3 are concentration dependent. Nucling, by interacting with galectin-3, also inhibits NF-κB signaling to regulate galectin-3 transcription. This would suggest for an autoregulatory circuitry for galectin-3 expression (44). Galectin-3 present in the extracellular sites, binds to different molecules expressed on T cells to induce their apoptosis in a caspase dependent manner (45). For example its interaction with CD45 expressed by T cells induces, in these cells, a heightened ROS production and phosphorylation of PKC which further activates the ERK pathway and caspase-9 activation. Both the N-terminus domain and CRD are essential

for the induction of apoptosis as galectin-3 lacking either of the domains fails to induce apoptosis (46). On the other hand when it binds to either CD29 and CD7, it leads to the release of mitochondrial cytochrome-c and activation of caspase-3 without involving caspase-8 (47).

Cellular adhesion, migration and angiogenesis

Galectin-3 can bind to different integrins and proteins present in the extracellular matrix, thereby affecting the process of cellular adhesion, migration and morphogenesis. Accordingly it was shown that galectin-3 reduced the adhesion of different carcinoma cell lines with

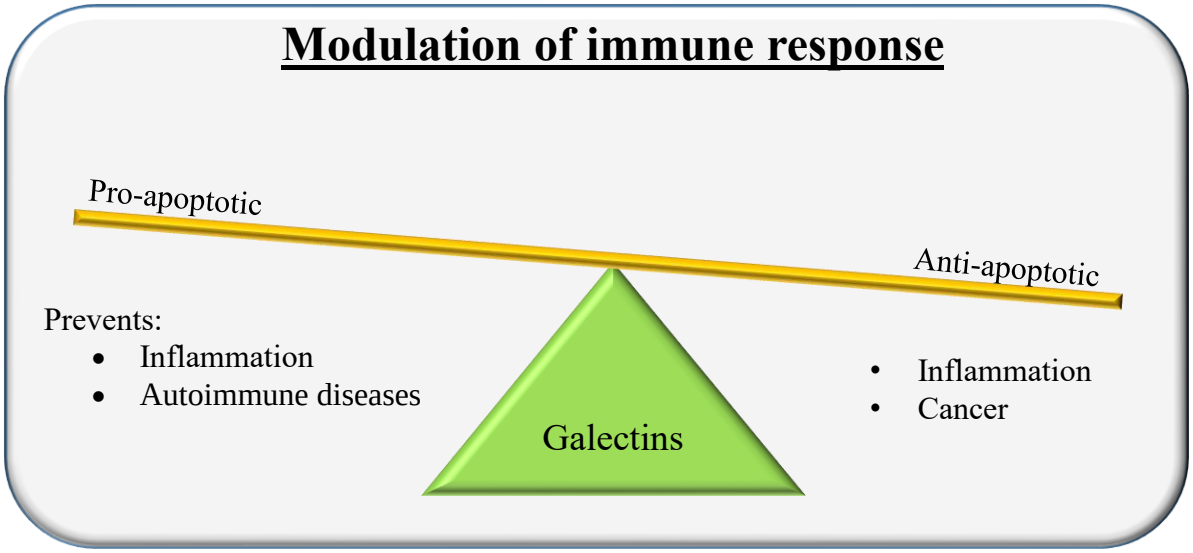

Figure no. 1.3. Role of galectin-3 in modulating apoptosis and the ensuing immune responses

extracellular matrix (ECM) proteins in a dose dependent manner (48). This property could contribute to the promotion of metastatic events. In other reports it was observed that after binding to its receptors on endothelial cells, galectin-3 up regulated αVβ3 that in turns enhanced angiogenesis by acting as a mediator between the integrins and the ECM proteins. The interaction between soluble factors such as VGEFR2 and αVβ3, NG2 and α3β1 is facilitated by galectin-3 (49–51) . Accordingly, galectin-3 and α3β1 interaction leads to the

migration of cells and thereby helping in the process of wound healing (52). Therefore, galectin-3 by interacting with ECM proteins could not only contributes to the tumorigenesis but also promote wound healing and the resolution of inflammation.

Role of galectin-3 during infections

Microbes such as bacteria, viruses, fungi, parasites have various glycoproteins on their surface through which they interact with their specific receptors available in the host cells. Such interactions either facilitate or inhibit their binding or cellular entry (53). The interacting partners vary depending on the pathogens, or the host species and the cell type involved. In general, animal lectins serve as the receptors for microbial surface glycans whose expression is greatly influenced by their encoded glycosyltransferases encoded (54–56). In the following section key roles of galectin-3 during bacterial and viral infections are discussed.

Galectin-3 as a modifier of bacterial infections

The bacterial cell wall is made up of peptidoglycans which consist of polysaccharides. The saccharides units are potential binding partners for galectins. Lipopolysaccharides (LPS) of gram-negative bacteria are known to bind galectins (57). The interaction between these two molecules results in the variable outcome for different gram-negative bacteria. Both the domains (N-terminus domain and CRD) of galectin-3 can bind to LPS independently. For example, the LPS of *Salmonella minnesota* R7 binds to N terminal region whereas that of *Klebsiella pneumoniae* has an affinity for CRD (58). The extracellular galectin-3 binds to *Neisseria meningitides* and increases its adhesion specifically to monocytes and macrophages, though this communication does not increase either its uptake or phagocytosis. On the contrary, it promotes infection (59). Galectin-3 is also expressed by epithelial cells in the reproductive tract mucosa of the urethra of males, cervix and fallopian tubes of females,

which are the potential sites for gonococci infections. Thus, the whole *Neisseria gonorrhoeae* or its purified derivatives such as lipooligosaccharides bind with galectin-3 in the *in vitro* cultures (60). This interaction could potentially contribute to the pathogenesis of gonococcal infections. Similarly, LPS of *Pseudomonas aeruginosa* binds to galectin-3 present on human corneal epithelial cells to promote ocular infection in the initial stages of host-pathogen interaction (61). During the pathogenesis of *Helicobacter pylori,* galectin-3 performs dual role either by promoting the infectivity or serving as a modifier of the infection. Thus, galectin-3 helps *H. pylori* adhere to the host cells in the initial stages of infection and this interaction is mediated by its O-antigens. Subsequently, *H. pylori* translocates its cytotoxin-associated antigen A into the gastric epithelial cells that in turn induces galectin-3 mRNA by activating ERK signalling pathways (62). Galectin-3 released in the extracellular spaces either serves as a chemoattractant to recruit the cells of innate immune origin to achieve anti-microbial functions or as an enhancer of infection by promoting adhesion of bacterium to the gastric epithelial cells. Invasive pathogens such as *Legionella pneumophila* and *Yersinia pseudotuberculosis* form pathogen associated vacuoles (PVs) inside the host cells. Galectin-3 could sense the components of secretion system of *L. pneumophila* and some of the pore proteins of *Y. pseudotuberculosis* present in such vacuoles and in so doing helps recruit IFN-γ inducible GTPase's to such PVs thereby participating in host defence (63). Mycolic acids (MA) and phosphatidylinositolmannosides, the membrane components of *Mycobacterium tuberculosis*, were shown to exhibit an affinity for galectin-3. The binding of MA to galectin-3 did not hamper latter's ability to bind sugar moieties but prevented its oligomerisation (64). The functional outcome of such an effect was not investigated but it could potentially reduce the pathogenesis. Galectin-3 was also found to localise in the phagosomes containing *M. tuberculosis* where it downregulated the activity of bacterial tyrosine kinase A (65, 66). Such an activity is known to play a critical role in the pathogenesis of tuberculosis by enhancing

bacterial persistence in the host. Galectin-3 not only binds to pathogenic bacteria but also to many species of the commensal microorganisms suggesting its indiscriminating activity between harmful and the helpful microbes. Such a property could be harnessed to alter the pathogenesis of microbial diseases as well (67). Thus, galectin-3 by binding to the microflora present in host could create a competition for the space and available nutrients thereby interfering with the colonization process.

Although this aspect will not be discussed in details, but galectin-3 could in fact modulate the immune response during fungal or the parasitic infections. While interacting with the oligomannans of *Candida spp.*, galectin-3 exhibits anti-microbial properties but the outcome of the interaction seems to be tissue specific during *Trypansoma cruzi* infection. Galectin-3 reduces the parasitic infectivity in the peritoneal macrophages to help control the systemic spread but, in the smooth muscles of coronary artery, such an interaction promotes infection by enhancing the adhesion between the host cell and the parasite (68, 69). One of the components of *Leishmania major*, the lipophosphoglycan specifically interacted with galectin-3 to cleave its N terminal region (70). This region is required for the oligomerisation associated activities of galectin-3. The consequence of such an interaction in the pathogenesis of leishmaniasis has not yet been investigated.

Galectin-3 as a modifier of viral infections

Viruses are the acellular entities that infect their host and manipulate different cellular components for survival. Galectin-3 plays vital roles during the binding step or the viral entry into the cells. The role of galectin-3 in modifying the pathogenesis of different strains of influenza virus has been studied. For example, H5N1 infection induced galectin-3 production in activated macrophages isolated from infected mice and was shown to induce inflammasome pathways leading to an enhanced IL-1β production. This aggravated the

severity of inflammatory reaction by promoting the cytokine storm (71). Contrary to these observations, Influenza A virus (Influenza A/Taiwan/CMUH01/2007(H1N1) infected MDCK cells, additionally treated with an antiviral drug aloe-emodin, up regulated galectin-3 to increase the expression of IFN-β, IFN-γ, PKR and 2′,5′–oligoadenylate synthetase (OAS) (72). In latter situation, the gamut of effector molecules induced could have a direct anti-viral activity in the cells thereby reducing the overall viral burden. With the reduced viral load the extent of cytokine storm was mitigated. The altered response pattern could also be due to the cell types involved. Similarly, galectin-3 depending on its relative levels and the localization could either promote or regulate the infectivity of susceptible cells by HIV. Galectin-3 via its N terminal region interacts with the proline rich region of Alix protein to help stabilise Alix-gag-p6 binding in the infected cells to promote HIV-1 budding (73). Galectin-3 alongside HIV is also present in the exosomes released from the infected dendritic cells (DCs) which in turn enhances the susceptibility of T cells to HIV-1 infection. This process is primarily mediated by an enhanced cellular fusion in which fibronectin as well as galectin-3 act to facilitate the fusion (74). Galectin-3 can also acts as an anti-viral agent when added exogenously to the HIV-1 infected THP1 derived macrophages (75). How it blocks HIV infectivity is not clear but could relate to its ability to interfere with the viral uptake by blocking the receptor for viral entry in these cells. Galectin-3 expression is also increased during HTLV-1 infection of T cells and it could enhance their metastatic potential as was also discussed in an earlier section (76). Junin virus, the causative agent of Argentine haemorrhagic fever causes an up regulation of galectin-3 expression in activated microglial cells but how it relates to the pathogenesis of the virus is not known (77). Recently it is reported that up regulated galectin-3 in the patient's serum can be used as a prognostic marker for Hepatitis C and B virus induced carcinoma (78, 79). Galectin-3 produced by corneal epithelial cells can bind to HSV-1 but not to HSV-2. Therefore, it is speculated that

galectin-3 could promote ocular HSV1 infection (80). Due to the increased levels of galectin-3 during zosteriform infection with HSV1, more macrophages and microglial cells infiltrated in the spinal dorsal horn and this contributed to a condition known as acute herpetic allodynia or reduced pain in mice (81). The pathophysiology of this disease as well as its molecular mediators are not well understood. MVMp (Minute virus of mice), a fibrotropic virus of parvoviridae family, also required galectin-3 for its efficient entry into the cells (82). Therefore, in most cases of viral infection, the extracellular galectin-3 acts as a bridge to facilitate interaction between the host and the pathogens either to enhance or reduce the pathogenicity depending on the virus involved.

Galectin 3 and γ-herpesviruses

γ-Herpesviruses are dsDNA viruses and are classified into two genra- Lymphocrytoviruses e.g., Epistein-Barr Virus (EBV) and Rhadinoviruses e.g., Kaposi's sarcoma-associated herpesvirus i.e. (KSHV) (83). Studying the pathogenesis of such viruses require a native host because of the species specificity. MHV68 infection of laboratory mice provides an accessible model system to study different aspects of pathogenesis and the host correlates of protection (84). Natural route of infection is still not clear but experimentally the virus can be injected through intranasal or intraperitoneal route to establish a latent infection. Upon intranasal infection, the virus infects mucosal epithelial cells and then migrates to spleen via mediastinal lymph nodes (MLNs) where it establishes latency in splenic B cells, peritoneal macrophages and dendritic cells (DCs). Acute stage of infection resolves after 9 to 14 days post infection (dpi) and then latency ensues where viral replication or its protein are undetectable by host immune system. $CD8^+$, $CD4^+$ T cells and B cells are the major players in the viral clearance, establishment and maintenance of latency. During acute stage of infection mainly $CD8^+$ T cells help clear the virus as a complete absence of $CD8^+$ T cells in mice lead to mortality within 12days post infection (85). $CD4^+$ T cells are essential in the

establishment of the latency and are the major producers of IFN-γ during reactivation. In the $CD4^+$ knockout mice, latency was delayed and the viral reactivation occurred frequently leading to their death within 2 – 3 months post infection (85, 86). B cells serve as the reservoir of the virus for the life of the host (87). Unlike other herpesviruses, γ-HV form latent infection irrespective of the dose and route of infection (88). The virus encodes several viral epitopes to activate $CD8^+$ T cells and many such epitopes are presented by $H2\text{-}D^b$ and $H2\text{-}K^b$ MHC I molecules (89). These viral epitopes are associated with genes expressed at different stages of infection, i.e. acute stage of replication, early latency and latent stage (90). Several specific genes are required for latency and M2 encoded protein is one of the major contributor. It is expressed in the cytoplasm of B cells and recognised by $CD8^+$ T cells during latency (91). The unique feature of persistent infection is that the immune cells do not undergo exhaustion unlike chronic infections and the cells remain functionally active (92). These observations suggest that some cellular or the extracellular regulators could fine tune the immune system and the viral control. Galectins could potentially serve such regulators.

Strategies to modify extracellular and intracellular galectin-3

We have described the role of galectin-3 in different pathophysiological conditions. CRD of galectin-3 binds to β-galactosides, so any host cells or the pathogens that express such saccharide units can potentially interact with galectin-3 molecules. Particularly during a direct host-pathogen interaction, galectin-3 is likely to facilitate infection. Therefore, one could argue on the relevance and the need of having such a molecule in the host. Galectin-3 was shown to dampen the activity of T cells either by inducing their apoptosis or serving as an immune checkpoint to regulate excessive inflammation and in so doing ameliorated autoimmune diseases. In order to understand the functions of galectin-3, it may be desirable to modulate the expression precisely. In the following section, different approaches that could

be used to modulate either the expression of galectin-3 or its neutralization to influence the disease outcomes are discussed.

The first approach is the manipulation of galectin-3 expressions at the genetic level. This could either be achieved by knock out (KO) i.e., complete removal or inducing a frame shift leading to disruption of the gene function in the whole organism or in a tissue/ cell specific deletion. A transient reduction in the expression of the target protein including galectin-3 could be achieved by its knock down (KD). If the disruption in the function of a gene is required in a cell specific manner or in a particular stage of cell differentiation, KD approach is usually preferred. For example if the disruption is required to only study the activation profile of immune cells or during a transition of effector cells into the memory population, one could resort to the KD approach. Different methods have be employed to regulate the expression of galectin-3 and could include an RNA interference based approach or the use of small molecules as inhibitors.

RNA interference

RNA interference approaches include the use of short hairpin RNA (shRNA) or small interfering RNA molecules (siRNA) to modify the expression of intracellular galectin-3. These approaches offer an advantage that the genetic material or the codons remain rather unaffected but specific small RNA sequences used help cleave the target mRNA only in such a way that most of it will be degraded; hence functional protein will be either absent or in less abundance. One disadvantage of such an approach is incomplete inhibition. In case of siRNA approach, pre-synthesised double-stranded RNA molecules are directly injected into the cells either by electroporation or lipid-mediated transfection. Most cells of the immune system have innate immune receptors such as TLRs. Therefore, such oligo's that are used to disrupt gene function could ,in fact, induce signaling events leading to the production of immune

effector molecules that might interfere with the physiological response in the target cells (93). For shRNA mediated KD, double-stranded short oligo's are ligated into a lentiviral or a retroviral cloning vectors and then co-transfected into susceptible cell lines such as HEK293T along with other packaging vectors. Once the recombinant viral particles are produced, such viruses are used for disruption of the target gene in the desired cells. shRNA is used for long term downregulation as there is a stable genomic integration assuring continuous supply of double-stranded RNA molecules (94).

Chemical inhibitors

Naturally occurring compounds like sugars or pectin derivatives and chemically synthesized compounds like thiogalactoside derivatives can also be used to manipulate the expression pattern or the relative abundance of galectin-3. Sugars bind to galectins through their CRDs, therefore such an approach does not specifically inhibit galectin-3. Recently it has been shown that the derivatives of pectin can also reduce the expression of galectin-3 though it failed to penetrate the cells (95). Thus, it does not influence the expression or the localization of intracellular galectin-3. Chemically synthesized compounds or those isolated from plants which could disrupt galectin-3 functions include TD139, GR-MD-02, GM-CT-01, and GCS-100. TD139 is in phase 2 clinical trials for managing idiopathic pulmonary fibrosis (96). Plant derivatives based galectin-3 inhibitors such as GR-MD-02 (derived from apples), GM-CT-01 and GCS-100 (from citrus fruits) are also in clinical trials (97).

Antibodies as biological reagents to elucidate molecular function

RNA interference and chemical inhibitors have limitations as they can have either off target effects or introduce aberrations in cells and therefore their physiological relevance might be of limited value. Most chemical inhibitors efficiently function extracellularly and therefore cannot inhibit the proliferative capacity of either transformed cells or activated cells by

modulating galectin-3 expression or localization. Therefore, there is a need to develop novel biologicals whose expression could be modulated as per the requirement to achieve the inhibition or inter-biomolecular interactions both intracellularly as well as extracellularly to help decipher molecular mechanisms in a better way. One class of biomolecules that fits the bill is antibodies. Antibodies bind to their counter structure with high precision. The intact antibody molecules or their derivatives currently constitute more than a billion dollar a year industry owing to their unparallel utility in biomedical, biotechnological and biological research. Beginning with the discovery of antibodies as anti-toxins by von Behring and Kitasato way back in 1901, the numerous modifications of such binders have been generated, tried and tested for many applications. These include generating monoclonal antibodies by using hybridoma technology to obtain antibodies specific to a given antigenic determinant. The large molecular mass and their inherent ability to act in the extracellular spaces once released from differentiated and activated B cells represent some of the known and yet to tackle hurdles in utilizing their full potential. The smaller versions of antibodies could be generated by performing protease digestions to obtain antigen binding fragments (Fab). However, this approach did not help greatly as the processed products tend to aggregate easily. However, with the advent of recombinant DNA technology, it became feasible to generate tailor-made binders such as scFv (single chain fragment variable). Such preparations are smaller in size and could also be expressed intracellularly if desired. However, not up-to the mark products were obtained even by with approach as extensive genetic engineering manipulations were needed. Such binders exhibited unstability and failed to withstand harsh conditions such as very low pH and high temperatures. Another issues with such products remained the random linkage of the variable region obtained from heavy (V_H) and light chain (V_L). This made the endeavour too tiresome for selecting out specific binders. Therefore, deciphering intracellular vs extracellular role of galectin-3 remained a challenge.

Intrabodies

Most of the above-mentioned drawbacks associated with antibody generation could be overcome if genetic material, encoding a naturally occurring heavy chain antibody is used as template for producing single domain antibodies (sdAbs). These antibodies came into existence when a unique class of heavy chain only antibodies (HCAb's) were discovered (98). Such antibodies were described in early 1990's and were characterised from the serum samples of dromedaries. Since then their existence in all the members of family camelidae and further illustration in some fishes was demonstrated (99). HCAb's were distinguished from classical heterotetrameric antibodies on the basis of their relative representation in blood, differential adsorption affinity matrices consisting of protein A and protein G and their smaller size (100). In dromedaries, there exist three types of IgG isotypes that are lacking in light chains and are known as IgG2a, IgG2c and IgG3 (98). Inspite of lacking three CDRs contributed by light chains, HCAb's bind target antigens with equivalent or more affinities when compared to the conventional Abs (101). Due to these attributes, HCAb's and their antigen recognizing domains (VHH) are considered as better therapeutics and diagnostic biologicals (102). VHH can be genetically constructed using the information encoded in the rearranged genomic segments of VDJ regions in B cells isolated from camelids. From our understanding of how immune system in vertebrates works, really the immunogens used for generating libraries do not critically hinder the applicability. Thus, every single vertebrate organism has the capability to respond to almost any antigen ever encountered or get to be encountered. Ablynx- a Belgium based biopharmaceutical company named VHH as nanobodies due to their smaller size (103). These domain antibodies are amenable for extensive genetic engineering and protein surgical procedures such as enzymatic linkage of two polypeptide or one polypeptide with other chemicals and therefore can be tailor-made for numerous applications that include bio-imaging (104), neutralization of pathogens and their

pathogenic entities (105, 106). Because of the extension of some CDRs particularly CDR2 and CDR3 leading to formation of pointing paratopes, even hidden epitopes are accessible to these binders (107). The size of VHH is very small, i.e., 13-15kD (102) and hence such binders easily penetrate tissue sites. One of their flip side, however is decrease in their half-life because of efficient clearance from the glomerulus filtration system. Nonetheless such antibodies can be generated into larger sized formulations such as dimers or tetramers, should such a need arise. These nanobodies can be selected for target antigens to provide specificity and can be further cloned and expressed intracellularly by retroviral or lentiviral mediated transfection. The utility of nanobodies or the single domain antibodies is well recognized in various fields of investigations ranging from theragnostics to crystal structure determination of various biomolecules (108, 109). sdAbs can also use to inhibit extracellular galectin-3 by incorporating signal sequences upstream of VHH such that these can be excreted outside of the cells. In nutshell, single domain antibodies can be a better reagent to neutralize the effects of galectin-3 inside as well as outside the cells.

Conclusion

Galectins family is ever expanding and the member proteins could have different affinities for the same ligands. Due to their expression in tissue/cell-specific manner and involvement in many diseases or clinical conditions, this protein family has come of age. This is especially true for galectin-3, one of the most studied members. Under normal conditions, galectin-3 participates in numerous cellular events and its function varies with the cellular localization and ligands involved. Galectin-3 influences the outcome of many diseases including tumorigenesis, autoimmunities as well as some infections. But how galectin-3 modulates the responsiveness of virus-specific $CD8^+$ T cells is less well understood and therefore is undertaken in the current study. Its role under specified circumstances can be usually predicted by using knockout mouse models. Such strategies eliminate molecular function

completely and therefore need to be supplemented with other non-genetic approaches such as disruption of protein-protein interactions using specific small molecules or the antibodies. In recent years many chemicals, as well as plant-based sugars, have been used to inhibit the functions of galectin-3. Although these inhibitors have shown promising results in *in vitro* and *in vivo* model systems and are currently in different phases of clinical trials, but the issues related to specificity reduce enthusiasm. In addition, the function of galectin-3 could not be disrupted intracellularly with such approaches. The specific binding can be taken care of when antibodies are used for such purposes but neither conventional antibodies nor scFv can penetrate the cell membrane. Moreover, the suitability of scFv to serve as intrabodies has yielded limited success. The discovery of Heavy chain antibodies (HCAb's) has given the required impetus to their intracellular expression and functional outcomes. The derivatives of sdAbs can disrupt protein-protein interactions intracellularly as intrabodies. The feasibility of such an approach was tested in this study where specific binders for galectin-3 were selected and used intracellularly.

The study was designed to first address the role of galectin-3 during anti-γ herpes viral $CD8^+$ T cell immunity using transnuclear and transgenic mice strains for a virus encoded epitopes and then to generate and characterise single domain antibodies selected from phage display technology not only against galectin-3 but also against other antigens such as those present in snake venom with the goal of establishing their utility.

References

1. Teichberg, V., and I. Silman. 1975. A beta-D-galactoside binding protein from electric organ tissue of Electrophorus electricus. *Proc. …* 72: 1383–1387.

2. Barondes, S. H., V. Castronovo, D. N. W. Cooper, R. D. Cummings, K. Drickamer, T. Felzi, M. A. Gitt, J. Hirabayashi, C. Hughes, K. ichi Kasai, H. Leffler, F. T. Liu, R. Lotan, A.

M. Mercurio, M. Monsigny, S. Pillai, F. Poirer, A. Raz, P. W. J. Rigby, J. M. Rini, and J. L. Wang. 1994. Galectins: A family of animal β-galactoside-binding lectins. *Cell* 76: 597–598.

3. Hirabayashi, J., and K. I. Kasai. 1993. The family of metazoan metal-independent β-galactoside-binding lectins: Structure, function and molecular evolution. *Glycobiology* 3: 297–304.

4. Hirabayashi, J., T. Hashidate, Y. Arata, N. Nishi, T. Nakamura, M. Hirashima, T. Urashima, T. Oka, M. Futai, W. E. G. Muller, F. Yagi, and K. I. Kasai. 2002. Oligosaccharide specificity of galectins: A search by frontal affinity chromatography. *Biochim. Biophys. Acta - Gen. Subj.* 1572: 232–254.

5. Liao, D. I., G. R. Vasta, H. Ahmed, O. Herzberg, and G. Kapadia. 2006. Structure of S-lectin, a developmentally regulated vertebrate beta-galactoside-binding protein. *Proc. Natl. Acad. Sci.* 91: 1428–1432.

6. Lobsanov, Y. D., M. A. Gitt, H. Leffler, S. H. Barondes, and J. M. Rini. 1993. X-ray crystal structure of the human dimeric S-Lac lectin, L-14-II, in complex with lactose at 2.9-Å resolution. *J. Biol. Chem.* 268: 27034–27038.

7. Raz, A., G. Pazerini, and P. Carmi. 1989. Identification of the Metastasis-associated, Galactoside-binding Lectin as a Chimeric Gene Product with Homology to an IgE-binding Protein. *Cancer Res.* 49: 3489–3493.

8. Leffler, H., S. Carlsson, M. Hedlund, Y. Qian, and F. Poirier. 2002. Introduction to galectins. *Glycoconj. J.* 19: 433–440.

9. Lensch, M., M. Lohr, R. Russwurm, M. Vidal, H. Kaltner, S. André, and H. J. Gabius. 2006. Unique sequence and expression profiles of rat galectins-5 and -9 as a result of species-specific gene divergence. *Int. J. Biochem. Cell Biol.* 38: 1741–1758.

10. Gitt, M. A., C. Colnot, F. Poirier, K. J. Nani, S. H. Barondes, and H. Leffler. 1998.

Galectin-4 and galectin-6 are two closely related lectins expressed in mouse gastrointestinal tract. *J. Biol. Chem.* 273: 2954–2960.

11. Houzelstein, D., I. R. Gonçalves, A. J. Fadden, S. S. Sidhu, D. N. W. Cooper, K. Drickamer, H. Leffler, and F. Poirier. 2004. Phylogenetic analysis of the vertebrate galectin family. *Mol. Biol. Evol.* 21: 1177–1187.

12. Liu, F. T., R. J. Patterson, and J. L. Wang. 2002. Intracellular functions of galectins. *Biochim. Biophys. Acta - Gen. Subj.* 1572: 263–273.

13. Wilson, T. J., M. N. Firth, J. T. Powell, and F. L. Harrison. 1989. The sequence of the mouse 14 kDa beta-galactoside-binding lectin and evidence for its synthesis on free cytoplasmic ribosomes. *Biochem. J.* 261: 847–52.

14. Ohyama, Y., J. Hirabayashi, Y. Oda, S. Ohno, H. Kawasaki, K. Suzuki, and K. ichi Kasai. 1986. Nucleotide sequence of chick 14K β-galactoside-binding lectin mRNA. *Biochem. Biophys. Res. Commun.* 134: 51–56.

15. Mehul, B., and R. C. Hughes. 1997. Plasma membrane targetting, vesicular budding and release of galectin 3 from the cytoplasm of mammalian cells during secretion. *J. Cell Sci.* 110 (Pt 1: 1169–78.

16. Menon, R. P., and R. C. Hughes. 1999. Determinants in the N-terminal domains of galectin-3 for secretion by a novel pathway circumventing the endoplasmic reticulum-Golgi complex. *Eur. J. Biochem.* 264: 569–576.

17. Liu, W., D. K. Hsu, H. Y. Chen, R. Y. Yang, K. L. Carraway, R. R. Isseroff, and F. T. Liu. 2012. Galectin-3 regulates intracellular trafficking of EGFR through alix and promotes keratinocyte migration. *J. Invest. Dermatol.* 132: 2828–2837.

18. Bänfer, S., D. Schneider, J. Dewes, M. T. Strauss, S.-A. Freibert, T. Heimerl, U. G. Maier, H.-P. Elsässer, R. Jungmann, and R. Jacob. 2018. Molecular mechanism to recruit

galectin-3 into multivesicular bodies for polarized exosomal secretion. *Proc. Natl. Acad. Sci.* 115: E4396–E4405.

19. Parolini, I., C. Federici, C. Raggi, L. Lugini, S. Palleschi, A. De Milito, C. Coscia, E. Iessi, M. Logozzi, A. Molinari, M. Colone, M. Tatti, M. Sargiacomo, and S. Fais. 2009. Microenvironmental pH is a key factor for exosome traffic in tumor cells. *J. Biol. Chem.* 284: 34211–34222.

20. Gong, H. C., Y. Honjo, P. Nangia-Makker, V. Hogan, N. Mazurak, R. S. Bresalier, and A. Raz. 1999. The NH2 terminus of galectin-3 governs cellular compartmentalization and functions in cancer cells. *Cancer Res.* 59: 6239–6245.

21. Roff, C. F., and J. L. Wang. 1983. Endogenous lectins from cultured cells. Isolation and characterization of carbohydrate-binding proteins from 3T3 fibroblasts. *J. Biol. Chem.* 258: 10657–10663.

22. Patterson, R. J., W. Wang, and J. L. Wang. 2002. Understanding the biochemical activities of galectin-1 and galectin-3 in the nucleus. *Glycoconj. J.* 19: 499–506.

23. Li, S. Y., P. J. Davidson, N. Y. Lin, R. J. Patterson, J. L. Wang, and E. J. Arnoys. 2006. Transport of galectin-3 between the nucleus and cytoplasm. II. Identification of the signal for nuclear export. *Glycobiology* 16: 612–622.

24. Davidson, P. J., S. Y. Li, A. G. Lohse, R. Vandergaast, E. Verde, A. Pearson, R. J. Patterson, J. L. Wang, and E. J. Arnoys. 2006. Transport of galectin-3 between the nucleus and cytoplasm. I. Conditions and signals for nuclear import. *Glycobiology* 16: 602–611.

25. Seetharaman, J., A. Kfanigsberg, R. Slaaby, H. Leffler, S. H. Barondes, and J. M. Rini. 1998. X-ray crystal structure of the human galectin-3 carbohydrate recognition domain at 2.1-Å resolution. *J. Biol. Chem.* 273: 13047–13052.

26. Tsay, Y. G., N. Y. Lin, P. G. Voss, R. J. Patterson, and J. L. Wang. 1999. Export of

galectin-3 from nuclei of digitonin-permeabilized mouse 3T3 fibroblasts. *Exp. Cell Res.* 252: 250–261.

27. Kudo, N., B. Wolff, T. Sekimoto, E. P. Schreiner, Y. Yoneda, M. Yanagida, S. Horinouchi, and M. Yoshida. 1998. Leptomycin B inhibition of signal-mediated nuclear export by direct binding to CRM1. *Exp. Cell Res.* 242: 540–547.

28. Park, J. W., P. G. Voss, S. Grabski, J. L. Wang, and R. J. Patterson. 2001. Association of galectin-1 and galectin-3 with Gemin4 in complexes containing the SMN protein. *Nucleic Acids Res.* 29: 3595–602.

29. Dagher, S. F., J. L. Wang, and R. J. Patterson. 2006. Identification of galectin-3 as a factor in pre-mRNA splicing. *Proc. Natl. Acad. Sci.* 92: 1213–1217.

30. Yoshii, T., T. Fukumori, Y. Honjo, H. Inohara, H. R. C. Kim, and A. Raz. 2002. Galectin-3 phosphorylation is required for its anti-apoptotic function and cell cycle arrest. *J. Biol. Chem.* 277: 6852–6857.

31. Mazurek, N., J. Conklin, J. C. Byrd, A. Raz, and R. S. Bresalier. 2000. Phosphorylation of the β-galactoside-binding protein galectin-3 modulates binding to its ligands. *J. Biol. Chem.* 275: 36311–36315.

32. Ochieng, J., V. Furtak, and P. Lukyanov. 2002. Extracellular functions of galectin-3. *Glycoconj. J.* 19: 527–535.

33. Wang, L., H. Inohara, K. J. Pienta, and A. Raz. 1995. Galectin-3 is a nuclear matrix protein which binds RNA. *Biochem. Biophys. Res. Commun.* 217: 292–303.

34. Shimura, T., Y. Takenaka, S. Tsutsumi, V. Hogan, A. Kikuchi, and A. Raz. 2004. Galectin-3, a novel binding partner of β-catenin. *Cancer Res.* 64: 6363–6367.

35. Menon, R. P., M. Strom, and R. C. Hughes. 2000. Interaction of a novel cysteine and histidine-rich cytoplasmic protein with galectin-3 in a carbohydrate-independent manner.

FEBS Lett. 470: 227–231.

36. Agrwal, N., J. L. Wang, and P. G. Voss. 1989. Carbohydrate-binding protein 35. Levels of transcription and mRNA accumulation in quiescent and proliferating cells. *J. Biol. Chem.* 264: 17236–17242.

37. Moutsatsos, I. K., J. M. Davis, and J. L. Wang. 1986. Endogenous lectins from cultured cells: Subcellular localization of carbohydrate-binding protein 35 in 3T3 fibroblasts. *J. Cell Biol.* 102: 477–483.

38. Chen, H.-Y., A. Fermin, S. Vardhana, I.-C. Weng, K. F. R. Lo, E.-Y. Chang, E. Maverakis, R.-Y. Yang, D. K. Hsu, M. L. Dustin, and F.-T. Liu. 2009. Galectin-3 negatively regulates TCR-mediated CD4+ T-cell activation at the immunological synapse. *Proc. Natl. Acad. Sci. U. S. A.* 106: 14496–501.

39. Kaur, M., D. Kumar, V. Butty, S. Singh, A. Esteban, G. R. Fink, H. L. Ploegh, and S. Sehrawat. 2018. Galectin-3 Regulates γ-Herpesvirus Specific CD8 T Cell Immunity. *iScience* 9: 101–119.

40. Yang Ry, Hsu Dk, and Liu Ft. 1996. Expression of galectin-3 modulates T-cell growth and apoptosis. *Proc. Natl. Acad. Sci. U. S. A.* 93: 6737–6742.

41. Van den Brûle, F. A., A. Bellahcene, P. Jackers, F. U. T. Liu, M. E. Sobel, and V. Castronovo. 1997. Antisense galectin-3 alters thymidine incorporation in human MDA-MB435 breast cancer cells. *Int. J. Oncol.* 11: 261–264.

42. Farhad, M., A. S. Rolig, and W. L. Redmond. 2018. The role of Galectin-3 in modulating tumor growth and immunosuppression within the tumor microenvironment. *Oncoimmunology* 7.

43. Yu, F., R. L. Finley, A. Raz, and H. R. C. Kim. 2002. Galectin-3 translocates to the perinuclear membranes and inhibits cytochrome c release from the mitochondria. A role for

synexin in galectin-3 translocation. *J. Biol. Chem.* 277: 15819–15827.

44. LIU, L., T. SAKAI, N. SANO, and K. FUKUI. 2004. Nucling mediates apoptosis by inhibiting expression of galectin-3 through interference with nuclear factor kappaB signalling. *Biochem. J.* 380: 31–41.

45. Stillman, B. N., D. K. Hsu, M. Pang, C. F. Brewer, P. Johnson, F. T. Liu, and L. G. Baum. 2006. Galectin-3 and galectin-1 bind distinct cell surface glycoprotein receptors to induce T cell death. *J. Immunol.* 176: 778–789.

46. Zhao, Z., L. Liu, G. Tai, H. Cheng, Y. Guan, Y. Zhou, H. Xue, and Z. Zhang. 2017. The N-terminal tail coordinates with carbohydrate recognition domain to mediate galectin-3 induced apoptosis in T cells. *Oncotarget* 8.

47. Fukumori, T., Y. Takenaka, T. Yoshii, H. R. C. Kim, V. Hogan, H. Inohara, S. Kagawa, and A. Raz. 2003. CD29 and CD7 Mediate Galectin-3-Induced Type II T-Cell Apoptosis. *Cancer Res.* 63: 8302–8311.

48. Ochieng, J., M. L. Leite-Browning, and P. Warfield. 1998. Regulation of cellular adhesion to extracellular matrix proteins by galectin-3. *Biochem. Biophys. Res. Commun.* 246: 788–791.

49. Nangia-Makker, P., Y. Honjo, R. Sarvis, S. Akahani, V. Hogan, K. J. Pienta, and A. Raz. 2000. Galectin-3 induces endothelial cell morphogenesis and angiogenesis. *Am. J. Pathol.* 156: 899–909.

50. Jun-ichi Fukushi,* Irwan T. Makagiansar, and W. B. S. 2004. NG2 Proteoglycan Promotes Endothelial Cell Motility and Angiogenesis via Engagement of Galectin-3 and α3β1 Integrin. *Mol. Biol. Cell* Vol. 15: 3580–3590.

51. Markowska, A. I., F.-T. Liu, and N. Panjwani. 2010. Galectin-3 is an important mediator of VEGF- and bFGF-mediated angiogenic response. *J. Exp. Med.* 207: 1981–1993.

52. Saravanan, C., F.-T. Liu, I. K. Gipson, and N. Panjwani. 2009. Galectin-3 promotes lamellipodia formation in epithelial cells by interacting with complex N-glycans on 3 1 integrin. *J. Cell Sci.* 122: 3684–3693.

53. Machala, E. A., B. P. McSharry, B. T. Rouse, A. Abendroth, and B. Slobedman. 2019. Gal power: the diverse roles of galectins in regulating viral infections. *J. Gen. Virol.* .

54. Baum, L. G., O. B. Garner, K. Schaefer, and B. Lee. 2014. Microbe-host interactions are positively and negatively regulated by galectin-glycan interactions. *Front. Immunol.* 5.

55. Dube, D. H., and C. R. Bertozzi. 2005. Glycans in cancer and inflammation - Potential for therapeutics and diagnostics. *Nat. Rev. Drug Discov.* 4: 477–488.

56. Kamili, N. A., C. M. Arthur, C. Gerner-Smidt, E. Tafesse, A. Blenda, M. Dias-Baruffi, and S. R. Stowell. 2016. Key regulators of galectin–glycan interactions. *Proteomics* 16: 3111–3125.

57. Li, Y., M. Komai-Koma, D. S. Gilchrist, D. K. Hsu, F.-T. Liu, T. Springall, and D. Xu. 2008. Galectin-3 Is a Negative Regulator of Lipopolysaccharide-Mediated Inflammation. *J. Immunol.* 181: 2781–2789.

58. Mey, A., H. Leffler, Z. Hmama, G. Normier, and J. P. Revillard. 1996. The animal lectin galectin-3 interacts with bacterial lipopolysaccharides via two independent sites. *J. Immunol.* 156: 1572–7.

59. Quattroni, P., Y. Li, D. Lucchesi, S. Lucas, D. W. Hood, M. Herrmann, H. J. Gabius, C. M. Tang, and R. M. Exley. 2012. Galectin-3 binds Neisseria meningitidis and increases interaction with phagocytic cells. *Cell. Microbiol.* 14: 1657–1675.

60. John, C. M., G. A. Jarvis, K. V. Swanson, H. Leffler, M. D. Cooper, M. E. Huflejt, and J. McLeod Griffiss. 2002. Galectin-3 binds lactosaminylated lipooligosaccharides from Neisseria gonorrhoeae and is selectively expressed by mucosal epithelial cells that are

infected. *Cell. Microbiol.* 4: 649–661.

61. Gupta, S. K., S. Masinick, M. Garrett, and L. D. Hazlett. 1997. Pseudomonas aeruginosa lipopolysaccharide binds galectin-3 and other human corneal epithelial proteins. *Infect. Immun.* 65: 2747–2753.

62. Fowler, M., R. J. Thomas, J. Atherton, I. S. Roberts, and N. J. High. 2006. Galectin-3 binds to Helicobacter pylori O-antigen: It is upregulated and rapidly secreted by gastric epithelial cells in response to H. pylori adhesion. *Cell. Microbiol.* 8: 44–54.

63. Feeley, E. M., D. M. Pilla-Moffett, E. E. Zwack, A. S. Piro, R. Finethy, J. P. Kolb, J. Martinez, I. E. Brodsky, and J. Coers. 2017. Galectin-3 directs antimicrobial guanylate binding proteins to vacuoles furnished with bacterial secretion systems. *Proc. Natl. Acad. Sci.* 201615771.

64. Barboni, E., S. Coade, and A. Fiori. 2005. The binding of mycolic acids to galectin-3: A novel interaction between a host soluble lectin and trafficking mycobacterial lipids? *FEBS Lett.* 579: 6749–6755.

65. Beatty, W. L., E. R. Rhoades, D. K. Hsu, F. T. Liu, and D. G. Russell. 2002. Association of a macrophage galactoside-binding protein with Mycobacterium-containing phagosomes. *Cell. Microbiol.* 4: 167–176.

66. Jaiswal, S., and K. K. Srivastava. 2018. Protein tyrosine kinase A modulates intracellular survival of mycobacteria through Galectin 3. *Biochem. Biophys. Res. Commun.* 498: 884–890.

67. Kavanaugh, D., M. Kane, L. Joshi, and R. M. Hickey. 2013. Detection of Galectin-3 Interaction with Commensal Bacteria. *Appl. Environ. Microbiol.* 79: 3507–3510.

68. Kleshchenko, Y. Y., T. N. Moody, V. A. Furtak, J. Ochieng, M. F. Lima, and F. Villalta. 2004. Human galectin-3 promotes Trypanosoma cruzi adhesion to human coronary artery

smooth muscle cells. *Infect. Immun.* 72: 6717–6721.

69. da Silva, A. A., T. L. Teixeira, S. C. Teixeira, F. C. Machado, M. A. dos Santos, T. C. Tomiosso, P. C. B. Tavares, R. T. e S. Brígido, F. A. Martins, N. S. de L. Silva, C. C. Rodrigues, M. C. Roque-Barreira, R. A. Mortara, D. S. Lopes, V. de M. R. Ávila, and C. V. da Silva. 2017. Galectin-3: A Friend but Not a Foe during Trypanosoma cruzi Experimental Infection. *Front. Cell. Infect. Microbiol.* 7: 1–9.

70. Pelletier, I., and S. Sato. 2002. Specific recognition and cleavage of galectin-3 by Leishmania major through species-specific polygalactose epitope. *J. Biol. Chem.* 277: 17663–17670.

71. Chen, Y. J., S. F. Wang, I. C. Weng, M. H. Hong, T. H. Lo, J. T. Jan, L. C. Hsu, H. Y. Chen, and F. T. Liu. 2018. Galectin-3 Enhances Avian H5N1 Influenza A Virus–Induced Pulmonary Inflammation by Promoting NLRP3 Inflammasome Activation. *Am. J. Pathol.* 188: 1031–1042.

72. Li, S. W., T. C. Yang, C. C. Lai, S. H. Huang, J. M. Liao, L. Wan, Y. J. Lin, and C. W. Lin. 2014. Antiviral activity of aloe-emodin against influenza A virus via galectin-3 up-regulation. *Eur. J. Pharmacol.* 738: 125–132.

73. Wang, S. F., C. H. Tsao, Y. T. Lin, D. K. Hsu, M. L. Chiang, C. H. Lo, F. C. Chien, P. Chen, Y. M. Arthur Chen, H. Y. Chen, and F. T. Liu. 2014. Galectin-3 promotes HIV-1 budding via association with Alix and Gag p6. *Glycobiology* 24: 1022–1035.

74. Kulkarni, R., and A. Prasad. 2017. Exosomes Derived from HIV-1 Infected DCs Mediate Viral trans-Infection via Fibronectin and Galectin-3. *Sci. Rep.* 7.

75. Xue, J., C. Fu, Z. Cong, L. Peng, Z. Peng, T. Chen, W. Wang, H. Jiang, Q. Wei, and C. Qin. 2017. Galectin-3 promotes caspase-independent cell death of HIV-1-infected macrophages. *FEBS J.* 284: 97–113.

76. Hsu, D., S. Hammes, I. Kuwabara, W. Greene, and F. Liu. 1996. Human T lymphotropic virus-I infection of human T lymphocytes induces expression of the β-galactoside-binding lectin, galectin-3. *Am. J. Pathol.* 148: 1661–1670.

77. Giusti, C. J. De, L. Alberdi, J. Frik, M. F. Ferrer, E. Scharrig, M. Schattner, and R. M. Gomez. 2011. Galectin-3 is upregulated in activated glia during Junin virus-induced murine encephalitis. *Neurosci. Lett.* 501: 163–166.

78. Sop, G., I. Alacacioglu, G. Bozkaya, A. Yuksel, E. Yuksel, A. Alacacioglu, M. Ulu, B. Pamukk, and A. Ari. 2015. Prognostic significance of serum galectin-3 levels in patients with hepatocellular cancer and chronic viral hepatitis. *Saudi J. Gastroenterol.* 21: 47.

79. Hsu, D. K., C. A. Dowling, K. C. G. Jeng, J. T. Chen, R. Y. Yang, and F. T. Liu. 1999. Galectin-3 expression is induced in cirrhotic liver and hepatocellular carcinoma. *Int. J. Cancer* 81: 519–526.

80. Woodward, A. M., J. Mauris, and P. Argueso. 2013. Binding of Transmembrane Mucins to Galectin-3 Limits Herpesvirus 1 Infection of Human Corneal Keratinocytes. *J. Virol.* 87: 5841–5847.

81. Takasaki, I., K. Taniguchi, F. Komatsu, A. Sasaki, T. Andoh, H. Nojima, K. Shiraki, D. K. Hsu, F. T. Liu, I. Kato, K. Hiraga, and Y. Kuraishi. 2012. Contribution of spinal galectin-3 to acute herpetic allodynia in mice. *Pain* 153: 585–592.

82. Garcin, P. O., I. R. Nabi, and N. Panté. 2015. Galectin-3 plays a role in minute virus of mice infection. *Virology* 481: 63–72.

83. Lacoste, V., A. Lavergne, B. de Thoisy, J. F. Pouliquen, and A. Gessain. 2010. Genetic diversity and molecular evolution of human and non-human primate Gammaherpesvirinae. *Infect. Genet. Evol.* .

84. Blaskovic, D., M. Stanceková, J. Svobodová, and J. Mistríková. 1980. Isolation of five

strains of herpesviruses from two species of free living small rodents. *Acta Virol.* .

85. Cardin, R. D. 2004. Progressive loss of CD8+ T cell-mediated control of a gamma-herpesvirus in the absence of CD4+ T cells. *J. Exp. Med.* .

86. Hu, Z., M. A. Blackman, K. M. Kaye, and E. J. Usherwood. 2015. Functional Heterogeneity in the CD4 + T Cell Response to Murine γ-Herpesvirus 68 . *J. Immunol.* .

87. Flaño, E., I.-J. Kim, D. L. Woodland, and M. A. Blackman. 2002. γ-Herpesvirus Latency Is Preferentially Maintained in Splenic Germinal Center and Memory B Cells. *J. Exp. Med.* .

88. Tibbetts, S. A., J. Loh, V. van Berkel, J. S. McClellan, M. A. Jacoby, S. B. Kapadia, S. H. Speck, and H. W. Virgin. 2003. Establishment and Maintenance of Gammaherpesvirus Latency Are Independent of Infective Dose and Route of Infection. *J. Virol.* .

89. Freeman, M. L., K. G. Lanzer, T. Cookenham, B. Peters, J. Sidney, T.-T. Wu, R. Sun, D. L. Woodland, A. Sette, and M. A. Blackman. 2010. Two Kinetic Patterns of Epitope-Specific CD8 T-Cell Responses following Murine Gammaherpesvirus 68 Infection. *J. Virol.* 84: 2881–2892.

90. Gredmark-Russ, S., E. J. Cheung, M. K. Isaacson, H. L. Ploegh, and G. M. Grotenbreg. 2008. The CD8 T-Cell Response against Murine Gammaherpesvirus 68 Is Directed toward a Broad Repertoire of Epitopes from both Early and Late Antigens. *J. Virol.* 82: 12205–12212.

91. Husain, S. M., E. J. Usherwood, H. Dyson, C. Coleclough, M. A. Coppola, D. L. Woodland, M. A. Blackman, J. P. Stewart, and J. T. Sample. 2002. Murine gammaherpesvirus M2 gene is latency-associated and its protein a target for CD8+ T lymphocytes. *Proc. Natl. Acad. Sci.* .

92. Cush, S. S., and E. Flano. 2009. Protective Antigen-Independent CD8 T Cell Memory Is Maintained during -Herpesvirus Persistence. *J. Immunol.* .

93. Marjorie Robbins, Adam Judge, and I. M. 2009. siRNA and Innate Immunity. *Oligonucleotides* 19: 89–102.

94. Mittal, V. 2004. Improving the efficiency of RNA interference in mammals. *Nat. Rev. Genet.* 5: 355–365.

95. Kolatsi-Joannou, M., K. L. Price, P. J. Winyard, and D. A. Long. 2011. Modified citrus pectin reduces galectin-3 expression and disease severity in experimental acute kidney injury. *PLoS One* 6.

96. 2017. TD139, A Novel Inhaled Galectin-3 Inhibitor for The Treatment of Idiopathic Pulmonary Fibrosis (IPF). Results from The First in (IPF) Patients Study. *QJM An Int. J. Med.* .

97. Girard, A., and J. L. Magnani. 2018. Clinical Trials and Applications of Galectin Antagonists. *Trends Glycosci. Glycotechnol.* 30: SE211–SE220.

98. Hamers-Casterman, C., T. Atarhouch, S. Muyldermans, G. Robinson, C. Hamers, E. B. Songa, N. Bendahman, and R. Hamers. 1993. Naturally occurring antibodies devoid of light chains. *Nature* 363: 446–448.

99. Greenberg, a S., D. Avila, M. Hughes, a Hughes, E. C. McKinney, and M. F. Flajnik. 1995. A new antigen receptor gene family that undergoes rearrangement and extensive somatic diversification in sharks. *Nature* 374: 168–173.

100. Rahbarizadeh, F., M. J. Rasaee, M. Forouzandeh, A. Allameh, R. Sarrami, H. Nasiry, and M. Sadeghizadeh. 2005. The production and characterization of novel heavy-chain antibodies against the tandem repeat region of MUC1 mucin. *Immunol. Invest.* 34: 431–452.

101. Daley, L. P., M. A. Kutzler, B. W. Bennett, M. C. Smith, A. L. Glaser, and J. A. Appleton. 2010. Effector functions of camelid heavy-chain antibodies in immunity to West Nile virus. *Clin. Vaccine Immunol.* 17: 239–246.

102. Muyldermans, S., C. Cambillau, and L. Wyns. 2001. Recognition of antigens by single-domain antibody fragments: The superfluous luxury of paired domains. *Trends Biochem. Sci.* 26: 230–235.

103. Snoeck, V. 2013. Current Experience in Immunogenicity Assessment of Next-Generation Biologics: Nanobodies. In *European Immunogenicity Symposium, Ablynx NV*.

104. Vaneycken, I., M. D'huyvetter, S. Hernot, J. de Vos, C. Xavier, N. Devoogdt, V. Caveliers, and T. Lahoutte. 2011. Immuno-imaging using nanobodies. *Curr. Opin. Biotechnol.* 22: 877–881.

105. Thanongsaksrikul, J., P. Srimanote, S. Maneewatch, K. Choowongkomon, P. Tapchaisri, S. I. Makino, H. Kurazono, and W. Chaicumpa. 2010. AVHH that neutralizes the zinc metalloproteinase activity of botulinum neurotoxin type A. *J. Biol. Chem.* 285: 9657–9666.

106. Safaee, L., S. Latif, M. Gargari, and I. Rasooli. 2013. International Journal of Infectious Diseases A novel nanobody against urease activity of Helicobacter pylori. *Int. J. Infect. Dis.* 17: 1–6.

107. Alzogaray, V., W. Danquah, A. Aguirre, M. Urrutia, P. Berguer, E. García Véscovi, F. Haag, F. Koch-Nolte, and F. a Goldbaum. 2011. Single-domain llama antibodies as specific intracellular inhibitors of SpvB, the actin ADP-ribosylating toxin of Salmonella typhimurium. *FASEB J.* 25: 526–534.

108. Lemaire, M., M. D'Huyvetter, T. Lahoutte, E. Van Valckenborgh, E. Menu, E. De Bruyne, P. Kronenberger, U. Wernery, S. Muyldermans, N. Devoogdt, and K. Vanderkerken. 2014. Imaging and radioimmunotherapy of multiple myeloma with anti-idiotypic Nanobodies. *Leukemia* 28: 444–7.

109. Loris, R., I. Marianovsky, J. Lah, T. Laeremans, H. Engelberg-Kulka, G. Glaser, S. Muyldermans, and L. Wyns. 2003. Crystal structure of the intrinsically flexible addiction

antidote MazE. *J. Biol. Chem.* 278: 28252–28257.

Chapter 2

Galectin-3 regulates γ-herpesvirus specific CD8 T cell immunity

Research described in this chapter is a slightly modified version of an article that in accepted for publication in *iScience* by Manpreet Kaur, Dhaneshwar Kumar, Vincent Butty, Sudhakar Singh, Alexandre Esteban, Gerald R. Fink, Hidde L. Poegh, and Sharvan Sehrawat.

Kaur M, Kumar D, Butty V, Singh S, Esteban A, Fink GR, Ploegh HL, Sehrawat S. Galectin 3 Regulates γ-Herpesvirus Specific CD8 T Cell Immunity. iScience. 2018 Nov 30;9:101-119.

In this chapter "our" and "we" refers to me and co-authors. My contribution in the paper includes (1) Selection of the topic (2) Compiling and interpretation of the literature (3) Designing experiments (4) understanding and interpretation of the results (5) Preparation of graphs and figures (6) Writing and editing

Abstract

To gain insights into the molecular mechanisms and pathways involved in the activation of γ-herpesvirus (MHV68)-specific TCR transnuclear $CD8^+$ T cells (TCR-TN cells), we performed a comprehensive transcriptomic analysis. Upon viral infection, we observed differential expression of several thousand transcripts encompassing various networks and pathways in activated compared to naïve TCR TN cells. Activated cells highly up regulated galectin-3, a member protein of galectin family. We therefore explored the role of galectin-3 in influencing anti-MHV68 immunity. Galectin-3 was recruited at the immunological synapse during activation of $CD8^+$ T cells and helped constrain their activation. The localization of galectin-3 to immune synapse was evident during the activation of naïve and memory $CD8^+$ T cells. Furthermore, galectin-3 knockout mice mounted a stronger MHV68-specific $CD8^+$ T cell response to the majority of viral epitopes examined. Such enhanced effector T cell responses in galectin-3 deficient animals led to better viral control. Targeting galectin-3 in $CD8^+$ T cells by strategies such as the use of small molecules or intrabodies to

disrupt its function may therefore serve to enhance their response to efficiently control infections.

Introduction

Timely induction of an adaptive immune response and the formation of effective immunological memory are essential for protective immunity against infectious disease (1). Appropriately activated $CD8^+$ T cells help control intracellular pathogens through recognition of peptides derived from pathogens in the context of class I MHC products. Induction of a $CD8^+$ T cell response requires the processing of three types of signal, delivered via peptide-MHC (p-MHC) complexes, co-stimulatory molecules and the prevailing cytokine milieu. Activated $CD8^+$ T cells expand to become effector cells that lyse their targets and so eliminate the intracellular pathogen (2). Several mechanisms then engage to regulate this response to limit possible damage caused by hyperactive immune cells (1).

Most pathogens establish an intricate relationship, manifested at many stages, with their host to ensure transmission, including invasion and the establishment of a productive infection. Barring few exceptions, pathogen-specific $CD8^+$ T cell responses are usually polyclonal in nature and recognize multiple epitopes specified by the invading pathogen (3). This applies in particular to complex pathogens such as poxviruses and herpesviruses (HV) in their natural hosts (4–7). Gamma-herpesviruses (γ-HV) are species-specific pathogens and therefore analysis of anti-γ-HV responses requires a natural host. Infection of mice with murine herpesvirus 68 (MHV68), is one of the most accessible model systems to study anti-γ-HV immunity and immunopathology (8–10). Various immune mediators induced in MHV68 infected mice display similarity to those induced during γ-HV infections in humans (11). Previously, we generated MHV68-specific $CD8^+$ T cell receptor transnuclear (TCR TN) mice by somatic cell nuclear transfer (SCNT) approach to investigate the contribution of

$CD8^+$ T cells to viral control (12). TCR TN mice use the physiological rearrangements of the endogenous antigen receptor loci. Therefore, $CD8^+$ TCR TN mice are likely to yield physiologically relevant primary T cell populations to investigate their responsiveness during infection (12, 13).

The efficiency with which T cells engage antigen-presenting cells (APCs) in an immunological synapse regulates their activation, differentiation as well as their functionality (14–17). The components of the immune synapse, such as the T cell receptor, co-receptors (CD3 with all its subunits), lineage differentiation surface glycoproteins such as CD4 and CD8, adhesion molecules and phosphatases (CD45), are extensively decorated with carbohydrates (18). Therefore carbohydrate-binding proteins (lectins) such as members of the galectin family may be critical in the formation, stabilization and disassembly of the immunological synapse. Galectins may also affect differentiation of T cells (19). Galectins bind to a variety of glycosylated proteins, expressed intracellularly or on the cell surface (20). Such interactions are either mediated by galectin glycan lattices or through specific receptor-ligand pairs (20). At least 15 different galectins have been identified and all have at least one conserved carbohydrate recognition domain (CRD), consisting of approximately 130 amino acids (21). Although galectins do not have classical secretory signals, some can nonetheless be released into extracellular space (22).

We performed RNA sequencing on MHV68-specific naïve and activated $CD8^+$ TCR TN T cells to gain insight into their function and phenotype. Activated TN cells isolated from virus-infected mice differentially expressed several thousand transcripts. We discovered several novel transcripts whose function remains to be fully defined in T cell biology. Among these, we found strong up regulation of galectin-3 in the virus-specific activated and expanded $CD8^+$ T cells in response to the MHV68 infection. We, therefore, investigated the role of galectin-3 in the activation of $CD8^+$ T cells during MHV68 infection,

as its contribution in anti-viral $CD8^+$ T cell immunity remains ill defined. Some studies have suggested a regulatory role of galectin-3 in $CD8^+$ T cell responses in autoimmune diseases and tumors (23, 24). In the tumor microenvironment, the extracellular galectin-3 interacted with effector molecule, IFN-γ owing to its extensive glycosylation and dampened its protective function against the developing tumor (24). We demonstrate that galectin-3 is recruited at the immunological synapse but predominantly acts intracellularly within $CD8^+$ T cells engaged to cognate peptide displayed by MHC I both during the primary and memory response. $CD8^+$ T cells lacking galectin-3 expanded more vigorously and produced enhanced cytokines as compared to WT $CD8^+$ T cells. Furthermore, galectin-3 knockout mice mounted a stronger virus-specific $CD8^+$ T cell response against most of the investigated epitopes and controlled virus better. Therefore, modulating the galectin-3 response pattern in $CD8^+$ T cells may serve as a strategy to enhance their function.

Methods

Mice, virus and cell lines used

Murine γ-herpesvirus (MHV68)-specific $CD8^+$ T cell transnuclear (TN) mice were generated and bred onto a C57BL/6 $Rag1^{-/-}$ background (12) TCR TN mice, C57BL/6 WT mice, OT1 TCR transgenic (tg) mice and galectin-3 knock out (KO) mice were bred and maintained at the AALAC-accredited animal facility of the Whitehead Institute for Biomedical Research, Cambridge, MA or at the Small Animal Facility for Experimentation at the Indian Institute of Science Education and Research Mohali. Age and gender-matched mice were used for experiments. All studies were carried out in accordance with procedures approved by the Massachusetts Institute of Technology Committee on Animal Care (CAC protocol # 1011-123-14) and Institute Animals Care and Use Committee (IACUC) of IISER Mohali. Whitehead Institute's Animal Welfare Assurance was approved and the approval number is

11/3/2009 (IACUC, A3125-01). Institutional Animal Ethics Committee (IAEC) of Indian Institute of Science Education and Research Mohali (IISER Mohali), constituted by the Committee for the Purpose of Control and Supervision of Experiments on Animals (CPCSEA) which is established under Chapter 4, Section 15(1) of the Prevention of Cruelty to Animals Act 1960. IAEC approved all the protocols and their numbers are; (IISERM/SAFE/PRT/2016/008, 009 and IISERM/SAFE/PRT/2017/011). All the experiments were performed strictly in accordance with the approved protocols. The cell lines (Vero cells, 3T12-3 and MDCK) were obtained from ATCC. All the viruses used were described earlier (25). The MHV-68, its recombinant version encoding for a SIINFEKL peptide (MHV68-M2 SIINFEKL) and influenza virus encoding SIINFEKL (WSN-SIINFEKL) were grown in 3T12-3 and MDCK cells respectively and stored at −80°C until further use.

Antibodies and Other Reagents

Fluorochrome-conjugated antibodies against mouse CD16/32, CD3a, CD8a, CD4, CD62L, CD69, CD44, B220, IFN-γ, CD11c, CD11b, CD45.1, CD45.2, PD1, KLRG1, TIM-3 and CCR7 were purchased from BD PharMingen. Anti-galectin-3 alexa fluor 647 and anti-galectin-3 PE antibody were obtained from eBioscience. Anti-Zap70-FITC was obtained from BD biolegend. A neutralizing anti-galectin-3 antibody (clone B2C10) was obtained from Thermofisher Scientific. Peptides were either synthesized in house at the Massachusetts Institute of Technology biopolymer facility or were obtained from GL Biochem. H-2K^b tetramers loaded with the indicated peptides were generated and used essentially as described (26). Tetramers carrying different peptides were generated by photochemical exchange of a conditional ligand (27). The peptide used for tetramer generation and intracellular cytokine staining (ICCS) assays include those derived from ORF9 (SVYGFTGV; H-2K^b restricted) and ORF75c (KSLTYYKL; H-2K^b restricted, SAIENYETF; H-2D^b restricted) for early

antigens and ORF6 (AGYIYYQL; H-2K^b restricted, AGPHNDMEI; H-2D^b restricted), ORF8 (KNYIFEEKL; H-2K^b restricted), ORF17 (SAITNHAAF; H-2D^b restricted) and ORF61 (p79) (TSINFVKI; H-2K^b restricted). For some experiments chicken ovalbumin-derived SIINFEKL peptide was used to probe OT1 or the endogenous cells.

Isolation of CD8$^+$ T cells

In order to isolate minimally manipulated CD8$^+$ T cells, negative selection kits from Miltenyi Biotec, Stem cell technology or Dynabeads™ Mouse CD8$^+$ T cells isolation kits were used. The purity of the CD8$^+$ T cells thus obtained was ascertained by flow cytometry. All procedures for cell separation were performed as per manufacturer's instructions. For some experiments cell sorting of fluorescent antibody-labelled cells was performed using a BD FACSAria™ II or BD FACSAria™ fusion instruments. The desired cell populations were obtained via a "dump" gate using antibodies against markers specific for cells other than CD8$^+$ T cells. For some experiments, antigen-specific CD8$^+$ T cells were isolated from infected mice using magnetic beads coated with class I MHC monomers.

Adoptive transfer of cells and virus infection

50x10^3 negatively separated MHV68-gB-ORF8-TCR TN CD8$^+$ T cells from H-2K^b - MHV68-gB-ORF8-TCR TN mice were adoptively transferred intravenously into CD45.1 congenic C57BL/6 or WT C57BL/6 mice one day before intra peritoneal infection with 5x10^5 pfu of MHV68. In some experiments, OT1 cells obtained from OT1 TCR tg mice were transferred in WT C57BL/6 mice, which were then infected with 5x10^5 pfu of MHV68 M2-SIINFEKL. In order to measure responses of endogenous memory CD8$^+$ T cells, an intranasal infection of 10 weeks old mice with WSN-SIINFEKL (5x10^2 pfu) was performed. The body weight was measured until 12 days post infection (dpi). Infected animals were euthanized using CO_2 asphyxiation at different dpi for further analyses. Single cell

suspensions obtained from lymphoid organs were analyzed for the number and phenotype of expanded cells. WT and Galectin-3 KO mice were infected with MHV68 by intraperitoneal or intranasal route. Lymphoid organs were analyzed to measure $CD8^+$ T cell responses. Lung tissues were collected to estimate viral loads.

RNA sequence analysis

FACS-purified naïve and MHV68 expanded K^b-ORF8-TCR TN $Rag1^{-/-}$ $CD8^+$ T cells were used for RNA isolation. The purity of sorted cells was verified by flow cytometry and was routinely > 99 percent. RNA was isolated from sorted cells using a kit from Qiagen. A Trueseq RNA sample Prep kit v2 from Illumina was used for RNA processing. 1µg of input total RNA was used and 18 cycles of PCR were performed and libraries were constructed. Paired end sequencing was performed. The sequence was mapped to mm9 using ELAND tool. Reads were counted in exons REFSEQ transcripts. Then, the count was normalized for reads per kb of mRNA per million (RPKM). For most analyses, transcripts below 5RPKM in paired samples were eliminated and genes that were selected had more than 1.5 fold or more than two-fold difference in any comparison as indicated in figure legends.

Network analysis for SDE genes in ORF8 TCR-TN mice infected with MHV-68

Using a cut off of 5 RPKM for any genes in either of the conditions and two fold differential expressions, we selected 1667 significantly differentially expressed (SDE) genes for network analysis. Network analysis was done using STRING (Search Tool for the Retrieval of Interacting Genes, https://string-db.org/) online tool. To filter out noise from the signals, we used stringent conditions. We obtained a protein-protein interaction (PPI) network that had an enrichment p value of less than 1.0^{-16}. Network with 498 SDE genes forming Nodes out of 1667 was obtained with STRING using default parameters. The STRING generated a .tsv file as an output that contained node1 (gene of our interest), node 2 (interacting partner). The

.tsv file (output from STRING) were opened in excel and analyzed for hub genes. Genes having more than five interacting partners yielded a total of 229 hub genes (Table 2.2). A gene was considered as a hub gene if it had more than 5 degree of centrality. The degree of centrality Cd(i) = deg(i) = |N(i)|, where deg (i) is the degree of node (i), and |N(i)| is the number of neighboring nodes to the node (i) (28). To further resolve the initially generated STRING network (that had genes which were not interacting), hub gene network was further made by STRING. Finally STRING network was generated to show Lgals genes as hub genes.

Phenotypic analysis of cells using flow cytometry

Spleen samples were extracted from different groups of animals and single cell suspensions were prepared. $1x10^6$ splenocytes were used for surface staining. Prior to the addition of specific antibody, cells were blocked with anti-Fc receptor antibody (CD16/32) for 20 min at 4°C. 1µg/ml of respective fluorochrome-labelled antibodies was added to the cell suspension and incubated for 30 minutes. After three rounds of washing with PBS-2%FCS, cells were analyzed by flow cytometry. To measure the relative expression of galectin-3 intracellularly and on the surface of activated cells, we performed surface staining as well as intracellular staining. Splenocytes from C57BL/6 mice were activated with anti-CD3 and anti-CD28 for 48 hrs at 37°C. After different time intervals, cells were stained with anti-galectin-3, anti-CD69 and anti-CD8. For intracellular cytokine staining (ICCS), $1x10^6$ of freshly isolated splenocytes or LN cells were cultured in 96-well round-bottomed plates in the presence of various concentrations of the indicated peptides and brefeldin A (5µg/ml) for 5 hr at 37°C in a humidified CO_2 incubator. At the end of the incubation period, cell surface staining, followed by ICCS was performed using a cytofix/cytoperm kit (BD Bioscience) as per manufacturer's instructions. Stained cells were analyzed by flow cytometry using a FACS

calibur (BD Bioscience) instrument and data was analyzed using FlowJo software (Tree star, OR). Cells were then analyzed by flow cytometry.

Immunofluorescence staining, confocal microscopy and co-localization analysis

To examine co-localization of galectin-3 with other molecules involved in immunological synapse formation during antigen-specific $CD8^+$ T cell activation, we performed confocal microscopy. SIINFEKL-specific endogenous or OT1 cells were activated by any of the following three approaches; class I MHC tetramer ($H\text{-}2K^b$ -SIINFEKL-tetramers-allophycocyanin)-coated coverslips, SIINFEKL-peptide pulsed BMDCs or magnetic beads coated with $H\text{-}2K^b$-SIINFEKL monomers. We investigated co-localization of galectin-3 with TCR marked by SIINFEKL peptide-loaded class I MHC tetramer ($H\text{-}2K^b$ -SIINFEKL-tetramer-allophycocyanin) and Zap70, a TCR-CD3 ζ-chain associated protein kinase involved in the initial stages of TCR signaling. Confocal laser scanning microscope from Olympus (FV10i-LIV / FV10i-DOC) that has a speed of 1.1 fps having 256 x 256 - 1024 × 1024 pixel resolution and FV10i-DOC: NA 0.4 /NA 1.35 objective was used for acquiring images. Fiji software was used for analyzing the images. This software was used to calculate the Pearson's correlation coefficient (PCC) for co-localization of the probes used as described elsewhere (29). To ascertain whether or not galectin-3 produced by $CD8^+$ T cells act intracellularly or extracellularly to control their activation, we performed neutralization experiments using α-lactose. α-lactose compete with galectins for their binding to carbohydrates and blocks the interaction (30). SIINFEKL peptide pulsed BMDCs were co-cultured with OT 1 cells in the presence of absence of 100 mM of α-lactose solution and the extent of localization of galectin-3 towards immune synapse was measured. Atleast 35 cells were counted for each group for calculating co-localization percentages for different molecules. Different methods of activation of $CD8^+$ T cells for confocal imaging are described in subsequent sections. To measure whether or not α-lactose indeed works we

measured the response of $CD8^+$ T cells in separate experiments. $CD8^+$ T cells were purified from lymph nodes of C57BL/6 mice and incubated with similar dose of α-lactose for 1 hour at 37°C. The cells were then washed three times with PBS and stimulated with anti-CD3 (coated) and anti-CD28 (soluble) for 12 hrs at 37°C. After activation, the cells were washed and stained with anti-CD69 and CD8 antibodies.

Activation of $CD8^+$ T cells with MHC I tetramers

Class I MHC ($H\text{-}2K^b$) SIINFEKL tetramer (allophycocyanin dye-conjugated) was coated on poly-lysine (Sigma Aldrich)-treated coverslips overnight at 4°C. The next day, coverslips were washed with sterile PBS and complete RPMI. SIINFEKL specific sorted $CD8^+$ T cells were added to these coverslips and incubated for different time intervals. Control cells were immobilized on poly-lysine treated coverslips in the absence of Class I MHC ($H\text{-}2K^b$) SIINFEKL tetramers. After incubation, cells were washed gently with PBS and were fixed and permeabilized using buffers from eBioscience (Intracellular fixation buffer and intracellular permeabilization buffer). This was followed by blockade with 5% FBS in permeabilization buffer. Cells were stained with mouse anti-galectin-3 (Thermofisher) and rabbit anti-Zap70 (Cell Signaling Technology) for 2 hrs at room temperature. After washing, cells were stained for 30 minutes with anti-mouse alexa fluor 568 (Thermofisher) and anti-rabbit alexa fluor 488 (Thermofisher). Thereafter cells were washed and mounted with fluoromount (Sigma Aldrich).

Activation of $CD8^+$ T cells with peptide pulsed APCs

APCs were generated from the bone marrow of C57BL/6 mice, using IL-4 and GM-CSF as described (25). $1x10^5$ APCs were placed on poly-lysine-treated coverslips and pulsed with SIINFEKL peptide (1μg/ml) for 2 hrs at 37°C. $4x10^5$ purified OT1 $CD8^+$ T were co-cultured with peptide-pulsed BMDCs for up to an hr. Cells were then stained as described in the previous section and analyzed by confocal microscopy.

In vivo activated cells analysis by immunofluorescence microscopy

$5x10^4$ or $1x10^5$ purified $CD8^+$ T cells from OT1 mice were adoptively transferred into gender-matched C57BL/6 mice. Subsequently, mice were infected intranasaly with $2x10^5$ pfu of MHV68-M2-SIINFEKL virus. At 6 or 55 dpi, mediastinal lymph nodes were collected and a single cell suspension was prepared. Cells were stained with class I MHC tetramer and were sorted by FACS. For some experiments, animals were infected with WSN-SIINFEKL and H-$2K^b$-SIINFEKL-specific $CD8^+$ T cells were isolated at 6 or 40 dpi using magnetic beads coated with SIINFEKL-class I MHC monomers. Briefly, one mg of M-270 streptavidin magnetic Dynabeads (Invitrogen) were incubated with 10 μg of biotinylated H-$2K^b$ monomers that were generated using UV cleavable peptide for two hours at 4°C with gentle shaking (5 rpm). After incubation, one ml of cold PBS was added gently and the beads were magnetically separated. The washing of monomers coated beads was repeated three times. Subsequently, the photocleavable ligand was exchanged with SIINFEKL peptide by UV exposure at 365nm for 60 min and three washings were performed subsequently to remove of any aggregated proteins. The H-$2K^b$-SIINFEKL coated beads thus prepared were mixed with $10x10^6$ lymphocytes obtained from the single cell suspension of spleens and mediastinal LN of virus infected mice. Beads and cells were incubated at 4°C for 90 min with gentle shaking (5rpm). Three times washing was performed with cold PBS using magnetic separation apparatus. The complex of beads and specific cells were added on polylysine-coated coverslips for 10 minutes at 37°C. Specific cells bound with beads were stained for galectin-3, Zap70 and DAPI for their subsequent analysis by confocal microscopy. The efficiency of sorting was ascertained cytofluorimetrically.

Generation of BMDCs

Bone marrow cells were isolated from the long bones of C57BL/6 mice. Cells were cultured with IL-4 (10ng/ml) and GM-CSF (10ng/ml) for four days in a humidified CO_2 incubator at 37°C. After differentiation, cells were analyzed by flow cytometry using anti-CD11b, CD11c and Class II MHC antibodies. More than 70 percent of cells were differentiated into DCs, as judged by expression of CD11c and activation associated molecules such as CD80, CD86 and Class II MHC.

Proliferation of cells

MACS-purified $CD8^+$ T cells from galectin-3 KO and WT animals were labelled with CFSE using protocols described elsewhere (12). Labelled cells were stimulated with plate-bound anti-CD3 (1μg/ml) and soluble anti-CD28 (1μg/ml) for varying times. Cells were then collected, washed and stained on ice with the indicated fluorochrome-labelled antibodies. After multiple rounds of washing with FACS buffer, cells were analyzed by flow cytometry. Culture supernatants were collected to measure secreted cytokines. To assess the influence of extracellular galectin-3 on the proliferation of $CD8^+$ T cells, $10x10^6$ OT1 cells were labelled with 2.5μM CFSE and $2x10^5$ of labelled cells were stimulated with plate bound anti-CD3 (1μg/ml) and soluble anti-CD28 (1μg/ml) antibodies in the presence or absence of anti-galectin-3 neutralizing antibody (10μg/ml). Cells were incubated at 37°C and CFSE dilution was measured at different time points.

ELISA for cytokine measurement

Culture supernatants were collected from stimulated cells, supplemented with a protease inhibitor cocktail (Roche Diagnostics) and stored at -20°C until use. The levels of IL-2 in the culture supernatants were measured by sandwich ELISA using the OptEIA kit for mouse IL-2 (BD Bioscience).

Extraction of lung tissue for virus titration

Lung tissues were collected from WT and Galectin-3 KO mice infected intranasaly with $5x10^5$ pfu of MHV-68 and euthanized by CO_2 asphyxiation six days post-infection. Blood vessels just above the liver were cut and mice were perfused with 10-15 ml of sterile PBµS by inserting a 25G needle into the right ventricle of the exposed heart. Lung tissues were weighed and frozen until use. Prior to titration of virus on 3T12-3 cells, lung tissues were thawed and homogenized with 500µl of DMEM without serum.

Statistical analysis

Student's "t" test and ANOVA tests were applied for statistical analysis to compare responses between groups, as indicated in the figure legends. The results are presented as mean ± SD. The p values are shown in the figures or figure legends and are represented as $^{*}p \leq 0.05$, $^{**}p \leq 0.01$, or $^{***}p \leq 0.001$.

Results

Phenotype of naïve and MHV68-stimulated TCR TN CD8$^+$ T cells

We compared the transcriptome of activated MHV68-specific ORF8 TCR TN CD8$^+$ T cells (12) with their naïve counterparts to gain insight into their function and phenotype. Both naïve and activated CD8$^+$ T cells were obtained from genetically comparable TCR TN mice (see schematic, Fig no. 2.1A). TN CD8$^+$ T cells expanded massively in response to MHV68 infection in congenic (CD45.1) mice that received 50x10^3 ORF TN cells prior to infection. At 6 days post infection, 35 to 40 percent of total CD8$^+$ T cells in spleens of infected mice were comprised of donor ORF8 TCR TN cells. Cells that responded to viral infection showed increased surface display of the activation markers such as CD44 and programmed cell death protein 1 (PD1) (Fig no. 2.1B), demonstrating a fresh recruitment of these cells in the course of the infection. Most of these cells produced IFN-γ in ICCS assays (12). We FACS-sorted activated ORF8 TCR TN CD8$^+$ T cells for further analysis as shown in Figure 2.1.

A

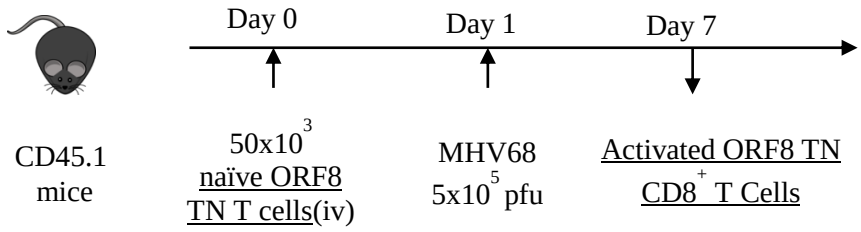

B

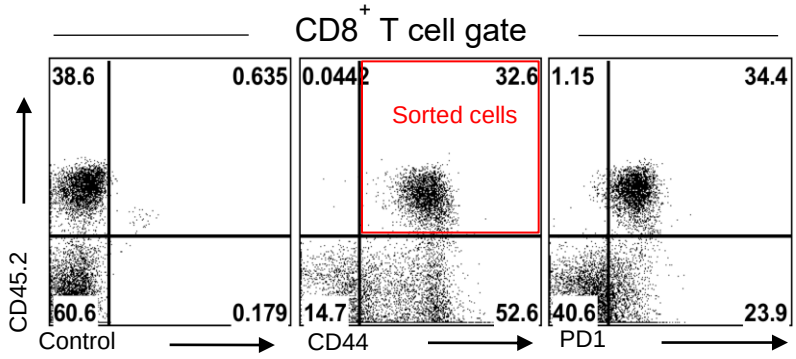

Figure no. 2.1. Phenotypic analysis of naïve and MHV68 expanded ORF8 TCR TN CD8$^+$ T cells. A. Schematic of the experiment. 50x10^3 Rag1$^{-/-}$ K^b-ORF8 TCR TN CD8$^+$ T cells were adoptively transferred in CD45.1 congenic C57BL/6 mice and recipients were infected with 5x10^5 pfu of MHV68 ip. On 6dpi, spleens were isolated and single cell suspensions were analyzed flow cytometrically using a panel of indicated cell surface markers. B. Representative FACS plots showing the phenotypic markers expressed by CD45.2 positive cell (Rag1$^{-/-}$ K^b-ORF8 TCR TN CD8$^+$ T cells) activated and expanded in response to viral infection.

RNAseq data and assessment of its quality

FACS-purified naïve cells and activated CD8$^+$T cells were processed for RNA isolation. Libraries were constructed and subjected to paired-end sequencing. Approximately one million reads of excellent quality for each sample were obtained. A high fraction of uniquely mapping reads having a minimal amount of ribosomal RNA sequences were obtained. Further analysis of RNAseq data showed a high percentage of junction reads, good exon/intron as well as exon/intergenic ratios and minimal 3'/5' bias in sequence coverage (Fig no. 2.2A). Some genes as exemplified by β_2m, Class I MHC, Tap1- did not change expression between naïve and activated TN cells and served as a point of reference with which to compare the observed changes (Fig no. 2.2B). Normalized RPKM and a $\log_2$ fold change of different genes from naïve and activated TN cells are shown in Table S1 (31) and in a scatter plot (Fig no. 2.2C). Ensembl entries (n = 11689) also present in our RNAseq data with more than 5 reads in either samples are shown in a scatter plot (Fig no. 2.2C). The extent of differential expression of a large majority of genes in activated as compared to naïve ORF8 TCR TN CD8$^+$ T cells was up to less than two-folds (Fig no. 2.2D). Top hits that were differentially expressed in TN cells are discussed in the following sections.

A

	Naïve	Day 6
Uniqper10M	0.62	0.59
Total	98405474	107360448
Uniq. Mapping	74296323	82907794
%Uniq. Mapping	75.5	77.22
Ribo. Mapping	47650	986561
%Ribo	0.64	1.19
Spice junctions	7411715	10282808
% Junctions	9.98	12.4
Exon/Introns	80.72	198.8
Exon/Intergenic	1859.99	4125.19
Log2(m(3'/5'))	0.38	0.31
Log2(m(3'/CDS))	-0.21	-0.25
Log2(m(CDS/5'))	0.59	0.55
sd(3'/5')	1.43	1.53
sd(3'/CDS)	0.97	1.1
sd(CDS/5')	1.33	1.45
Insert size mean (bp)	173.6	179
Insert size stdv (bp)	67.1	60.3

B

Gene	Naïve RPKM	D6 RPKM	Day6/ Naïve
Tap1	153	147	1.041
ß2m	2362	1743	1.3
H2(D1)	156	169	0.98

C

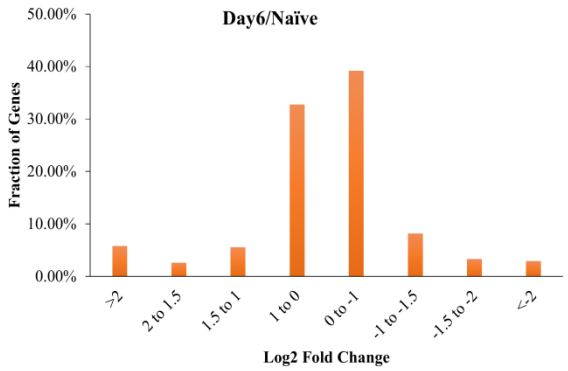

D

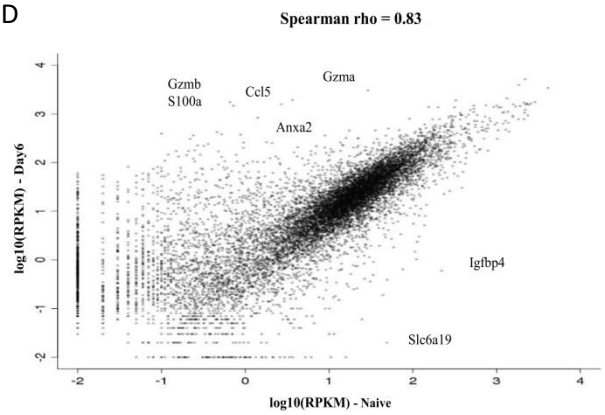

Figure no. 2.2 Sorted CD45.2^{+} CD44^{hi} cells that were expanded due to MHV68 infection and their naïve counterparts were used for RNA sequencing. A. Key attributes for analyzing the quality of RNA seq data. B. The number of reads (RPKM) recorded for some of the control genes. RPKM (Reads per kilobase per million mapped reads) = total exon reads/mapped reads (million) x exon length (Kbp) C. Bar diagram show the extent by which the fraction of genes are differentially expressed. D. Scatter plot shows the differential expression of transcripts in naïve and 6 dpi activated TN CD8^{+} T cells.

Analysis of transcriptome of naïve and activated TCR TN CD8$^+$ T cells

Our initial analyses involved the number of reads for the α (TRAV10N801, TRAJ33*01) and β chains (TRBV31*01, D1*01 and TRBJ2-2*01) of the specific TCR used by ORF8 TCR TN CD8$^+$ T cells (12). We found a high degree of sequence coverage across the expected TCR α and β chains (Fig no. 2.3A). As TCR expression is down regulated in stimulated T cells in the acute phase of response, fewer reads were obtained for the TCR chains in activated CD8$^+$ T cells (Fig no. 2.3A).

Of the several thousand transcripts differentially expressed in activated TN CD8$^+$ T cells, many have not been reported to exhibit a similar expression pattern Table S1(31). We also compared our RNAseq data with the transcriptome of two of the commonly used CD8$^+$ TCR transgenic (tg) mice (OT1 and P14) as these mice have provided excellent insights into the differentiation pathways of antigen-specific CD8$^+$ T cells (32, 33). The comparison revealed that more transcripts were differentially expressed in TCR TN CD8$^+$ T cells (Fig no. 2.3B and C, Table S1 (31). The varying TCR affinities of TN T cells as compared to the tg cells, the usage of endogenous TCR loci for receptor assembly by TN cells as compared to other tg cells, the influence of microenvironment generated during respective infection may all contribute to the observed differences. Varying affinity of peptide recognition by TCRs of TN and tg cells was shown by tetramer dissociation assays in an earlier work (12). The possible contribution of differences in microenvironment and co-stimulatory molecules, as are expected to occur in a natural γ-herpesvirus infection, versus antigen delivery by other means, was not investigated further. Multiple transcripts were clustered in different pathways such as cell cycle progression, apoptosis signaling, DNA replication, hypoxia response via hypoxia inducing factors, oxidative stress response, T cell activation, the ubiquitin-proteasome pathway and the p53 pathway (Fig no. 2.3D). A compilation of different

biological processes represented by differentially expressed transcripts in ORF8 TN cells is shown in Tables S2 and S3 (31).

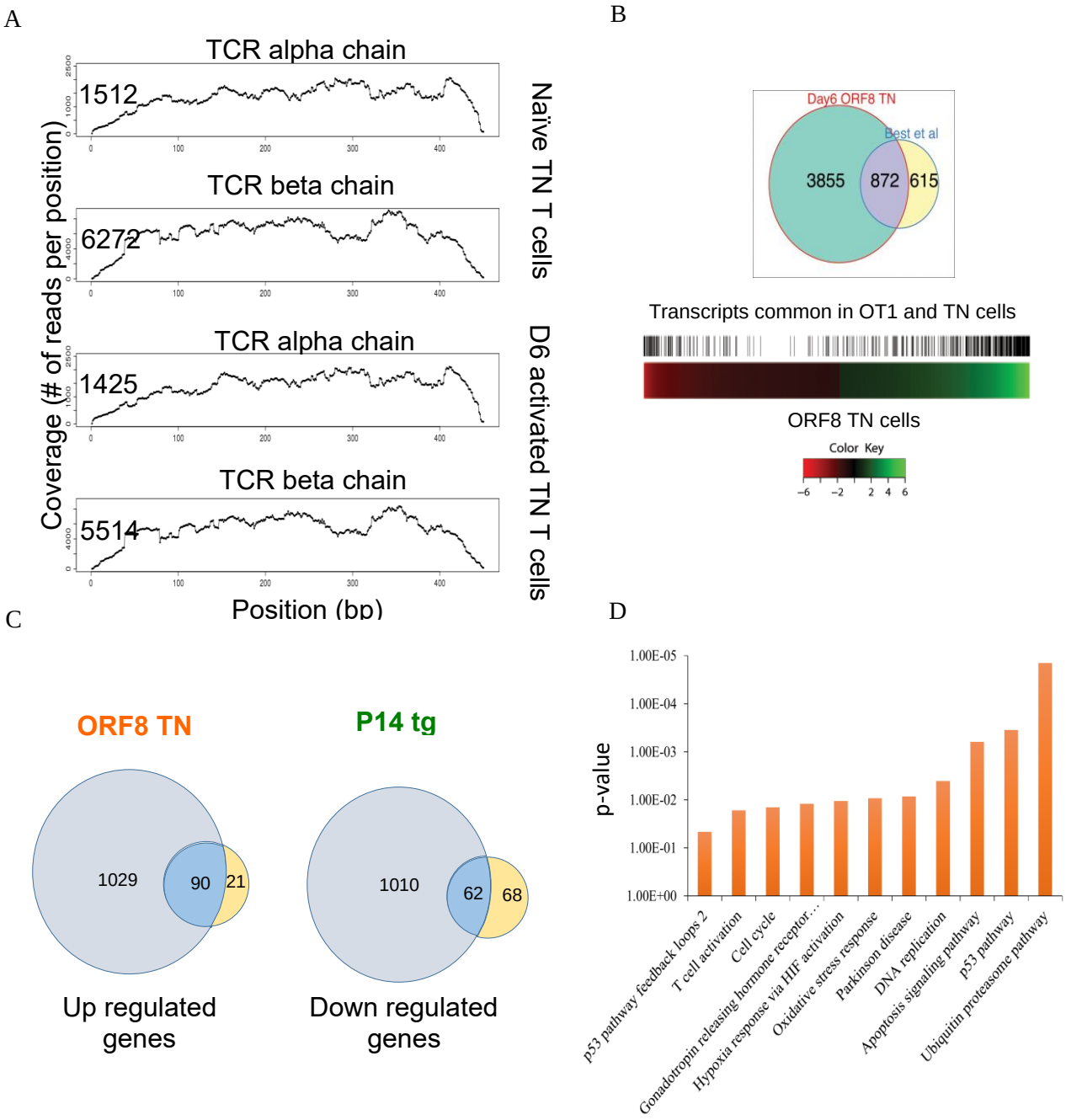

Figure no. 2.3. **Transcriptomic analysis of naïve and activated ORF8 TCR TN CD8$^+$ T cells.** A. Intensity of the reads recovered from RNAseq data present in the rearranged VDJ and VJ of β- and α-chains of TCR in naïve and activated H-2K^b-ORF8 TCR TN CD8$^+$ T cells. B. A comparison of transcriptome of TN cells CD8$^+$ T cells, tg OT1 cells and tg P14

$CD8^+$ T cells that were activated by γ-Herpesvirus, Listeria monocytogenes and Lymphocytic choriomeningitis virus (LCMV) Armstrong infection respectively. Upper panel; Venn diagram shows the comparisons of transcriptome of OT1 cells and ORF8 TCR TN $CD8^+$ T cells that were differentially expressed atleast 1.5 fold in both the cell types. Lower panel; Heat map of 1.5 fold differentially expressed transcripts in ORF8 TCR TN $CD8^+$ T cells (lower heat map) and those that are common in OT1 cells and ORF8 TN cells (upper heat map). C. A comparison of differential transcriptome of ORF8 TN cells and P14 tg cells in the acute phase of a MHV68 and LCMV infection. Pi chart shows the numbers of genes up or down regulated by two fold in the respective cell types, D. Gene ontology panther pathway analysis of differentially expressed transcripts in ORF8 TCR TN $CD8^+$ T cells for the biological processes represented.

Gene ontology (GO) panther pathway analysis

Genes encoding different classes of proteins that were differentially expressed by activated TN cells included nucleic acid binding proteins, G-protein coupled receptors, ribosomal proteins, transcription factors, ligand-gated ion channels, signaling molecules and adaptors, chaperones, growth factors, cell adhesion molecules, cytoskeletal proteins, splicing factors,

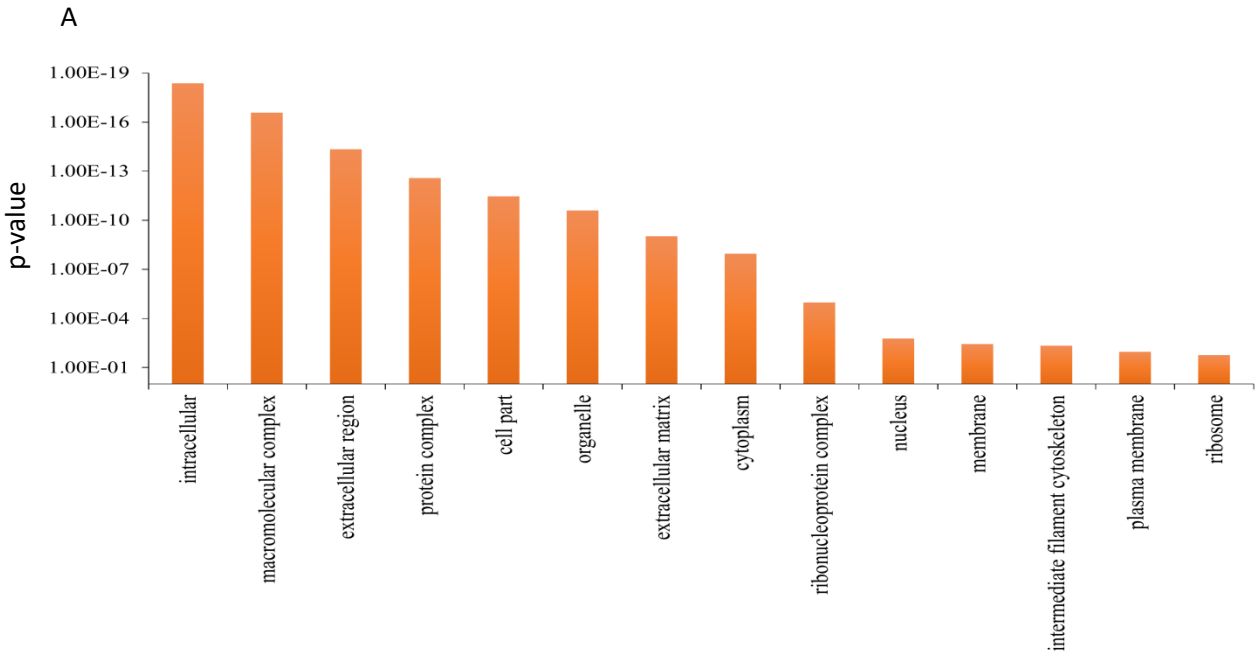

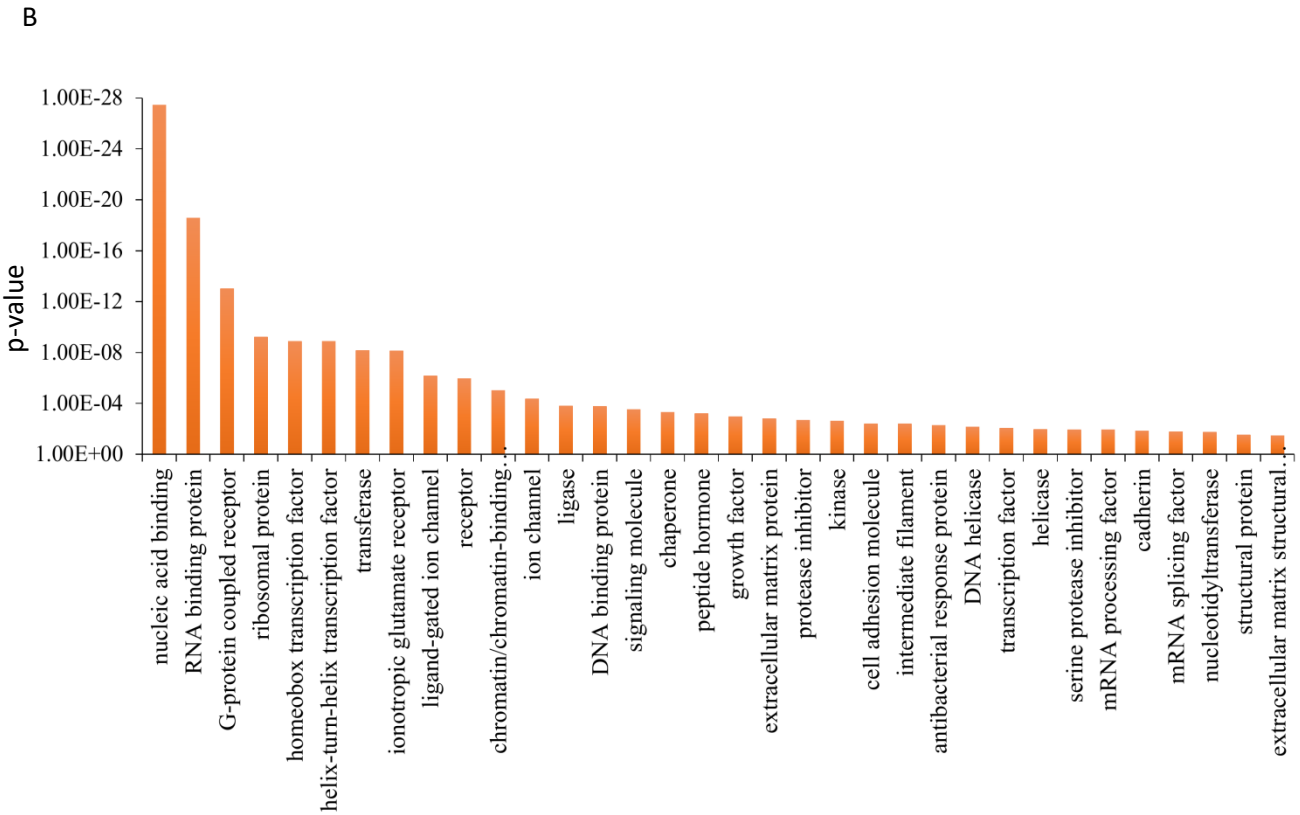

Figure no. 2.4. Gene ontology (GO) panther pathway analysis of differentially expressed transcripts in activated and naïve ORF8 TCR TN CD8$^+$ T cells. A. Bar diagram depicts the p-values of transcripts represented for cellular compartment. B. Bar diagram depicts the p-values of transcripts represented for the class of proteins.

extracellular matrix as well as structural proteins (Fig no. 2.4A and B).

Our RNAseq data showed that transcripts for many genes were differentially expressed in activated TN cells associated with the effector functions of CD8$^+$ T cells (Fig no. 2.4A and Table S1 (31)). We validated altered expression of some of the genes differentially expressed in activated TN cells by cytofluorimetry and these include CD62L, TIM-3, PD1, CD44, CCR7, galectin-3, IFN-γ at the protein product level (Fig no. 2.1B, Fig no. 2.5A&B) (12).

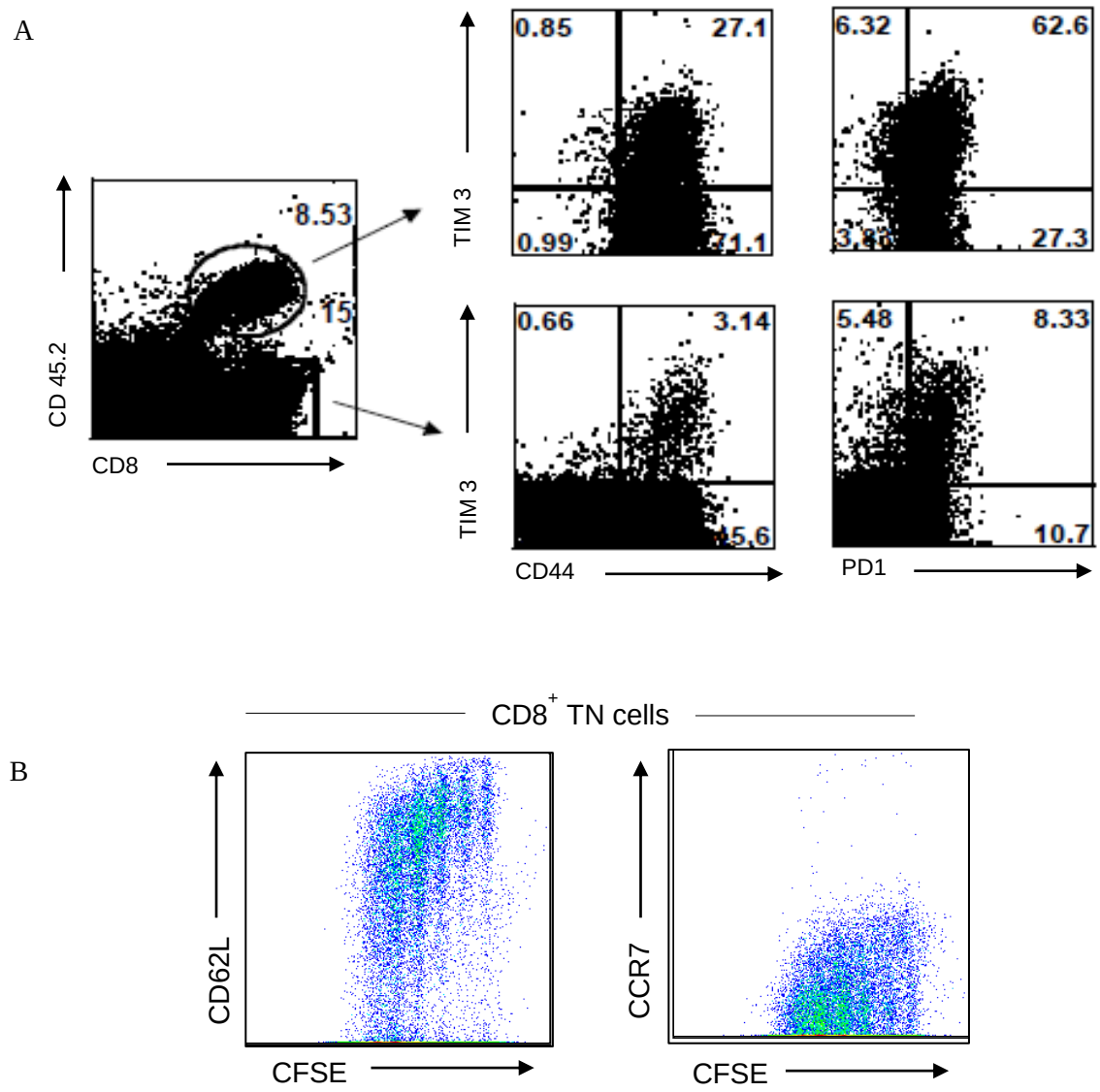

Figure no. 2.5. Analyzing the expression of some of the genes at protein level in activated TN cells as compared to naïve TN cells. A. Representative FACS plots show the expression of TIM-3 and PD1 by donor and endogenous $CD8^+$ T cells. For each experiment at least four animals were included and experiments were repeated two times with similar results. B. CFSE labelled ORF8 TN T cells were stimulated with BMDCs pulsed with the cognate KNYIFEEKL peptide for three days. Representative FACS plots show the expression of CD62L and CCR7 in dividing TCR TN $CD8^+$ T cells. Representative FACS plots are shown.

Expression profile of MHV68 specific $CD8^+$ T cells upon virus infection

$CD8^+$ T cells exponentially expand during the acute phase of infection and acquire a differentiation program that helps them migrate to the site(s) of infection to control infection (34). Several genes differentially expressed by activated ORF8 TN cells represent such events (Table S1 (31)). In brief, transcripts for genes that encode for proinflammatory cytokines such as IFN-γ (up by 40 fold), granzymes B, A and K (up by 300 to 900 fold); chemokine receptors such as CCR5 (up by 77 fold) and the chemokine RANTES (up by 300 fold) were highly up regulated in activated TN T cells as compared to their naïve counterparts. Annexin II, a vesicular protein that facilitates extracellular transport of other proteins was highly expressed (up by 250 fold) in activated TN cells, suggesting its critical role in effector functions of $CD8^+$ T cells. Similarly, transcription factors that promote cellular proliferation and help produce several effector molecules were highly up regulated in expanded TN T cells. Some examples include Tbet (up by 93 fold), Zbtb32 (up by 67 fold), polycomb-group repressive complex 1 (up by 40 fold) and E2f2 (up by 35 fold). Other genes that are associated with activation and fate determination of $CD8^+$ T cells such as *klrc1* (up by 54-fold), *lag3* (up by 48-fold), *klrg1* (up by 30-fold), *havrc2* (TIM-3: up by 30-fold), *pdcd1* (PD1: up by 26-fold), *ctla4* (CTLA-4: up by 17-fold) were also significantly up regulated in TN cells. As genes responsible for encoding Ca^{++}-binding proteins such as those of S100 family (*s100a6, s100a4, s100a9, s100a10, s100a8*) were up regulated up to 100-fold by activated TN $CD8^+$ T cells. Most of these proteins are involved in differentiation and cell cycle progression and are known to modulate tubulin polymerization (35). Genes encoding galectin-1 (*lgals1*: up by 87-fold) and galectin-3 (*lgals3*: up by 140-fold) were among the highly up regulated genes in activated TN T cells. In this study we decided to investigate the role of galectin-3 in anti γ-herpes virus $CD8^+$ T cell immunity, as will be described below. Numerous genes were down regulated in virus-reactive activated ORF8 TN T cells compared

to naïve TN cells (Table S1 (31)). The extent of down regulation was more than 40-fold for five genes, between 20- to 40-fold for six genes, between 10- to 20-fold for approximately 40 genes, between 5-10 fold for more than 100 genes and up to two fold for several thousand genes (Fig no. 2.6A & B and Table S1 (31)).

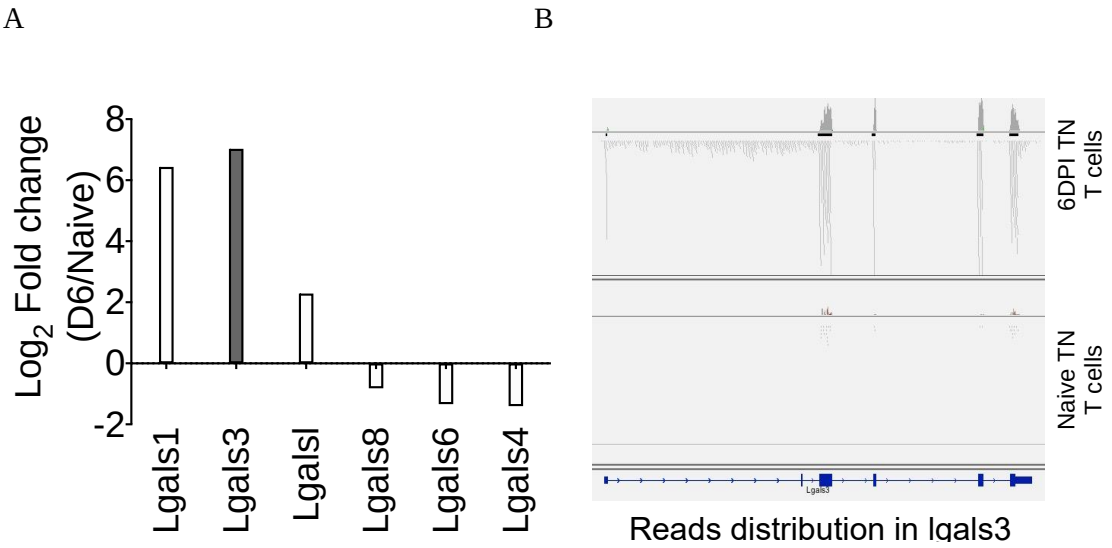

Figure no. 2.6. CD8$^+$ T cells up-regulate galectin-3 expression upon TCR and co-receptor ligation. A. Bar diagram shows a fold change in the expression of transcripts for different galectins in naïve and activated TCR TN CD8$^+$ T cells as a result of MHV68 infection as analyzed from RNAseq data. B. IgV snapshots to show the frequency of reads encompassing the exons (filled rectangles on the bottom line) vs intron (line without rectangles) of galectin-3 gene (Lgals3) in activated ORF8 TN CD8$^+$ T cells (6dpi) and their naïve counter parts.

One of the most down-regulated genes in activated TN cells was *igfbp4* (down by 131-fold), which encodes insulin-like growth factor-binding protein 4. This molecule is involved in differentiation of helper cells such as Th1, Th17 and regulatory T cells (36). Whether or not this molecule plays a role in differentiation of CD8$^+$ T cells has not been investigated. Genes that encode for transporters of amino acids (*slc6a19;* down 42-

fold, *slc6a5;* down 37-fold, *slc2a7*; down 11-fold) were highly down regulated in activated TN T cells compared to ion transporters (*slc4a1, slc7a1*), urea (*slc14a1*), and carbohydrates (*slc35b3*). This suggests that during the acute phase of a $CD8^+$ T cell response, fate and function are greatly influenced by transport and metabolism of amino acids or by redox potential (37, 38). The gene for the actin regulator, FAM101B was also down regulated in activated TN cells. FAM101B localizes to the perinuclear space and helps stabilize perinuclear actin filament bundles (39). Its function in $CD8^+$ T cell differentiation remains to be investigated. A gene, *st6gal1* which encodes ST6 β–galactoside α-2,6-sialyltransferase, was down regulated by 22-fold in activated TN cells which might suggest a differential modification, particularly the capping of molecules such as CD45 with α-2,6 sialic acid during development of T cells in the thymus as compared to their glycosylation profile during their herpesvirus induced activation in the periphery (40). Many such issues remain less well studied. The glycosylation status of different proteins in $CD4^+$ T cells is known to control their differentiation program, but studies investigating its role in $CD8^+$ T cell differentiation are limited (41). IL-7R (*il7r* : down by 25 fold) specifically marks precursors of memory $CD8^+$ T cells during the acute phase of infection (42). Similar to its expression pattern, genes for other molecules such as GPR114 (*gpr114* : down by 17-fold), IFN-γR2 (*ifngr2* : down by 16-fold), vasoactive intestinal peptide receptor 1 (*Vipr1* : down by 15-fold), interferon-inducible members of the *schlafen* family ; *slfn5* (down by 15 fold), adhesion molecule with Ig-like domain 2 ; *amigo2* (down by 14-fold), TNF receptor superfamily member 25 ; *tnfrsf25* (down by 14 fold) were among those down regulated in activated TN $CD8^+$ T cells. Many of these molecules have been implicated in T cell differentiation but the role of others remains to be explored (43, 44).

Apart from the genes described in this section, several thousand differentially expressed genes are listed in table 2.1and S1 (31).

Table 2.1. A list on unmapped genes using Gene Ontology analysis

0610007P14Rik	1810043G02Rik	4632434I11Rik	AI467606	BC094916	D14Abb1e	Gm9846	Mll5	Phf17	Wdr20a	Zfp526
0610009D07Rik	2010012O05Rik	4833420G17Rik	AI597468	Beta-s	D4Wsu53e	Gpi1	Mnf1	Pion	Wdr67	Zfp579
0610010F05Rik	2010015L04Rik	4930422G04Rik	AI837181	Bloc1s2a	D5Ertd579e	Grlf1	Mrp63	Rab1	Wdr85	Zfp580
0610010K14Rik	2010107E04Rik	4930427A07Rik	AI846148	Bmyc	D8Ertd82e	Gtpbp5	Nrp	Rnaset2a	Zfp110	Zfp592
0610030E20Rik	2010111I01Rik	4930432K21Rik	AK010878	C030006K11Rik	Ddx39	Gyg	Nt5c3l	Rnaset2b	Zfp12	Zfp652
0610037L13Rik	2210016L21Rik	4930444A02Rik	Akr1b3	C030046E11Rik	Dnahc8	Gyk	Nup62-il4i1	Rpl34-ps1	Zfp146	Zfp653
1110004F10Rik	2210404J11Rik	4930453N24Rik	Akr1e1	C230052I12Rik	Dnalc4	H2-Ke2	Pagr1a	Rpl36al	Zfp182	Zfp661
1110008F13Rik	2210404O07Rik	4930486L24Rik	Anks1	C330006A16Rik	Dnase2a	H2-Ke6	Pcdhga1	Rps3a1	Zfp207	Zfp664
1110008J03Rik	2300009A05Rik	4930503L19Rik	Atad3a	C330027C09Rik	E130309D02Rik	H2-T9	Pcdhga10	Serpinb6a	Zfp260	Zfp672
1110008P14Rik	2310011J03Rik	4930579G24Rik	Atp5k	C87436	E130311K13Rik	H3f3b	Pcdhga11	Sfrs18	Zfp276	Zfp687
1110034G24Rik	2310022B05Rik	4932438A13Rik	Atpbd4	C920025E04Rik	E330009J07Rik	Hba-a1	Pcdhga12	Solh	Zfp280c	Zfp692
1110059E24Rik	2310035C23Rik	4933434E20Rik	AU022252	Calm2	E430025E21Rik	Hba-a2	Pcdhga2	Spata5l1	Zfp280d	Zfp71-rs1
1190002N15Rik	2310039H08Rik	5730508B09Rik	AW549877	Calm3	Eef1b2	Hist1h4c	Pcdhga3	Spin2	Zfp281	Zfp710
1190007I07Rik	2310042D19Rik	5830415F09Rik	AW554918	Car12	Efha2	Hist1h4i	Pcdhga5	Stx4a	Zfp287	Zfp74
1300018J18Rik	2410066E13Rik	6030458C11Rik	B630005N14Rik	Car15	Eif2c1	Hmga1-rs1	Pcdhga6	Stxbp3a	Zfp318	Zfp740
1500009L16Rik	2410131K14Rik	6330403M23Rik	B930041F14Rik	Car2	Eif2c2	Hnrpll	Pcdhga7	Supt16	Zfp329	Zfp770
1500032L24Rik	2510002D24Rik	6330416G13Rik	Baat1	Car5b	Eif2c3	Hras1	Pcdhga8	Supt20	Zfp335	Zfp771
1600002H07Rik	2610019F03Rik	8430410A17Rik	BC003965	Ccdc90a	Fam108c	Jhdm1d	Pcdhga9	Supt4a	Zfp354c	Zfp784
1600014C10Rik	2610301B20Rik	9030617O03Rik	BC004004	Cd24a	Fam86	Klhdc5	Pcdhgb1	Sypl	Zfp365	Zfp821
1700017B05Rik	2700029M09Rik	9430023L20Rik	BC016423	Cenpc1	Fam92a	Klra12	Pcdhgb2	Tgtp2	Zfp367	Zfp827
1700020L24Rik	2700060E02Rik	9930012K11Rik	BC029214	Chmp1b	Fasl	Klra23	Pcdhgb4	Tmem170	Zfp369	Zfp85-rs1
1700025G04Rik	2700094K13Rik	9930104L06Rik	BC030336	Cldn25	Fem1a	Lrdd	Pcdhgb5	Tmem48	Zfp382	Zfp865
1700037H04Rik	2810403A07Rik	A130010J15Rik	BC030867	Cnih	Fh1	Lrrc33	Pcdhgb7	Tmem8	Zfp422	Zfp932
1700066M21Rik	2810417H13Rik	A230046K03Rik	BC037034	Csda	Gbp3	Lsmd1	Pcdhgb8	Tmsb15b2	Zfp445	Zkscan14
1700088E04Rik	3010026O09Rik	A230050P20Rik	BC048403	Ctps	Gm13826	Man1a	Pcdhgc3	Trp53	Zfp451	Zkscan6
1700094D03Rik	3110057O12Rik	A430005L14Rik	BC049715	Cxx1b	Gm20604	Mettl21d	Pcdhgc4	Trp53bp2	Zfp507	Znrd1as
1810013L24Rik	3230401D17Rik	A730008H23Rik	BC052040	Cyp4v3	Gm5506	Mll1	Pcdhgc5	Trp53i13	Zfp513	
1810022K09Rik	4632415K11Rik	AA414768	BC055324	Cyp51	Gm5918	Mll2	Pgm1	Txn1	Zfp518a	
1810037I17Rik	4632428N05Rik	AB124611	BC056474	D030056L22Rik	Gm6251	Mll3	Phf15	Ube2cbp	Zfp523	

Table 2.2. Hub genes and their numbers of interactions(Cut off ≥ 5 interactions)

Genes	Interaction	Genes	Interaction	Genes	Interaction	Genes	Interaction
Mcm5	141	Cdkn3	55	Rfc4	27	Cdc25b	11
Prc1	136	Ckap2	55	Kif15	26	Fanca	11
Mad2l1	129	Ccne1	54	Tyms	26	Zbtb32	11
Kif20a	125	Fzr1	54	Racgap1	26	Ube2s	11
Rad51ap1	119	Ercc6l	54	Rad51c	26	Tpi1	11
Top2a	118	Fignl1	54	Tuba1b	25	Pak6	11
Smc2	117	Kif22	53	Nasp	24	Bard1	10
Zwilch	116	Kntc1	52	Dscc1	24	Plcg2	10
Cenpf	114	Rpa2	52	Fancd2	23	Cd24a	10
Kifc1	111	Rfc3	51	Tubb3	23	**Lgals3**	**10**
Cdca8	109	Gins2	51	Myo5a	22	Il10ra	10
Ect2	107	Kif23	51	Pbk	21	Hsp90aa1	9
Lig1	105	Tipin	51	Tuba1c	21	Cit	9
Cep55	103	Ccne1	51	Wee1	20	Ly6c2	9
Birc5	102	Anln	50	E2f2	20	Il2ra	9
Kif20b	101	Ccna2	50	Tubb4b	20	Cdkn2c	9
D2Ertd750e	101	Bub1	50	Pmf1	20	H2-Aa	8
Ube2c	100	Ezh2	50	H2-Ab1	20	Fbxo5	8
Ttk	98	Gen1	49	Cdca3	20	Kif11	8
Cdca2	97	H2afx	48	Polq	20	S1pr5	8
Rfc5	92	Rrm1	48	Shcbp1	20	Tnfrsf13c	8
Tacc3	92	Cenpn	47	Cd68	20	Vim	8
Oip5	90	Arhgef39	46	Mcm4	19	Dck	8
Mcm3	89	Mcm8	46	Stil	18	Ly6c1	8
Kif2c	89	Ccne2	45	E2f8	18	Irf8	8
Mcm2	88	Pcna	45	Prr11	18	Gng2	7
Spc24	88	Rad51	45	Mcm10	17	Anxa2	7
Cenpi	88	Cdca7	45	Il2rb	17	Prdm1	7
Arhgap11a	88	Parpbp	44	Itgb1	17	Plek	7
Espl1	86	Tpx2	43	Ska3	17	Mapre2	7
Cenph	86	Depdc1b	42	Trip13	16	Ankle1	7
Ccnf	83	Cks1b	40	Fam54a	16	Nsl1	6
Nusap1	81	E2f1	39	Cdk1	15	Gna15	6
Cenpe	79	Gins1	39	Rbbp8	15	**Lgals1**	**6**
Kif4	75	Neil3	38	Apitd1	15	Dhfr	6
Ccdc99	75	Slbp	37	Bora	15	Mpp6	6
Bub1b	74	Tfdp1	35	Pif1	15	Cd74	5
Orc1	74	Cenpl	34	Itgax	15	Gmnn	5
Clspn	74	Nuf2	34	Serpinb1a	15	Cdt1	5
Dbf4	73	Eme1	34	Serpinb6b	15	H2-Eb1	5
Hmgb2	69	Itgam	34	Mastl	15	Cdc20	5
Exo1	67	Troap	33	Aurkb	14	Asf1b	5
Cenpm	67	Casp3	33	Ccr2	14	Txn1	5
Tcf19	67	Plk4	32	Cxcr3	14	Pmch	5
Plk1	64	Mcm6	32	Chaf1b	14	Gpr55	5
Ccnb2	64	Prim1	31	Kif18b	14	Gzma	5
Skp2	64	Recql4	31	Ccl5	14	Mybl2	5
Chek1	62	Fen1	31	Prim2	13	Brca1	5
Foxm1	61	Hells	30	Rrm2	13	Pdcd1	5
Spag5	61	Ndc80	29	Cenpp	13	Ctla4	5
Ska1	60	Ccr5	29	Dclk2	13	Icos	5
Gtse1	60	Kif18a	28	BC055324	13	Rgs1	5
Ckap2l	60	Incenp	28	Iqgap3	13	Hopx	5
Chtf18	59	Cdk2	28	Cd19	12	Dusp5	5
Paf	57	Sgol2	28	Ms4a1	12	Myo1f	5
Mis18bp1	56	Brip1	28	Stmn1	12	Ddias	5
Aurka	55	Ube2t	27	Rcc1	12		
Dsn1	55	Nek2	27	Fgr	12		

Network analysis for significantly differentially expressed genes during activation of MHV68 specific TCR-TN CD8^{+} T cells

It is technically challenging to explore in depth all of the genes whose expression changes significantly upon TN cell activation. Therefore, we performed a network analysis for those genes that were highly differentially expressed in naïve and activated TN cells (Fig no. 2.7). In brief, the STRING network analysis revealed 229 nodes, which interacted with each other by 7892 edges and the average node degrees was 68.9. The average local clustering coefficient was found to be 0.721. A value of clustering coefficient nearing zero suggests no clustering while the value 1 represents maximal clustering (40). Many of the genes present in the network have been studied during differentiation of T cells expanded during infectious agents (32, 33, 45).

A

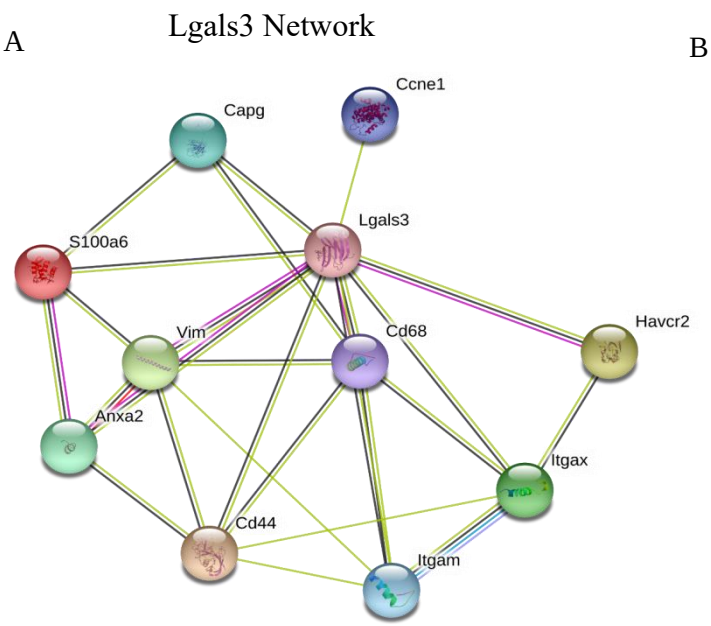

B

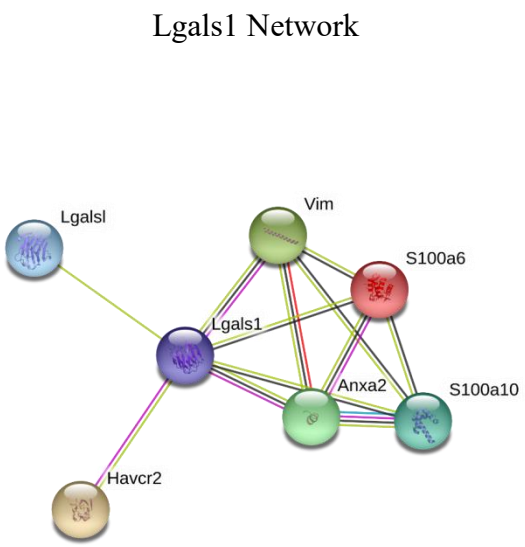

We focused our further analysis on the family of galectins that have critical role in immune responses during infection, autoimmunities and cancers. We generated a STRING network for galectins encoded by lgals genes (Fig no. 2.7A-C). Two such networks were obtained in

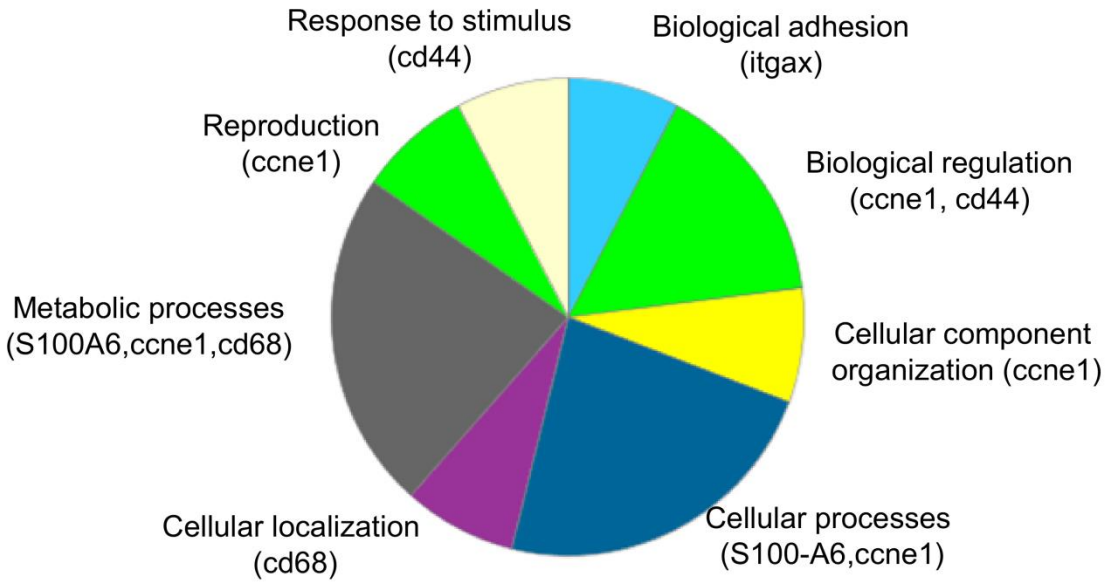

Figure no. 2.7. **Computational analysis of RNAseq data to generate STRING network to investigate protein-protein interactions (PPI).** A. STRING network of differentially expressed genes having a cut off criteria of 5RPKM in both samples and a two-fold change in expression between naïve and activated TN cells. Hub genes having equal to or more than 5 interactions with a p value < 1.0e-^{16} were used for network generation. A and B. STRING Network is generated to show Lgals genes as hub genes, Lgals3 (A) and Lgals1 (B). Lgals3 interacted with 10 partners while Lgals1 interacted with 6 partners. Both networks had a PPI enrichment p value < 1.0e-16. C. Lgals3 gene and its interacting partner (7 out of 10 genes were mapped through PANTHER) to investigate different biological process. *Itgam*, *capg*, and *Anxa2* were not mapped through PANTHER.

which Lgals3 and Lgals1 served as hub genes. The network with Lgals3 revealed 10 interacting partners while the one with Lgals1 revealed only six interacting partners each having a high PPI enrichment scores and p value of less than 1.0e-16 (Fig no. 2.7A and B). Lgals3 had more interacting partners and additionally included many partners of Lgals1. Given its critical role during activation of T cells, we chose galectin-3 for elucidating its role in CD8^{+} T cells response induction during γ-HV (Fig no. 2.7C) (19).

Expression of Galectin 3 in activated $CD8^+$ T cells

We analyzed and compared the transcriptional expression profile of all the members of galectin family in naïve and the virus-activated ORF8 TCR TN $CD8^+$ T cells (Fig no. 2.8A). Galectin 3 showed increased expression in activated TN T cells (up ~140-fold) (Fig no. 2.8A and B). The expression of galectin-3 by polyclonal $CD8^+$ T cells induced during γ-HV infection in the spleen is shown in Figure 2.8A. We also measured expression of galectin-3 protein in adoptively transferred TN cells as well as endogenous $CD8^+$ T cells that expanded in response to MHV68 infection in recipient congenic (CD45.1) mice (Fig no. 2.8B). While a few naïve $CD8^+$ T cells (less than 10%) showed galectin-3 expression, all virus-specific endogenous (~2% of total $CD8^+$ T cells) as well as donor TN $CD8^+$ T cells (97.4% of total $CD8^+$ T cells) scored positive for galectin-3 expression 6 dpi in spleen samples (Fig no. 2.8B). Endogenous MHV68-ORF8-specific $CD8^+$ T cells were likewise analyzed for galectin-3 expression in the absence of an adoptive transfer. A large majority of H-$2K^b$-ORF8-Tet^+ $CD8^+$ T cells in peripheral blood (Fig no. 2.8C) expressed galectin-3.

To investigate the kinetics of galectin-3 protein induction in $CD8^+$ T cells, we stimulated sorted $CD8^+$ T cells from WT mice with anti-CD3 and anti-CD28 antibodies. Intracellular and extracellular expression of galectin-3 was measured (Fig no. 2.8D and E). Upon activation, $CD8^+$ T cells up regulated intracellular pool of galectin-3 to a larger extent as compared to its surface expression (Fig 2.8E). More $CD8^+$ T cells expressed intracellular galectin-3 (~30% at 16 hours and more than 70% at 70 hours post stimulation) (Fig 2.8D). As expected, a large majority of $CD8^+$ T cells additionally up regulated CD69 upon stimulation (Fig 2.8D). The total galectin-3 expressing cells as detected in these assays are also likely to include the cells expressing surface galectin-3 as well. Therefore, we measured its expression in both the permeabilized and intact cells (Fig 2.8E). These experiments revealed a predominant intracellular expression of galectin-3 in activated cells (Fig 2.8E).

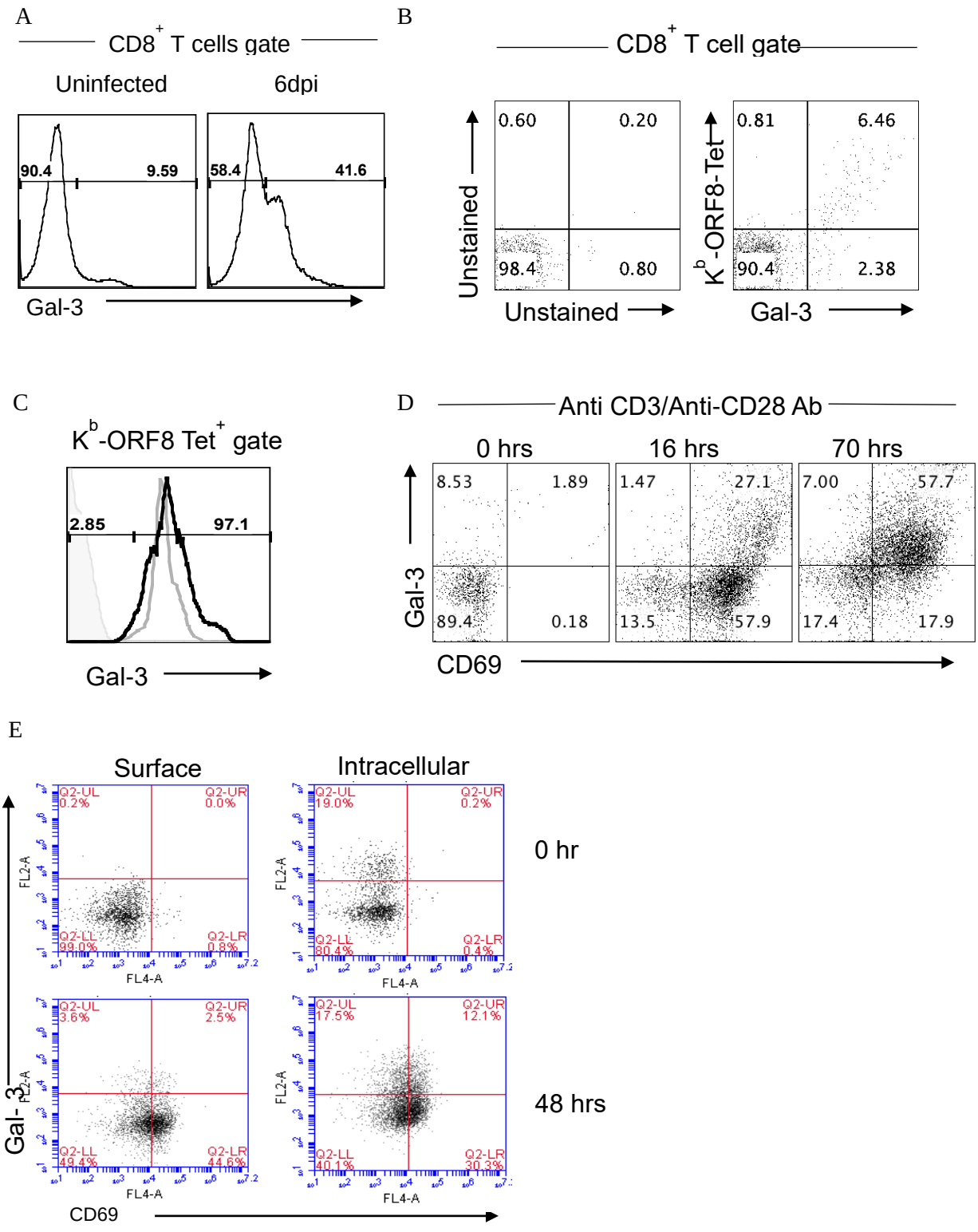

Figure no. 2.8. Expression kinetics of Galectin-3 on activated CD8$^+$ T cells. A. 50x10^3 TN cells were transferred in congenic CD45.1 mice and 6 days later the expression of galectin-3 was measured on total CD8$^+$ T cells. B. Galectin-3 expression was measured flow cytometrically in H-2K^b-KNYIFEEKL specific CD8$^+$ T cells on 6dpi to measure intracellular

galectin-3 expression. The staining with specific antibodies followed Fc receptors blocking. Bold black lines in overlaid histogram represent expression of galectin-3 in $CD45.1^+$ (endogenous $CD8^+$ T cells; ~2% of total $CD8^+$ T cells) and grey line represents galectin-3 expression in donor $CD45.2^+$ (TCR TN cells; 97.3% of total $CD8^+$ T cells). C. C57BL/6 mice were infected with MHV68 and $CD8^+$ T cells from peripheral blood were analyzed for intracellular galectin-3 at 10dpi. FACS plots show the expression of galectin-3 in K^b-ORF8 tetramer positive cells. The protocol used does detect cell surface and intracellular pool of galectin-3. D. Purified $CD8^+$ T cells were stimulated by soluble anti-CD3 (1μg/ml) and anti-CD28 (1μg/ml) in the presence of IL-2 in a round-bottomed plate for 16 and 70 hours. The expression of surface CD69 and intracellular galectin-3 was analyzed. Representative FACS plots are shown for all the experiments. E. *In vitro* activation of magnetically sorted $CD8^+$ T cells using anti-CD3 (coated) and anti-CD28 (soluble) antibodies to measure intracellular (permeabilized cells) and surface (without permeabilization) galectin-3. The cells were stimulated for two days and the expression level of galectin-3 was measured as described in transparent methods section. Activated cells predominantly up regulated intracellular galectin-3 but its expression on cell surface was affected to a lesser extent.

Galectin-3 is recruited at the immunological synapse during $CD8^+$ T cell activation

During induction of $CD8^+$ T cell responses, the TCR recognizes the peptide-MHC complex that is central to the immunological synapse. Other constituents are recruited subsequently. Most proteins that participate in the immune synapse are glycosylated. Galectin-3, through its CRD, could interact with them to influence T cell activation (46). We performed confocal microscopy to investigate whether galectin-3 expressed either at basal level in $CD8^+$ T cells or up regulated after stimulation of naïve and memory $CD8^+$ T cells is recruited to the immunological synapse. The extent of co-localization was measured and quantified as described (29). After the TCR is ligated with cognate ligand, signaling events create docking sites for the cytosolic adapter molecule Zap70, which is recruited upon phosphorylation of ζ-chain of the co-receptor. We stimulated antigen-specific OT1 cells with immobilized H-$2K^b$-

SIINFEKL-tetramer-allophycocyanin and stained for galectin-3 and Zap70. Un-stimulated cells served as controls. A diffuse and low level of expression for Zap70 was seen in naïve cells (Fig no.2.9A and E-F). The extent of co-localization of galectin-3 with Zap70 was ~50% in un-stimulated cells. Within 10 minutes of incubation with MHC I tetramer, co-localization of galectin-3 with the MHC I tetramer increased (~70 percent) as did galectin-3 with Zap70 (more than 70 percent) (Fig no. 2.9B). The extent of co-localization remained high at 20 minutes but began to diffuse at 60 minutes post stimulation (Fig no. 2.9C and D). Diffuse staining for Zap70 was apparent at 60 minutes (Fig no. 2.9D). Upon TCR stimulation, galectin-3 expressed at basal level in $CD8^+$ T cells is co-localized with Zap70.

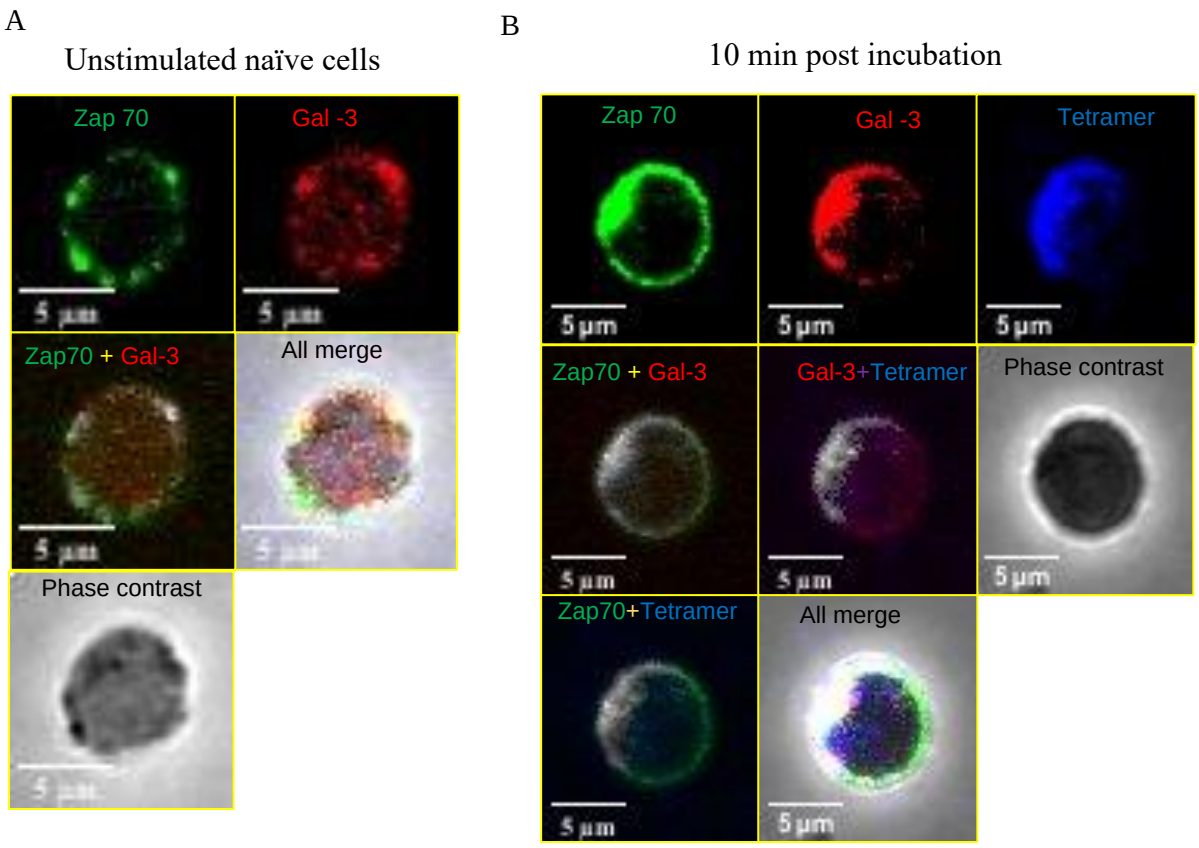

C

20 min post incubation

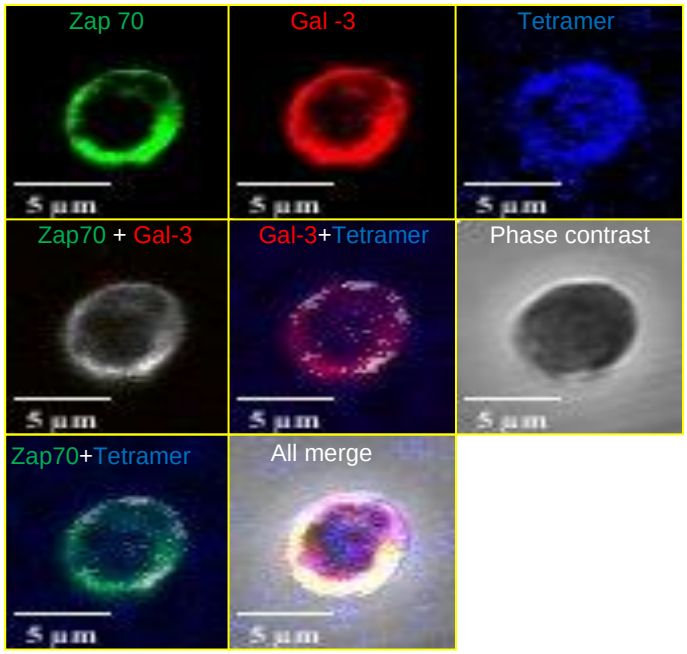

D

1 hrs post incubation

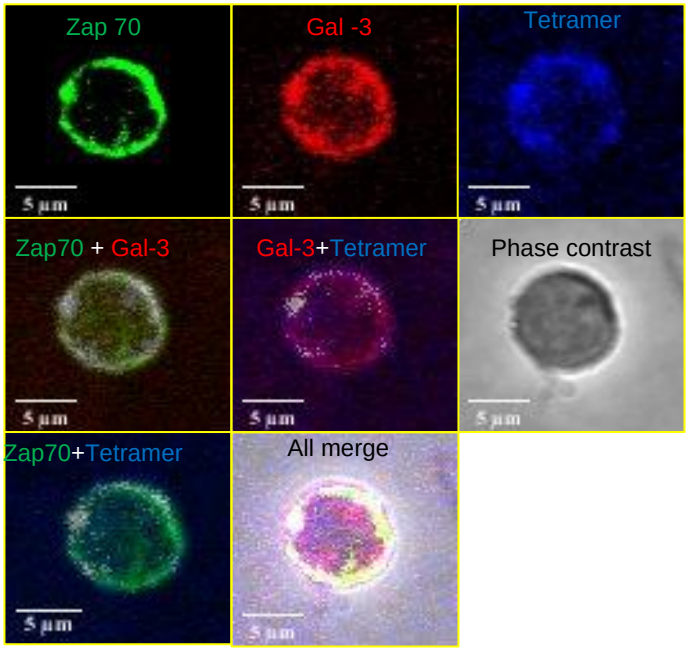

E

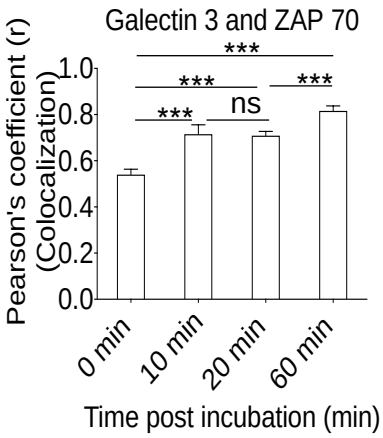

F

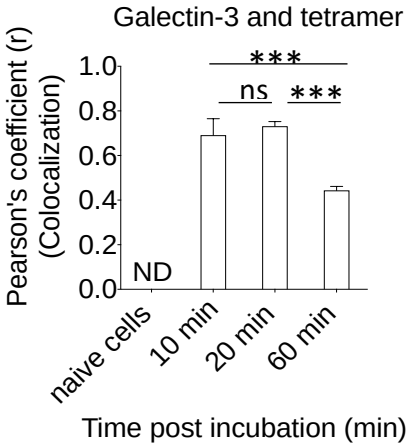

G

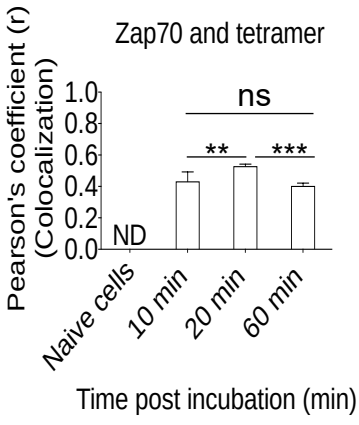

Figure no. 2.9. Galectin-3 expressed by TCR stimulated CD8$^+$ T cells is recruited at immunological synapse. Antigen-specific CD8$^+$ T cells from OT1 mice were negatively selected by MACS purification and subsequently stimulated with specific peptide-loaded class I MHC tetramer (H-2K^b-SIINFEKL-Tetramer-APC conjugated and immobilized on coverslips). Purified CD8$^+$ T cells were added onto coverslips and incubated for varying times. At indicated time, cells were stained for different molecules and confocal images were acquired as described in material and method section. A. OT1 cells incubated for 60 min on coverslips in the absence of H-2K^b tetramers were analyzed for different markers. Representative micrographs for individual staining and co-localization of Zap70, galectin-3 and tetramer are shown. B-D. OT1 cells incubated for 10 min (B), 20 min (C) and 60 min (D) on coverslips in the presence of H-2K^b tetramers were similarly analyzed for different markers. Representative images for each group are shown. E-G. Cumulative data for co-localization experiments obtained from more than 30 different cells is shown. Tukey multiple comparisons test was used to determine the level of significance.

Next, we investigated whether galectin-3 up regulated in previously stimulated CD8$^+$ T cells is recruited to the immunological synapse upon their re-stimulation. To this end, OT1 cells were stimulated *in vitro* using anti-CD3 and anti-CD28 antibodies for 72 hours. These cells were then co-cultured with SIINFEKL-pulsed BMDCs and stained for galectin-3 and Zap70. Cells not re-stimulated with peptide-pulsed BMDCs exhibited diffuse staining for galectin-3 (Fig no. 2.10A, upper panel). Within 10 minutes of co-culture with peptide-pulsed BMDCs, galectin-3 localized towards the immune synapse (IS) and remained so until 60 minutes; Figure 2.10A lower three panels and Figure 2.10B. In these experiments, we did not observe enhanced expression and recruitment of Zap70 to the immunological synapse in re-stimulated cells. CD8$^+$ T cells become temporarily refractory to re-stimulation as the TCR (47).

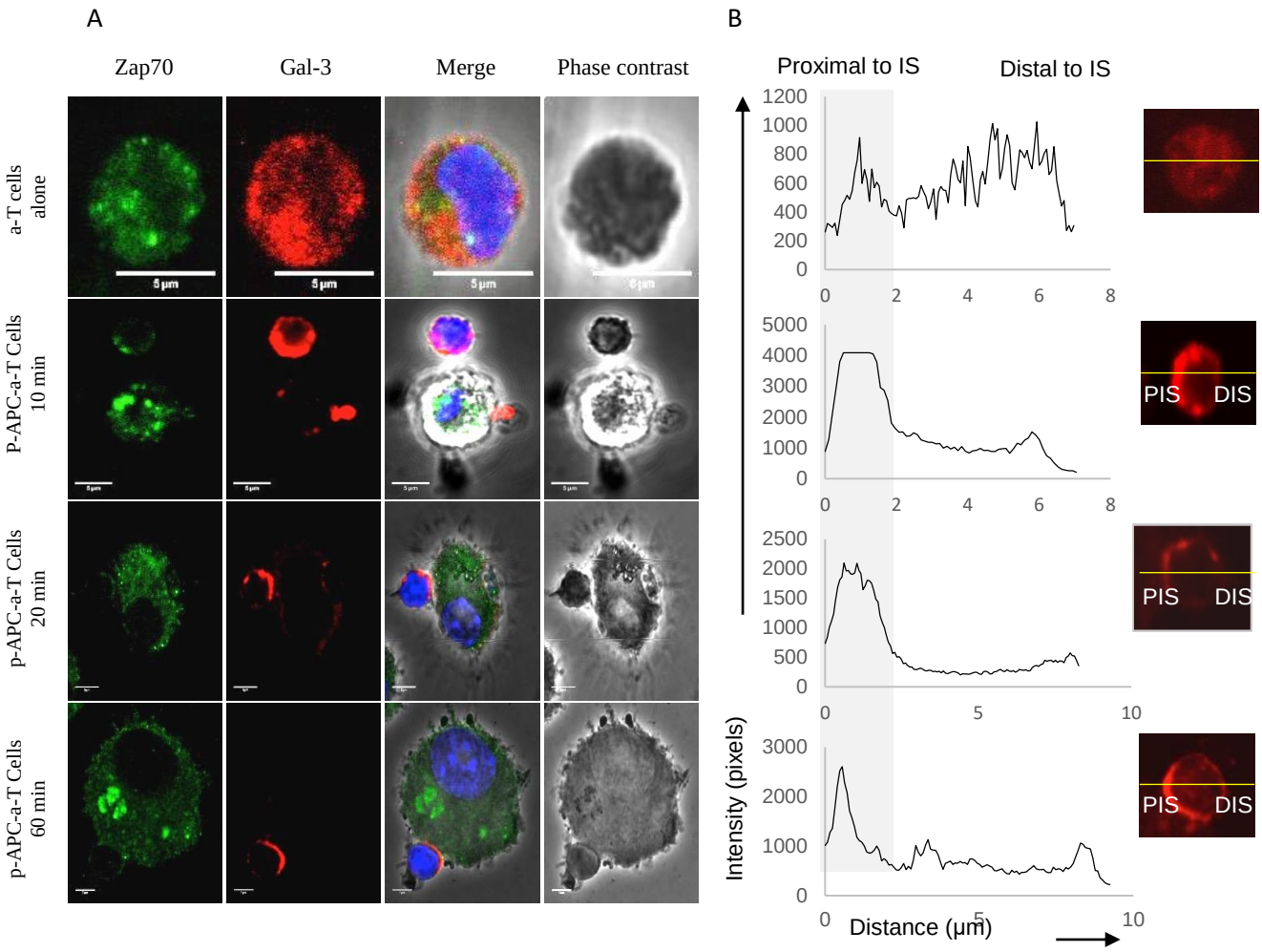

Figure no. 2.10 Galectin-3 is recruited at immunological synapse after restimulation of *in vitro* activated CD8$^+$ T cells. A. MACS purified OT 1 cells were stimulated in vitro using anti-CD3 and anti-CD28 antibodies for 72 hours. Thereafter cells were washed and co-cultured with SIINFEKL peptide pulsed BMDCs for indicated time. Thereafter cells were stained for different markers and analyzed by confocal microscopy for distribution of galectin-3. A. Micrographs show the expression of different molecules and their migration towards immunological synapse involving activated OT1 T cells and BMDCs at different time post stimulation. B. The intensity of galectin-3 expressed in OT1 cells that migrated towards BMDCs is shown. Shaded area represents intensity of fluorescent probe proximal to immunological synapse (PIS) as compared to the intensity observed distal to immunological synapse (DIS).

We also performed co-localization experiments using $CD8^+$ T cells that were expanded as a result of viral infections and isolated in the acute phase of response at 6dpi (Fig no. 11A). Galectin-3 was up regulated in antigen-specific $CD8^+$ T cells responding to invading viral infections. We used two different viruses (a γ-HV (MHV68) and Influenza virus) to investigate galectin-3 expression and localization in reactive $CD8^+$ T cells (Fig no. 2.11B and C). Activated cells were then stained to assess co-localization of galectin-3 with class I MHC tetramers and Zap70. Staining of $CD8^+$ T cells with class I MHC tetramers marked the expression of TCR. We observed significant co-localization of galectin-3 with MHC tetramers (~40%) and Zap70 (more than 80%). In addition Zap70 and class I-MHC tetramers also exhibited a co-localization to the extent of 40% (Fig no. 2.11B and C). Therefore, our results show that galectin-3 is recruited at the immune synapse during activation of $CD8^+$ T cells.

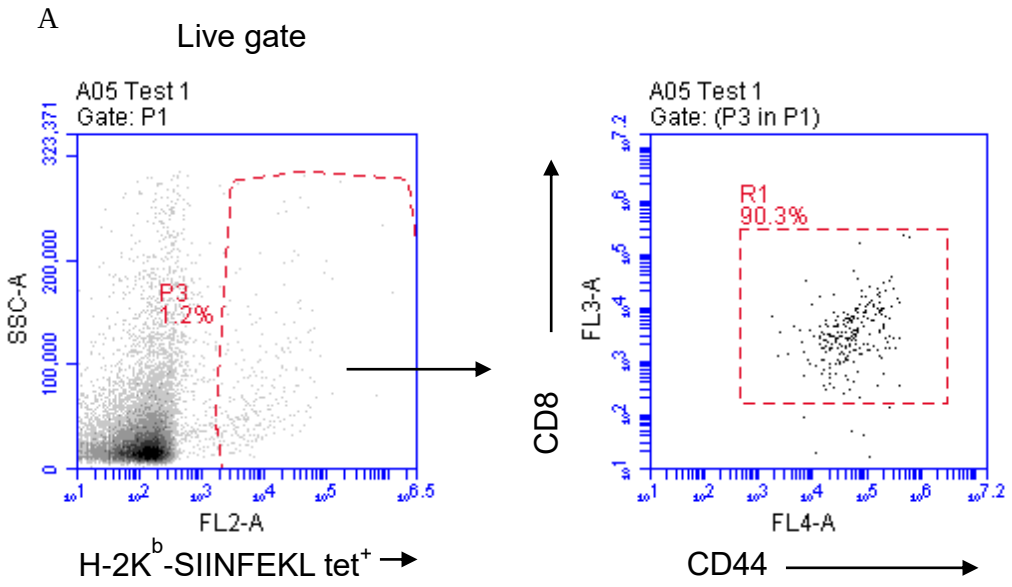

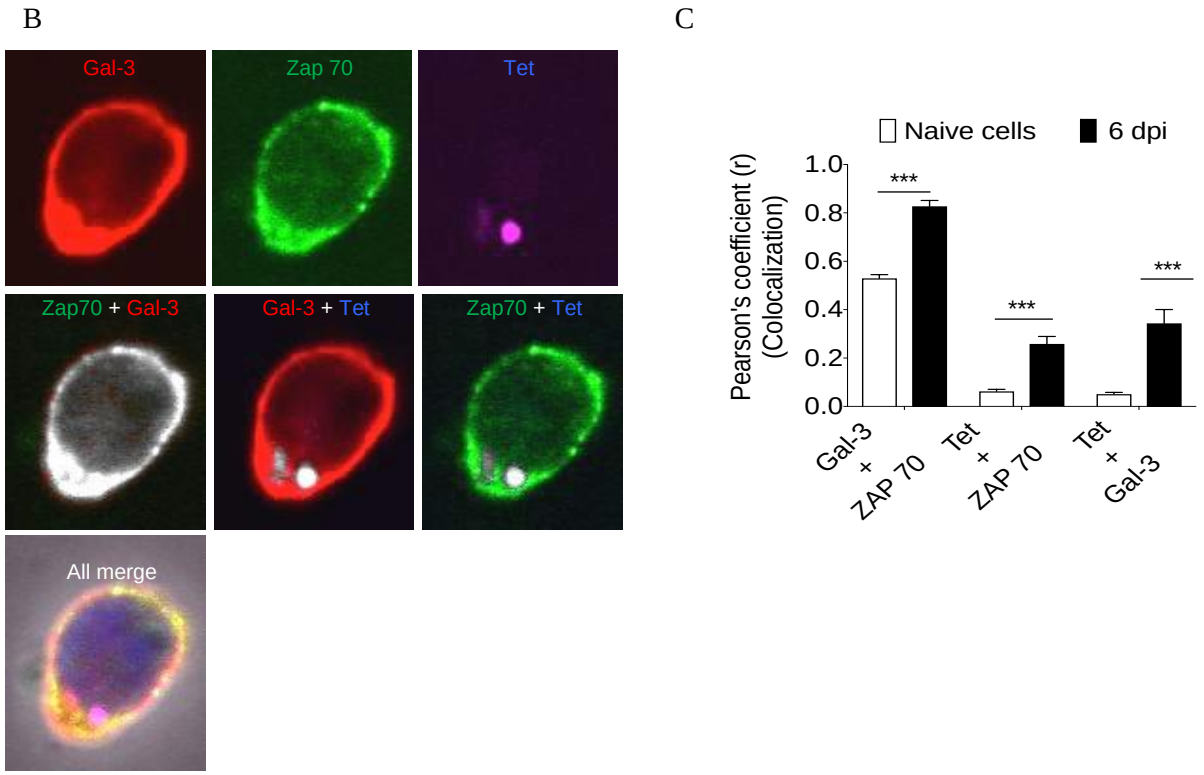

Figure no. 2.11 Galectin-3 is recruited at immunological synapse after restimulation of *in vivo* activated CD8$^+$ T cells. A. 50x10^3 OT1 cells were transferred into C57BL/6 mice, which were then infected with MHV68 M2-SIINFEKL through intranasal route. On 5dpi, PBMCs were analyzed for SIINFEKL specific CD8$^+$ T cells. B. OT1 cells were transferred in C57BL/6 mice one day prior to the infection with MHV68 M2-SIINFEKL. Six days post infection, H-2K^b-SIINFEKL tetramer positive cells were FACS sorted and stained for galectin-3 and Zap70. Micrographs show staining of different molecules. C. Bar graphs represent co-localization of different molecules in input control cells and OT 1 cells obtained from infected animals at 6dpi. More than 35 cells were analyzed for each time points.

While analyzing co-localization of galectin-3 at immune synapse, we added α-lactose to the co-culture of activated OT1 cells and SIINFEKL pulsed BMDCs to determine whether or not CD8$^+$ T cells produced galectin-3 acts intracellularly or extracellularly. α-lactose inhibits interaction between CRD of galectins and carbohydrate moieties present on other proteins (30). Addition of α-lactose, which is likely to act extracellularly by competing with

galectins for binding to glycosylated proteins, did not alter the expression kinetics and recruitment of galectin-3 or Zap70 towards the proximal end of the immune synapse (Fig no. 2.12A and B). Whether or not α-lactose treatment of cells during their activation influences the activation of $CD8^+$ T cells was also measured cytofluoremetrically 12 hrs post stimulation with plate bound anti-CD3 and soluble anti- CD28 antibodies (Fig no. 2.12E). $CD8^+$ T cells stimulated in the presence of α-lactose displayed an impaired activation profile as measured by CD69 staining (Fig no. 2.12E). α-lactose may not only act to compete with galectin-3 but with other galectins as well. Therefore, we investigated the influence of extracellular galectin-3 neutralization by specific antibody clone (B2C10) that was previously shown to bind extracellular galectin-3 (24, 48). We also performed experiments using this clone to validate its ability to bind cell surface as well as extracellular galectin-3 (Fig no. 2.12D). As naive and activated $CD8^+$ T cells did not display significant amount of galectin-3 on their surface (Fig no. 2.12E), we reasoned the primary immune cells other than those expressing CD8 molecule could be used to demonstrate its surface detection. Splenocytes as well as lymph node cells did not express galectin-3 on their surface but about 25% of total splenocytes and 12% of lymph node cells that were CD8 negative show its surface expression (Fig no. 2.12F). Additionally, we performed galectin-3 pull down experiments using B2C10 clone of anti-galectin-3 that will demonstrate its ability to bind a soluble extracellular galectin-3. The results shown in Figure 2.12D, demonstrate that a polypeptide of about 30kDa, the molecular mass of galectin-3, was specifically bound by anti-galectin-3 antibody. The result of surface galectin-3 neutralization experiments using anti-galectin 3 antibodies are described in one of the later sections.

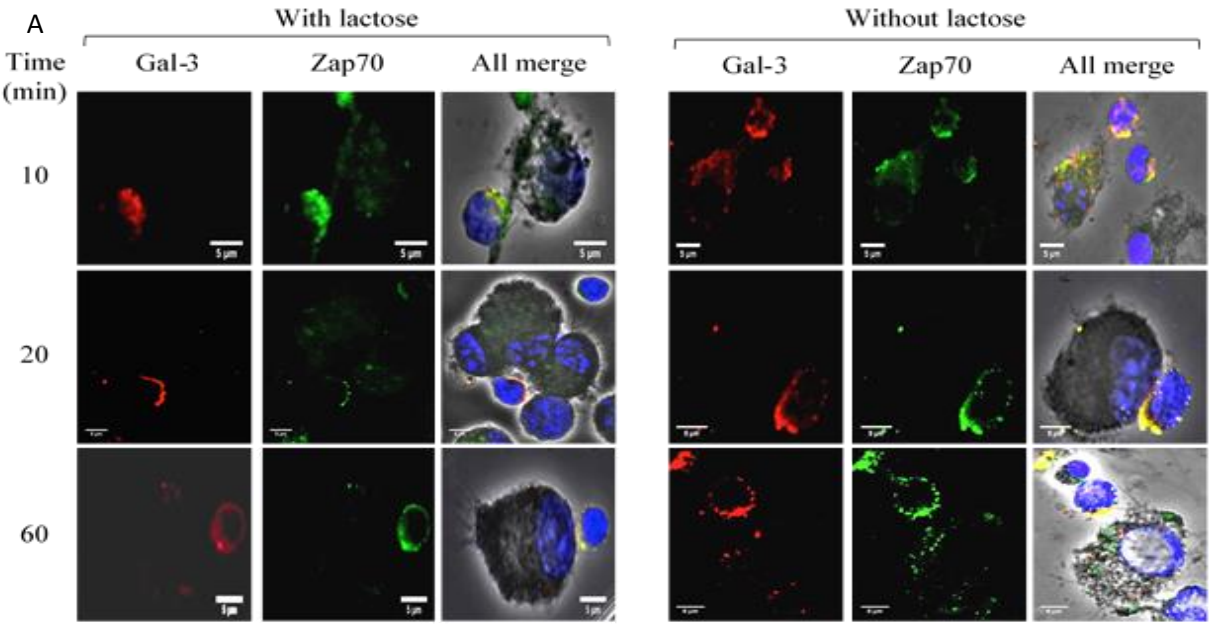
A
With lactose
Without lactose
Time (min)
Gal-3
Zap70
All merge
10
20
60

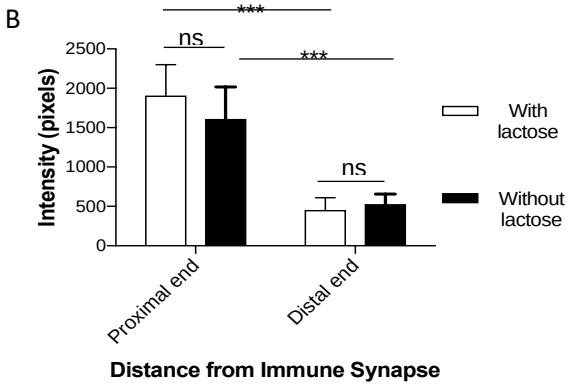
B
***
ns
***
ns
Intensity (pixels)
2500
2000
1500
1000
500
0
With lactose
Without lactose
Proximal end
Distal end
Distance from Immune Synapse

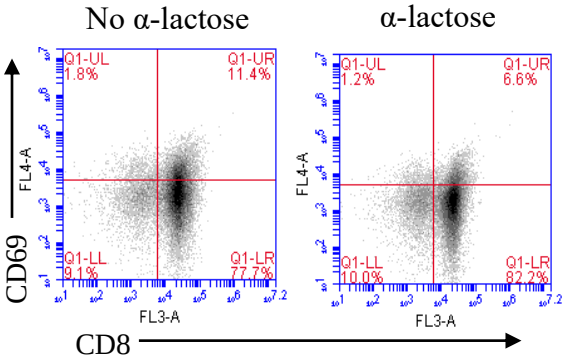
C
No α-lactose
α-lactose
Q1-UL 1.8%
Q1-UR 11.4%
Q1-LL 9.1%
Q1-LR 77.7%
Q1-UL 1.2%
Q1-UR 6.6%
Q1-LL 10.0%
Q1-LR 82.2%
FL4-A
FL3-A
CD69
CD8

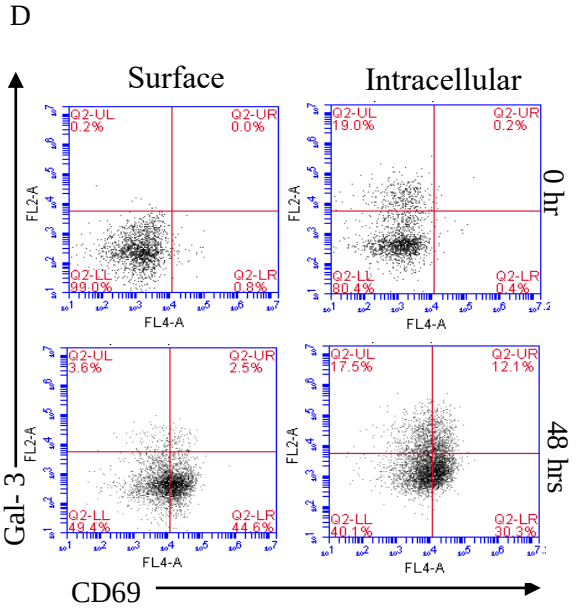
D
Surface
Intracellular
Q2-UL 0.2%
Q2-UR 0.0%
Q2-LL 99.0%
Q2-LR 0.8%
Q2-UL 19.0%
Q2-UR 0.2%
Q2-LL 80.4%
Q2-LR 0.4%
0 hr
Q2-UL 3.6%
Q2-UR 2.5%
Q2-LL 49.4%
Q2-LR 44.6%
Q2-UL 17.5%
Q2-UR 12.1%
Q2-LL 40.1%
Q2-LR 30.3%
48 hrs
FL2-A
FL4-A
Gal- 3
CD69

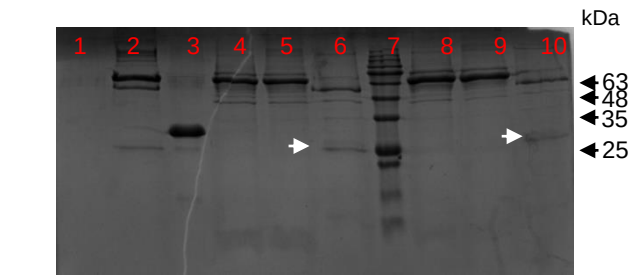
E
kDa
1
2
3
4
5
6
7
8
9
10
63
48
35
25

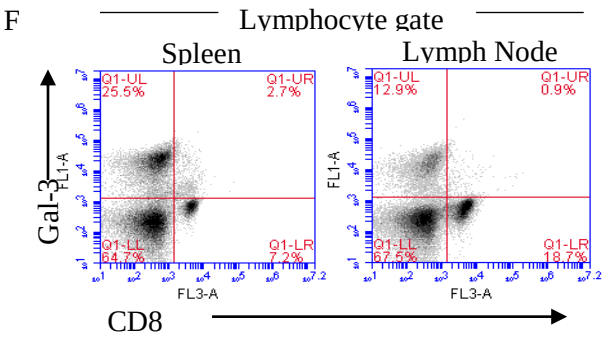
F
Lymphocyte gate
Spleen
Lymph Node
Q1-UL 25.5%
Q1-UR 2.7%
Q1-LL 64.7%
Q1-LR 7.2%
Q1-UL 12.9%
Q1-UR 0.9%
Q1-LL 67.5%
Q1-LR 18.7%
FL1-A
FL3-A
Gal-3
CD8

Figure no. 2.12. An influence of α-lactose on the recruitment of intracellular vs extracellular galectin-3 at the immunological synapse was analyzed. SIINFEKL peptide pulsed BMDCs were co-cultured with OT 1 cells FACS-sorted from infected animals at 6dpi in the presence of absence of 100 mM of α-lactose solution and the extent of localization of galectin-3 towards immune synapse was measured. A minimum of 35 cells was counted for each group for calculating co-localization percentages for different molecules. A. Representative confocal micrographs for the co-localization of galectin-3 and Zap70 are shown. B. Bar diagram depicting the intensity of galectin-3 at the proximal and distal end of OT1 cells in contact with peptide-pulsed BMDCs for 35 cellular contacts for each sample is shown. C. Measuring the influence of a-lactose on $CD8^+$ T cell activation. $CD8^+$ T cells were purified from lymph node of C57BL/6 mouse and incubated with 277mM of α-lactose for 1 hour at 37°C. The cells were then washed three times with PBS and stimulated with anti-CD3 (coated) and anti-CD28 (soluble) for 12 hrs at 37° C. After activation the cells were washed and stained with anti-CD69 and anti-CD8 antibodies. D-F. A demonstration that the clone (B2C10) of antibody used for neutralization of galectin-3 can bind and detect extracellular surface expressed galectin-3. D. A galectin-3 pull-down by the neutralizing antibody (B2C10) from the lysates of spleen cells and lymph node cells. Different samples prepared from pull down experiments were resolved on a 12% SDS-PAGE. lane 1: dye, lane 2: beads with IgG1 (blocking antibody, 3mg), lane 3: recombinant galectin-3 (3mg), lane 4: input splenocytes lysate, lane 5: residual sample from splenocytes lysate after pull-down, lane 6; pull-down fraction from splenocytes lysate, lane 7: molecular weight marker (MWM), lane 8: input lymph node cell lysate, lane 9: residual sample from splenocytes lysate after pull-down, lane 10: pull-down fraction from lymph node cells. In lanes 6 and 10, a faint band of galectin-3 corresponding to 30kDa is retrieved (white arrow marked), bonds corresponding to heavy chain (~50kDa) and light chain (25kDa) of IgG1 molecules are also visible. High molecular mass bands might represent aggregated products and the carrier protein in antibody preparation. F. Splenocytes from C57BL/6 mice were isolated to stain for CD8 and galectin-3. Gated lymphocytes are shown for anti-CD8 and galectin-3 staining. While $CD8^+$ T cells expressed low levels of galectin-3, $CD8^-$ T cells demonstrate significant population of surface galectin-3 expressing cells.

Galectin-3 is recruited to IS during re-stimulation of virus specific memory CD8$^+$T cells

Long-term protective immunity to intracellular infections or vaccines is critically dependent on memory response. Therefore, we investigated whether or not galectin-3 is also involved in regulating the immune synapse formation by virtue of its localization at proximal end during the activation of memory CD8$^+$ T cells. We infected OT1 cells recipient mice with MHV68-SIINFEKL and analyzed CD8$^+$ T cells in the memory stage (55 days post infection) by flow cytometry and confocal microscopy (Fig no. 2.13A). All H-2K^b-SIINFEKL specific CD8$^+$ T cells expressed high level of CD44 (CD44^{hi}) but low level of CD62L (CD62L^{lo}) and IL-7R (IL-7R^{lo}) (Fig no. 2.13B). This phenotype is previously reported during a persistent γ-HV (MHV68) infection (49). Galectin-3 co-localized with Zap70 and tetramers to the extent of ~80% and ~40% (Fig no. 2.13C-D) while co-localization of Zap70 with tetramers was ~ 30% in stimulated H-2K^b SIINFEKL-specific cells with immobilized tetramers. Therefore, similar to what was observed during the initial activation of naïve CD8$^+$ T cells after MHV68 infection, the stimulation of specific memory CD8$^+$ T cells exhibited galectin-3 recruitment at the immune synapse.

A

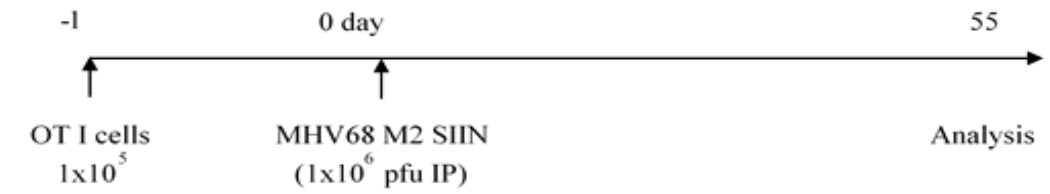

B

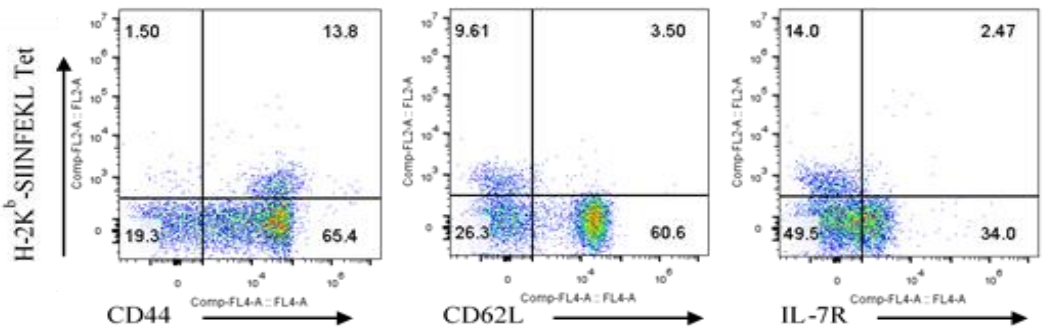

C

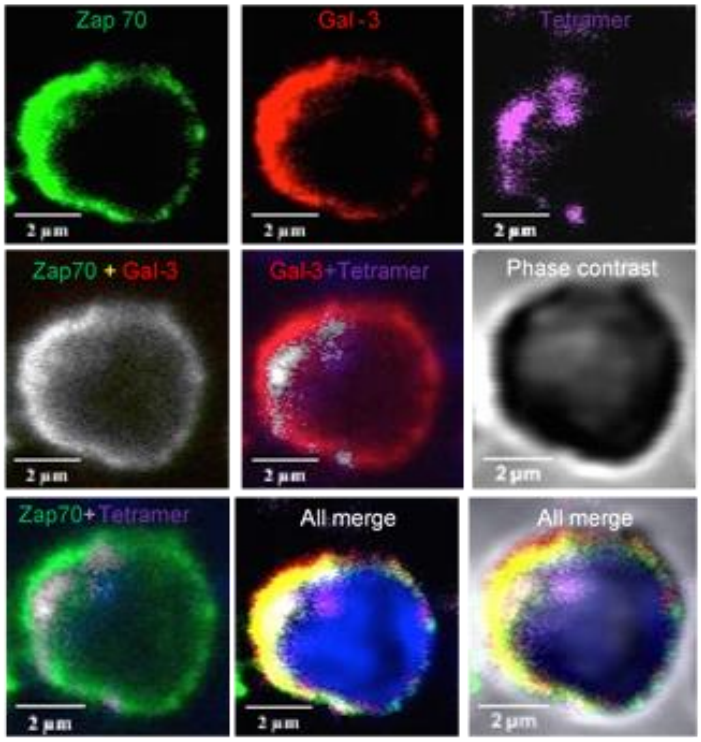

D

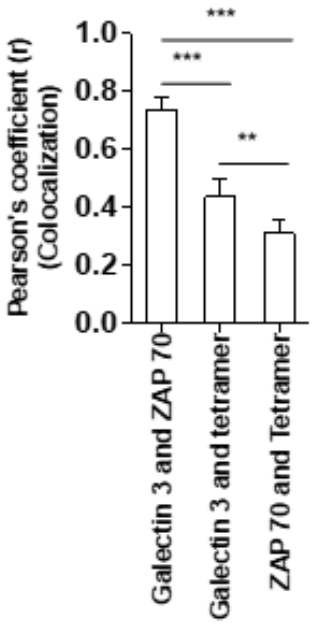

Figure no. 2.13 Galectin-3 expressed by memory cells generated during γ-HV (MHV-68 M2 SIINFEKL) and during their recall response is recruited at immunological synapse. A. $1x10^5$ OT1 cells were adoptively transferred in C57BL/6 mice one day before infection with MHV68-M2SIINFEKL virus. B. Phenotypic characterization of H-$2K^b$-SIINFEKL specific CD8 T cells was performed flow cytometrically. Representative FACS plots are shown. C-D. H-$2K^b$-SIINFEKL specific CD8 T cells were FACS purified at 55dpi and stimulated by H-$2K^b$-SIINFEKL tetramer coated on coverslips for one hour. Thereafter cells were stained for different markers and analyzed by confocal microscopy for distribution of galectin-3. C. Representative confocal micrographs show the expression of different molecules. D. Bar graphs represent co-localization of different molecules in H-$2K^b$-SIINFEKL cells. More than 30 cells were analyzed.

The phenotype of memory $CD8^+$ T cells generated during a persistent infection is distinct from those generated during an acute viral infection. We therefore analyzed memory cells generated during an acute infection with influenza virus. We infected mice with an

influenza virus encoding a SIINFEKL epitope (WSN-SIINFEKL) and analyzed endogenous antigen-specific memory $CD8^+$ T cells at 40 days post infection (Fig no. 2.14). Infected mice demonstrated a transient drop in body weight (Fig no. 2.14B). H-$2K^b$-SIINFEKL-specific $CD8^+$ T cells isolated in the acute phase of response demonstrated a high expression of activation marker CD44 and KLRG1 (Fig no. 2.14C). When analyzed during memory stage after 40 dpi, H-$2K^b$-SIINFEKL-specific $CD8^+$ T cells were heterogeneously stained for CD44, CD62L and IL-7R, a phenotype distinct from those of memory cells generated during persistent MHV68 infection (Fig no. 2.14E). Sorted H-$2K^b$ SIINFEKL-specific $CD8^+$ T cells during the acute (Fig no. 2.14D) as well as memory stage (Fig no. 2.14 F-G) of infection were analyzed for recruitment of galectin-3 at the immune synapse. As shown in Figure 2.14D and E and F, galectin-3 was recruited alongside Zap70 at the synapse formed between SIINFEKL-specific $CD8^+$ T cells and H-$2K^b$ SIINFEKL control beads.

Taken together, our results demonstrate that galectin-3 is up regulated in antigen-specific $CD8^+$ T cells upon MHV68 as well as Influenza virus infection and is recruited to the immunological synapse during their primary as well as memory stimulation.

A

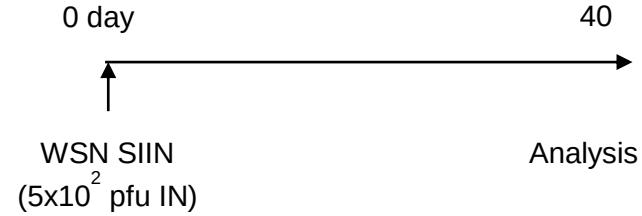

B

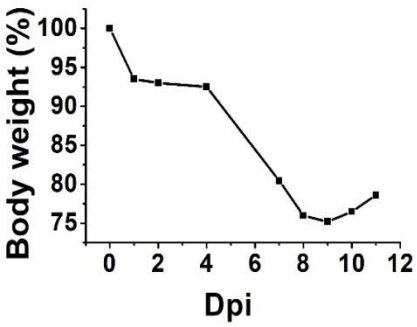

C

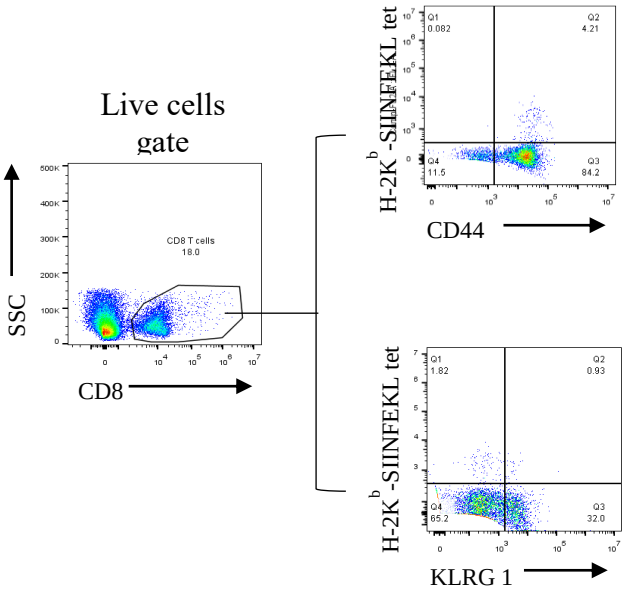
Live cells
gate
SSC
CD8
CD8 T cells
18.0
H-2K^b-SIINFEKL tet
CD44
Q1 0.082
Q2 4.21
Q4 11.5
Q3 84.2
H-2K^b-SIINFEKL tet
KLRG 1
Q1 1.82
Q2 0.93
Q4 65.2
Q3 32.0

D

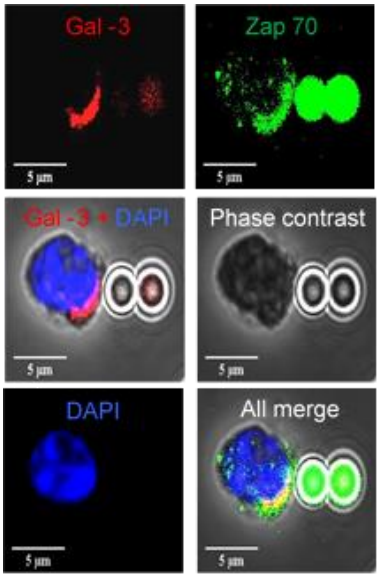
Gal -3
Zap 70
Gal -3 + DAPI
Phase contrast
DAPI
All merge
5 µm

E

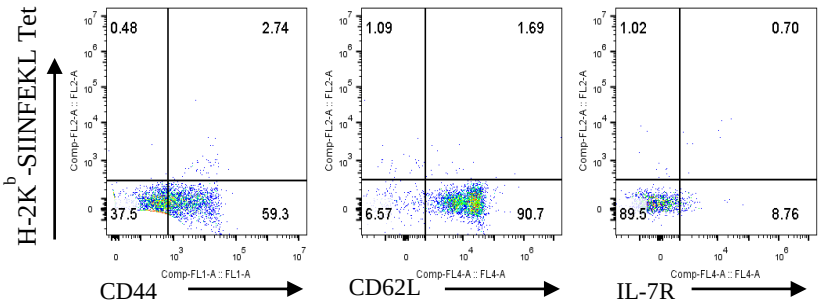
H-2K^b-SIINFEKL Tet
0.48
2.74
37.5
59.3
CD44
1.09
1.69
6.57
90.7
CD62L
1.02
0.70
89.5
8.76
IL-7R

F

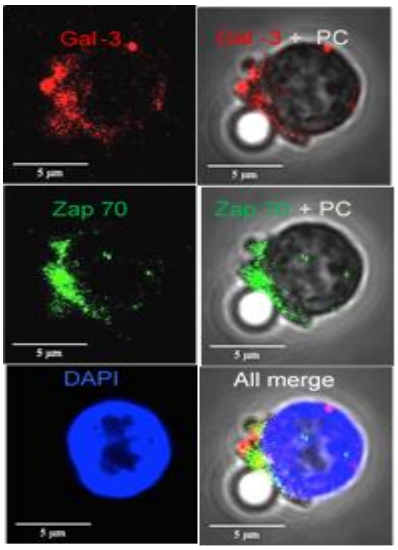
Gal -3
Gal -3 + PC
Zap 70
Zap 70 + PC
DAPI
All merge
5 µm

G

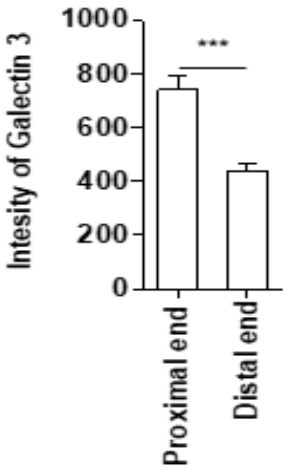
Intesity of Galectin 3
1000
800
600
400
200
0
***
Proximal end
Distal end

Figure no. 2.14. Galectin-3 expressed by memory cells generated during WSN-SIINFEKL and during their recall response is recruited at immunological synapse. A.C57BL/6 mice were infected with WSN-SIINFEKL through intranasal route and disease progression and phenotypic analysis of antigen-specific $CD8^+$ T cells was measured. B. Body weight of infected animals was monitored for up to 12 days and is shown as change in body weight as compared to the original. C. On 6dpi, mediastinal LN single cell suspensions were analyzed for the phenotype of endogenous SIINFEKL specific $CD8^+$ T cells. Representative FACS plots are shown. D. H-$2K^b$-SIINFEKL-specific $CD8^+$ T cells were magnetically sorted and analyzed for co-localization of galectin-3 and Zap70 towards the immune synapse. E. Phenotypic characterization of endogenous H-$2K^b$-SIINFEKL specific $CD8^+$ T cells at 40dpi was performed flow cytometrically. Representative FACS plots are shown. F. Representative confocal micrographs show the expression and co-localization of different molecules. G. Bar diagram show the intensity (pixels) of galectin-3 at the proximal and distal end of specific cells and H-$2K^b$ monomer coated beads contacts. At least 30 such contacts were counted.

Galectin-3 regulates proliferation and cytokine production by $CD8^+$ T cells

Having established that galectin-3 is recruited to the immunological synapse in $CD8^+$ T cells after stimulation, we investigated whether extracellular galectin-3 neutralization improves activation and cytokine production by $CD8^+$ T cells *in vitro*. We stimulated purified CFSE labelled $CD8^+$ T cells with bound anti-CD3 and soluble anti-CD28 antibodies in the presence or absence of a neutralizing anti-galectin-3 antibody (Fig no. 2.15A). In the absence of an antibody treatment, approximately, 10% and 70% of $CD8^+$ T cells divided at 72 and 96 hours post stimulation, respectively, upon incubation with anti-CD3 (1µg/ml of plate bound) and soluble anti-CD28 antibodies (Fig no. 2.15B and C). Extracellular galectin-3 neutralization with neutralizing antibody did not affect the proportion of divided cells as measured by CFSE dilution assays at 72 and 96-hours post stimulation (Fig no. 2.15B and C).

To further investigate a cell autonomous contribution of galectin-3 in activating $CD8^+$ T cells, we magnetically isolated $CD8^+$ T cells from WT and galectin-3 KO mice and stimulated equal numbers of CFSE-labelled $CD8^+$ T cells, by application of different

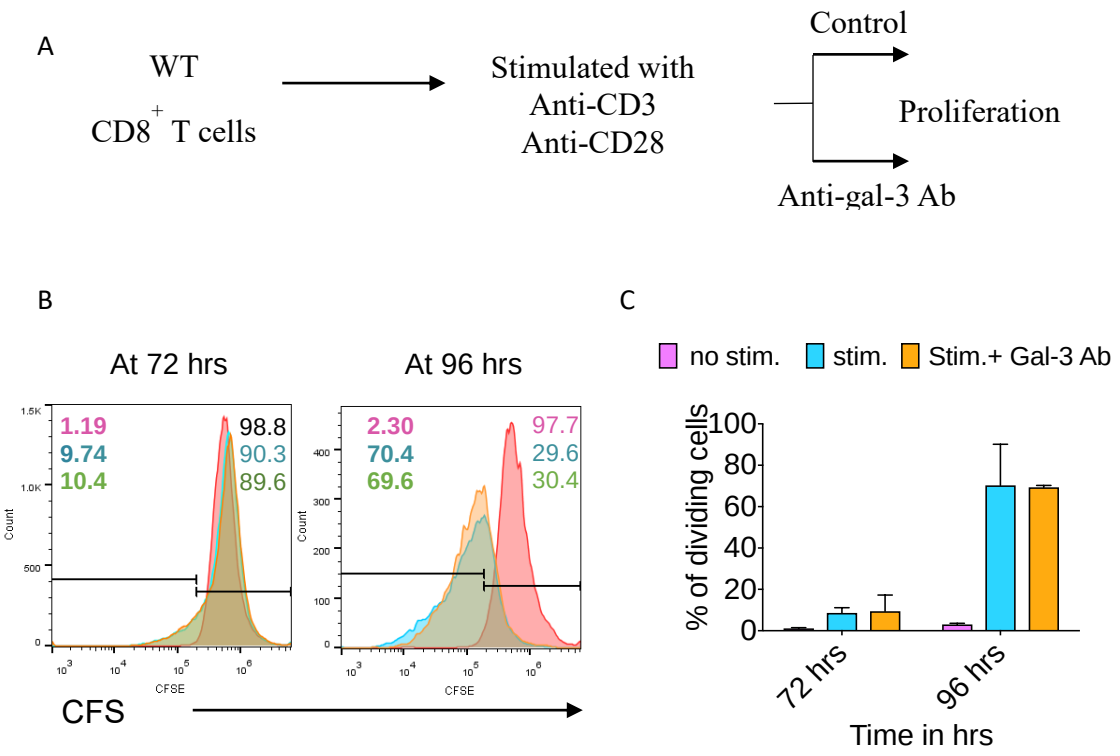

Figure no. 2.15. Cell autonomous intracellular expression of galectin-3 in $CD8^+$ T cells is responsible for regulating their proliferation. A. Purified $CD8^+$ T cells labelled with CFSE were stimulated with plate bound anti-CD3 (1µg/ml) and soluble anti-CD28 (1µg/ml) antibodies in the presence or absence of neutralizing anti-galectin-3 (10µg/ml) antibody. The proliferation was measured by CFSE dilution. B. A schematic of the experiment is shown. C. Representative overlaid histograms show the proliferation of $CD8^+$ T cells in the presence or absence of anti-galectin-3 antibody. The numbers written in bold fonts represent the numbers of divided cells in unstimulated cells (pink), stimulated cells (blue) and stimulated cells added with anti-galectin-3 antibody (orange). D. Bar diagram show the percentage of divided cells at 72 hrs and 96 hours in $CD8^+$ T cells stimulated in the presence or absence of anti-galectin-3 antibody.

concentrations of soluble anti-CD3 and anti-CD28 (1µg/ml) antibodies. We measured CFSE dilution as an indicator of proliferation and IL-2 production in culture supernatants as an indicator of their functionality (Fig no. 2.16A). More $CD8^+$ T cells from galectin-3 KO mice proliferated than those from WT mice at all the concentrations of anti-CD3 antibody tested (Fig no. 2.16B-C). Galectin-3-deficient $CD8^+$ T cells produced more IL-2 than WT $CD8^+$ T cells in response to anti-CD3/anti-CD28 antibody treatment (Fig no. 2.16D). We also stimulated splenocytes from galectin-3 KO and WT mice with anti-CD3/anti-CD28 antibodies and measured their proliferation and cytokine production. Similar to the response of $CD8^+$ T cell, total T cells that also included responding $CD4^+$ T cells from galectin-3 KO mice produced more IL-2 than their WT counterparts (Fig no. 2.16E).

A

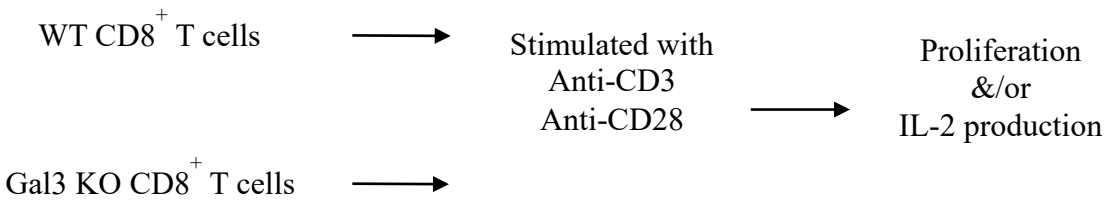

B

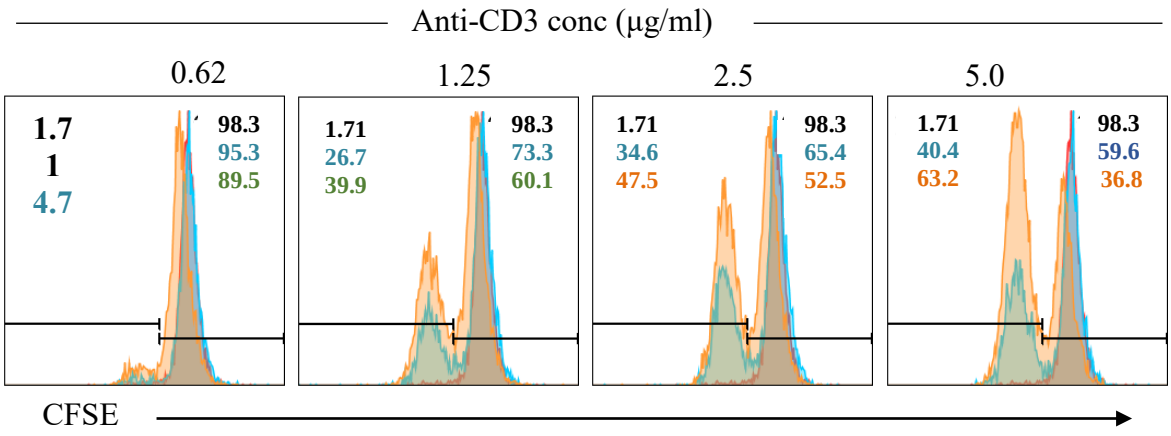

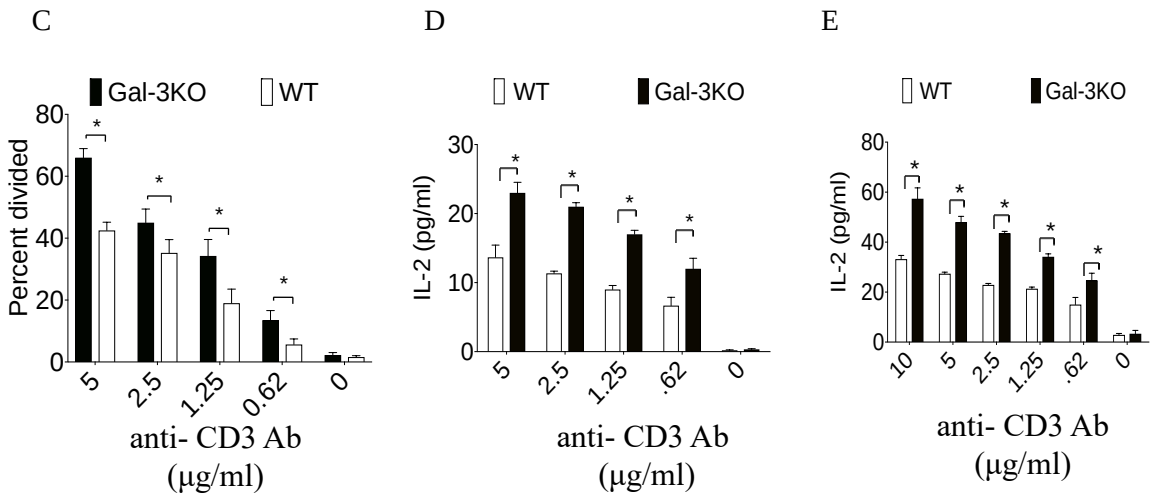

Figure no. 2.16. Cell autonomous intracellular expression of galectin-3 in CD8$^+$ T cells is responsible for regulating their proliferation and cytokine production. A. A schematic of the experiment is shown. CD8$^+$ T cells were MACS purified from WT and galectin-3 KO mice and labelled with CFSE. Labelled cells were then stimulated in vitro with indicated concentration of soluble anti-CD3 and 1μg/ml of anti-CD28. Dilution of CFSE in CD8$^+$ T cells was measured cytofluorimetrically and IL-2 levels were measured in the culture supernatants by sandwich ELISA. B. Histograms show the proliferation of WT and galectin-3 deficient CD8$^+$ T cells at indicated concentrations of anti-CD3. The numbers written in bold fonts represent the numbers of divided cells in unstimulated (black), WT (blue) and galectin-3 deficient CD8$^+$ T cells (orange). C. Bar diagram show the percentage of divided cells from galectin-3 KO and WT animals when stimulated with indicated concentrations of anti-CD3. D. Bar diagrams show IL-2 levels in the culture supernatants of WT and galectin-3 deficient cells. E. Total splenocytes isolated from WT and galectin-3 KO animals were stimulated with indicated concentrations of anti-CD3 and 1μg/ml of anti-CD28 for 60 hours and IL-2 levels were measured by ELISA. Bar diagrams show the levels (mean±SD) of IL-2 for three separate wells in WT and galectin-3 KO animals at indicated concentration of anti-CD3. The experiments were repeated three times with similar results.

A deficiency of galectin-3 in T cells is therefore responsible for their enhanced proliferation and cytokine production and galectin-3 could predominantly acts in a cell autonomous manner and intracellularly to inhibit T cell functions.

Galectin-3 deficiency enhances MHV68-specific $CD8^+$ T cell response

After demonstrating a regulatory intracellular function of galectin-3 during the immunological synapse formation, we explored whether a loss of galectin-3 expression has functional consequences in modulating a virus-specific $CD8^+$ T cell response. We infected WT and galectin-3 KO mice with MHV68 (Fig no. 2.17A) and measured the magnitude of virus-specific $CD8^+$ T cells isolated from spleens by MHC tetramer staining and ICCS assays. Galectin-3 KO animals mounted a stronger virus-specific $CD8^+$ T cell response than WT animals (Fig no. 17B-E). Using MHC tetramers, we investigated recognition of $CD8^+$ T cell epitopes derived from five different ORFs of MHV68. Both early (ORF9 and ORF75c) as well as late (ORF6, ORF8, ORF17 and ORF61) MHV68 antigens were examined (4, 5). Galectin-3 KO mice showed greater expansion of their virus-specific $CD8^+$ T cells than WT mice (Fig no. 2.17B-C). Intracellular cytokine assays were performed to measure IFN-γ producing cells in response to $H\text{-}2K^b$ and $H\text{-}2D^b$ -restricted peptides. The frequencies of cytokine-producing splenic $CD8^+$ T cells were significantly higher for most of the epitopes for galectin-3 KO animals than those for WT animals (Fig no. 2.17D and E). ORF61 and ORF75c-reactive $CD8^+$ T cells expanded to a greater extent than those recognizing other ORFs (Fig no. 2.17). $CD8^+$ T cells that recognize ORF61, a ribonucleotide reductase, may be critically involved in maintenance of viral latency (4, 5). ORF75c, a tegument protein of MHV68, exhibits ubiquitin E3 ligase activity and can target degradation of promyelocytic leukemia (PML), essential for the pathogenesis of γ-HV-induced transformation and in modulating apoptosis (50). An ORF75c null virus is compromised in its ability to establish latency as well (51). Thus, enhancing the frequency of $CD8^+$ T cells specific for ORF75c and ORF61 may be a means of interfering with γ-HV mediated pathogenesis. A lack of galectin-3 signaling in virus-specific $CD8^+$ T cells by enhancing their responsiveness could perhaps improve protection against this γ-HV.

A

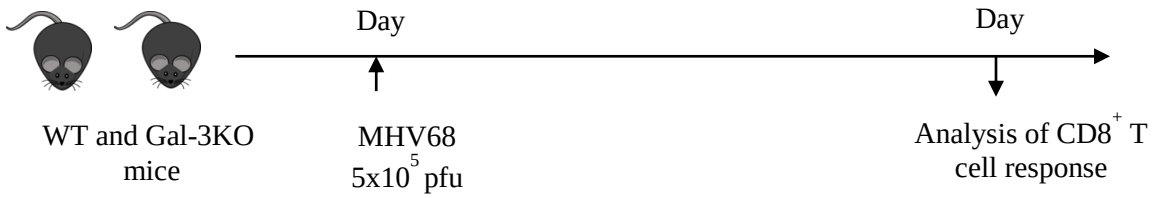
Day
Day
WT and Gal-3KO mice
MHV68 5x10^5 pfu
Analysis of CD8+ T cell response

B

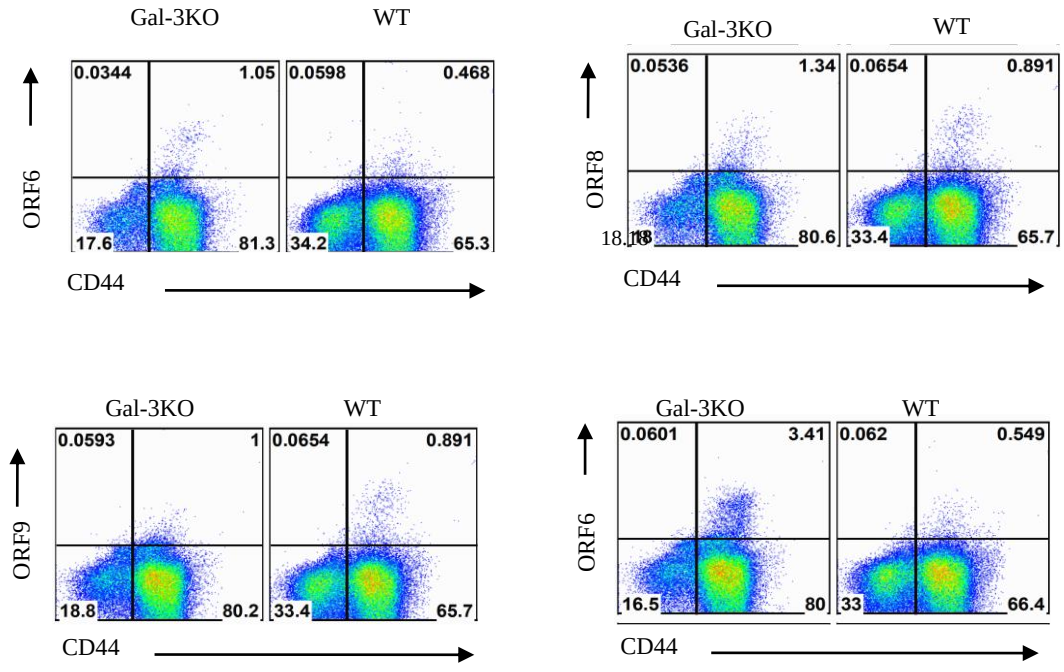
Gal-3KO
WT
ORF6
CD44
0.0344
1.05
17.6
81.3
0.0598
0.468
34.2
65.3
ORF8
0.0536
1.34
80.6
0.0654
0.891
33.4
65.7
ORF9
0.0593
1
18.8
80.2
0.0654
0.891
33.4
65.7
0.0601
3.41
16.5
80
0.062
0.549
33
66.4

C

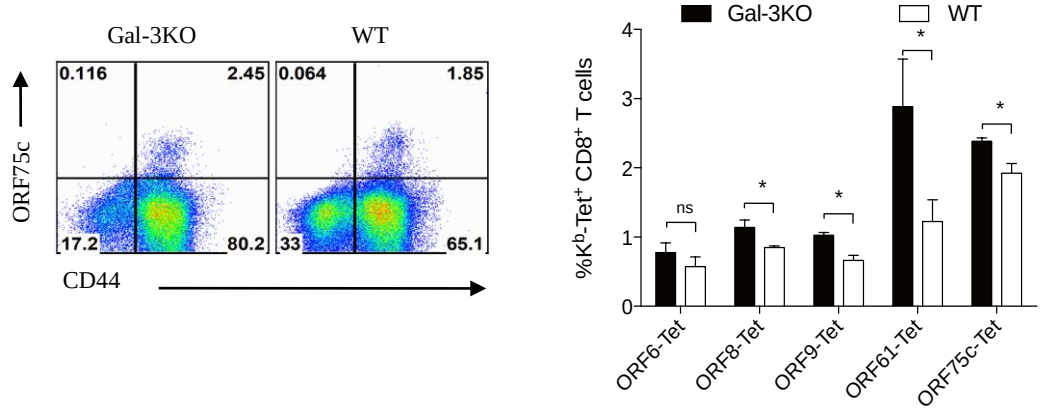
Gal-3KO
WT
ORF75c
CD44
0.116
2.45
17.2
80.2
0.064
1.85
33
65.1
%Kb-Tet+ CD8+ T cells
ns
*
ORF6-Tet
ORF8-Tet
ORF9-Tet
ORF61-Tet
ORF75c-Tet

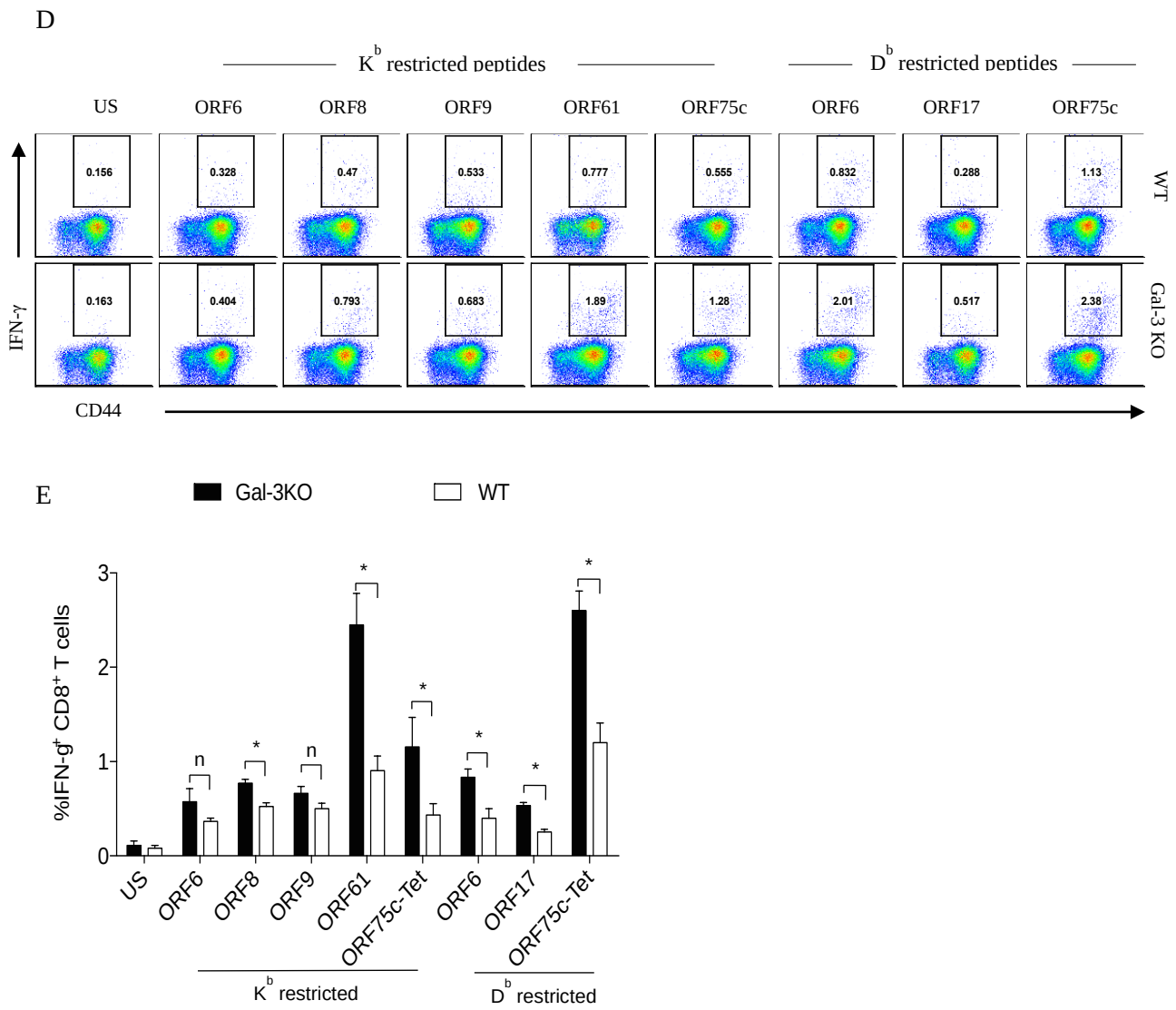

Figure no. 2.17. Galectin-3 deficiency enhances magnitudes of γ-HV specific CD8$^+$ T cells. A. A schematic of the experiment to investigate influence of galectin-3 in anti-MHV68 specific CD8$^+$ T cell responses. Galectin-3 KO and C57BL/6 WT mice were ip infected with MHV68 and splenocytes were analyzed for surface TCR expression and intracellular cytokine staining. B. Representative FACS plots show the frequencies of respective tetramer specific cells in spleen samples of infected WT and galectin-3 KO mice. Tetramers for respective ORFs were generated using a UV mediated photo cleavage reaction and the exchange was performed to displace conditional ligand with peptides sequences derived from the indicated ORFs of MHV68. C. Bar diagrams show the frequencies of respective peptide-specific CD8$^+$ T cells measured from at least four different animals per group. The experiments were repeated at least two times with similar results. D. Representative FACS

plots show IFN-γ producing $CD8^+$ T cells measured using ICCS assays. Splenocytes from WT and galectin-3 KO animals were stimulated with peptides derived from indicated ORFs of MHV68 and the cells were analyzed using flow cytometry. E. Bar diagrams show the frequencies (mean±SD) of IFN-γ producing cells reactive to class I MHC epitopes of indicated ORFs derived peptides measured for four WT and galectin-3 KO animals per group.

Enhanced MHV68 specific $CD8^+$ T cell response leads to more efficient viral control in galectin-3 KO mice

We asked whether or not a stronger anti-viral $CD8^+$ T cell response in galectin-3 KO mice would help control the virus more efficiently than in WT mice. Galectin-3 KO and WT animals were infected intranasaly with MHV68 so that we could measure replicating virus in lung tissues. The functionality of anti-viral $CD8^+$ T cells and viral titers in lung tissues of infected animals were then measured (Fig no. 2.18A). We measured the frequencies of activated $CD8^+$ T cells i.e., TIM-3^+, $CD44^+$ and TIM-3^+CD44^+ $CD8^+$ T cells in the mediastinal lymph nodes of MHV68-infected galectin-3 KO and WT mice (Fig no. 2.18B-E). TIM-3 expression on $CD8^+$ T cells marks antigen-experienced cells (52). More TIM-3^+CD8^+ T cells were present in the LN of galectin-3 KO animals (10.6%) than in WT animals (4.6%) (Fig no. 2.18B-E). Only a subset $CD44^{hi}CD8^+$ T cells expressed TIM-3 (Fig no. 2.18C). Galectin-3 KO animals also had more activated $CD8^+$ T cells ($CD44^{hi}$ $CD8^+$: 18% in WT and 31% in galectin-3 KO mice) (Fig no. 2.18D-E). The frequencies of IFN-γ positive $CD8^+$ T cells isolated from MLN were measured by ICCS assays in response to known MHV68-specific $CD8^+$ T cell targets. Seven out of these eight peptides evoked significantly more IFN-γ positive $CD8^+$ T cells in galectin-3 KO animals (Fig no. 2.18F-G).

This was true for both H-2K^{b}- and H-2D^{b}-restricted epitopes. Viral titers were measured in lung tissues of galectin-3 KO and WT mice and showed up to a 100-fold reduction in galectin-3 KO mice on 6 dpi (Fig no. 2.18H).

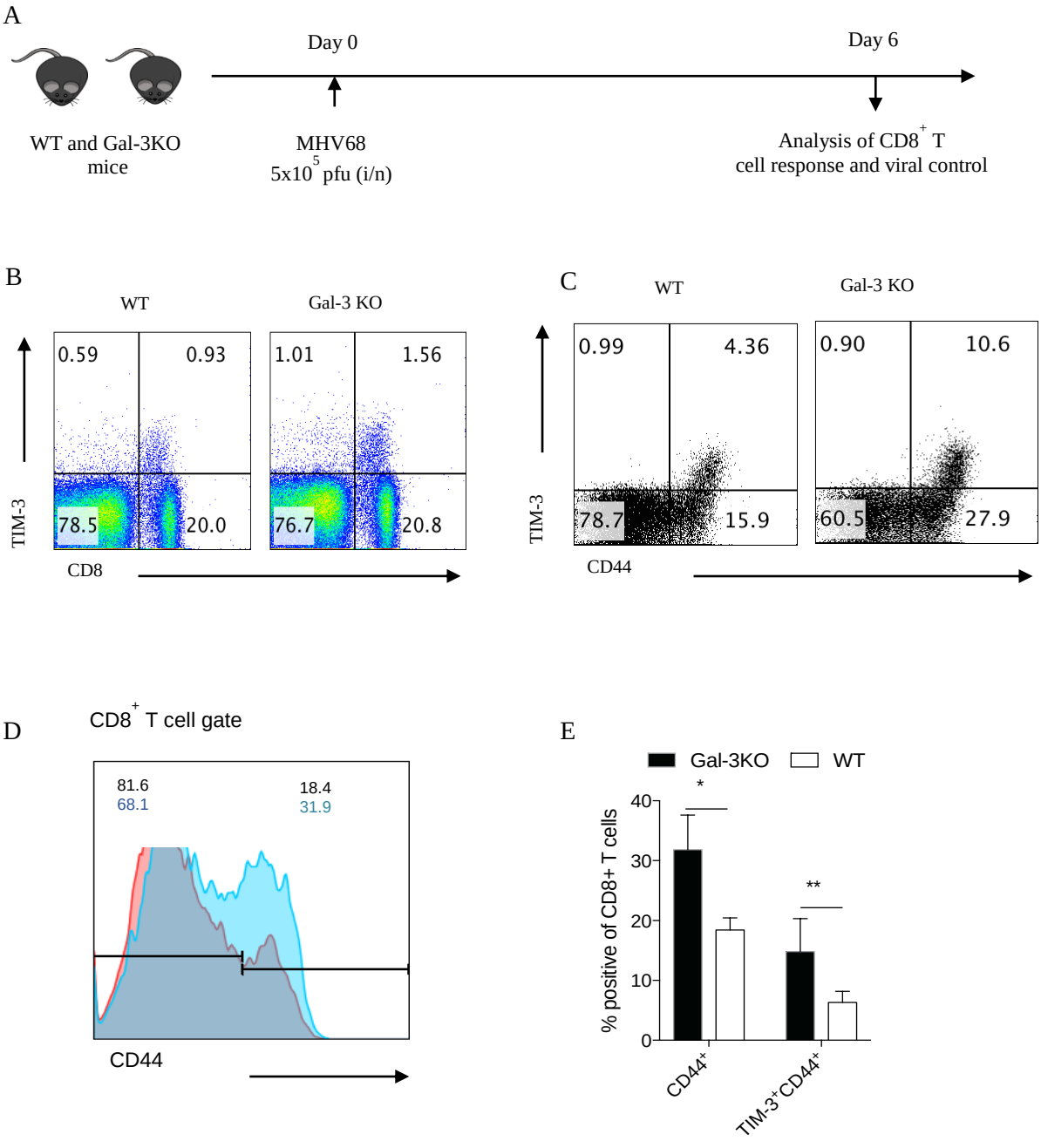

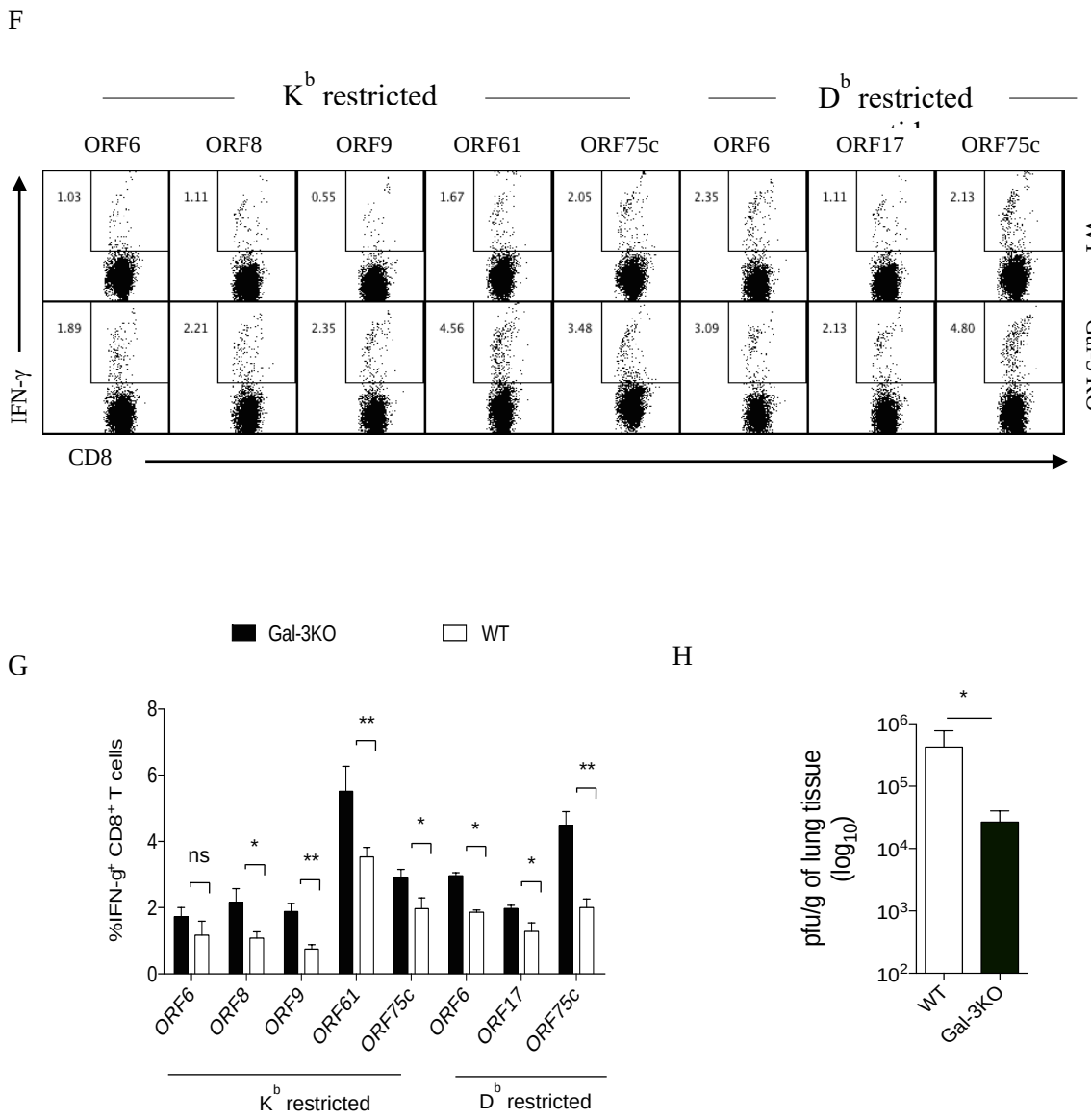

Figure no. 2.18. Galectin-3 deficient animals efficiently control γ-HV infection. A. A schematic of the experiments is shown. Galectin-3 KO and C57BL/6 WT mice were intranasally infected with $5x10^5$ pfu of MHV68. Mediastinal lymph nodes were analyzed at 6 dpi by surface staining and intracellular cytokine staining for measuring the phenotype and functions of $CD8^+$ T cells. Lungs were collected from the infected animals and the viral titers were measured. B. Representative FACS plots show the frequencies of TIM-3^+ activated $CD8^+$ T cells in live cell gate isolated from the lymph nodes of WT and galectin-3 KO mice. C. FACS plots of $CD8^+$ T cell gated population show the expression of CD44 and TIM-3 in $CD8^+$ T cells from WT and galectin-3 KO mice. D. Histograms show the expression of CD44 in gated $CD8^+$ T cells isolated from lymph nodes of WT and galectin-3 knockout mice. Numbers in overlaid histograms represent proportion of $CD44^{lo}$ and $CD44^{hi}$

populations of WT (regular font) and galectin-3 knockout (bold font). E. Bar diagrams show the percentage of $CD44^+$ and $CD44^+TIM\text{-}3^+$ $CD8^+$ T cells in WT and galectin-3 KO animals. F. FACS plots show the frequencies of IFN-γ positive cells in response to different MHC class I ($H\text{-}2K^b$ and $H\text{-}2D^b$ restricted) epitopes derived from ORFs of MHV68. G. Bar diagrams showing the frequencies (mean±SD) of IFN-γ producing $CD8^+$ T cells from a representative experiment in which four WT and four galectin-3 KO animals were used. H. Bar diagram shows virus titers in the lungs of the four animals each from WT and galectin-3 KO group at 6dpi. The experiments were repeated two times with similar results.

Galectin-3 contributed by cells other than $CD8^+$ T cells does not affect virus-induced expansion of specific $CD8^+$ T cells.

Many cell types, including T cell, B cells, myeloid cells and stromal cells may produce galectin-3 (19). We investigated whether or not galectin-3 contributed by cells other than $CD8^+$ T cells affects the expansion of virus-specific $CD8^+$ T cells. We transferred $50x10^3$ ORF8 TCR TN $CD8^+$ T cells into WT and galectin-3 knockout mice one day prior to MHV68 infection and measured the frequencies of expanded cells 7 days later (Fig no. 2.19A). Both endogenous and transferred ORF8-specific TN cells were analyzed. The proportion of activated and expanded ORF8 TCR TN $CD8^+$ T cells was similar in both the galectin-3 KO and WT animals (Fig no. 2.19B and C), suggesting a negligible effect of exogenous galectin-3 in the magnitude of γ-HV-specific $CD8^+$ T cells. Galectin-3 deficiency therefore may exert a cell-autonomous phenotype in $CD8^+$ T cells expanded during MHV68 infection.

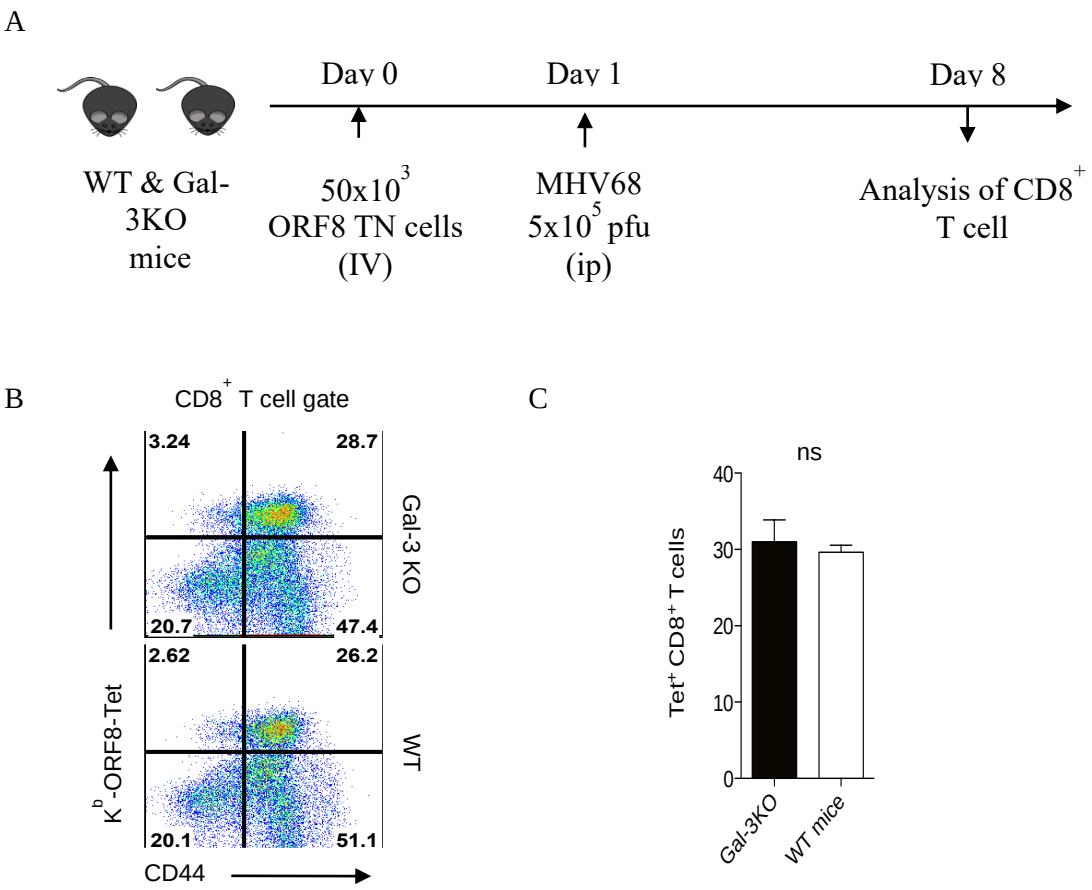

Figure no. 2.19. Expansion of virus-specific CD8$^+$ T cells during acute phase of infection is not influenced by exogenous galectin-3. A. A schematic of the experiments is shown. 50x10^3 ORF8 TN cells were adoptively transferred into WT and galectin-3 KO animals, which were then i.p. infected with MHV68. At 6dpi, the frequencies of ORF8-Tetramer positive cells were analyzed. B. Representative FACS plots show the frequencies of K^b-ORF8 tetramer positive cells in the spleen samples of animals. C. Bar diagrams show the frequencies (mean ± SD) of H-2K^b-ORF8 CD8$^+$ T cells obtained from three WT and galectin-3 KO animals. The experiments were repeated two times with similar results.

Discussion

Gamma-herpesviruses exhibit species-specificity. Insights into their pathogenesis are therefore gained using a natural host. The host correlates of protection to γ-herpesviruses may also be confounded by host specific elements. Due to an absence of a reliable animal model, studies of host pathogen interactions involving γ-HV have suffered. MHV68 infection of mice offers one of the accessible model for studying host immunity and immunopathology to such viruses (11). We previously generated a $CD8^+$ TCR TN mouse model that serves as a source of homogeneous γ-herpesviruses specific $CD8^+$ T cells (12). Such cells arguably provide physiological pattern subject to their genesis method. We performed RNA sequencing on naïve and activated MHV68-specific $CD8^+$ TCR TN T cells, the latter isolated in the acute phase of infection, to obtain insights into molecules and pathways that may be critical to their function. Genes for many transcripts encompassing different biological processes, cellular components, and classes of proteins and of diverse molecular function were differentially expressed. Many of these transcripts have not been reported previously to exhibit a similar expression pattern in the acute phase of other virus infections (32, 33). Further analysis showed that more than three hundred transcripts in our dataset were not mapped to the existing Gene Ontology database (Table 2.2). The transcriptional analysis of endogenous $CD8^+$ T cells is commonly confounded by representation of innumerable TCR affinities, as the analyzed cell population is heterogeneous. The transcriptomic data on differentiating single cell is limited but could provide valuable information. RNAseq data of differentiating TN $CD8^+$ T cells could provide further insight into their phenotypic and functional attributes. These RNAseq data could uncover new angles of attack to investigate $CD8^+$ T cell biology. Of course, not only transcription but also the translational status determines the fate of differentiating $CD8^+$ T cells (53). Numerous genes differentially expressed in activated TN $CD8^+$ T cells suggest

that during differentiation of T cells the translational machinery may be impaired, which could contribute to contraction of almost 95% of antigen-reactive $CD8^+$ T cells.

$CD8^+$ T cells expand massively to resolve the intracellular infection. Most of the expanded pathogen-specific effector cells are then contract (1). The mechanisms responsible for their induction, expansion and elimination are not entirely well understood and may very well show considerable heterogeneity, depending on the pathogen involved. The role of galectins in the pathogenesis of infection is beginning to be understood better (54). Galectins play diverse roles in immunity upon infection, in autoimmune diseases and cancer (55). Through direct interactions with the pathogen or by modulating the microenvironment in which pathogens reside, galectins can either promote or prevent viral infections (54). For example, galectin-1 could promote HIV infection of macrophages by directly binding to its surface glycoproteins and thereby serving as a bridge between the virus and immune cells (56, 57). Galectins can also help attract susceptible immune cells to sites of infection (58). Viruses such as HIV, EBV, Nipah virus and herpesvirus 1 modulate the expression of various galectins in host cells (54). One could therefore argue that galectin-3 deficiency might interfere with a productive replication of γ-HV such that the overall antigen levels are reduced. We observed enhanced anti-viral $CD8^+$ T cell immunity in galectin-3 KO mice which would rather represent an under estimation virus-specific $CD8^+$ T cells. Galectin-3 deficient animals mounted a stronger anti-MHV68 $CD8^+$ T cell response to seven out of eight epitopes, regardless of their restriction by different MHC haplotypes ($H\text{-}2K^b$ or $H\text{-}2D^b$). In doing so a better viral control was achieved. Similarly an enhanced expansion and cytokine production by co-receptor stimulated $CD8^+$ T cells was observed suggesting that disruption of galectin-3 signaling could enhance overall magnitude of T cell responses.

During activation of $CD8^+$ T cells, actin microfilaments help coalesce the glycoproteins involved in the formation of immunological synapse (16). Our RNAseq data showed up regulation of two members of the galectin family i.e., galectin-3 (up ~140-fold) and galectin-1 (up ~87-fold) in activated TN $CD8^+$ T cells during the acute phase of infection with MHV68. Galectin-3 has one CRD but exhibits a greater tendency to multimerize upon binding to glycoconjugates than other galectins (59). This effect is attributed to its non-lectin N-terminal domain, which is rich in proline and glycine residues (60). Therefore extensive studies deciphering the role of galectin-3 during initial stages of T cell activation have been performed. Accordingly, exposure of T cells to exogenous galectin-3 might cause their apoptosis, while endogenous expression of galectin-3 was found to exert an anti-apoptotic function (61). However, we earlier showed that activated $CD8^+$ T cells during HSV1 infection did not undergo apoptosis upon treatment with exogenous galectin-3 (52). Therefore, the influence of galectin-3 on immune cells could be context of concentration as well condition dependent.

Galectin-3 is recruited to the immunological synapse during activation of $CD4^+$ T cell response (46). In view of its up regulation in MHV68-specific TCR TN $CD8^+$ T cells, we investigated whether galectin-3 expression has functional consequences in resolving the infection. We find that galectin-3 expression was up regulated at transcriptional and at a protein product level upon viral infections as well in co-receptor stimulated $CD8^+$ T cells within 16 hours and the expression further increased on 3 days post stimulation (Fig no. 2.6&2.8). This was true for MHV68 as well as influenza virus expanded antigen-specific $CD8^+$ T cells thereby attesting to the fact that pathogen-specific elements and their interaction by host could play a role in fine tuning T cell responses (Fig no. 2.13 and 2.14.). The milieu generated during some chronic infection is enriched in inhibitory cytokines such as IL-10 that could promote the activity of glycosyltransferases such as Mgat5 that in turn

promoted the N-linked glycans modification for various surface proteins (62). Galectin-3 might interfere with the recruitment of such proteins during activation of T cells and thereby increasing the threshold of TCR signaling. This effect may be predominantly extracellular in nature. Our investigation focusing on intracellular versus extracellular involvement of galectin-3 in shaping T cell responses against γ-HV revealed predominantly an intracellular role of this molecule as the neutralization of extracellular galectin-3 either by α-lactose or by anti-galectin-3 antibody did not seem to influence the recruitment of galectin-3 to immune synapse or the proliferation of stimulated cells (Fig no. 2.10, 2.11, 2.12 and 15). The α-lactose treatment could also interfere with the activity of other galectins, which was also reflected in experiments investigating its role in the activation of T cells. Accordingly, in some of the experiment where α-lactose was added during the activation of $CD8^+$ T cells impaired their activation that might suggest the role of other players (Fig no. 2.12C). Therefore, the experiments aimed at the neutralization of galectin-3 function by an antibody provided more relevant information with respect to its intracellular versus extracellular role in the cellular activation (Fig no. 2.15). That the antibody used could affect extracellular galectin-3 neutralization was shown earlier (24, 48). Our experiments also demonstrate the binding of the antibody to extracellular galectin-3 (Fig no. 2.12E & F). Intracellular role of galectin-3 in fine tuning IS could be independent of CRD. Thus some studies did show such an effect that was majorly contributed by Chrps (63).

We observed that upon their co-culture with cognate-peptide pulsed APCs, galectin-3 rapidly recruited to the immunological synapse in $CD8^+$ T cells undergoing a primary as well as secondary stimulation (Fig no. 2.9-2.14). Expression of galectin-3 compromised the magnitude of virus-specific $CD8^+$ T cells to clear the virus, as galectin-3 deficient $CD8^+$ T cells showed an enhanced frequency for almost all the epitopes of MHV68. The ability of galectin-3 to constrain anti-viral immunity is counter intuitive but its presence at the

immunological synapse could help attenuate spontaneous activation of the TCR to avoid immunopathological reactions particularly to self-antigens (64). Development and maintenance of peripheral $CD8^+$ T cells requires sustained low affinity interactions that involve self-peptides loaded onto MHC I molecules (65). Therefore, the presence of galectin-3 at synapse could act as a break to constrain any possible hyperactivity. Galectin-3 is also thought to compromise the activity of cytotoxic $CD8^+$ T cells during some autoimmune diseases as well as in the tumor microenvironment (23, 66, 67). In a tumor environment the interaction of galectin-3 with T cells effector cytokine, IFN-γ compromised its protective function and the effect is extracellular in nature. However, how galectin-3 acts to constrain anti-viral $CD8^+$ T cell immunity during herpesviruses is still not understood and was elucidated in this study. We found that galectin-3 contributed by cells other than $CD8^+$ T cells had little influence in impairing the induction, activation and expansion of MHV68-specific TN $CD8^+$ T cells *in vivo* (Fig no. 2.19). The role for galectin-3 in $CD8^+$ T cells during a γ herpesvirus is thus cell-autonomous.

The distribution of single positive $CD4^+$ and $CD8^+$ T cells in the thymi of galectin-3 KO and WT animal were similar suggesting that during development of these cells galectin-3 may not be playing a major role and predominantly regulates reactivity of T cells in periphery (31). The observation that memory $CD8^+$ T cells when recalled by antigenic stimulation does induce the recruitment of regulatory galectin-3 to immune synapse can have implication in designing the regimen for priming and boosting vaccine specific $CD8^+$ T cell immunity. Our results suggest that modifying galectin-3 function in $CD8^+$ T cells and not in a generic manner could be considered as a strategy to enhance anti-viral $CD8^+$ T cell immunity, for example through disruption of its localization to the immune synapse by using small molecules or intrabodies or by manipulation of its glycosylation status or even by adjusting the expression levels of galectin-3 itself.

References

1. Ahmed, R., and D. Gray. 1996. Immunological memory and protective immunity: understanding their relation. *Science* 272: 54–60.

2. Zinkernagel, R. M. 1996. Immunology taught by viruses. *Science* 271: 173–8.

3. Wong, P., and E. G. Pamer. 2003. CD8 T C ELL R ESPONSES TO I NFECTIOUS P ATHOGENS. *Annu. Rev. Immunol.* 21: 29–70.

4. Freeman, M. L., K. G. Lanzer, T. Cookenham, B. Peters, J. Sidney, T.-T. Wu, R. Sun, D. L. Woodland, A. Sette, and M. A. Blackman. 2010. Two Kinetic Patterns of Epitope-Specific CD8 T-Cell Responses following Murine Gammaherpesvirus 68 Infection. *J. Virol.* 84: 2881–2892.

5. Gredmark-Russ, S., E. J. Cheung, M. K. Isaacson, H. L. Ploegh, and G. M. Grotenbreg. 2008. The CD8 T-Cell Response against Murine Gammaherpesvirus 68 Is Directed toward a Broad Repertoire of Epitopes from both Early and Late Antigens. *J. Virol.* 82: 12205–12212.

6. Amanna, I. J., M. K. Slifka, and S. Crotty. 2006. Immunity and immunological memory following smallpox vaccination. *Immunol. Rev.* 211: 320–337.

7. Moutaftsi, M., B. Peters, V. Pasquetto, D. C. Tscharke, J. Sidney, H.-H. Bui, H. Grey, and A. Sette. 2006. A consensus epitope prediction approach identifies the breadth of murine TCD8+-cell responses to vaccinia virus. *Nat. Biotechnol.* 24: 817–819.

8. Nash, A. A., and B. M. Dutia. 2008. Murine Gammaherpesvirus 68. In *Encyclopedia of Virology* Elsevier. 372–378.

9. Nash, A. A., B. M. Dutia, J. P. Stewart, and A. J. Davison. 2001. Natural history of murine gamma-herpesvirus infection. *Philos. Trans. R. Soc. Lond. B. Biol. Sci.* 356: 569–79.

10. Sehrawat, S., D. Kumar, and B. T. Rouse. 2018. Herpesviruses: Harmonious Pathogens but Relevant Cofactors in Other Diseases? *Front. Cell. Infect. Microbiol.* 8: 177.

11. Barton, E., P. Mandal, and S. H. Speck. 2011. Pathogenesis and Host Control of Gammaherpesviruses: Lessons from the Mouse. *Annu. Rev. Immunol.* 29: 351–397.

12. Sehrawat, S., O. Kirak, P.-A. Koenig, M. K. Isaacson, S. Marques, G. Bozkurt, J. P. Simas, R. Jaenisch, and H. L. Ploegh. 2012. CD8(+) T cells from mice transnuclear for a TCR that recognizes a single H-2K(b)-restricted MHV68 epitope derived from gB-ORF8 help control infection. *Cell Rep.* 1: 461–71.

13. Kirak, O., E.-M. Frickel, G. M. Grotenbreg, H. Suh, R. Jaenisch, and H. L. Ploegh. 2010. Transnuclear Mice with Predefined T Cell Receptor Specificities Against Toxoplasma gondii Obtained via SCNT. *Science (80-.).* 328: 243–248.

14. Mempel, T. R., S. E. Henrickson, and U. H. von Andrian. 2004. T-cell priming by dendriticcells in lymph nodes occurs in three distinct phases. *Nature* 427: 154–159.

15. Fooksman, D. R., S. Vardhana, G. Vasiliver-Shamis, J. Liese, D. A. Blair, J. Waite, C. Sacristán, G. D. Victora, A. Zanin-Zhorov, and M. L. Dustin. 2010. Functional anatomy of T cell activation and synapse formation. *Annu. Rev. Immunol.* 28: 79–105.

16. Dustin, M. L., and J. A. Cooper. 2000. The immunological synapse and the actin cytoskeleton: molecular hardware for T cell signaling. *Nat. Immunol.* 1: 23–29.

17. Viola, A., A. Lanzavecchia, Y. Sakakibara, and A. Lanzavecchia. 1996. T Cell Activation Determined by T Cell Receptor Number and Tunable Thresholds. *Science (80-.).* 273: 104–106.

18. Qian, D., and A. Weiss. 1997. T cell antigen receptor signal transduction. *Curr. Opin. Cell Biol.* 9: 205–12.

19. Hsu, D. K., H.-Y. Chen, and F.-T. Liu. 2009. Galectin-3 regulates T-cell functions. *Immunol. Rev.* 230: 114–127.

20. Van Kooyk, Y., and G. A. Rabinovich. 2008. Protein-glycan interactions in the control of innate and adaptive immune responses. *Nat. Immunol.* 9: 593–601.

21. Rabinovich, G. A., L. G. Baum, N. Tinari, R. Paganelli, C. Natoli, F. T. Liu, and S. Iacobelli. 2002. Galectins and their ligands: amplifiers, silencers or tuners of the inflammatory response? *Trends Immunol.* 23: 313–20.

22. Hughes, R. C. 1999. Secretion of the galectin family of mammalian carbohydrate-binding proteins. *Biochim. Biophys. Acta* 1473: 172–85.

23. Kouo, T., L. Huang, A. B. Pucsek, M. Cao, S. Solt, T. Armstrong, and E. Jaffee. 2015. Galectin-3 Shapes Antitumor Immune Responses by Suppressing CD8+ T Cells via LAG-3 and Inhibiting Expansion of Plasmacytoid Dendritic Cells. *Cancer Immunol. Res.* 3: 412–423.

24. Gordon-Alonso, M., T. Hirsch, C. Wildmann, and P. van der Bruggen. 2017. Galectin-3 captures interferon-gamma in the tumor matrix reducing chemokine gradient production and T-cell tumor infiltration. *Nat. Commun.* 8: 793.

25. Sehrawat, S., P.-A. Koenig, O. Kirak, C. Schlieker, M. Fankhauser, and H. L. Ploegh. 2013. A catalytically inactive mutant of the deubiquitylase YOD-1 enhances antigen cross-presentation. *Blood* 121: 1145–1156.

26. Altman, J. D., P. A. Moss, P. J. Goulder, D. H. Barouch, M. G. McHeyzer-Williams, J. I. Bell, A. J. McMichael, and M. M. Davis. 1996. Phenotypic analysis of antigen-specific T lymphocytes. *Science* 274: 94–6.

27. Bakker, A. H., R. Hoppes, C. Linnemann, M. Toebes, B. Rodenko, C. R. Berkers, S. R. Hadrup, W. J. E. van Esch, M. H. M. Heemskerk, H. Ovaa, and T. N. M. Schumacher. 2008. Conditional MHC class I ligands and peptide exchange technology for the human MHC gene products HLA-A1, -A3, -A11, and -B7. *Proc. Natl. Acad. Sci. U. S. A.* 105: 3825–30.

28. Pavlopoulos, G. A., M. Secrier, C. N. Moschopoulos, T. G. Soldatos, S. Kossida, J. Aerts, R. Schneider, and P. G. Bagos. 2011. Using graph theory to analyze biological networks. *BioData Min.* 4.

29. Dunn, K. W., M. M. Kamocka, and J. H. McDonald. 2011. A practical guide to evaluating colocalization in biological microscopy. *AJP Cell Physiol.* 300: C723–C742.

30. Demetriou, M., M. Granovsky, S. Quaggin, and J. W. Dennis. 2001. Negative regulation of T-cell activation and autoimmunity by Mgat5 N-glycosylation. *Nature* 409: 733–739.

31. Kaur, M., D. Kumar, V. Butty, S. Singh, A. Esteban, G. R. Fink, H. L. Ploegh, and S. Sehrawat. 2018. Galectin-3 Regulates γ-Herpesvirus Specific CD8 T Cell Immunity. *iScience* 9: 101–119.

32. Best, J. A., D. A. Blair, J. Knell, E. Yang, V. Mayya, A. Doedens, M. L. Dustin, A. W. Goldrath, and T. I. G. P. Immunological Genome Project Consortium. 2013. Transcriptional

insights into the CD8(+) T cell response to infection and memory T cell formation. *Nat. Immunol.* 14: 404–12.

33. Wherry, E. J., S.-J. Ha, S. M. Kaech, W. N. Haining, S. Sarkar, V. Kalia, S. Subramaniam, J. N. Blattman, D. L. Barber, and R. Ahmed. 2007. Molecular Signature of CD8+ T Cell Exhaustion during Chronic Viral Infection. *Immunity* 27: 670–684.

34. Kaech, S. M., and W. Cui. 2012. Transcriptional control of effector and memory CD8+ T cell differentiation. *Nat. Rev. Immunol.* 12: 749–761.

35. Donato, R., B. R. Cannon, G. Sorci, F. Riuzzi, K. Hsu, D. J. Weber, and C. L. Geczy. 2013. Functions of S100 proteins. *Curr. Mol. Med.* 13: 24–57.

36. Miyagawa, I., S. Nakayamada, K. Nakano, K. Yamagata, K. Sakata, K. Yamaoka, and Y. Tanaka. 2017. Induction of Regulatory T Cells and Its Regulation with Insulin-like Growth Factor/Insulin-like Growth Factor Binding Protein-4 by Human Mesenchymal Stem Cells. *J. Immunol.* 199: 1616–1625.

37. Lin, L., S. W. Yee, R. B. Kim, and K. M. Giacomini. 2015. SLC transporters as therapeutic targets: emerging opportunities. *Nat. Rev. Drug Discov.* 14: 543–60.

38. Böhmer, C., A. Bröer, M. Munzinger, S. Kowalczuk, J. E. J. Rasko, F. Lang, and S. Bröer. 2005. Characterization of mouse amino acid transporter B ^{0} AT1 (slc6a19). *Biochem. J.* 389: 745–751.

39. Gay, O., B. Gilquin, F. Nakamura, Z. A. Jenkins, R. McCartney, D. Krakow, A. Deshiere, N. Assard, J. H. Hartwig, S. P. Robertson, and J. Baudier. 2011. RefilinB (FAM101B) targets filamin A to organize perinuclear actin networks and regulates nuclear shape. *Proc. Natl. Acad. Sci. U. S. A.* 108: 11464–9.

40. Clark, M. C., and L. G. Baum. 2012. T cells modulate glycans on CD43 and CD45 during development and activation, signal regulation, and survival. *Ann. N. Y. Acad. Sci.* 1253: 58–67.

41. Toscano, M. A., G. A. Bianco, J. M. Ilarregui, D. O. Croci, J. Correale, J. D. Hernandez, N. W. Zwirner, F. Poirier, E. M. Riley, L. G. Baum, and G. A. Rabinovich. 2007. Differential glycosylation of TH1, TH2 and TH-17 effector cells selectively regulates susceptibility to cell death. *Nat. Immunol.* 8: 825–834.

42. Kaech, S. M., J. T. Tan, E. J. Wherry, B. T. Konieczny, C. D. Surh, and R. Ahmed. 2003. Selective expression of the interleukin 7 receptor identifies effector CD8 T cells that give rise to long-lived memory cells. *Nat. Immunol.* 4: 1191–1198.

43. Slebioda, T. J., T. F. Rowley, J. R. Ferdinand, J. E. Willoughby, S. L. Buchan, V. Y. Taraban, and A. Al-Shamkhani. 2011. Triggering of TNFRSF25 promotes CD8+ T-cell responses and anti-tumor immunity. *Eur. J. Immunol.* 41: 2606–2611.

44. Geserick, P., F. Kaiser, U. Klemm, S. H. E. Kaufmann, and J. Zerrahn. 2004. Modulation of T cell development and activation by novel members of the Schlafen (slfn) gene family harbouring an RNA helicase-like motif. *Int. Immunol.* 16: 1535–1548.

45. Wherry, E. J., and R. Ahmed. 2004. Memory CD8 T-cell differentiation during viral infection. *J. Virol.* 78: 5535–45.

46. Chen, H.-Y., A. Fermin, S. Vardhana, I.-C. Weng, K. F. R. Lo, E.-Y. Chang, E. Maverakis, R.-Y. Yang, D. K. Hsu, M. L. Dustin, and F.-T. Liu. 2009. Galectin-3 negatively regulates TCR-mediated CD4+ T-cell activation at the immunological synapse. *Proc. Natl. Acad. Sci. U. S. A.* 106: 14496–501.

47. Demotte, N., V. Stroobant, P. J. Courtoy, P. Van Der Smissen, D. Colau, I. F. Luescher, C. Hivroz, J. Nicaise, J.-L. Squifflet, M. Mourad, D. Godelaine, T. Boon, and P. van der Bruggen. 2008. Restoring the Association of the T Cell Receptor with CD8 Reverses Anergy in Human Tumor-Infiltrating Lymphocytes. *Immunity* 28: 414–424.

48. Yip, P. K., A. Carrillo-Jimenez, P. King, A. Vilalta, K. Nomura, C. C. Chau, A. M. S. Egerton, Z.-H. Liu, A. J. Shetty, J. L. Tremoleda, M. Davies, T. Deierborg, J. V. Priestley, G. C. Brown, A. T. Michael-Titus, J. L. Venero, and M. A. Burguillos. 2017. Galectin-3 released in response to traumatic brain injury acts as an alarmin orchestrating brain immune response and promoting neurodegeneration. *Sci. Rep.* 7: 41689.

49. Jennings, R. N., J. M. Grayson, and E. S. Barton. 2014. Type I interferon signaling enhances CD8+ T cell effector function and differentiation during murine gammaherpesvirus 68 infection. *J. Virol.* 88: 14040–9.

50. Ling, P. D., J. Tan, J. Sewatanon, and R. Peng. 2008. Murine Gammaherpesvirus 68 Open Reading Frame 75c Tegument Protein Induces the Degradation of PML and Is Essential for Production of Infectious Virus. *J. Virol.* 82: 8000–8012.

51. Gaspar, M., M. B. Gill, J.-B. Lösing, J. S. May, and P. G. Stevenson. 2008. Multiple Functions for ORF75c in Murid Herpesvirus-4 Infection. *PLoS One* 3: e2781.

52. Sehrawat, S., P. B. J. Reddy, N. Rajasagi, A. Suryawanshi, M. Hirashima, and B. T. Rouse. 2010. Galectin-9/TIM-3 Interaction Regulates Virus-Specific Primary and Memory CD8+ T Cell Response. *PLoS Pathog.* 6: e1000882.

53. Araki, K., M. Morita, A. G. Bederman, B. T. Konieczny, H. T. Kissick, N. Sonenberg, and R. Ahmed. 2017. Translation is actively regulated during the differentiation of CD8+ effector T cells. *Nat. Immunol.* 18: ni.3795.

54. Vasta, G. R. 2009. Roles of galectins in infection. *Nat. Rev. Microbiol.* 7: 424–438.

55. Rabinovich, G. A., and M. A. Toscano. 2009. Turning "sweet" on immunity: galectin–glycan interactions in immune tolerance and inflammation. *Nat. Rev. Immunol.* 9: 338–352.

56. Ouellet, M., S. Mercier, I. Pelletier, S. Bounou, J. Roy, J. Hirabayashi, S. Sato, and M. J. Tremblay. 2005. Galectin-1 acts as a soluble host factor that promotes HIV-1 infectivity through stabilization of virus attachment to host cells. *J. Immunol.* 174: 4120–6.

57. Mercier, S., C. St-Pierre, I. Pelletier, M. Ouellet, M. J. Tremblay, and S. Sato. 2008. Galectin-1 promotes HIV-1 infectivity in macrophages through stabilization of viral adsorption. *Virology* 371: 121–129.

58. Sano, H., D. K. Hsu, L. Yu, J. R. Apgar, I. Kuwabara, T. Yamanaka, M. Hirashima, and F. T. Liu. 2000. Human galectin-3 is a novel chemoattractant for monocytes and macrophages. *J. Immunol.* 165: 2156–64.

59. Lepur, A., E. Salomonsson, U. J. Nilsson, and H. Leffler. 2012. Ligand induced galectin-3 protein self-association. *J. Biol. Chem.* 287: 21751–6.

60. Menon, R. P., and R. C. Hughes. 1999. Determinants in the N-terminal domains of galectin-3 for secretion by a novel pathway circumventing the endoplasmic reticulum-Golgi complex. *Eur. J. Biochem.* 264: 569–576.

61. Fukumori, T., Y. Takenaka, N. Oka, T. Yoshii, V. Hogan, H. Inohara, H. Kanayama, H.-R. C. Kim, and A. Raz. 2004. Endogenous Galectin-3 Determines the Routing of CD95 Apoptotic Signaling Pathways. *Cancer Res.* 64: 3376–3379.

62. Smith, L. K., G. M. Boukhaled, S. A. Condotta, S. Mazouz, J. J. Guthmiller, R. Vijay, N. S. Butler, J. Bruneau, N. H. Shoukry, C. M. Krawczyk, and M. J. Richer. 2018. Interleukin-10 Directly Inhibits CD8+ T Cell Function by Enhancing N-Glycan Branching to Decrease Antigen Sensitivity. *Immunity* 48: 299–312.e5.

63. Bawumia, S., E. A. M. Barboni, R. P. Menon, and R. C. Hughes. 2003. Specificity of interactions of galectin-3 with Chrp, a cysteine- and histidine-rich cytoplasmic protein. *Biochimie* 85: 189–194.

64. Radosavljevic, G., V. Volarevic, I. Jovanovic, M. Milovanovic, N. Pejnovic, N. Arsenijevic, D. K. Hsu, and M. L. Lukic. 2012. The roles of Galectin-3 in autoimmunity and tumor progression. *Immunol. Res.* 52: 100–110.

65. Ziegler, A., C. A. Müller, R. A. Böckmann, and B. Uchanska-Ziegler. 2009. Low-affinity peptides and T-cell selection. *Trends Immunol.* 30: 53–60.

66. Nangia-Makker, P., V. Balan, and A. Raz. 2008. Regulation of Tumor Progression by Extracellular Galectin-3. *Cancer Microenviron.* 1: 43–51.

67. Fortuna-Costa, A., A. M. Gomes, E. O. Kozlowski, M. P. Stelling, and M. S. G. PavÃ£o. 2014. Extracellular Galectin-3 in Tumor Progression and Metastasis. *Front. Oncol.* 4: 138.

Chapter 3

Attempts at modifying intracellular galectin-3 using small molecule inhibitors and specific intrabodies

In this chapter “our” and “we” refers to me and co-investigator. My contribution in the chapter includes (1) Selection of the topic (2) Compiling and interpretation of the literature (3) Designing experiments (4) understanding and interpretation of the results (5) Preparation of graphs and figures (6) Writing and editing

Abstract

Galectin-3 produced by many cell types is critically involved in counter-regulation of T cell responses during diseases caused by cancers, autoimmune diseases as well as infections. Intracellular galectin-3 seemingly plays a predominant negative regulatory function during the induction as well as re-stimulation of γ-HV specific $CD8^+$ T cells by virtue of its recruitment to the immunological synapse to regulate their efficient activation. Sugar based molecules that can efficiently compete for carbohydrate binding sites of galectin-3 have shown beneficial effects to modulate disease outcome but their intracellular targeting and specificity remained major hurdles. We explored the utility of single domain antibodies to address these issues. We generated a phage display library of $2.2x10^6$ clones of sdAbs using genetic scaffold of rearranged VHH derived from camelids. We then selected five clones using recombinant galectin-3 as the bait and demonstrated their binding affinity to galectin-3 by western blotting. We also demonstrated the intracellular expression of single domain antibodies using an in-house modified retroviral vector. Our results therefore pave the way for intracellular targeting of galectin-3 using intrabodies.

Introduction

Galectins are the β-galactoside binding lectins and currently constitute a family of over 15 members (1). Galectin-3 is an extensively studied member, a feat attributed to its involvement in capacious conditions ranging from tumors to autoimmunities. There is evidence that galectin-3 could modulate the pathogenesis of infectious diseases caused by parasites, bacteria as well as some viruses. However, there is ambiguity in its mechanisms of action as it relates to its functioning intracellulary or in the extracellular spaces. In the previous chapter we have demonstrated that intracellular galectin-3 hampers activation of $CD8^+$ T cells during γ-herpesvirus infections Therefore, to achieve an adequate response, galectin-3 function might have to be modified selectively, both during the primary as well as secondary stimulation of $CD8^+$ T cells. Thus, the inherent role of regulatory molecules such as galectin-3 could be to control excessive inflammation and prevent any adverse autoimmune response (2). Therefore, different strategies that involve genetic disruption chemically synthesised small molecules, plants derived products, and conventional antibodies have been tested. As galectins have CRDs to bind sugar moieties, carbohydrates based inhibitors were obvious choice for targeting their functions. Some examples of these inhibitors include GR-MD-02 (Galactoarabino-rhamnogalaturonate),GM-CT-01(galactomannan isolated from seeds of Cyamopsis tetragonoloba), G3-C12 (ANTPCGPYTHDCPVKR peptide), HH1-1 (arabinogalactan polysaccharide derived from safflower), TD139 (3,3'-Dideoxy-3,3'-bis-[4-(3-fluorophenyl) -1H-1,2,3- triazol-1-yl]-1,1' – sulfanediyl -di- ß-D- galactopyranoside; (2S,3R,4S,5R,6R)-4- [4-(3-Fluorophenyl)triazol-1-yl] -2-[(2S,3R,4S,5R,6R) -4-[4-(3-fluorophenyl)triazol-1-yl]- 3,5-dihydroxy-6-(hydroxymethyl) oxan-2-yl] sulfanyl-6-(hydroxymethyl)oxane-3,5-diol) (3–5). However, the specificity and cell penetrability remained one of the major challenges for such compounds. Monoclonal antibodies targeting either the CRD (clone; 14D11.2D2) or the N-terminal region

of galectin-3 (clone 1F5.D4 & clone 7D4.A1) conferred the affinity and much needed specificity for the respective regions but such binders failed to penetrate the cells and therefore discouraged their optimal utility in targeting galectin-3 in live cells (6). For an inhibitor to target a protein intracellularly, it should be stable in the cellular environment, has to have a smaller molecular mass and should be able to bind to its counter structures with specificity and greater affinity.

A class antibodies could potentially accomplish aforesaid actions yielding appropriate aftereffects. These are the single domain antibodies (sdAb) that are the actual antigen binding regions of heavy chain antibodies (HCAbs) known to exist in all the members of family camelidae and cartilaginous fishes (7, 8). Unlike conventional antibodies, such immunoglobulins lack both light chains as well as C_H1 domain (9). Their mere existence and how could an antibody molecule in absence of CDRs contributed by light chains can bind to their complementary counter structures startled many. The first clue came from the sequence analyses of such antibodies. Thus, C_H1 domain could possibly have been deleted because of a single point mutation (G to A transition) at the conserved 5' splicing site of the intron allowing an alternative splicing of the heavy chain to eliminate C_H1 domain (10). The removal of C_H1 domain is likely to make its association with light chains superfluous. The question next in order was about the stability of these antibodies in the absence of light chains. The conserved hydrophobic residues in the framework region 2 of the variable domain were replaced by hydrophilic amino acids that could counterpoise the loss of light chain and yield functional products good for all practical purposes (9). However many more questions remain unanswered about the biogenesis of such binders, but their natural existence and impending adoption animated molecular biologists, biotechnologist and immunologists alike to expedite the exploitability of their unreached yet useful potential as biological reagents. Recombinant DNA technology admixed with chemical biology approaches were

employed to generate uncountable and immensely useful ambidextrous biological tools to decipher biological events. The sequence of events begin with the library generation, surface display of such binders using well characterised microbes such as yeast, bacteriophages or even the subcellular organelles such as ribosomes followed by selection procedures. The most favoured selection process is the biopanning that involves immobilising the biomolecule of interest on synthetic solid surfaces followed by establishing and disrupting interactions to select out and amplifying the sequence of choice (11). These procedures made it possible to generate binders in literally inexhaustible supply. Because of their small size i.e. 10-15kDa such binders are also called one of the followings: domain antibodies, nanobinders, nanobodies, monbodies, VHH or sdAbs (12). Such terminologies are used interchangeably without discrimination.

Some of the unique features of VHH include: a) Their molecular weight ranges from 10-15 kDa. Small size however makes them to pass through glomerulus filtration system within few hours thereby limiting the retention. However, depending upon the requirement, the retention time could be altered by approaches such as their cross linking with serum albumins or polyethylene glycol (13). b) The complementary determining region 3 (CDR3) is extended and can therefore form paratope that can recognise hidden or the cryptic epitopes usually inaccessible to paratopes of conventional antibodies. The enlarged CDR3 is further stabilised by extra disulphide bonds between CDR1 and CDR3 (14). c) Such binders can withstand the extreme temperatures as well as pH conditions (15). Due to this property, they can be given orally or can be used in tropical countries where temperature fluctuations are all the more common. d) VHH exhibit greater homology with human VH, making it unlikely to evoke host immune responses, when injected *in vivo* for different purposes (9). e) VHHs are soluble in most aqueous solutions and can penetrate the tissues including blood brain barrier (16).

sdAbs libraries are prepared by cloning the specific amplicon encoding for VHH in phagemid vectors followed by biopanning for the desired antigen using phage display technology (17). This technique was first introduced by Prof. George P. Smith in 1985, since then it has come of age and is extensively used to display peptides and proteins on the surface of bacteriophages. It requires three components i.e. the phagemid vector for cloning of VHH genes, TG1 strain of *E. coil* for the transformation and expression of VHH and helper phage particles for display of VHH as a fusion product with one of the coat protein on its surface. A unique feature or distinct property which makes phagemids different from the plasmid is the presence of f1 ori sites for bacteriophage to allow for replication like a single stranded DNA and pack the foreign genes into phage particles. Apart from that they have pIII or pVIII protein encoding gene for incorporating inframe the foreign gene that could be expressed as fusion protein displayed on the surface of bacteriophage (Fig no. 3.1). For protein display on the surface either the minor coat proteins i.e. pIII or major coat protein i.e. pVIII are designated. Choice of phage protein partner depends on the desired affinity vs avidity effect of the VHH for specific antigen. The VHH genes are cloned into phagemid vector followed by its transformation into TG1 bacterial strain. TG1 is a suppressor strain which does not recognise the stop codon (TGA) so it encodes protein beyond TGA and express the VHH as fusion protein but when the same phagemid is transformed in non-suppressor strains which can recognise the amber stop codon then stop protein synthesis after TGA codon. This causes the proteins to be displayed on the surface of bacteriophage to be selected against the antigen of choice by biopanning. Specific binders can be eluted either by organic solvents or acidic pH buffers. Eluted phages containing phagemids are further amplified by infecting TG1 bacteria or analysing by sequencing. Upon selection of binders the VHH is further subcloned in a desirable vector either to purify the product or express these antibodies intracellularly as intrabodies.

Materials and methods

Primers used

All the primers used for cloning, amplification and site directed mutagenesis are provided in table 3.1.

Table no. 3.1: A complete listing of all the primers used.

S.No.	Primer name	Binding region	Nucleotide sequence
1.	CALL001	Forward primer – leader sequence to CH2 exon	GTCCTGGCTGCTCTTCTACAAGG
2.	CALL002	Reverse primer – CH2 exon to leader sequence	GGTACGTGCTGTTGAACTGTTCC
3.	MKS04	forward primer for phage display- *Xho I*	TCACTCGAGATGGATGTGCAGCTGCAGGAGTC
4.	MKS05	reverse primer for phage display- *Not I* (nested with tag)	GGAGTGCGGCCGCTGGAGA
5.	MKS06	forward primer for phage display- *Nco I* (Nested)	TGCCATGGATGTGCAGCTGCAGGAGTCTG
6.	MKS07	reverse primer for phage display- *Bam HI* (nested)	CGGGATCCCTAGTGGTGATGGTGATGATGACTAGTGCGGCCGCTGGAGACG
7.	MKS08	reverse primer for phage display- *Bam HI* (nested , without tag)	CGGGATCCTCAACTAGTGCGGCCGCTGGAGACG
8.	MKS09	5’ sequencing primer -specific to vector	GTTGTGTGGAATTGTGAGCGG
9.	MKS10	3’ sequencing primer -specific to vector	CCACAGACAGCCCTCATAG
10.	MKS11	Forward primer for phage display- *Nco I* (Nested) (plasmid and phagemid both)	CATGCCATGGATGTTCAGCTGCAAGAGTCTGGAGG
11.	MKS12	Reverse primer for phage display- *Xho I* (Nested) (only plasmid insertion)	CCGCTCGAGTCGTCCGCTGGAGACGGTGACCTG
12.	MKS13	reverse primer for phage display- *Bam HI* (Nested) (plasmid as template and	CGCGGATCCATCTCAGTGGTGGTGGTG

		phagemid insertion)	
13.	MKS14	Reverse primer for phage display *Kpn I* (Nested)	CAAGGGTACCTCGTCCGCTG GAGACGGTGACCTG
14.	MKS15	Reverse primer for phage display- *Xho I* replaced by *Kpn I* (Nested) (for modified phagemid)	GTGGTGGTGGTGATGGTGGG TACCTCGTCCGCTGGAGAC
15.	MKS18	Forward primer for SDM	CTGGCAGCTCAGTTGGCCTCC ATGGCCCAGGTGC
16.	MKS19	Reverse primer for SDM	GCACCTGGGCCATGGAGGCC AACTGAGCTGCCAG
17.	MKS22	Reverse primer of VHH- FR4	GAAATGCGGCCGCTGTGGAG ACGGTGACCTG
18.	MKS23	Forward primer of VHH- FR1	GGCCTCCATGGCCGATGTTCA ACTGCAGGAGTCAGGAGGAG GCTCG
19.	MKS24	Reverse primer to add *myc* tag at 3'of retroviral vector backbone	GGGACCCAGGTCACCGTCTC CACAGCGGCCGCGGAGCAGA AGCTGATCTCAGAGGAGGAC CTGAATTCGCC
20.	LTV1	Forward primer to include *Age I* at 5'of VHH	CTAGACCGGTCCATGGCCGA TGTTCAACTGCAGGAGTC
21.	LTV2	Reverse Primer to include *Eco RI* at 3'of VHH	CGGGAATTCGCGGCCGCTGT GGAGACGGTGACCTGG
22.	pMKO.1 GFP FP	Forward primer for sequencing-specific to vector	GCGCCGGAATTGAAGATCTG TCG
23.	pMKO.1 GFP RP	Reverse primer for sequencing-specific to vector	GGTCGACCACTGTGCTGGCG AATTCAAAA
24.	SV40 FP	Forward primer for SV40 promoter (*Bgl II* site)	CCGGCTGTGGAATAGATCTG TGTGTCAGTTAG
25.	SV40 RP	Reverse primer for SV40 promoter (*Age I* site)	GTTAAGCCAGTAAGCTTACC GGTTTTGCAAAAGCCTAGGC C
26.	Gal3 FP	Forward primer for Galectin-3 (*Nco I* site)	GTCCACCATGGATATGGCAG ACAGCTTTTCGCTTAAC
27.	Gal3 RP	Reverse primer for Galectin-3 (*Not I* site)	ATATGCGGCCGCGATCATGG CGTGGTTAGCACTGGTGAGG
28.	T7 promoter	Binds to promoter	TAATACGACTCACTATAGGG
29.	T7 terminator	Binds to terminator sequence	GCTAGTTATTGCTCAGCGG

Cloning of recombinant Galectin-3

RNA was isolated from $1x10^6$ RAW macrophages by trizol method (18). cDNA was then synthesized by using cDNA synthesis kit from TAKARA. Gal-3 was amplified using 2% cDNA as template 500nM of each primer, 200µM dNTP, 1.5mM extra $MgCl_2$ and 1U of phusion polymerase in 1X HF buffer. The final volume of reaction mixture was made upto 100µl by using MQ. One cycle of initial denaturation at 98°C for 30sec, 30 cycles involving denaturation at 98°C for 15 sec, annealing at 64.8°C for 35 sec and extension for 45 sec at 72°C and final extension for 5 minutes at 72°C was performed. PCR product was digested and used for ligation with double digested pET22b vector. Transformation was done in DH5α chemical competent cells and on next day colony PCR was performed. It was further confirmed by double digestion (by using *Nco I* and *Not I* enzymes) of PCR positive clones.

Purification of galectin 3

Chemically competent *origami* strain of *E. coli* cells were transformed with 10ng of isolated plasmids from DH5α cells. The induction of protein was done with 1mM IPTG at 37°C for six hrs. To measure the induction of recombinant galectin-3, 0.2 OD value equivalent of uninduced and induced cultures were resolved using 12% SDS- PAGE. For scaling up the production of recombinant gal-3, the induction was performed at 18°C for 16 hrs and then cultures were pelleted down at 5000 rpm. Protein purification was done by two methods.

a) Extraction by using lysozyme

One gm of the bacterial pellet was treated with 100µl of lysozyme (100mg/ml prepared in 15mM Tris and 50mM NaCl (Tris-NaCl buffer) buffer) followed by sonication (15min pulse on/off with 40 amplitude) for 30 minutes on ice. The samples were then centrifuged at 10000 rpm for 30 minutes and the supernatants were passed through Ni-NTA columns. Galectin-3 bound to Ni-NTA beads was eluted in Tris-NaCl buffer containing 400mM imidazole.

b) Purification from inclusion bodies

A major fraction of galectin-3 was present in the inclusion bodies and therefore was purified under denaturing conditions by slightly modifying the original protocol (19). The purified protein was then refolded using a rapid dilution method in refolding buffer having 400mM L-arginine, 100mM Tris-base, 5mM reduced glutathione, 0.5mM oxidised glutathione and 1mM EDTA. (20). The purity was assessed by resolving the purified protein by 12% SDS-PAGE.

Modifications of phagemid and retroviral cloning vectors

a) Modification of phagemid vector by site directed mutagenesis

Phagemid vector, pSEX81, was obtained from progen Biotechnik. Originally the vector contained 5' *Nco I* and 3' *Not I* sites for cloning but we found the frequent occurrence of *Nco I* site in the CDR's of VHH. Therefore, *Nco I* site was replaced by *Sfi I*, the latter being a 13mer site, at the 5' end by site directed mutagenesis. The possibility of occurring a 13mer site was low. 50ng template vector was incubated with 200µM dNTP's, 1U Pfu polymerase, 125ng of each primers in 1x reaction buffer (Thermo Fisher Scientific) under the following conditions: initial denaturation at 95°C 1 min, 18 cycles of denaturation 95°C 50 sec, amplification 60°C 50 sec and extension 68°C 5 min and the final extension was performed at 68°C for 7 min. The amplified product was then treated with *Dpn I* for one hour at 37°C. This mixer was used to transform TG1 electro competent cells. The presence of *Sfi I* site was confirmed with restriction digestion followed by horizontal gel electrophoresis and sequencing. The digestion reaction was performed for 1µg of vector DNA in two steps, first incubating at 37°C for two hrs and then 50°C for additional two hours.

b) Modification of retroviral cloning vector

For retroviral mediated transfection, pMKO.1GFP vector was a gift from William Hahn (Addgene plasmid #10676). In this vector, first U6 promoter was replaced with another SV40 promoter by restriction digestion and ligation. The U6 promoter designed for shRNA oligos was removed by a two-step double digestion reaction involving the first step with *Bgl II* (at 37 °C in NEB 2.1 buffer for 2hrs) and the second step with *Age I* (at 37 ° C in cutsmart buffer for 1 hr). The amplified SV40 promoter sequence was ligated using the same sites (*Bgl II and Age I*). Ligation was performed at 25°C for two hrs and the ligated mixture was transformed into DH5α competent cells. Positive clones were identified by colony PCR by using forward and reverse primers binding specifically to the insert and the vector, respectively. Further confirmation was done by double digestion using *Bgl II* (at 37 °C in NEB 2.1 buffer for 2hrs) and *Eco RI* (at 37 ° C in cutsmart buffer for 1 hr) enzymes. Additionally, a myc tag was added at the C terminus by using the primers; LTV 1 and MKS.24 between the 5'*Age I* and 3' *Eco RI* sites.

Transfection of HEK293T cells

$1x10^5$ of HEK293T cells were plated in 6 well plate and incubated overnight at 37°C. Next day cells were washed gently with PBS and then transfection mixture was poured into the wells. For preparing transfection mixture, 10µl of lipofectamine-3000 was preincubated with 240µl of Opti-MEM media for 10 minutes at RT followed by the addition of 1µg of plasmid DNA solution (i.e. 10µl of plasmid in 240µl of Opti-MEM medium). The mixture was incubated for 30 minutes at RT and was then added to the cells. Cells were then incubated at 37°C for five hrs and the transfection mixture was replaced with complete DMEM subsequently. After 25 hrs of transfection, cells were observed under the fluorescence

microscope for the GFP signal and cell lysates were prepared to probe electroblotted membranes with *anti-c-myc* antibody

Colony PCR

Single colonies were picked and used as templates for amplifying the insert using 500nM of each primer, 200µM dNTP, 1.5mM extra $MgCl_2$ and 1U of HF polymerase in 1X HF buffer. The final volume of reaction mixture was made upto 100µl with MQ. The PCR conditions used were: One cycle of initial denaturation at 98°C for 50sec, 30 cycles of denaturation at 98°C for 30 sec, annealing at 64.8°C for 35 sec, extension for 45 sec at 72°C and the final extension for 5 minutes at 72°C. All the PCRs for amplifying galectin-3, SV40 promoter, c-myc tag and VHH screenings were performed using the annealing temperatures of 64.8°C.

Generation of single domain antibody library

Total RNA was isolated from PBMCs by trizol method and cDNA was prepared by using cDNA synthesis kit from TAKARA. PCR was done in two steps. In first PCR step the region between leader sequence to C_H2 exon yielded the amplicons in the range of 750-800base pairs that corresponded to the entire fragment antigen binding (Fabs) of IgG1, IgG2 and IgG3. In order to amplify VHH sequences from only IgG2 and IgG3 antibodies, a second PCR was performed by using primers from FR1 to FR4. The template for the second reaction was gel extracted from PCR amplicon obtained in the first cycle that corresponded to the HCAbs (IgG2 and IgG3) (21). The VHH thus amplified in second PCR was cloned in a phagemid vector (pSEX81) obtained from Progen Biotechnik. The vector was mutated to incorporate sequence for *Sfi I* at 5' end by site directed mutagenesis as described earlier. This mixture was used to transform TG1 electro competent cells. *Sfi I* site was confirmed with digestion and sequencing. VHH amplicons and vector were digested O/N first with *Not I* HF and then with *Sfi I* at 50°C. Digested vector and insert were purified from agarose gel and

then ligated into 1:10 ratio for 2 hrs 30 min at 25°C. Ligated product was used to transform TG1 ultra competent cells (Lucigen). Library size was calculated by using following formula:

$$\text{Library size} = \frac{\text{No. colonies X Dilution factor}}{\text{Volume used for plating (µl)}}$$

M13K07 amplification and titration

a) Production and isolation of helper phage (M13K07)

Initially M13K07 was obtained from NEB and used as an inoculum for further propagation. Secondary culture of TG1 bacteria at 0.4 OD value was infected with MK13K07 in 1:20 dilution (1 bacterium with 20 phage particles) for 30 min in static conditions and then 50µg/ml kanamycin was added to the media and incubated for overnight at 37°C with rotation at 180rpm. Overnight culture was centrifuged in 50ml falcons at 4000rpm for 30 minutes. To 40 ml of the supernatant, 10ml of sterile PEG/NaCl solution was added. It was allowed to precipitate in ice for 1 hr and then centrifuged at 4°C, 4000rpm for 1 hr. The whitish pellet was dissolved in minimum volume of PBS and heated at 70°C for 60 seconds. Again it was centrifuged at 4°C, 12000rpm for 10 mins. Supernatant was stored at -80°C.

b) Phage titration

Different dilutions i.e. 10^{-4} to 10^{-14} were prepared from newly amplified phage particles. 100µl of each dilution was mixed with 100µl of TG1 cells in their mid log growth phase and incubated for 30 mins without shaking at 37°C. The inoculated bacteria were mixed with 5ml of top agar and poured on 2XYT plates. After overnight incubation, the plaques were counted.

Biopanning of the phage display library for antigens

a) Revival of library

Library was stored in the form of 1ml aliquots and one such aliquot contained $1x10^{10}$ bacteria to represent the whole repertoire of VHH. For the revival of library, one aliquot was resuspended in 500ml 2XYT media containing 20% glucose and 100µg/ml ampicillin. It was incubated at 37°C for 3-4 hrs until an OD value of 0.4 was reached. The culture was then infected with $2x10^{12}$ bacteriophage particles for 30 min under static conditions and subsequently centrifuged at 4000rpm for 20min. The pellet was resuspended in fresh 2XYT media containing 100µg/ml ampicillin and 50µg/ml kanamycin and then grown for overnight at 37°C. Next day the recombinant phage particles were purified by PEG/NaCl method and used for Biopanning.

b) Biopanning

Polystyrene plates were coated with 100µl/well of refolded recombinant galectin-3 (20µg/ml stock) overnight at 4°C. Next day the plates were washed three times with 0.05% PBST buffer and blocked with 5% skim milk along with 50mM α-lactose for 2 hrs ta RT. Additional controls were used for blocking. The plates were then washed three times and $1x10^{11}$ recombinant bacteriophages were added per well and a further incubation was done for 1 hr 30 min at RT. After incubation the plates were washed with 0.5% PBST 25 times. To elute strong binders triethlylamine was added for 30 min followed by neutralisation using Tris buffer (pH 7.4).

Phage ELISA

One hundred µl of galectin-3 (10µg/ml) was coated in 96 well polystyrene ELISA plates overnight at 4°C. Next day the plates were washed three times with 10mM PBS-0.05% Tween-20 (PBST) and blocked with 3%BSA in PBST for 2 hrs at RT. After blocking and

washing, 100µl of 3 fold diluted phages from each colony were added to the wells. Plates were incubated for one and a half hour at RT and then washed with PBS containing 0.5% Tween-20. After three washing, 1:5000 dilutions of mouse anti-pVIII antibodies were added for one and a half hour. Plates were then washed for three times with PBST and anti-mouse alkaline phosphatase was added. The plates were then incubated for one and a half hour. After three washings plates were developed by adding 200µl per well of pNpp substrate obtained from Sigma Aldrich (1mg/ml in glycine buffer). Reaction was stopped with 50µl of 3M NaOH per well and absorbance was recorded at 405nm.

Western blotting

Induced and uninduced bacterial cultures with the same OD values or the purified galectin-3 were subjected to SDS-PAGE for 2 hrs at 100V. PVDF membrane was charged with methanol for 20sec and then soaked in the transfer buffer for 5min. The resolved polypeptides were transferred to charged PVDF membranes at constant 15mA. The membranes were then blocked with 5% skim milk in 0.05% PBST for 2hrs at RT followed by incubation with 1:2000 dilution of anti-galectin-3 mouse antibody for 1 hr 30 min. The membranes were then washed three times in 0.05% PBST and incubated with 1:20000 dilution of anti-mouse alkaline phosphatase conjugated antibody. The membranes were developed by using X-ray machine.

Statistical analysis

Student's “t” test and ANOVA tests were applied for statistical analysis to compare responses between groups, as indicated in the figure legends. The results are presented as mean ± SD. The p values are shown in the figures or figure legends and are represented as $^{*}p \leq 0.05$, $^{**}p \leq 0.01$, or $^{***}p \leq 0.001$.

Results

Small molecules as galectin-3 inhibitors

Some chemically synthesised small molecules were shown to bind galectins (22). We obtained one such derivative, thiogalactoside derivative, known as Di-(3-deoxy-3-(4-((butylamino)carbonyl)-1H-1,2,3- triazol-1-yl)-β-D-galactopyranosyl)sulfane (kindly provided by Prof. Ulf Nilson). It displayed a strong affinity for galectin-3 (23nm) (23). Therefore, we tested the ability of this inhibitor to influence the activation of $CD8^+$ T cells stimulated in the presence of anti-CD3 and anti-CD28 antibodies. In addition we also measured the response of anti-viral $CD8^+$ T cells in experimentally infected mice with HSV1 that were additionally injected with the inhibitor. First we perfomed *in vitro* experiments to optimise at what dose the inhibitor could have specific effect without causing cellular toxicity does not kill the cells then we performed *in vivo* experiments (Figure no. 3.1 A&B). We then performed experiments to measure the response of anti-viral $CD8^+$ T cells and repeated such experiments many times but obtained no significant difference in either the magnitude of H-$2K^b$-SSIFARL-tet^+CD8^+ T cells or in cytokine producing cells between the two groups i.e. control and inhibitor treated gps (Figure 3.1C). These observations were surprizing but clue us in considering the possibility whether the inhibitor is working intracellularly or only neutralising the extracellular galectin-3. We performed *in vitro* kinetics of galectin-3 expression in activated $CD8^+$ T cells and the ability of the inhibitor to neutralize or mask galectin-3 thereby making it unapparent for detection. 1µM of the inhibitor was added to stimulated cells. These cells were stimulated with anti-CD3 and anti-CD28 and divided into two groups, i.e. with or without inhibitor. In unstimulated cells (at 0 times), galectin-3 was predominantly present intracellularly and its surface expression was negligible (Figure 3.1D). After 48 hrs of stimulation, a large proportion of $CD8^+$ T cells expressed the activation marker CD69. In stimulated cells added with inhibitor, there was no change in the

intracellular expression of galectin-3 (38.6% ± 2% in control i.e. without inhibitor vs 37.9% ± 3.2% in Test group i.e where inhibitor was added) but the surface staining was significantly reduced (12.5% ± 1.4% in control vs 0.4% ± 0.2% in test group) (Fig no. 3.1E). This provided us with an explanation why no significant difference was observed in the magnitude of virus-specific $CD8^+$ T cells or their cytokine producing ability in control vs treated animals as the inhibitor might have predominantly worked extracellularly. These results were inconcordance with our earlier reported results in chapter 2.

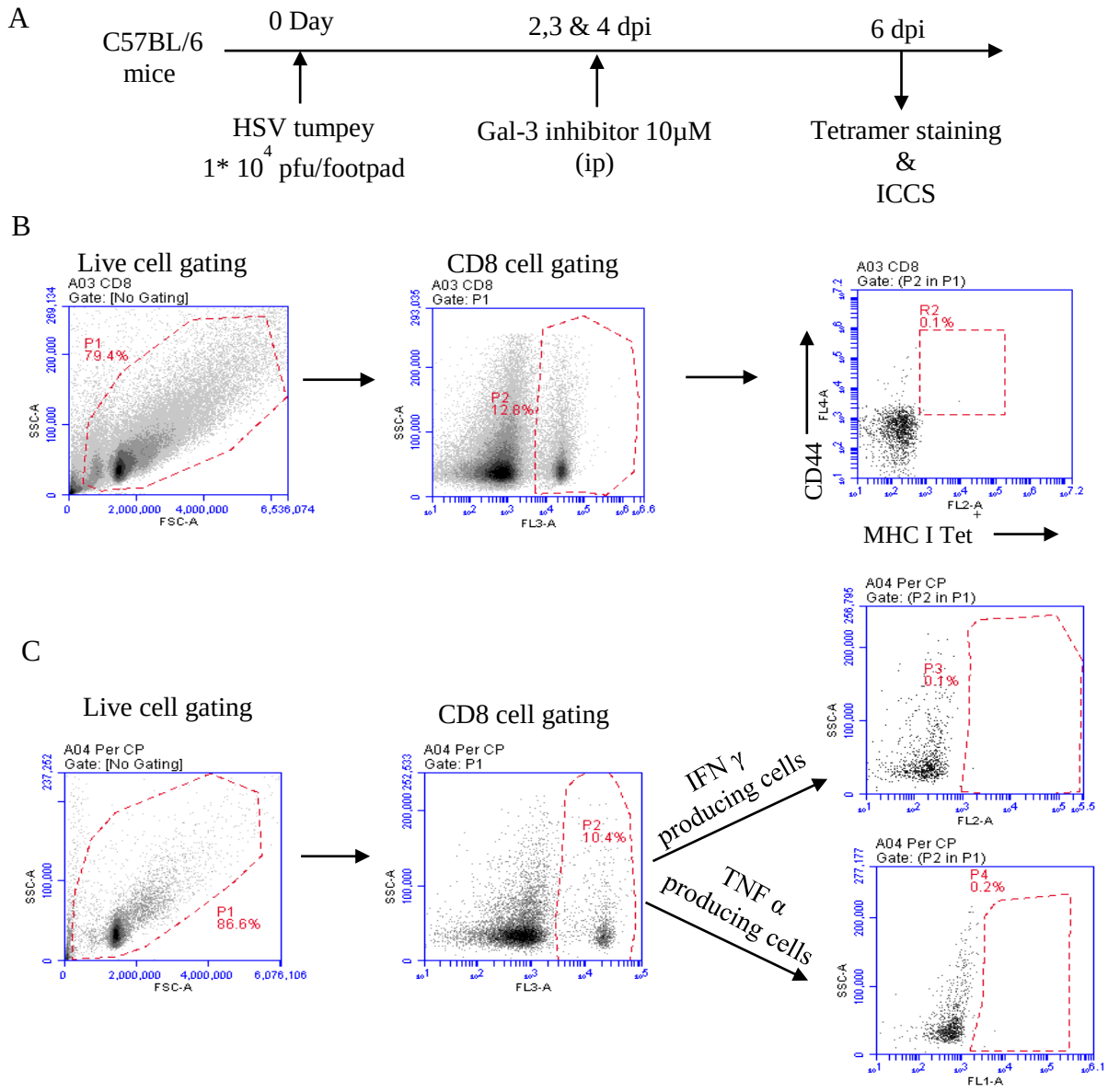

D

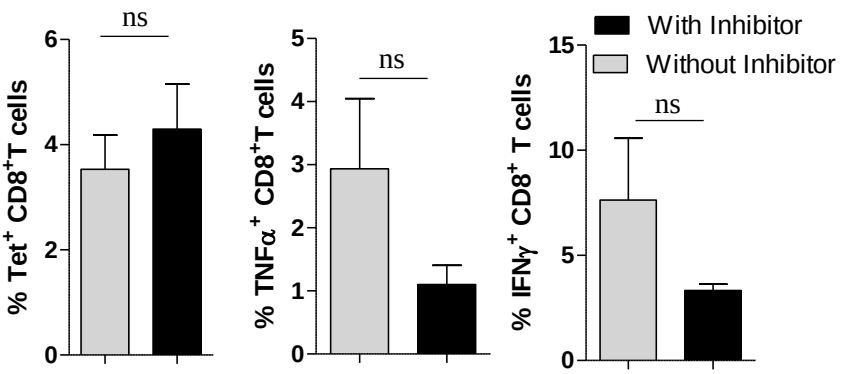

E

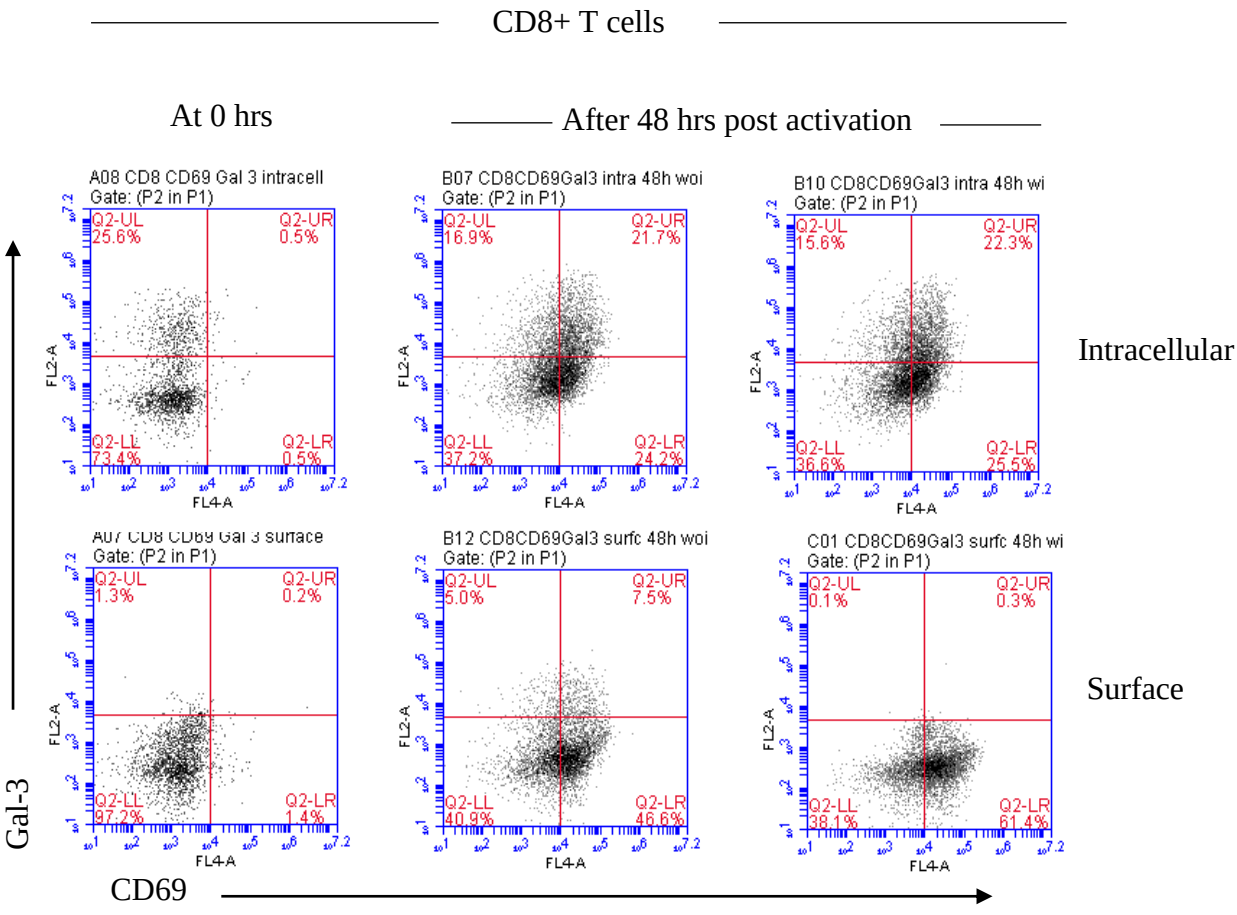

Figure no. 3.1. Measuring the effects of gal-3 inhibitor in modulating CD8$^+$ T cells *in vivo* and *ex vivo*. A. A schematic of the experiments performed using HSV1 infection in C57/BL/6 mice. B&C. Gating strategies for H-2Kb-SSIEFARL-Tet$^+$ CD8$^+$ T cells (B) and intracellular cytokine production (C), D. Measuring *in-vivo* effects of gal-3 inhibition on the magnitude of virus-specific CD8$^+$ T cells during HSV1 infection, D. Measuring *ex-vivo* effects of gal-3 inhibitor stimulated cells from spleens .

Expression of recombinant galectin-3

To disrupt galectin-3 function intracellularly, we required recombinant protein that can easily be cloned and expressed as a fluorescent protein to decipher its intracellular localisation as well as function using specific binders. Moreover, the desired amount of protein could be obtained for selecting anti-gaectinl-3 single domain antibodies from the phage display technology. Galectin-3 was amplified, cloned and expressed using converted cDNA isolated from RAW cell lines. Initially three different annealing temperatures were used to optimise conditions for galectin-3 amplification using the primers pairs, Gal3 FP and Gal3 RP (Fig no. 3.2A). For large scale amplification, the annealing temperature of 64.8°C was used. The amplified product was cloned in pET22b vector using 5' *Nco I* and 3' *Not I* sites and transformed into DH5*α* strain of *E. coli*. We obtained 10 times more colonies in test reaction as compared to self-ligation. A total of 32 colonies were screened for the presence of insert by using vector specific primers (i.e. T7 promoter and T7 terminator binding primers) and 14 colonies were judged positive for the insert (marked with asterisk sign in yellow colour in Fig no. 3.2B). For the protein expression, plasmids isolated from the cultures of all the 14 clones were transformed in *Origami* strain of *E.coli* and shortlisted clones were induced with 1mM of IPTG for the expression of galectin-3 at 37°C for 6 hrs in a 96 well plate format. After the induction, the 0.4 OD value equivalents from induced and uninduced cultures were loaded and resolved using 12% SDS-PAGE gels. One gel was used for the staining (Fig no. 3.2 C) and other was probed with anti-galectin-3 antibody by western blotting (Fig no. 3.2D). Galectin-3 was cloned in pET22b vector and expressed as a fusion product with $(HIS)_6$ at C terminal making it easier for the purification using Ni-NTA beads. For a large scale production and purification of recombinant galectin-3, clone 26 was used. Initially it was purified by using lysozyme mediated cell lysis but the yield was poor as a major chunk of protein was expressed in inclusion bodies. Therefore, we purified the protein

from inclusion bodies by using 8M urea and then performed the refolding as described in material and methods (Fig no. 3.2E & F). Refolded protein was used for biopanning of specific single domain antibodies from the phage display library and subsequent experiments.

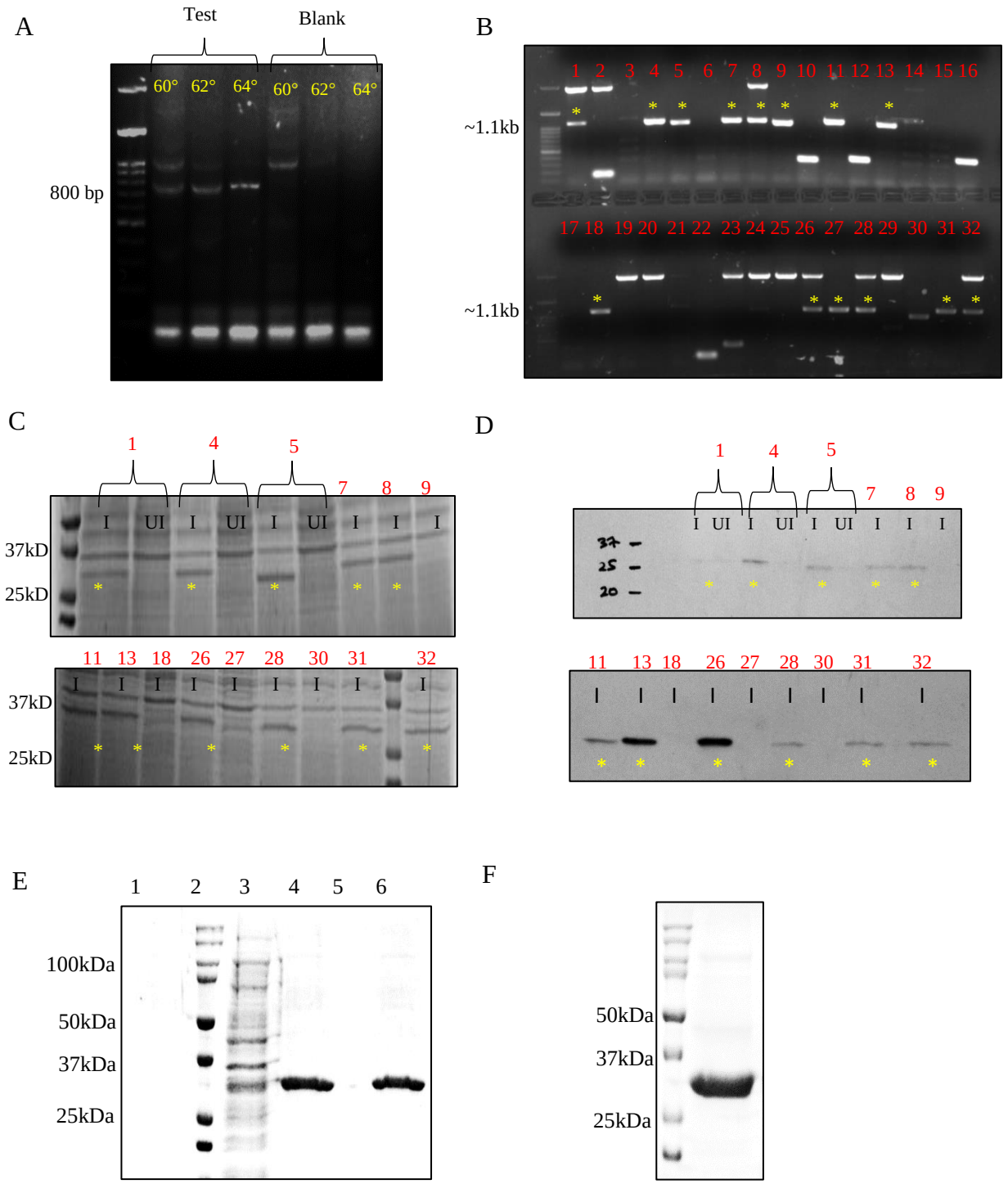

1. Dye, 2. Marker, 3. Eluted protein,
5. Empty, 6.Beads

Figure no. 3.2. Cloning and the expression of recombinant gal-3. A. PCR amplification of gal-3 at different temperatures is shown, B. The transformants were screened by Colony PCR of randomly picked colonies using using pET22b specific primers, C & D. Images show the induction of shortlisted clones (marked as asterisk sign) using 12% SDS-PAGE (C) and Western blotting (D), E & F. Gel pictures of Ni-NTA purified (E) and refolded recombinant gal-3 (F).

Library generation and phagemid modifications

Camelids have unique types of antibodies that are composed of only the heavy chain dimers. The antigen binding region is only contributed by a single domain. We generated phagemid libraries for single domain antibodies using coding sequence in the VHH. The schematic of library generation is showed in Fig no. 3.3A. Collected PBMC's from 50ml of camel's blood were used for RNA isolation by Trizol method (Fig no. 3.3B). To cover the the maximum repertoire possible, we used 5µg RNA as a template for cDNA synthesis and then amplified the region between leader sequence and 5' region of C_H2 domain. This step would amplify the genes from both conventional as well HCAbs that could easily be identified and resolved in 2% agarose gel owing to the size difference of the amplicon as the HCAbs lack C_H1 domains (Fig no. 3.3C). We obtained a higher migrating bands around 900bp (corresponding to the amplicons for conventional antibodies) and two bands in 700-750 range (representing the amplicons of HCAbs i.e. IgG2 and IgG3) (Fig no. 3.3C). The lower migrating bands were purified from gel by using a gel extraction kit and the product was used for amplifying VHH. In this step, the amplicons for HCAbs were used as template so contamination by VH was removed. The size of VHH band that we obtained ranged from 350-450bp (Fig no. 3.3D).

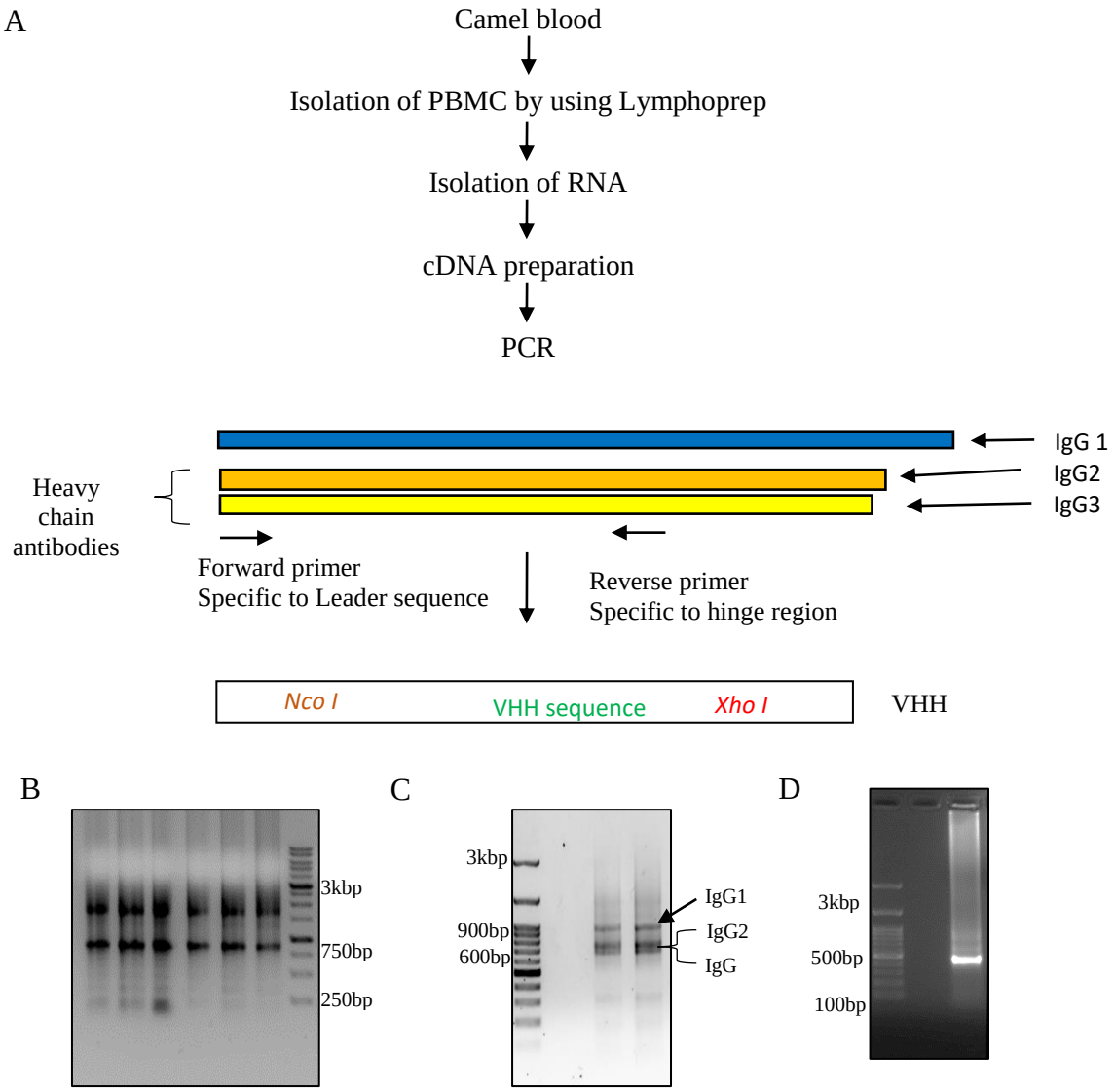

Figure no. 3.3. Amplification of V_HH for the generation of single domain antibodies library. A. A schematic of different steps used for the library generation, B. Isolation of RNA from PBMCs and its analysis by gel electophoresis, C. Amplification of Fabs of IgG isotypes by using cDNA as the template. The upper band corresponds to IgG1 and the lower bands corresponds to IgG2 and IgG3 D. Amplified V_HH using Fab of HCAbs as a template.

Initially we used phagemid vector pSEX81 that did not have any $(HIS)_6$ tag and the stop codon after multiple cloning sites (Fig no3.4). Therefore we performed experiments to incorporate $(HIS)_6$ tag and a stop codon in the same vector so that upon transformation in non-suppressor starin of *E. coli*, VHH does not express the protein beyond stop codon. To

this end, we first cloned VHH in the pET22b by using *Nco I* at 5' and *Xho I* at 3' site in such a way that $(HIS)_6$ tag and stop codon occur in frame downstream to the insert gene, VHH.

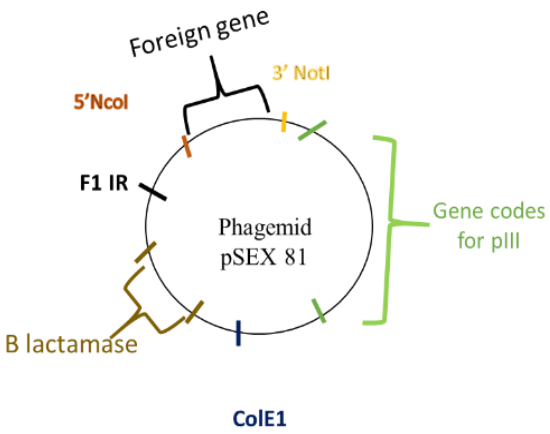

Figure no. 3.4. Pictorial map of pSEX 81 phagemid vector.

For cloning VHH in the plasmid vector, MKS 11 & 12 primers were used to amplify VHH with *Nco I* at 5' and *Xho I* at 3' sites. The insert and the vector were digested with these two

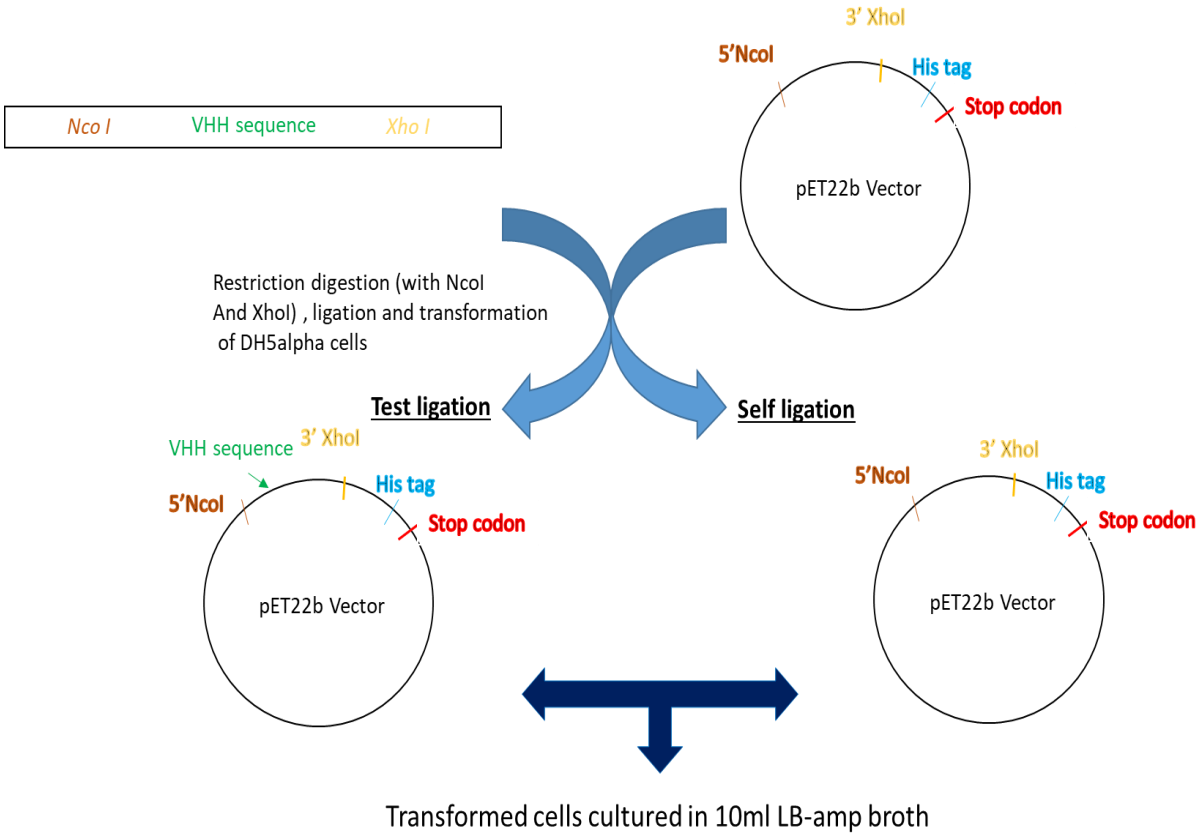

Figure no. 3.5. A schematic for cloning V_HH in pET22b plasmid vector.

enzymes and ligated by using T4 DNA ligase. The transformed DH5α *E. coli* strain was grown in 10ml of LB Amp medium and after 14 hrs of incubation, the plasmids were isolated by using a plasmid isolation kit (Fig no. 3.5). The plasmid that contained VHH sequences between *NcoI* and *XhoI* was used as template for MKS 11 &13 primers. We factored in the possibility that there would be different VHH sequences as a few ng of amplified VHH were used and the primers used were those specific to framework regions. MKS 13 primer contained *BamHI* site and the complementary region for stop codon and some of the bases of $(HIS)_6$ tag so it could efficiently bind to the plasmid vector backbone and in so doing amplified the product 5' *NcoI*- VHH-*XhoI*-$(HIS)_6$ tag-Stop codon-*BamHI* 3' (Fig no. 3.6).

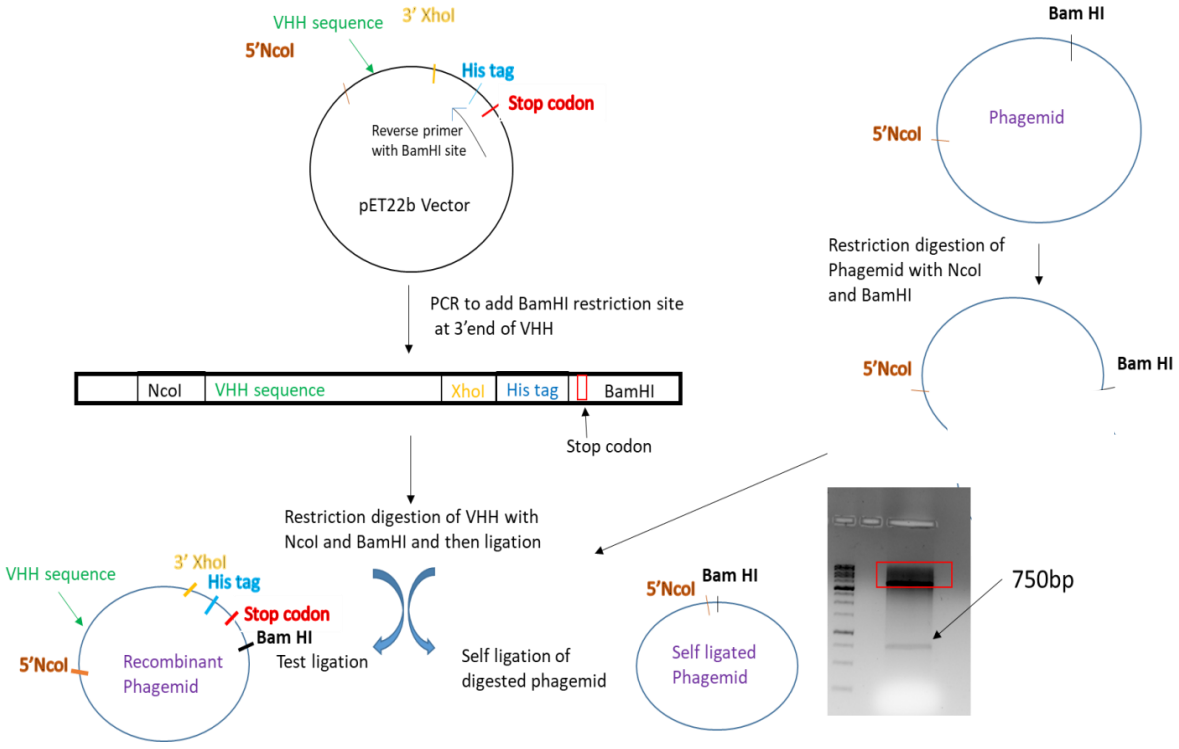

Figure no. 3.6. A schematic used for the addition of VHH along with $(HIS)_6$ tag and Stop codon into phagemid vector.

All VHH amplicons were ligated into pSEX81 phagemid by using 5' *NcoI* and 3'*BamHI* sites as depicted in Figure no. 3.6. The transformation was performed in TG1 strain of *E. coli*

as DH5*a* is not compatible strain for phagemids. After the transformation, the phagemids were isolated that contained $(HIS)_6$ tag and stop codon after VHH sequences (Fig no. 3.6).

We then attempted to clone the whole amplified repertoire into the modified phagemid but faced another hurdle. Thus, the *XhoI* site was present in the backbone of phagemid vector. So we planned to replace the 3' *XhoI* with *KpnI* site that was neither present in the vector backbone or in the VHH sequence. However, we realised subsequently that a single colony was picked and the VHH sequence analysed did not have Kpn1 site. As

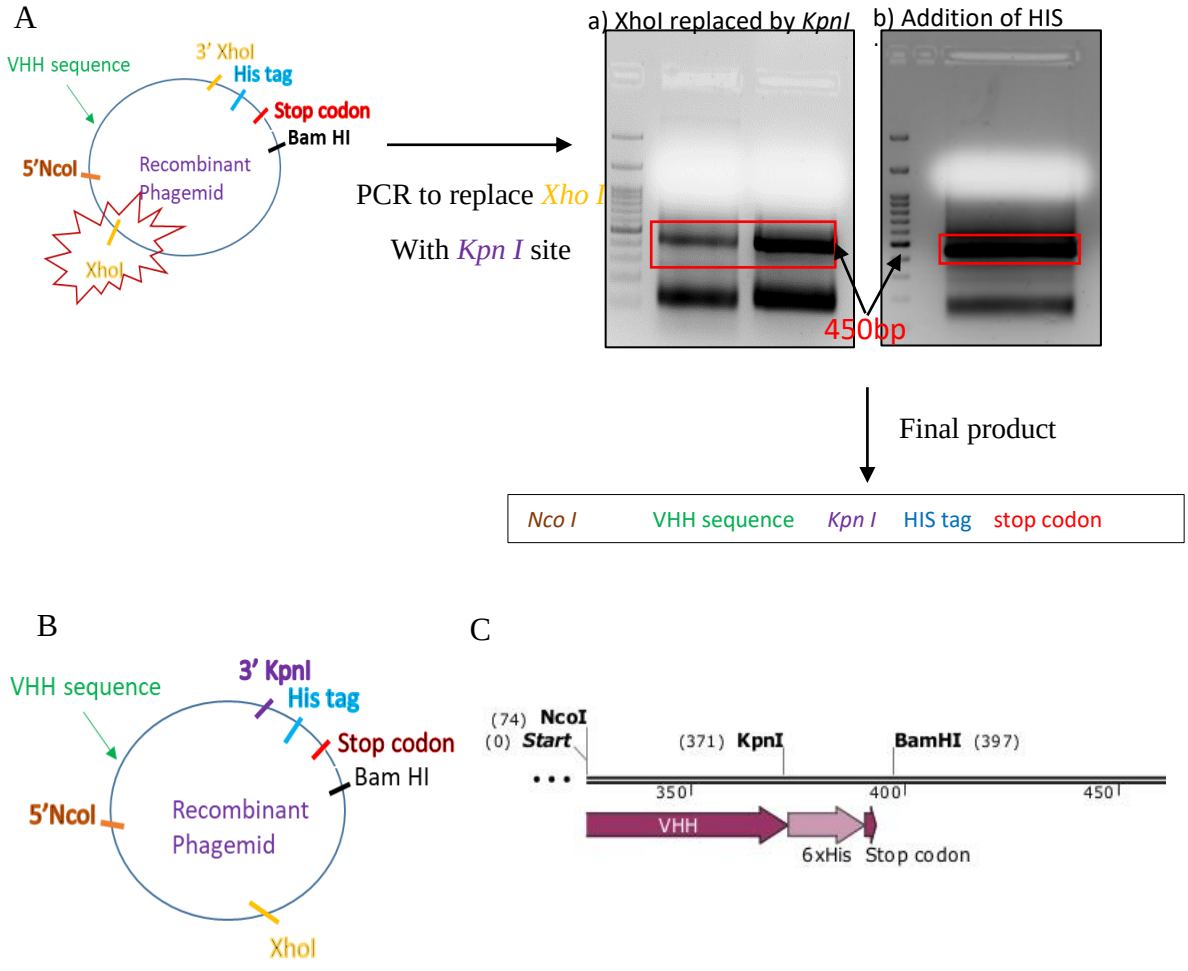

Figure no. 3.7. Modification of phagemid with KpnI site. A. Two step PCR where panel shows the replacement of XhoI site with KpnI and panel b represents the addition of HIS tag and stop codon at 3' end of VHH, B. Vector map with KpnI site and other additional features, C. sequencing results of one of the phagemid clone with KpnI site.

we discovered later other sequences did have the site. Totally undermining this fact we initiated experiments to incorporate Kpn1 site in the reverse primer. The PCR was done in two steps where in the first step we used VHH sequences as the template and amplified these sequences using same forward primer MKS11 carrying at 5' *NcoI* and the reverse primer MKS 14 having *KpnI* site at 3' end. The PCR product thus obtained was used as template for second PCR with MKS 15 primers in order to add downstream features and we finally obtained 5' *NcoI*-VHH-*KpnI*-$(HIS)_6$ tag-Stop codon-*BamHI* 3' (Fig no. 3.7A). These amplicons were digested and ligated into phagemid vector followed by transformation into TG1 *E. coli* strain (Fig no. 3.7B). All the modified sites were verified by sequencing results (Fig no. 3.7C). We then amplified VHH sequences using different combinations of MKS primers as shown in Figure no. 3.8A. Multiple digestions were performed using different sets of enzymes (Fig no. 3.8B). We observed unexpected digestion pattern for a few clones. Thus, after digestion, we observed three instead of two bands i.e. apart from those originating from vector backbone we two more bands of approximately ~100bp and ~300bp size were visible. To get better clarity, we performed single digestion of VHH from these clones with *NcoI*, *KpnI* and *BamHI* and found that *NcoI* was cleaving the insert at two sites i.e. at the beginning of VHH sequence and 100 bp later. Similarly *KpnI* also cleaved the insert at two sites i.e. after 100bp from 5' end and at 3' end (Fig no. 3.8C). From sequencing results we found that *NcoI* was present in CDR1 and *KpnI* was present in the FR2. Given the hypervariability of antibody sequences, it becomes difficult to predict the restriction sites in the CDRs and any occurrence of sequences for hexa cutter always remain a possibility. Further the protein sequence of these framework regions remain conserved but at DNA level but because of the degeneracy of codons, a different nucleotide sequence could encode for the same amino acid as was the case for *KpnI* site. The first two amino acids in the Framework region 2 are tryptophan and tyrosine which is conserved in all VHH's. Tryptophan is encoded by TGG

and tyrosine by TAT and TAC but when it is TAC then along with TGG i.e. TGGTAC, the *Kpn I* restriction site is created. In this way it was difficult to choose a 6mer restriction site.

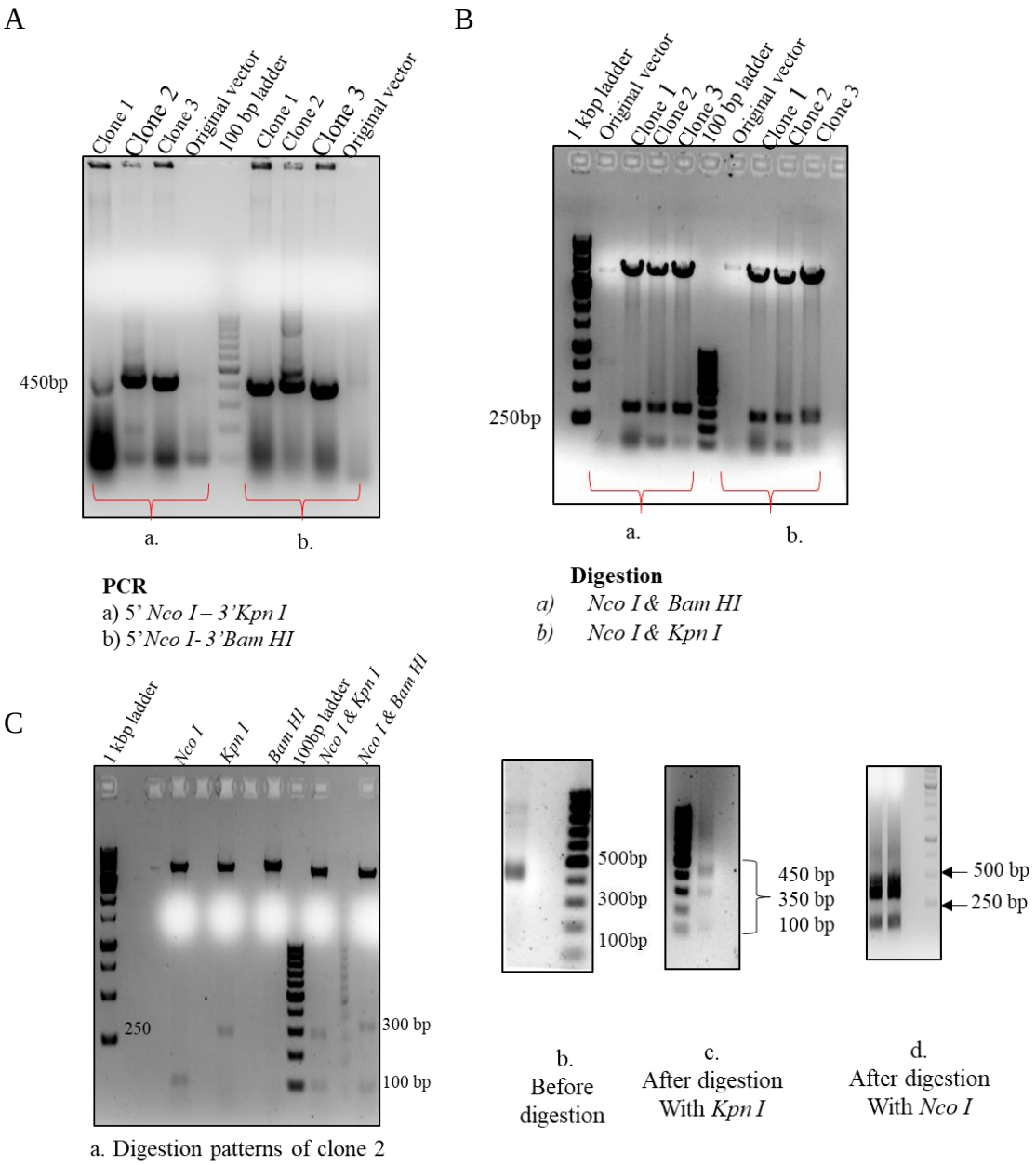

Figure no. 3.8. **Experiments aimed at trouble shooting for library generation.** A. PCR amplification and restriction digestion of VHH containing phagemid clones with different sets of indicated enzymes. C. Gel picture (a) shows the digestion pattern of clone 2 with *Nco I, Kpn I* and *Bam HI* alone versus their double digestions. Gel pictures depicts the pattern of same VHH before (b) and after digestion with *Kpn I (c)* and *Nco I (d).*

To overcome these problems, we decided to incorporate *Sfi I*, a 13mer site at 5' end of original phagemid vector and for 3' end we used an 8mer *Not I* site that being already in the

vector. *Not I* is GC rich site and therefore could create problems during the amplification of VHH, we therefore introduced null mutations in the reverse primer, MKS22. *Sfi I* site was added in the vector by site directed mutagenesis (as described in materials and methods) and then confirmed this site by digestion as well as by analysing sequencing results (Figure no. 3.9 A & B).

Once we ensured that all the modifications were present in the phagemid vector, we then performed experiments on a small scale to ascertain whether or not a fusion product of VHH and bacteriophage coat protein pIII could be induced. Four different phagemids containing VHH sequences were induced for protein expression followed by probing with

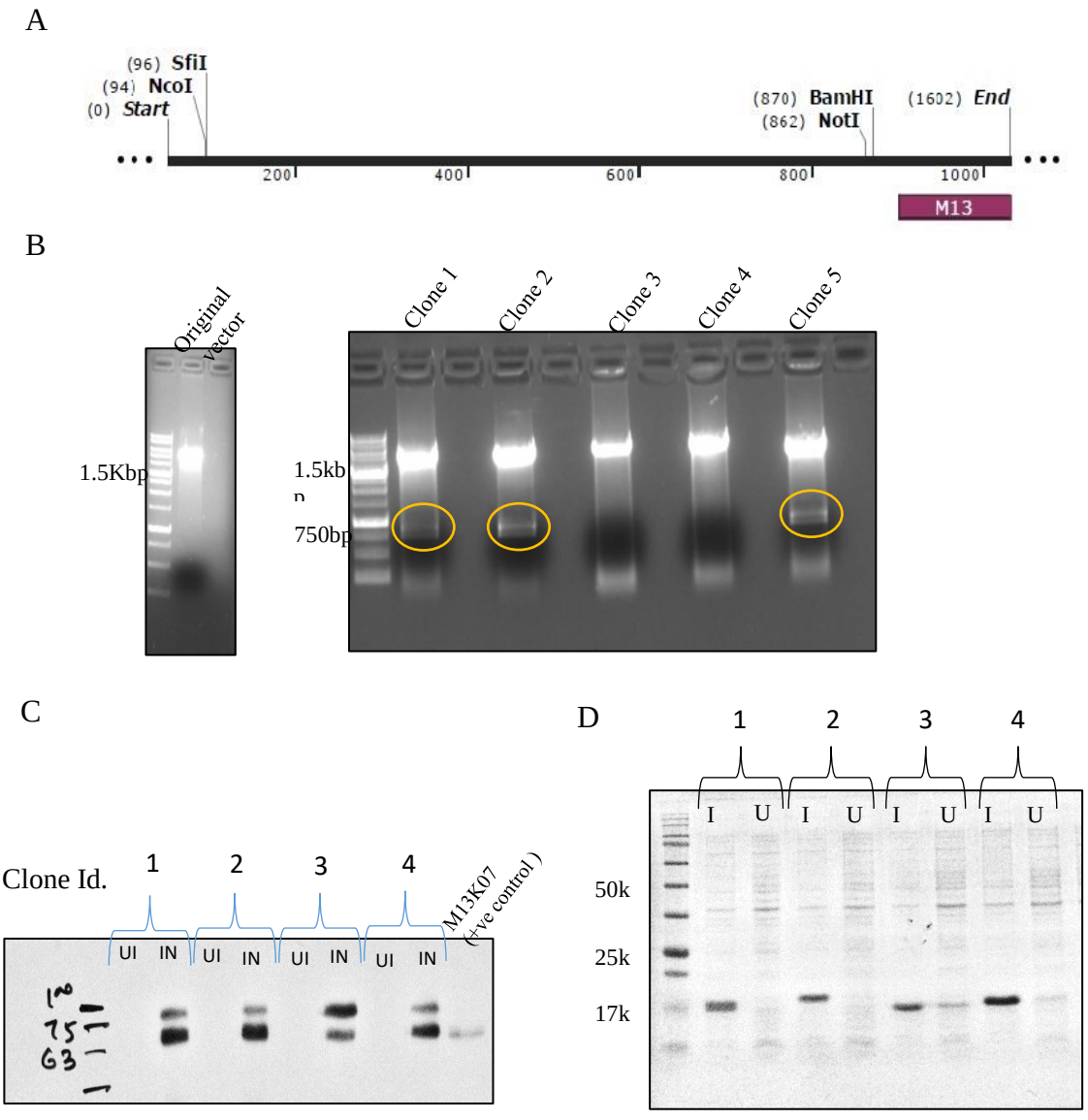

Figure no. 3.9. Site directed mutagenesis to incorporate 13mer *sfi I* site in the phagemid and establishing the success of work flow for library generation. A. Sequencing results shows the presence of *Sfi I* site in proximation to the *Nco I site* at 5'end B. Digestion pattern of original vector versus different clones with incorporated *Sfi I* and *Bam HI site* C. Immunoblotting of four clones induced with IPTG in comparison to their uninduced counterparts using anti-pIII antibody, D. SDS-PAGE after subcloning of V_HH from the phagemid to pET22b plasmid vector and a demonstration of VHH induction with IPTG.

anti-pIII antibody. We observed the expression of fused product (VHH + pIII) in four out of four clones. The expression nonetheless was at varying levels as expected. Later, we established the display of these VHHs on the surface of bacteriophages. Then we performed subcloning of these VHHs in the pET22b vector and the induction of protein was confirmed (Fig 3.9 C & D).

After optimising the flow of work involving the expression of VHH from the phagemid to plasmid, we prepared the library at large scale. We digested 20µg of purified phagemid vector and 5µg of insert and then ligated in 1:10 ratio using T4 DNA ligase. We obtained 22 million transformants which could represent the size of the library. 50 clones randomly selected from such libraries were analysed by colony PCR as well as double digestion using *Nco I* and *Not I* sites to confirm the presence of insert. We obtained 94% clones positive for the inserts (Fig no. 3.10). The sequencing results revealed that all the clones had conserved mutations canonical for VHHs.

Biopanning of galectin-3 specific single domain antibodies

The phage display library thus generated was used for biopanning against recombinant purified and refolded galectin-3. We obtained a five-fold greater number of colonies when galectin-3 was used as compared to the control plates but surprisingly all the clones appear to be shorter sequences for VHH (200bp instead of 450bp) when analysed by colony PCR.

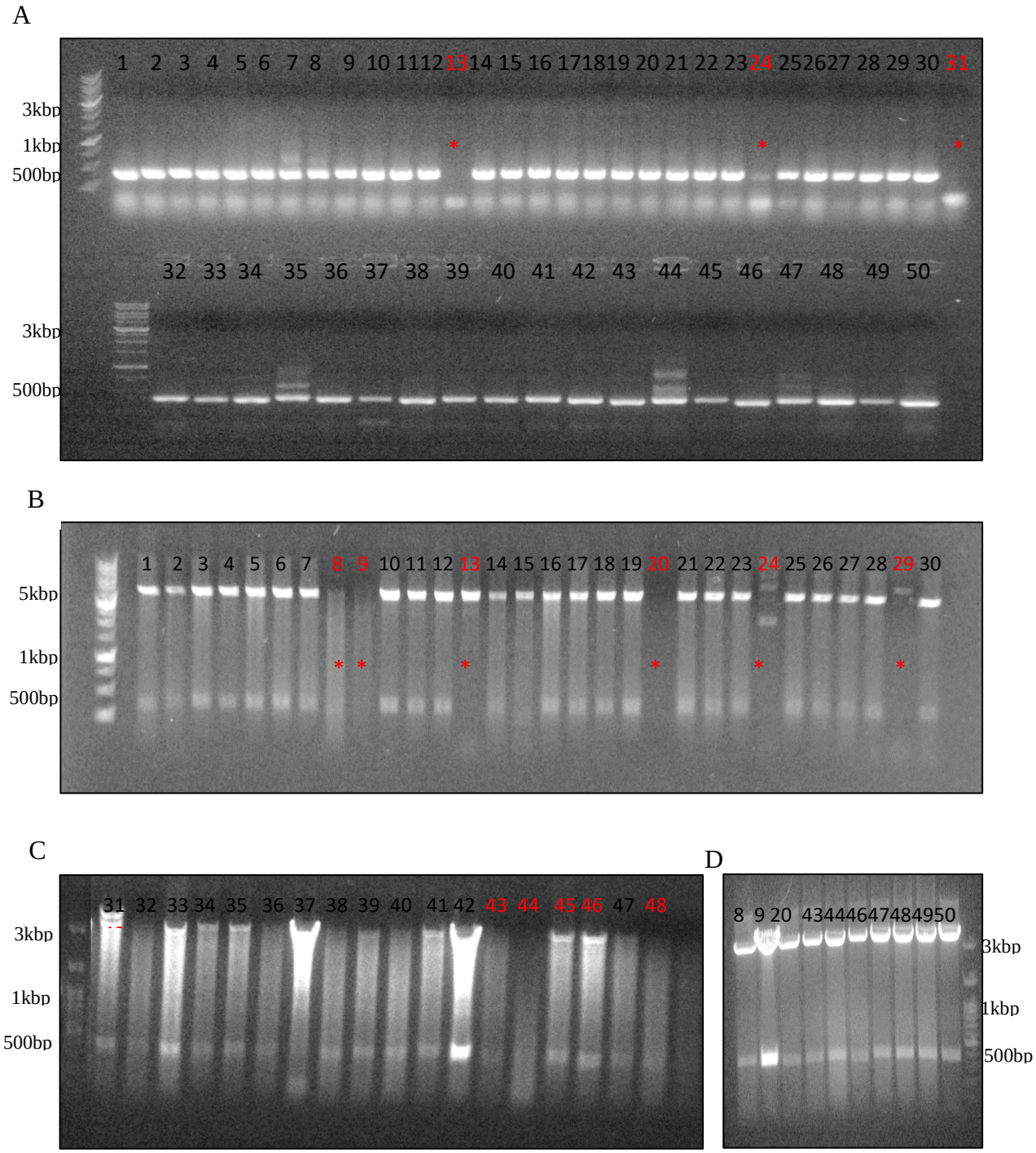

Figure no. 3.10 Ascertaining the quality of library by colony PCR. A. 50 clones were analysed by colony PCR to identify the presence of V_HH inserts, B & C. *NcoI* and *Not I* restriction enzymes were used to digest the vector from same clones. D. Select clones that showed negative results in the first reaction were reanalysed by restriction digestion..

(Fig no. 3.11 A & B). We currently have no plausible explanation for the observed results but it could be attributed to the poor resolution of amplified products in the gels or due to the

presence of *Not I* sites in either CDR2 or CDR3. These sites were used for inserting the amplified VHHs in the vector backbone. Upon integration of truncated products in the vector the bacterial colonies with shorter sequences might have overgrown those carrying full length products. Such a phenomenon is reported earlier (24). We performed the biopanning again in the presence or the absence of α-lactose so as to prevent non-specific interactions effected by CRD of galectin-3. The addition of α-lactose did not significantly alter the numbers of colonies obtained but interestingly we obtained full length VHHs as revealed by screening of colonies by colony PCR. Randomly selected colonies were probed using phage ELISA but no significant differences were observed between test colonies expressing VHHs as fusion protein and displayed on the surface of phage particles versus the control phages (M13K07 helper phages). The reason could be a direct binding or strong interactions between phages and galectin-3. To verify this, we performed western blotting and probed electrophoretically resolved galectin-3 with the anti-galectin-3 antibody as a positive control and M13K07 as a test sample. Further with in M13K07 group, one strip was incubated with *anti-pIII* and second with *anti-pVIII* antibody. As expected there was band with anti-galectin-3 antibody but we observed positive signal with anti-pVIII antibody as well. This suggested that phage particles could bind to galectin-3 (Figure no. 3.11 C). We alternatively performed this experiment where polypeptide from phage particles were resolved by SDS-PAGE and probed with $(HIS)_6$ tagged galectin-3. We observed positive bands with different molecular weights (Figure no. 3.11 D). Due to these reasons we did not proceed further with phage ELISA after biopanning hence subcloned the VHH genes directly into the modified pET22b vector where it expressed with a biotin tag, thrombin cleavage site and $(HIS)_6$ tag. We used three full length and two truncated VHH clones for probing in western blotting where 2° culture at 0.4 OD was induced with 1mM IPTG for 6 hrs at 37°C then cells were lysed in the lysis buffer. As VHH was biotinylated so positive signals were detected by using streptavidin protein

conjugated with HRP. We observed that all clones were positive for galectin-3 binding (Figure 3. 11 E).

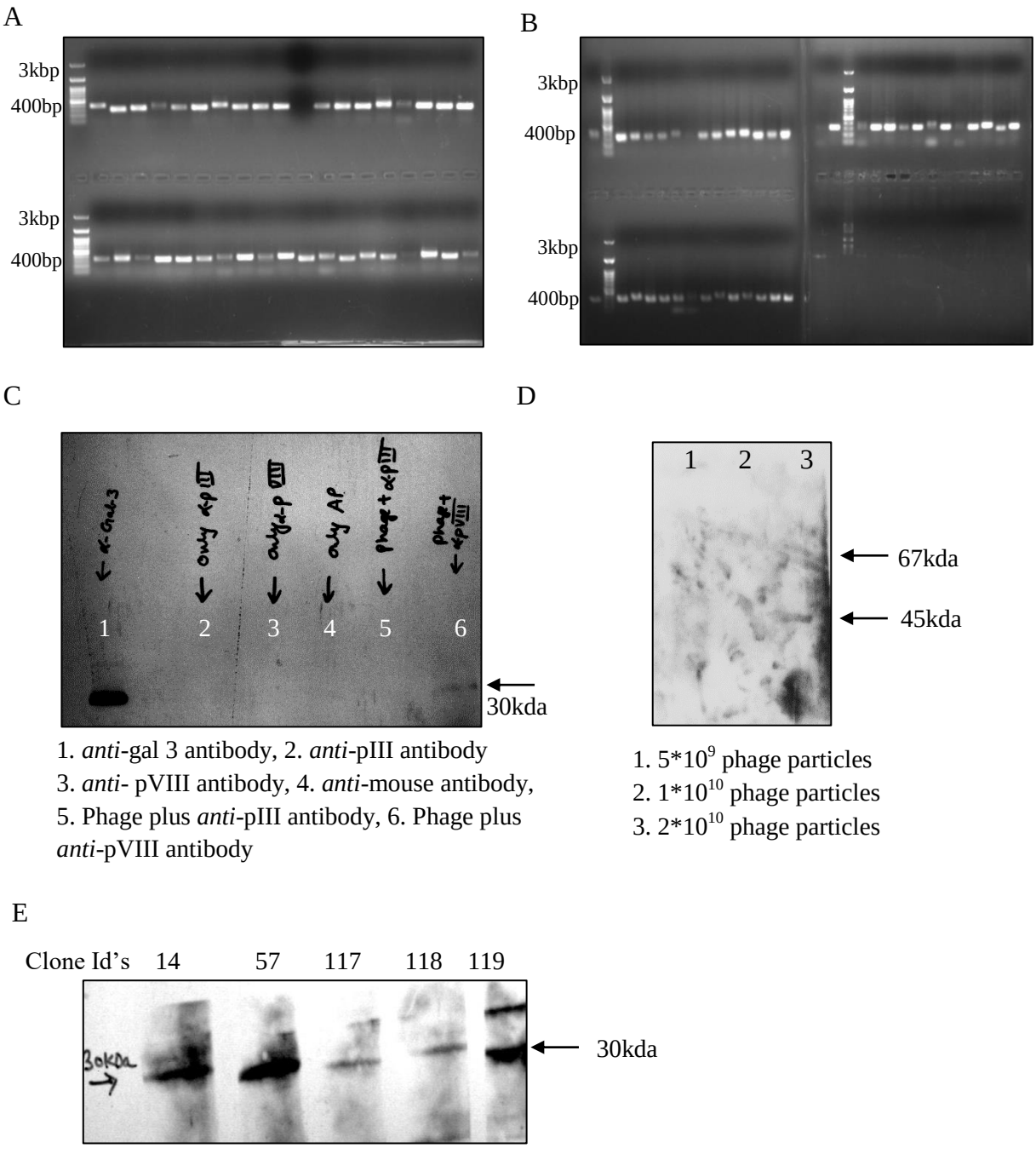

Figure no. 3.11. Biopanning for galectin-3. A & B. Colony PCR by using vector specific primers (MKS09 & MKS 10), C. Galectin-3 was probed with different set of antibodies and/or in combination with phage particles, D. Different concentrations of Phage particles are probed with $(HIS)_6$ tagged galectin 3, E. Western blotting showing that all 5 VHH clones bind to galectin 3.

Retroviral vector modifications and production of intrabodies

Once we selected VHHs for galectin-3, we attempted to express such binders intracellularly so that such binders could disrupt galectin-3 function in the cells of our interest. We used a retroviral based system to produce the sdAbs inside the cells. pMKO.1 GFP cloning vector that contains U6 promoter upstream of cloning sites i.e. 5' *Age I* and 3' *Eco RI* sites was used. U6 promoter is used for cloning of short oligos but is not suitable for full length genes because RNA polymerase II does not bind to U6 promoter and hence no mRNA copies and eventually no protein product are produced. We first modified the pMKO.1 GFP vector for the cloning of full genes.

a) Replacement of U6 with SV40 promoter

pMKO.1 GFP vector contains two copies of SV40 promoter, one for GFP expression and other for 3' LTR's. We reasoned that if SV40 is used for GFP expression then it can also be used for the expression for any full length gene. We therefore used one of these SV40 as a template for PCR (SV40 FP and SV40 RP primers) and amplified SV40 with 5' *Bgl II* and 3' *Age I* sites as U6 promoter was present in between two restriction sites i.e. 5' *Bgl II* and 3' *Age I.* For the replacement of U6 promoter, a sequential digestion was performed in two step as the two enzymes are incompatible with each other. The vector DNA was first incubated with *Bgl II* enzyme in the presence of NEB2 buffer for 2 hrs at 37°C followed by purification using isopropanol precipitation method. The product was then incubated with *Age I* enzyme in Fast digest buffer (Thermo Fisher Scientific) for 1 hr at 37°C. After digestion and CIP treatment of the vector, both the insert and vector backbone were purified from agarose gel by a gel purification kit. The ligation was performed in 1:5 ratio of vector to insert at 25°C for 2 hrs followed by transformation in DH5α bacteria. There was more than 5 fold difference in the test versus self-ligated colonies. Successful replacement of U6 with SV40 was confirmed using colony PCR as well double digestion with *Bgl II* and *Age I.* As there were

already two SV40 promoters in the vector backbone so for performing colony PCR, we used forward primer that was insert specific and reverse primer as vector specific. We got specific

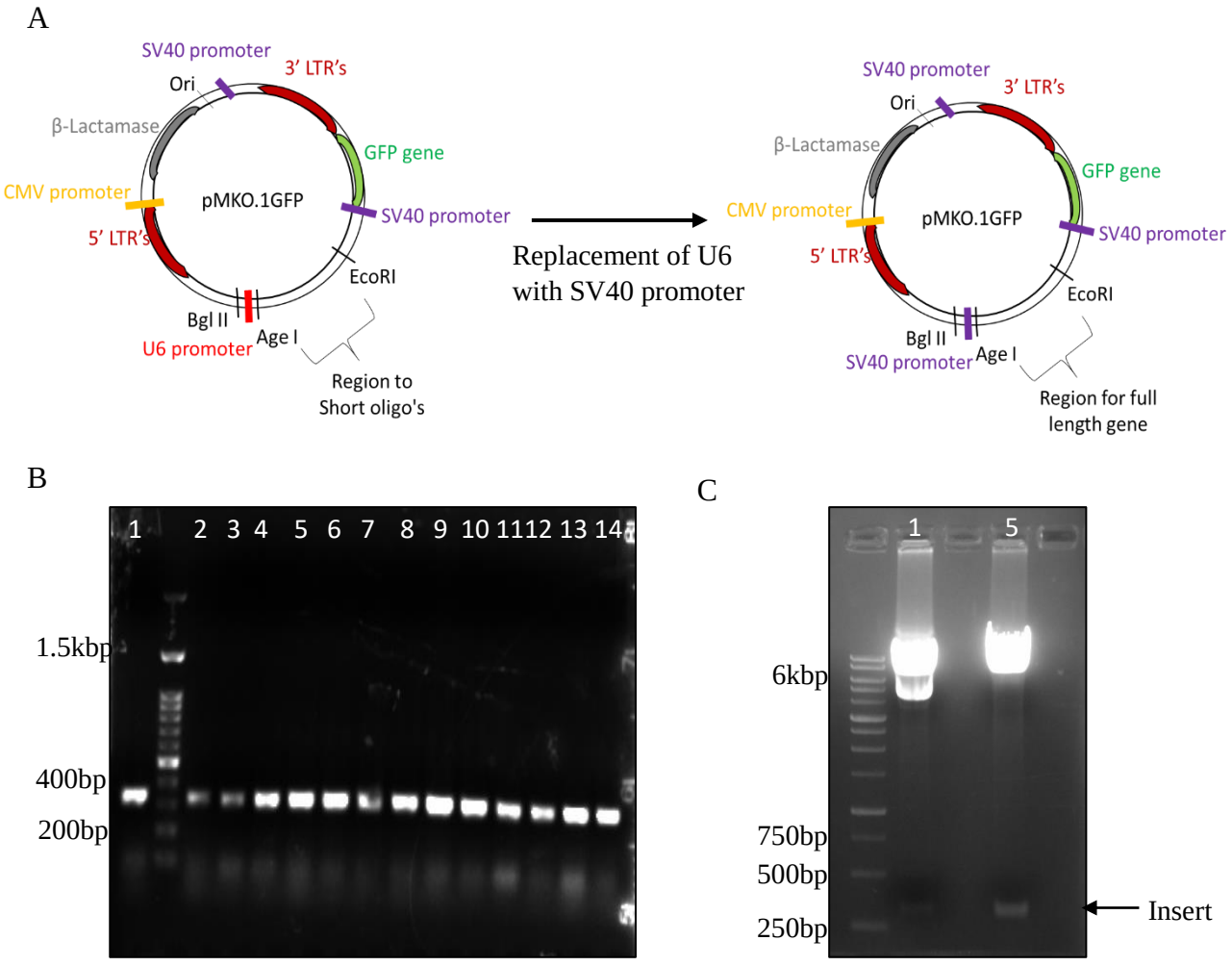

Figure no. 3.12. Replacement of U6 with SV40 promoter. A. Schematic of Vector modification, B. Colony PCR by using insert and vector specific primers, C. Double digestion of shortlisted clones.

band of 350bp for almost all the clones (gel picture of few clones has shown in Fig no.3.12 B &C) suggesting for the amplification of the newly integrated SV40 promoter.

b) Addition of c-myc in vector backbone

After integration of SV40 promoter, vector could efficiently be used to clone full length genes but the unavailability of an appropriate tag would make it difficult to screen for the translated product of the inserted gene (such as the VHH) under SV40 promoter. We

A

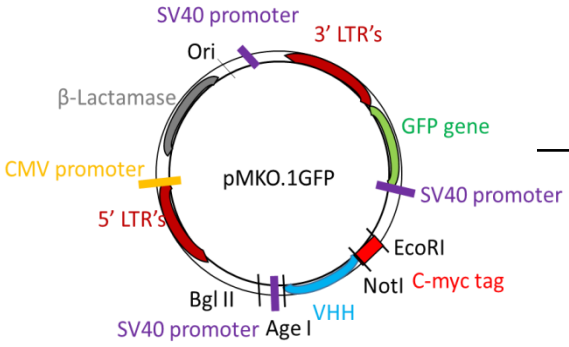

Digestion with *Nco I*

Expected digestion pattern

Original vector (bp)	Final vector (bp)
96	96
137	115
1689	137
1829	688
3016	1491
	1689
	3014

B

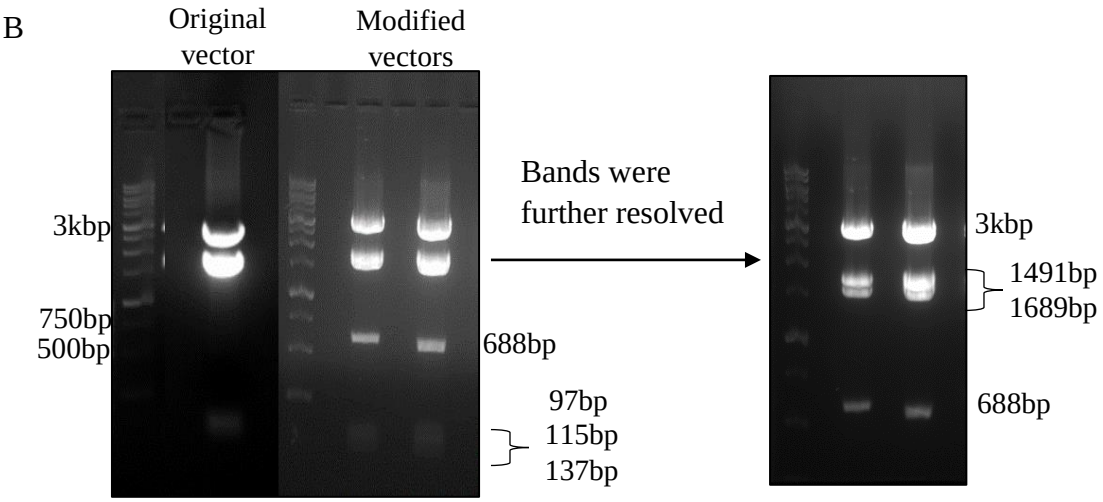

Figure no. 3.13. Restriction mapping of modified pMKO.1GFP vector. A. Restriction digestion map of modified vector and its expected band pattern, B. Digestion pattern of original vector versus modified vector and further it was resolved to visualise the bands around 1500bp length.

therefore incorporated a *c-myc* in the vector backbone using two PCR steps. To standardise the conditions, we used a VHH specific for another characterised antigen. The final PCR amplicon contained 5' *Age I* -VHH - *Not I* - *c-myc tag- Eco RI* 3'. To confirm the appropriate modification the vector and the PCR product were digested with *Age I* and *Eco RI* and ligated in 1:5 ratio of vector to the insert. Clones with positive insert were identified directly by double digestion where 32 clones were grown in 1ml LB Amp and the plasmids were isolated by a plasmid isolation kit followed by digestion with *NcoI* HF restriction enzyme (Fig no 3.13). The original vector contained 5 sites for *Nco I* enzyme and once it gets modified then

two additional sites were expected, one in SV40 promoter (newly integrated) and the second in VHH sequence so as expected we obtained 7 bands after digestion.

c) Production of intrabodies

For intrabodies production, we used the modified vector containing VHH sequence. The vector was transfected in HEK293T cells and after 24 hrs of transfection the expression of GFP was observed using a fluorescent microscope (Figure no. 3.14 A). GFP was also expressed under SV40 promoter so the expectation was that the VHH gene would also be expressed in HEK293T cells. For confirming whether this is true, we prepared the lysate of these cells and performed western blotting with *anti-c-myc* antibody. Indeed we obtained positive signal in first two lanes where the lysates from two different samples were loaded. As a positive control we used a *c-myc* tagged bacterial protein that also had a same molecular weight (Figure no. 3.14B). Therefore, we demonstrated that indeed specific VHH is expressed intracellularly and hence can be used to target its ligands inside the cells. With the availability of such a modified vector, other genes can also be cloned and expressed intracellularly.

A

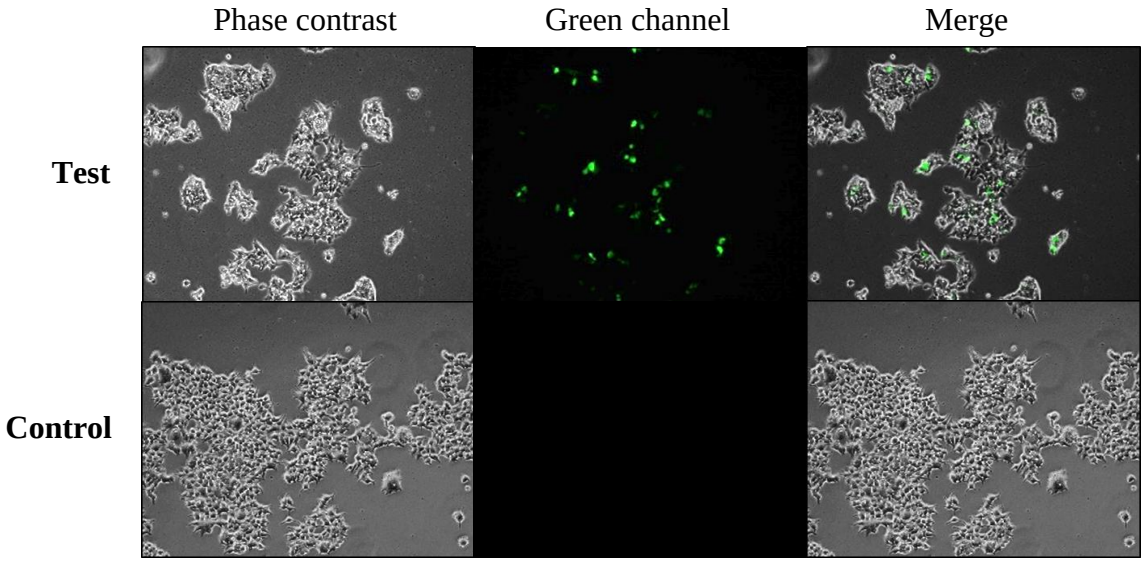

B

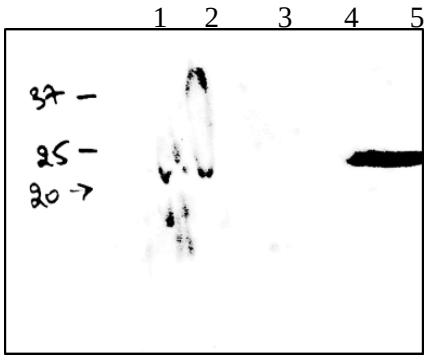

1,2, & 3.sdAb clones, 4.Negative control 5.Positive control

Figure no. 3.14. Production of intrabodies. A. Fluorescence images after 24hrs post transfection, B. HEK 293T cell lysate was probed in western blot by anti-c myc antibody.

For primary cells, this modified vector in combination with packaging vector should be used to transfect HK293T cells where after 24 hrs post transfection, retroviral particles will be released from the cells and culture supernatant can be used to infect the primary cells.

Conclusions

We have generated single domain antibody library from the camel's blood by using modified phagemid vector and panned out domain antibodies for galectin-3. We have standardised the production of intrabodies in mammalian cells by using modified retroviral cloning vector. Both cloning as well as packaging vector can be used to co-transfect HEK293T cells and then retroviral particles can be collected from cell supernatant which can be used to infect primary cells. Once primary cells gets retroviral particles then sdAb's for galectin-3 can expressed inside the cells and used to modulate the migration of galectin-3 towards the synapse hence its negative effects can be minimized in a cell specific manner.

References

1. Hirabayashi, J., and K. I. Kasai. 1993. The family of metazoan metal-independent β-galactoside-binding lectins: Structure, function and molecular evolution. *Glycobiology* 3: 297–304.

2. Toscano, M. A., A. G. Commodaro, J. M. Ilarregui, G. A. Bianco, A. Liberman, H. M. Serra, J. Hirabayashi, L. V. Rizzo, and G. A. Rabinovich. 2014. Galectin-1 Suppresses Autoimmune Retinal Disease by Promoting Concomitant Th2- and T Regulatory-Mediated Anti-Inflammatory Responses. *J. Immunol.* 176: 6323–6332.

3. Yao, Y., L. Zhou, W. Liao, H. Chen, Z. Du, C. Shao, P. Wang, and K. Ding. 2019. HH1-1, a novel Galectin-3 inhibitor, exerts anti-pancreatic cancer activity by blocking Galectin-3/EGFR/AKT/FOXO3 signaling pathway. *Carbohydr. Polym.* 204: 111–123.

4. Iurisci, I., A. Cumashi, A. A. Sherman, Y. E. Tsvetkov, N. Tinari, E. Piccolo, M. D'Egidio, V. Adamo, C. Natoli, G. A. Rabinovich, S. Iacobelli, and N. E. Nifantiev. 2009. Synthetic inhibitors of galectin-1 and -3 selectively modulate homotypic cell aggregation and tumor cell apoptosis. *Anticancer Res.* 29: 403–410.

5. Chen, W. S., Z. Cao, H. Leffler, U. J. Nilsson, and N. Panjwani. 2017. Galectin-3 inhibition by a small-molecule inhibitor reduces both pathological corneal neovascularization and fibrosis. *Investig. Ophthalmol. Vis. Sci.* 58: 9–20.

6. Thapi, D., M. Stasenko, T. White, S. J. Walderich, N. Feit, F. Weis-Garcia, and D. R. Spriggs. 2018. Abstract 1776: High-affinity anti-galectin-3 antibodies targeting oncogenic properties in serous ovarian cancer. *Cancer Res.* 78: 1776–1776.

7. Hamers-Casterman, C., T. Atarhouch, S. Muyldermans, G. Robinson, C. Hammers, E. B. Songa, N. Bendahman, and R. Hammers. 1993. Naturally occurring antibodies devoid of light chains. *Nature* 363: 446–448.

8. Greenberg, a S., D. Avila, M. Hughes, a Hughes, E. C. McKinney, and M. F. Flajnik. 1995. A new antigen receptor gene family that undergoes rearrangement and extensive somatic diversification in sharks. *Nature* 374: 168–173.

9. Vu, K. B., M. A. Ghahroudi, L. Wyns, and S. Muyldermans. 1997. Comparison of llama V(H) sequences from conventional and heavy chain antibodies. *Mol. Immunol.* 34: 1121–1131.

10. Khong Nguyen, V., R. Hamers, L. Wyns, and S. Muyldermans. 1999. Loss of splice consensus signal is responsible for the removal of the entire C(H)1 domain of the functional camel IGG2A heavy-chain antibodies. *Mol. Immunol.* 36: 515–524.

11. Deschacht, N., K. De Groeve, C. Vincke, G. Raes, P. De Baetselier, and S. Muyldermans. 2010. A Novel Promiscuous Class of Camelid Single-Domain Antibody Contributes to the Antigen-Binding Repertoire. *J. Immunol.* 184: 5696–5704.

12. Spinelli, S., L. Frenken, D. Bourgeois, L. De Ron, W. Bos, T. Verrips, C. Anguille, C. Cambillau, and M. Tegoni. 1996. The crystal structure of a llama heavy chain variable domain. *Nat. Struct. Biol.* 3: 752–757.

13. Adams, R., L. Griffin, J. E. Compson, M. Jairaj, T. Baker, T. Ceska, S. West, O. Zaccheo, E. Davé, A. D. G. Lawson, D. P. Humphreys, and S. Heywood. 2016. Extending the half-life of a fab fragment through generation of a humanized anti-human serum albumin Fv domain:

An investigation into the correlation between affinity and serum half-life. *MAbs* 8: 1336–1346.

14. Muyldermans, S., T. Atarhouch, J. Saldanha, J. A. R. G. Barbosa, and R. Hamers. 1994. Sequence and structure of vh domain from naturally occurring camel heavy chain immunoglobulins lacking light chains. *Protein Eng. Des. Sel.* 7: 1129–1135.

15. Van Der Linden, R. H. J., L. G. J. Frenken, B. De Geus, M. M. Harmsen, R. C. Ruuls, W. Stok, L. De Ron, S. Wilson, P. Davis, and C. T. Verrips. 1999. Comparison of physical chemical properties of llama V(HH) antibody fragments and mouse monoclonal antibodies. *Biochim. Biophys. Acta - Protein Struct. Mol. Enzymol.* 1431: 37–46.

16. Rutgers, K. S., R. J. A. Nabuurs, S. A. A. van den Berg, G. J. Schenk, M. Rotman, C. T. Verrips, S. G. van Duinen, M. L. Maat-Schieman, M. A. van Buchem, A. G. de Boer, and S. M. Van der Maarel. 2011. Transmigration of beta amyloid specific heavy chain antibody fragments across the in vitro blood-brain barrier. *Neuroscience* 190: 37–42.

17. McCafferty, J., A. D. Griffiths, G. Winter, and D. J. Chiswell. 1990. Phage antibodies: filamentous phage displaying antibody variable domains. *Nature* 348: 552–554.

18. Chomczynski, P., and N. Sacchi. 1987. Single-step method of RNA isolation by acid guanidinium thiocyanate-phenol-chloroform extraction. *Anal. Biochem.* 162: 156–159.

19. Maggi, M., and C. Scotti. 2017. Enhanced expression and purification of camelid single domain VHH antibodies from classical inclusion bodies. *Protein Expr. Purif.* 136: 39–44.

20. Garboczi, D. N., D. T. Hung, and D. C. Wiley. 1992. HLA-A2-peptide complexes: refolding and crystallization of molecules expressed in Escherichia coli and complexed with single antigenic peptides. *Proc. Natl. Acad. Sci.* 89: 3429–3433.

21. Conrath, K. E., M. Lauwereys, M. Galleni, a. Matagne, J. M. Frère, J. Kinne, L. Wyns, and S. Muyldermans. 2001. β-Lactamase inhibitors derived from single-domain antibody fragments elicited in the Camelidae. *Antimicrob. Agents Chemother.* 45: 2807–2812.

22. Chan, Y. C., H. Y. Lin, Z. Tu, Y. H. Kuo, S. T. D. Hsu, and C. H. Lin. 2018. Dissecting the structure–Activity relationship of galectin–Ligand interactions. *Int. J. Mol. Sci.* 19.

23. Salameh, B. A., I. Cumpstey, A. Sundin, H. Leffler, and U. J. Nilsson. 2010. 1H-1,2,3-Triazol-1-yl thiodigalactoside derivatives as high affinity galectin-3 inhibitors. *Bioorganic Med. Chem.* 18: 5367–5378.

24. 'T Hoen, P. A. C., S. M. G. Jirka, B. R. Ten Broeke, E. A. Schultes, B. Aguilera, K. H. Pang, H. Heemskerk, A. Aartsma-Rus, G. J. Van Ommen, and J. T. Den Dunnen. 2012. Phage display screening without repetitious selection rounds. *Anal. Biochem.* 421: 622–631.

Chapter 4

Phospholipase A2 specific single domain antibody neutralizes snake venom induced cellular and organismal toxicity

In this chapter “our” and “we” refers to me and co-investigators. My contribution in the chapter includes (1) Selection of the topic (2) Compiling and interpretation of the literature (3) Designing experiments (4) understanding and interpretation of the results (5) Preparation of graphs and figures (6) Writing and editing

Abstract

Snakebites continue to pose serious public health threat in many parts of the world. Anti-sera of animal origin have been the mainstay of therapeutic interventions for managing snakebites but associated ill effects are numerous. We tested whether anti-venom single domain antibody (sdAb) obtained by biopanning from phage display library of camelid VHH could neutralize the cellular and organismal toxicity in zebrafishes. Experimentally intoxicated zebrafishes were not only better protected by a prior neutralization of injected venom by sdAbs but also by their therapeutic injection. The venom neutralized zebrafishes also maintained the tissue integrity. Furthermore, such antibodies effectively neutralized the cellular toxicity as measured by *in vitro* assays. The sdAbs specifically interacted with phospholipase A2, gp12 of Russell viper venom with nanomolar affinity, resisted denaturation upto 65°C (T_m > 62.9°C), remained stable for a month at 37°C and maintained their structures between pH range of 2 to 10. Therefore, monoclonal single domain antibodies specific for venom components obtained from phage display libraries can serve as an effective therapeutic intervention for managing envenoming due to snakebites and help save lives.

Introduction

Envenoming due to snakebites and the ensuing mortality is a major public health problem in tropical and subtropical countries. As many as five million snakebites occur annually with approximately 50% envenoming rates leading to a quarter of a million deaths worldwide (1). A large majority of rural population, tribes, farm workers, fishermen, herdsmen, construction workers as well as personnel on expeditions in uninhabitable locations are mostly affected from snakebites. Most of the bitten patients particularly in resource-limited countries are not even admitted to hospitals for various reasons therefore the actual numbers are likely to be significantly more (2–4).

The members of family Elapidae and Viperidae such as *Daboia russelii* (Russell's viper), *Naja naja* (spectacled cobra), *Bungarus caeruleus* (common krait) and *Echis carinatus* (saw scaled viper) contribute to the loss of life and morbidity in a decreasing order particularly in Asian countries (5). The cardiovascular and nervous systems are initially affected by hematotoxins or the neurotoxins present in the venom (6, 7). The dose and duration of injected venom decides the severity of disease and mortality if such cases are not attended to in a timely fashion. The mortality is due to loss of vital organs function. A large proportion of snakebite survivors develop one or more types of permanent disabilities (8–10). About 70-90% of venom's dry weight consists of molecules that range from organic acids to large proteins, which act either in isolation or in synergy to cause the pathogenesis. Enzymes such as oxidoreductases, transferases, hydrolases, hyaluronidases, phospholipases, lyases are considered as major contributors of toxicity (11).

Approximately 80% population worldwide depends on traditional medicine for treating snakebites, the efficacy of which is highly questionable (12). Anti-venom serum (AVS) of animal origin has been the cornerstone therapy for managing snakebites. AVS

used for venom neutralization may be monovalent that targets venom from a single species of snake or polyvalent that neutralize venom from more than one species. AVS injections cause various ill effects that range from anaphylaxis to serum sickness and if not treated in a timely fashion could be life threatening (13–15). Moreover, the current demand of AVS exceeds the supply globally, which further underscore the need of developing better alternatives. This calls for finding innocuous alternatives having better biological and biophysical properties. The startling discovery that all members of camelidae family possess a significant proportion of their serum antibodies that lack light chains but nonetheless were able to bind to antigens with an equivalent and better affinities, paved the way for exploiting their unique features as potential therapy (16). We tested whether such antibodies could serve to neutralize the toxicological effect of the Russell viper venom in cellular assays as well as in the vertebrate host. We also explored whether or not zebrafish could be used for screening the toxicological effect of Russell viper venom and its neutralization by monoclonal sdAbs obtained by phage display technology. We demonstrated that single domain antibodies obtained from phage display library effectively neutralized the venom induced toxicological effects. Such formulations effectively protected primary and established immune cells from venom-induced cytotoxicity. A prior neutralization of venom by sdAbs or their therapeutic administration enhanced survival of experimentally intoxicated zebrafishes as well as restored organ integrity. Furthermore, sdAbs displayed superior biophysical, biochemical and biological properties that included an extended shelf life. Therefore, specific sdAbs could serve as an effective therapeutic intervention to manage envenoming due to snakebites

Materials and Methods

Biochemical characterization of Russell viper venom RVV

A. Gel filtration chromatography: For the fractionation of RVV components, 40mg of crystallized venom was dissolved in 1ml of 10 mM PBS and passed through 0.22µm filters. The sample was injected into Hi Prep 16/60 200HR column (UNICHROMAT 1500 system GE Healthcare Life Sciences) and 0.5ml fractions were collected at the flow rate of 0.2ml/min.

B. Sodium dodecyl sulphate - polyacrylamide gel electrophoresis (SDS-PAGE): Fraction from each of the peaks were pooled and run using reducing as well as non-reducing SDS-PAGE for analysis of their polypeptide profile. Additionally, the whole venom was also resolved simultaneously. Indicated concentrations of venom and its different fractions obtained by chromatography were mixed with equal volume of 2x Laemmlie sample buffer (LSB) with or without carrying β-mercaptoethanol.

C. Mass spectrometry (MS): Lyophilized RVV powder obtained from local vendors was stored at -20°C until use. RVV was dissolved in PBS to obtain 100µg in 65µl concentration and then 25µl of 100mM ammonium bicarbonate (ABC) was added so as to make the final concentration of 25mM in 100µl volume. To this solution, 10µl of Tri butyl phosphine (TBP) was added for reduction and incubated at 37°C for 30 minutes. For the alkylation process, the cocktail was treated with 100µl of 40mM idoacetamide (IAA) in 25mM ABC solution for 30 minutes at 37°C. By using speed vacuum, its volume was reduced to 50µl. We then added 1µl of solubilization buffer to trypsin vial followed by 49 µl of reaction buffer. Both the solutions (50µl reduced and alkylated protein plus 50µl trypsin solution) were mixed and kept for O/N at 37

°C (17). Samples were then acquired using Waters™ synapt G2-Si Q ToF Mass spectrometer with electrospray shotgun mode.

Measuring cytotoxicity by RVV

We used primary cells (mice $CD4^+$ and $CD8^+$ T cells) and Jurkat cells for measuring toxicological effects on venom. $CD4^+$ and $CD8^+$ T cells were isolated from spleens and lymph nodes of C57BL/6 mice using 'Dynabeads untouched mouse $CD4^+$ and $CD8^+$ T cells kits. Different concentrations of Russell's viper venom (0.1, 1, 10 & 100µg per well) were used and in some wells no venom was added to serve as control. Then the cells were added and incubated for different time periods (0, 0.5, 1, 2 and 4 hrs) at 37°C. The viability of cells was checked using trypan blue dye exclusion method. The cells were also stained for with Annexin V and PI to assess the cytotoxicity using flow cytometry. Additionally, different concentrations of eight different fractions obtained from gel filtration chromatography were used. Then, cells were added and incubated for different time at 37°C. Cells were also stained using acridine orange and Ethidium bromide and images were analyzed by fluorescence microscope with at a magnification of 100x (18).

Measuring toxicological effects of individual fraction of RVV

Jurkat cells and HEK293T cells were incubated with 10µg of whole RVV and equivalent concentrations of its isolated fractions for two hrs at 37°C. The Jurkat cells were then washed three times, and stained with Annexin V and PI followed by acquisition using a flow cytometer. HEK293T cell line being semi adherent were only analyzed microscopically at 400X magnification.

Effect of RVV on the cell cycle

Jurkat cells were grown in serum free RPMI media for 24hrs and then incubated with 10µg of RVV in complete media for 4 hrs. After that cells were washed with 10 mM PBS and

kept in 70% chilled ethanol for 2 hrs at -20°C. Then cells were washed and incubated with 50µl of RNAse solution (stock 50µg/ml) for 30 minutes at 37°C. For staining equal volume of PI solution (stock 50µg/ml) was used and BD FACS Accuri was used to acquire and analyze samples.

ELISA for measuring specific antibody response

Peripheral blood samples were collected from unexposed or immune camels to collect the PBMCs and serum samples. For performing ELISA, 100µl of RVV and its various fractions (10µg/ml) were coated in 96 well polystyrene ELISA plates overnight at 4°C. Next day the plates were washed three times with 10mM PBS-0.05% Tween-20 (PBST) and blocked with 3% BSA in PBST for 2 hrs at room temperature. After blocking and washing, 10 fold serial dilutions of serum samples were added and plates were incubated for one and a half hour at room temperature. After extensive washings, 10^{-4} dilution of mouse anti-camel antibodies were added and plates were incubated one and a half hour at RT. Plates were then washed for three times with PBST and anti-mouse alkaline phosphatase was added. The plates were incubated for one and a half hour. After three washings plates were developed by adding 200µl per well of pNpp substrate obtained from sigma Aldrich (1mg/ml in glycine buffer). Reaction was stopped with 50µl of 3M NaOH per well and the absorbance values were recorded at 405nm. In some experiments the binding stringency was achieved using 10 fold higher concentration of Tween-20.

Determination of antibody titres

The purified HCAbs were used for generating hyperimmune sera in mice following established protocols (19). Antibody titres of the mice anti-camel IgG3 whole serum was determined from A_{450} values of their log dilutions using the formula:

Log antibody titre = X+ (A-C/A-B) x D

Where

X = Log dil. of the test sample having A_{405} immediately lower than cut-off value.

A = A_{405} of the test sample dil. immediately higher than the cut-off A_{405} value.

B = A_{405} of the test sample dil. immediately lower than the cut-off A_{405} value

C = Cut-off A_{405} value

(C = Mean A_{405} of the negative samples + 3x Standard deviation)

D = Log dil. factor i.e. 1

Biopanning

The methods described in the chapter 3 were followed for selection of sdAbs against RVV. Only one round of biopanning was performed with 10µg of RVV. The reactivity of displayed VHH was established by phage ELISA.

Subcloning and protein purification

The cloned VHH sequences were confirmed by PCR and restriction digestion using *Nco I* HF and *Not I* HF for 3 hrs at 37°C. Digested VHH sequences were gel extracted using PCR purification kit (Invitrogen) and ligated to the double digested pET22b vector. The ligated product was transformed in chemically competent DH5α cells. Next day, colonies were picked and grown in LB amp medium overnight. Plasmids purification was done by miniprep kits (Invitrogen). 10ng of isolated plasmids were transformed in chemical competent *E. coli Origami* cells. Protein induction was achieved at 18°C for 16 hrs and thereafter the cells were pelleted down at 5000 rpm. Two methods were used for protein purification. i) The cell pellet was suspended in lysozyme (100µl of 100mg/ml lysozyme) and then sonicated (amplitude at 40) with 1min pulse on/1min pulse off for 8 cycles on ice. The cell lysate was centrifuged at 10, 000 rpm for 30 minutes and the supernatant thus obtained was passed through Ni-NTA column. The elution was performed in Tris-NaCl buffer containing 400mM imidazole. ii) As the substantial amount of induced protein was

present in the inclusion bodies, therefore we also attempted to purify and refold induced VHH. Purification from inclusion bodies was performed under denaturing conditions as described earlier (20). The protein was then refolded using refolding buffer as described earlier (21) with addition of 400mM L-arginine (Sigma). To check for the purity, eluted protein was loaded on SDS-PAGE. For further purity, refolded protein was loaded on gel filtration column and based on the absorbance at 280 nm and different fractions were collected.

Binding assays

For binding kinetics Bio layer interferometry (BLI) was performed using BLltz system with Ni-NTA probes (ForteBio). 150µl of 50µg/ml HIS tagged VHH was loaded on the probes for 5 minutes and the excess of unbound VHHs were washed out by incubating in PBS. For the association/ binding, the immobilized VHH was incubated with different concentrations of RVV and for dissociation kinetics the probe was placed in PBS. All incubations were done at RT for 5 minutes. After each round, probe was re-charged by placing sensor in 10mM glycine for 1 minutes and then PBS for 5 minutes and finally for 1 minutes in 10mM Nickel sulphate solution..

Molecular docking

PDB files for V_HH and sPLA2 were generated by using I-TASSER online server (22–24). Then, ClusPro2.0 server (http://ClusPro.bu.edu/) was used to predict possible interactions between V_HH and sPLA2 in the antibody mode with V_HH selected as receptor and sPLA2 selected as the ligand (25). Docked structure having minimum ClusPro score was selected and further analysed using the PyMOL Molecular Graphics System, Version 2.0 Schrödinger, LLC.

Determining the specificity for sdAbs

The pull-down experiments were performed for determining the specific component of RVV interacting with the selected specific VHH-$(HIS)_6$. 100µl of Ni-NTA conjugated magnetic beads (Qiagen) were washed and incubated with the mixture of 50µg VHH and 100µg neat venom in 100µl PBS at room temperature (RT) while gently shaking at 10 rpm for 1 hr. Only beads were used for the control experiments keeping all other components as such. These beads were washed three times with PBS and finally re-suspended into 10µl PBS. Samples were prepared in 2x Laemmli sample buffer at 95°C for 5 min and resolved using a 15% SDS-PAGE.

Phospholipase A2 activity assay

The phospholipase activity was measured by using a matrix carrying 4% of egg yolk in 0.9% agarose solution (45°C) in 10mM Calcium chloride. Plates were prepared and the wells were punched in the gel in which 10µl of sample was poured (PBS, Neat RVV or fraction 7). Plates were incubated at 37°C for 20hrs and then diameter of clear zones were measured as described earlier (26). In order to measure the inhibitory activity of phospholipase A_2 by specific sdAb, a prior incubation of either the whole RVV or the separated fraction 7 was done and then the cocktail was added to the wells of prepared gel.

Thermal and pH Stability of sdAbs

To measure the effect of temperature on the structural integrity of VHH, thermal kinetics was performed. Pure preparations of sdAbs were incubated at different temperatures ranging from 20°C to 90°C for 10 min at each point and T_m was calculated from their circular dichroism (CD) spectra (27). Similar experiments were performed where the VHH were incubated in the buffers varying in pH values ranging from 2 to 13 followed by analysis by using CD spectra.

In vitro and *in vivo* neutralization of RVV by specific sdAbs

We performed *in vitro* and *in vivo* experiments to investigate whether or not sdAbs neutralize toxicity caused by RVVs. For *in vitro* neutralization, graded doses of specific sdAbs were pre-incubated with 10µg of RVV on ice for 30 minutes then added to Jurkat cells (0.5 million per well of 96 well plate) and the cells were stained using annexin V and PI followed by flow cytometric analysis 2 hrs later.

For *in vivo* neutralization, 6µg of sdAbs were pre-incubated with 10µg of RVV for 30 minutes on ice and then the cocktail was injected into zebrafishes intraperitoneally. Un-injected or only RVV in PBS injected zebrafishes served as control for such experiments. After 0.5 hour of injection another dose of 6µg was injected. Control animals were similarly injected with the same volume of diluent and the experimental animals were followed for more than 10 hours duration. At the termination of experiment, all the zebrafishes were scarified exposing to cold temperature and carefully dissected to collect internal organs such as intestines. Intestines thus isolated from control and sdAbs neutralized venom intoxicated animals were treated with different concentrations of sucrose and fixed in 5% paraformaldehyde. The fixed organs were then embedded into blocks with optimal cutting temperature (OCT) compound. These blocks were stored at -80°C until further use. Similar experiments were conducted for measuring the efficacy of purified HCAbs from sera samples.

Histological investigation

The frozen tissue blocks were used for preparing sections of intestines from different groups using a cry-sectioning machine and slides were prepared. Tissue sections were then stained using hematoxylin and eosin (H&E) dyes with slight modifications from original protocol (28) and visualized using 10X objective lenses.

Statistical analysis

One-way ANNOVA with Tukey's multiple comparison tests and two way ANOVA for more than three groups were used. The p value below 0.05 considered as significant. * <0.05, ** <0.01 and *** <0.001.

Results

Generation of anti-camel antibodies

From Camel sera samples, HCAb's were isolated by ammonium sulphate precipitation method and further purified by gel filtration chromatography (Fig no. 4.1A). Different fractions were loaded on SDS-PAGE and later fractions were pooled which contains only HCAb's (Fig no. 4.1B). HCAB' were further purified by using protein A and G conjugated magnetic beads (Fig no. 4.1C) where IgG2 and IgG3 were eluted at different pH buffers. Final product was used to immunize Balb/c mice (29) and hyperimmune serum was collected before every booster dose. After two booster doses, final serum was collected and antibody production was checkedby different immunological techniques. First we did most basic technique i.e. Agarose gel immunodiffusion assay where three wells were punched in the agarose gel layer and then antigen i.e. Camel HCAb's were added to the 2nd well. Mice preimmune and hyperimmune serum were added to the well no. 1 and 3 respectively. We observed a precipitation line between the well no. 2 and 3 (Fig no. 4.1D). It shows that antibody titer was quite high which was further calculated by ELISA i.e 10^6 (Fig no. 4.1E) and antibody specificity was established by western blotting (Fig no. 4 .1F&G).

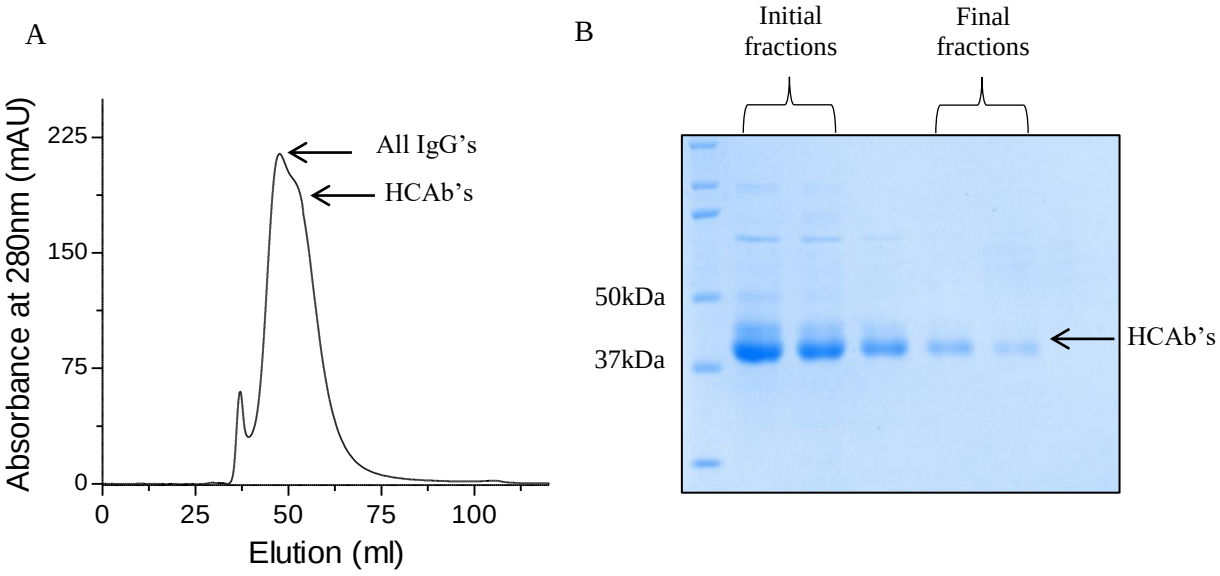

C

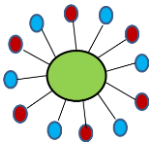

Protein A and Protein G attached to the magnetic bead

Elution of IgG2 at pH 4.5

IgG2

Elution of IgG3 at pH 3.5

IgG3

D

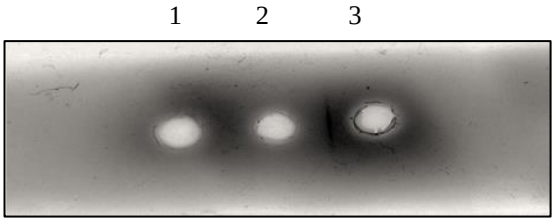

1. Pre-immune serum, 2. Antigen (HCAb's)

3. Hyper-immune serum (HIS)

E

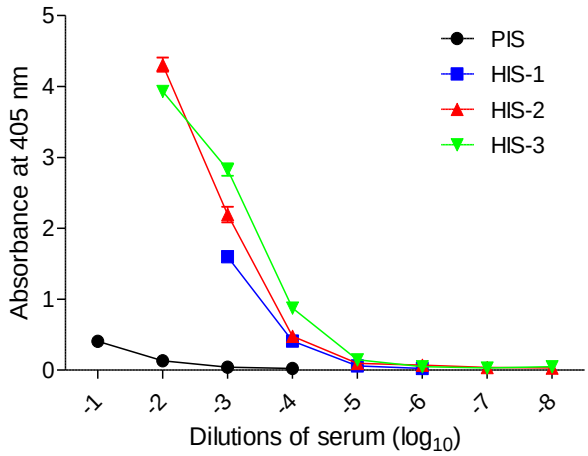

F

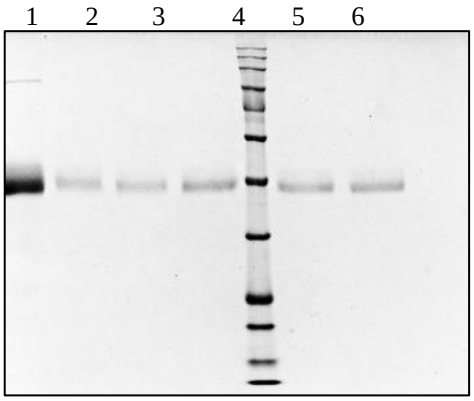

1. Before purification, 2. Supernatant, 3. Washing, 4. IgG2, 5. MWM, 6 & 7. IgG3, 8. Dye

G

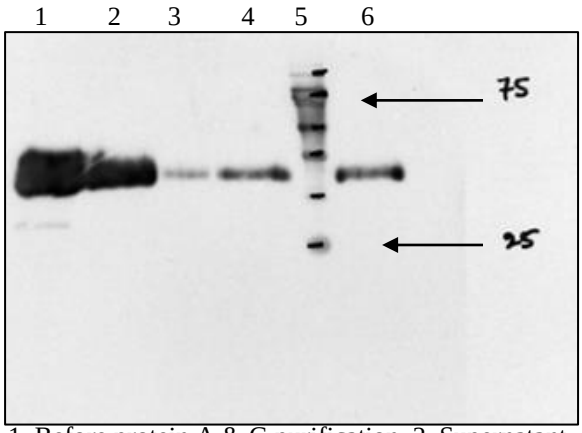

1. Before protein A & G purification, 2. Supernatant, 3. Washing, 4. IgG2, 5. MWM, 6. IgG3

Figure no. 4.1. Generation of anti-camel HCAbs antibodies. A. & B Gel filtration chromatograph and SDS-PAGE showing the all IgG's in initial fractions and only HCAb's (IgG2 and IgG3) in later fractions, C. Schematic of Protein A and G based purification of HCAb's, D. AGID showing precipitation line between 2^{nd} and 3^{rd} well, E, Hyperimmune serum collected after each booster dose and used to calculate the antibodv titre after final dose.

Characterization of RVV

The polypeptide profile of freshly reconstituted RVV was obtained by resolving its components using a non-reducing SDS-PAGE. Eight different fractions of RVV obtained by gel filtration were also simultaneously resolved by electrophoresis. The representative chromatogram and the polypeptide profile are shown in Figure 4.2A and 2B. We obtained more than 15 different identifiable polypeptide bands in a 12% reducing and non-reducing gels (Fig no. 4.2B). The various fractions obtained by gel filtration revealed some distinct polypeptide bands while the molecular weight of other polypeptides were shared among multiple fractions (Fig no. 4.2B). We therefore analyzed the whole RVV by MS analysis. The results obtained are shown in table 4a. Various enzymes such as acidic and basic secretory phospholipase A2, serine protease inhibitors, C-type lectins such as snalecs, proteins involved in activating blood coagulation factors V and X, amino acid oxidizing enzymes etc were identified in the RVV based on their PLGS scores (Table 4a). Some selected fractions were also subjected to MS analysis. Major proteins in fraction 1 were amino acid oxidases, Zinc metalloproteinase-disintegrin-like, vimentins etc. In addition factor X activating heavy and light chains were recovered from the fraction 1 (Table 4b). The peptide coverage from fraction 4 revealed the presence of proteins such as acidic, basic and neutral phospholipase A2, serine proteases and the subunits of proteins that activate factor X of the blood coagulation system. In addition, the caspases recruitment domain fragment 4 (CARD4) proteins was also present in this fraction (Table 4c). Many of these proteins are responsible

for causing apoptosis of cells, blood clotting, cellular adhesion as well as inflammatory reactions.

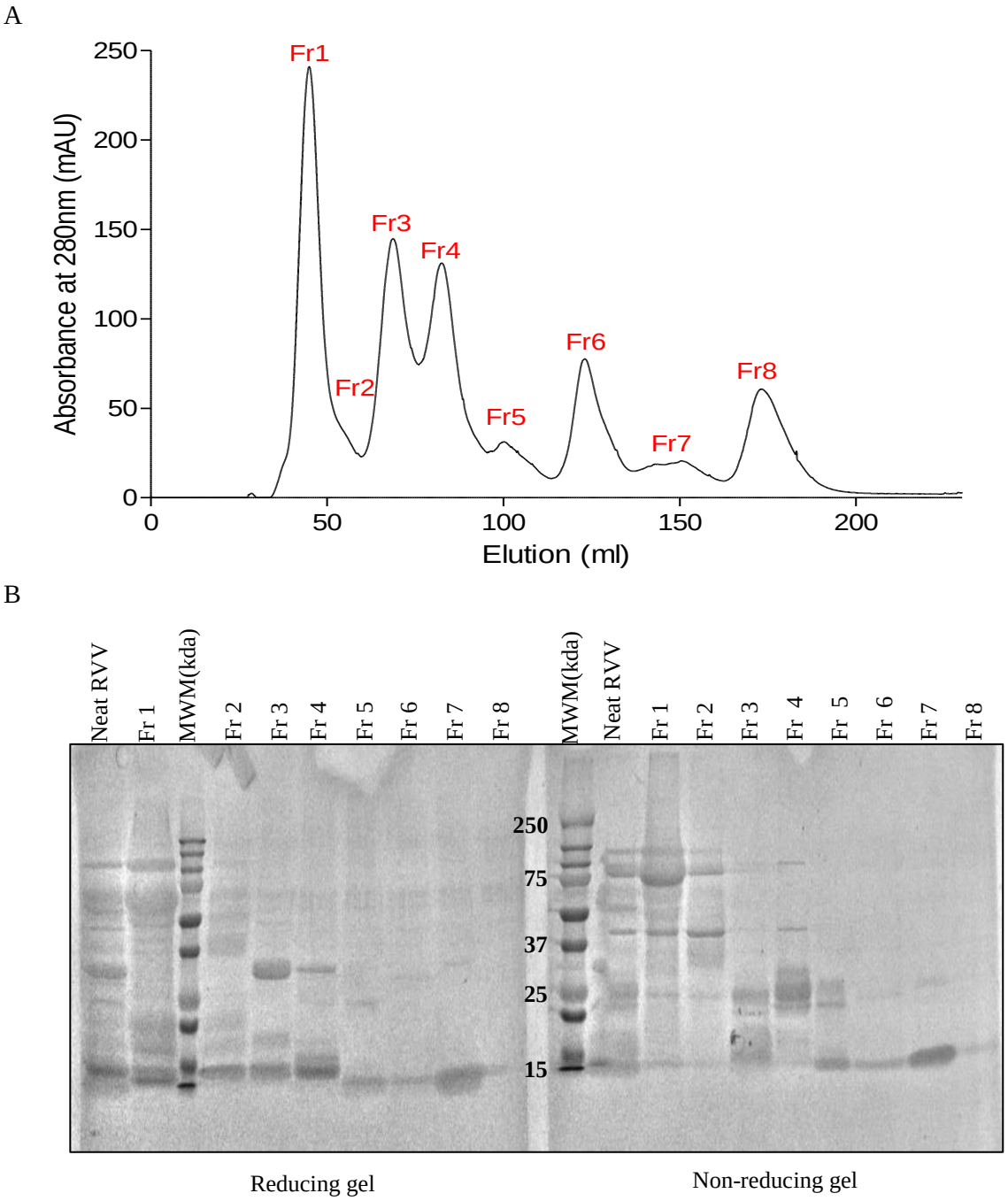

Figure no. 4.2. Preliminary analysis of RVV. A. Gel filtration chromatograph, B. Polypeptide profile under reducing as well non-reducing conditions.

Table no. 4.1a. Mass spectrometric analysis of neat RVV.

Accession	Description	mW (Da)	pI (pH)	PLGS Score
Q7T2R1	Acidic phospholipase A2 daboiatoxin A chain OS=Daboia siamensis PE=1 SV=1	15384	4.4561	9189.087
Q2ES51	Phospholipase A2-IV OS=Daboia russelii PE=2 SV=1	15112	5.0493	5552.593
A8CG89	Basic phospholipase A2 Drk-b1 OS=Daboia russelii PE=1 SV=1	15853	8.2397	4724.177
P0DKX1	Neutral phospholipase A2 RVV-PFIIc' (Fragment) OS=Daboia russelii PE=1 SV=1	2192	7.793	4471.857
B2YHV5	Phospholipase A2 OS=Daboia siamensis GN=PLA2S3 PE=3 SV=1	15468	4.4136	3848.604
A8CG82	Basic phospholipase A2 DsM-b1/DsM-b1' OS=Daboia siamensis PE=1 SV=1	15832	8.2397	3393.998
P00990	Kunitz-type serine protease inhibitor 2 OS=Daboia siamensis PE=1 SV=1	6845	8.2998	3190.139
P0DJP5	Acidic phospholipase A2 Drs-PLA2 (Fragment) OS=Daboia siamensis PE=1 SV=1	2012	11.4888	1779.744
Q2ES49	Kunitz-type serine protease inhibitor 2 OS=Daboia russelii PE=2 SV=1	9676	10.0415	1426.438
T1P647	Factor X activator light chain 2 OS=Daboia russelii PE=2 SV=1	18311	5.5254	1344.81
K4GT33	Caspase recruitment domain family member 4 (Fragment) OS=Daboia russelii GN=CARD4 PE=4 SV=1	35443	8.9194	783.4761
A8CG87	Acidic phospholipase A2 Drk-a2 OS=Daboia russelii PE=2 SV=1	15574	4.73	705.3512
F2Q6F3	Cysteine-rich seceretory protein Dr-CRPB (Fragment) OS=Daboia russelii PE=2 SV=1	25027	8.0845	687.632
V9I1K1	Venom nerve growth factor 1 OS=Daboia russelii PE=2 SV=1	27424	8.4814	677.2955
F2Q6F2	Cysteine-rich seceretory protein Dr-CRPK OS=Daboia russelii PE=2 SV=1	26670	7.0327	622.0593

Table 4.1b. Mass spectrometric analysis of fraction 1

Accession No.	Description	mW (Da)	pI (pH)	PLGS Score
G8XQX1	L-amino-acid oxidase OS=Daboia russelii PE=1 SV=1	56852	8.4463	2136.782
K9JAW0	Factor X activator heavy chain OS=Daboia russelii PE=2 SV=1	69474	5.981	1036.854
K9JBV0	p68 alpha subunit OS=Daboia siamensis PE=2 SV=1	17984	5.2339	517.9565
K9JDE8	Dabocetin beta subunit OS=Daboia russelii PE=2 SV=1	18011	6.3823	511.0542
K9JCB2	Factor X activator light chain 2 OS=Daboia russelii PE=2 SV=1	18260	6.0923	225.8476
B8K1W0	Zinc metalloproteinase-disintegrin-like daborhagin-K OS=Daboia russelii PE=1 SV=1	69509	5.9238	157.5799
B9TVZ4	Zinc finger homeobox protein (Fragment) OS=Daboia russelii GN=ZEB2 PE=4 SV=1	32169	8.1724	68.7573
Q8UVG8	Vimentin OS=Daboia russelii PE=2 SV=1	52816	4.9058	58.5073

Table 4.1c. Mass spectrometric analysis of fraction 4

Accession No.	Description	mW (Da)	pI (pH)	PLGS Score
Q7T2R1	Acidic phospholipase A2 daboiatoxin A chain OS=Daboia siamensis PE=1 SV=1	15384	4.4561	9189.087
Q2ES51	Phospholipase A2-IV OS=Daboia russelii PE=2 SV=1	15112	5.0493	5552.593
A8CG89	Basic phospholipase A2 Drk-b1 OS=Daboia russelii PE=1 SV=1	15853	8.2397	4724.177
P0DKX1	Neutral phospholipase A2 RVV-PFIIc' (Fragment) OS=Daboia russelii PE=1 SV=1	2192	7.793	4471.857
B2YHV5	Phospholipase A2 OS=Daboia siamensis GN=PLA2S3 PE=3 SV=1	15468	4.4136	3848.604
A8CG82	Basic phospholipase A2 DsM-b1/DsM-b1' OS=Daboia siamensis PE=1 SV=1	15832	8.2397	3393.998
P00990	Kunitz-type serine protease inhibitor 2 OS=Daboia siamensis PE=1 SV=1	6845	8.2998	3190.139
P0DJP5	Acidic phospholipase A2 Drs-PLA2 (Fragment) OS=Daboia siamensis PE=1 SV=1	2012	11.4888	1779.744
Q2ES49	Kunitz-type serine protease inhibitor 2 OS=Daboia russelii PE=2 SV=1	9676	10.0415	1426.438
T1P647	Factor X activator light chain 2 OS=Daboia russelii PE=2 SV=1	18311	5.5254	1344.81
K4GT33	Caspase recruitment domain family member 4 (Fragment) OS=Daboia russelii GN=CARD4 PE=4 SV=1	35443	8.9194	783.4761
A8CG87	Acidic phospholipase A2 Drk-a2 OS=Daboia russelii PE=2 SV=1	15574	4.73	705.3512
F2Q6F3	Cysteine-rich secretory protein Dr-CRPB (Fragment) OS=Daboia russelii PE=2 SV=1	25027	8.0845	687.632
V9I1K1	Venom nerve growth factor 1 OS=Daboia russelii PE=2 SV=1	27424	8.4814	677.2955
F2Q6F2	Cysteine-rich secretory protein Dr-CRPK OS=Daboia russelii PE=2 SV=1	26670	7.0327	622.0593

Determining the immunogenicity of RVV components

The whole RVV and all the different fractions were probed for their antigenicity using two different immunoassays: ELISA and western blotting. Equal protein concentrations (10µg/well) of the whole RVV and the fractionated components were coated onto ELISA plates and immune sera obtained from camels were screened for the presence of specific antibodies to identify immunogenic fractions of the RVV. The results show the immunogenicity of the whole venom as well as different components in the fractionated venom (Fig no. 4.3A). We used two different concentrations of tween-20 i.e. 0.05% like normal ELISA or western blot and another is 0.5%. With 0.05% tween-20, the immunogenicity of fractions 1 to 4 was more as compared to that of other fractions but as we increased the percentage of the detergent then the absorbance of different fractions has been changed, i.e. neat, Fr5 and 1 have maximum while 4,6 and 7 have overlapped absorbance and other fractions showed minimum absorbance. (Fig no. 4.3 A&B). In order to identify the immunogenicity of molecular species present in the RVV, the whole RVV and different fractions obtained by chromatographic separation were electrophoresed to resolve in a 12% reducing and non-reducing gel and the polypeptides thus obtained were electro blotted on a PVDF membrane (GE Healthcare Lifesciences). The membranes were then probed for the identification of polypeptides against which specific antibodies were generated. The major response in the whole RVV was directed against protein band of 35kD and 15kD (Fig no. 4.3C). The major polypeptide bands detectable by anti-sera were present in six out of 8 fractions. Fraction 6 and 8 did not show a positive reaction. The polypeptides in Fr 1 (65, 25 and 15kD), Fr 3 (35 and 15kD), Fr 4 (15kD), Fr 5 (15kD) and Fr 7(11kD) exhibited greater immunogenicity (Fig no. 4.3C).

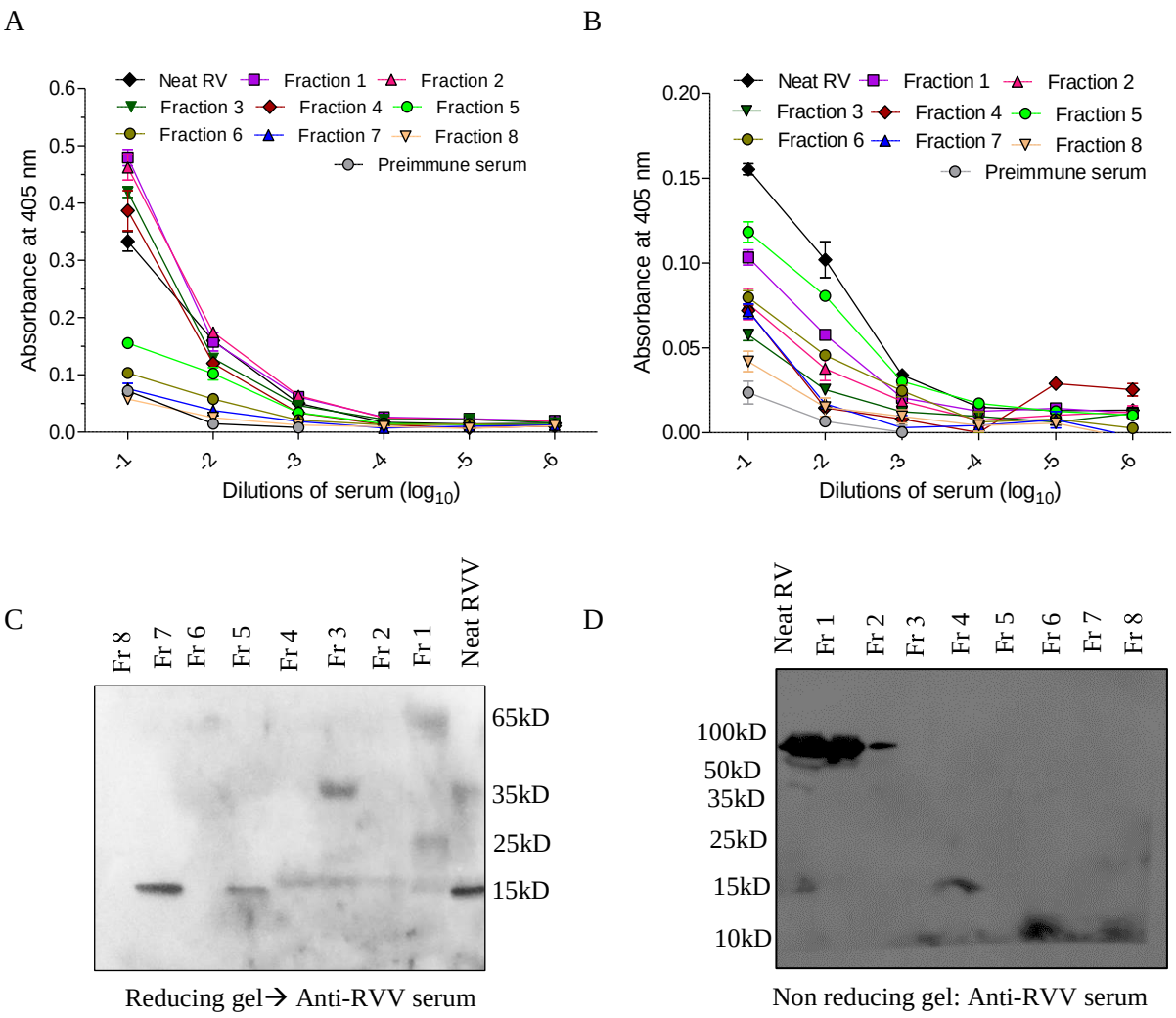

Figure no. 4.3. Immunogenicity of neat RVV and its fractions. A & B. Indirect ELISA with 0.05% and 0.5% tween-20 respectively, C&D. Immunoblotting with camel serum under reducing and non-reducing conditions (gels) respectively.

Selection and characterization of RVV specific sdAbs from phage display libraries

The phage display library of VHH from camelids was previously generated and 22 million transformants were obtained (as described in previous chapter). 10µg of neat RVV per well was used for Biopanning. There was more than five-fold difference in the numbers of colonies between test (where RVV was coated) vs control plates (no antigen). After biopanning, we screened the colonies by phage ELISA and found 5 out of 288 positive clones. Surprisingly all 5 clones had the same sequence. We then subcloned the VHH into

original as well as modified pET22b vector and transformed into origami *E. coli* strain. From original vector the sdAb would be expressed with $(HIS)_6$ tag but in modified vector we added biotin acceptor sequence so as to produce *in vivo* biotinylated VHH along with $(HIS)_6$ tag. We then purified sdAbs under denaturing conditions and the yield was 25mg/L. VHH or sdAb had a molecular mass of 17 kDa and its purity is shown in (Fig no. no. 4.4A). As the function of VHH is governed by its structural integrity, we performed CD spectral analysis and observed β sheets (because of a peak in range between 210-220nm) (Fig no. no. 4.4B). There was also a peak at 230nm that could be due to side chains in the tertiary structures (30). The RVV specific sdAb clone was selected by biopaning from the phage display libraries using RVV coated plates and the specificity of the interaction was initially confirmed by phage ELISA. To identify the interacting partner/s for sdAb from the components of RVV, we performed a pull-down assay. Ni-NTA magnetic beads were first incubated with VHH-$(HIS)_6$ and then with neat RVV as described in the materials and method section. The bound mixture after extensive washings was resolved by a reducing SDS-PAGE and different controls were simultaneously included. We observed a specific band migrating close to 10kDa size that was absent in other controls such as the only sdAbs or the only beads. This experiment was also repeated with only fraction 7 also and we got repeatable results (Fig no. 4.4C&D). We cut out the specific band and performed a MALDI MS/MS where the spectra were searched against NCBI protein database for *Daboia russelii* (taxid 8707) using a Crux mass spectrometry analysis tool-kit employing target-decoy strategy (31, 32). Precursor ion/mass tolerance was kept 1.2 Da and fragment ion/mass tolerance at 0.6 Da. To improve the outcome of identification procedures, semi-tryptic digestion was performed and only upto one-missed cleavage was allowed. Protein with $-10*\log_{10}$ posterior error probability (PEP) scores greater than 20 was considered as positive. Using these criteria, we identified group 12B secretory phospholipase A2 *(Daboia*

russelii, Accession no ASU45046.1, MW 10.5kDa) as the specific interacting partner for sdAbs (33). Some additional polypeptide bands were recovered with beads alone which could be due to the presence of histidine patches in these proteins that could interact with Ni-NTA beads (34). The band of 10.5kDa was also present when the whole RVV and fraction 7 were probed using VHH-$(His)_6$ and a secondary *anti*-$(His)_6$ -HRP antibody by western blotting (Fig no. no. 4.4E) as well as when biotinylated VHH and streptavidin-HRP conjugate were used (Fig no. 4.4F-G)**.** We further confirmed our results by measuring its phospholipase activity by using egg yolk as a substrate. Neat RVV in different dilutions was used as a positive control. Due to specific reactivity of fraction 7, 10µg of fraction 7 was also included in such assays. We observed a clear zone after 10-15 hrs of incubation and the diameter of the zone increased with the more concentration of loaded protein (Fig no. 4.4H).

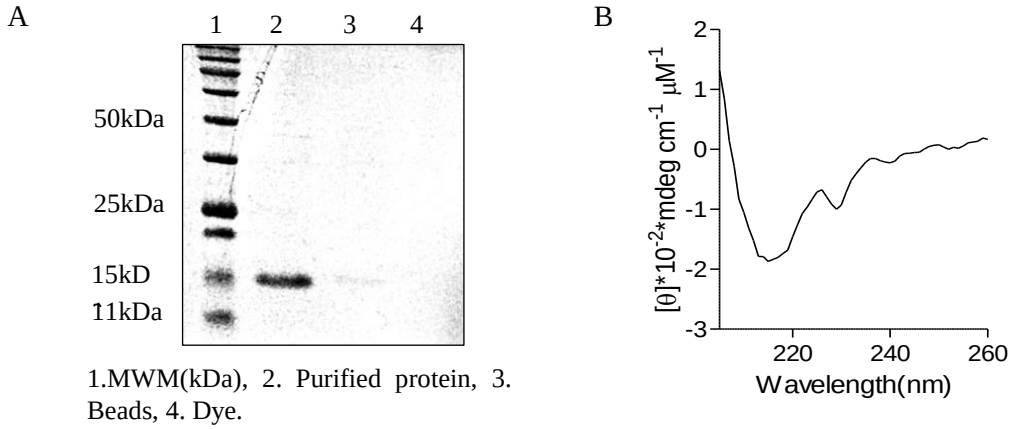

1.MWM(kDa), 2. Purified protein, 3. Beads, 4. Dye.

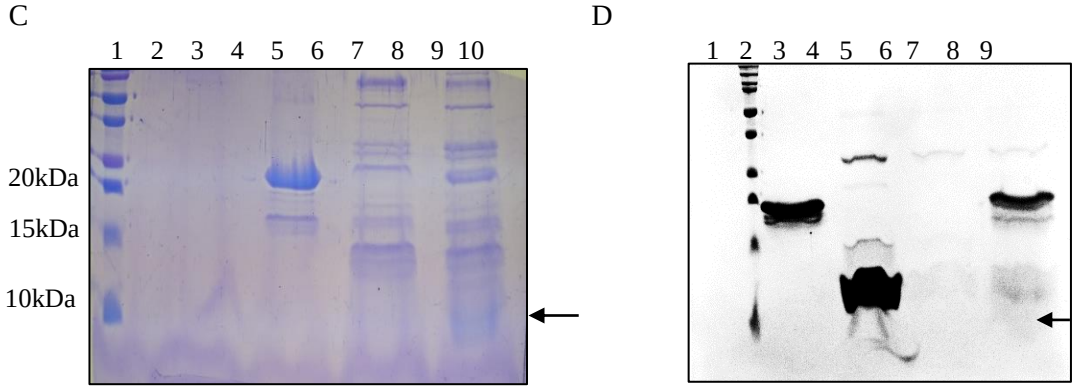

1- MWM; 2,4,6,8 &10 8 &10 10 ely, C&D 5- VHH with beads; 7- RVV with beads, 9- beads plus VHH and RVV

1.Dye, 2. MWM, 3.Beads + sdAb, 4,6,8&10. Empty, 5. Fraction 7, 7. Beads + Fr 7, 9. Beads+sdAb+Fr 7

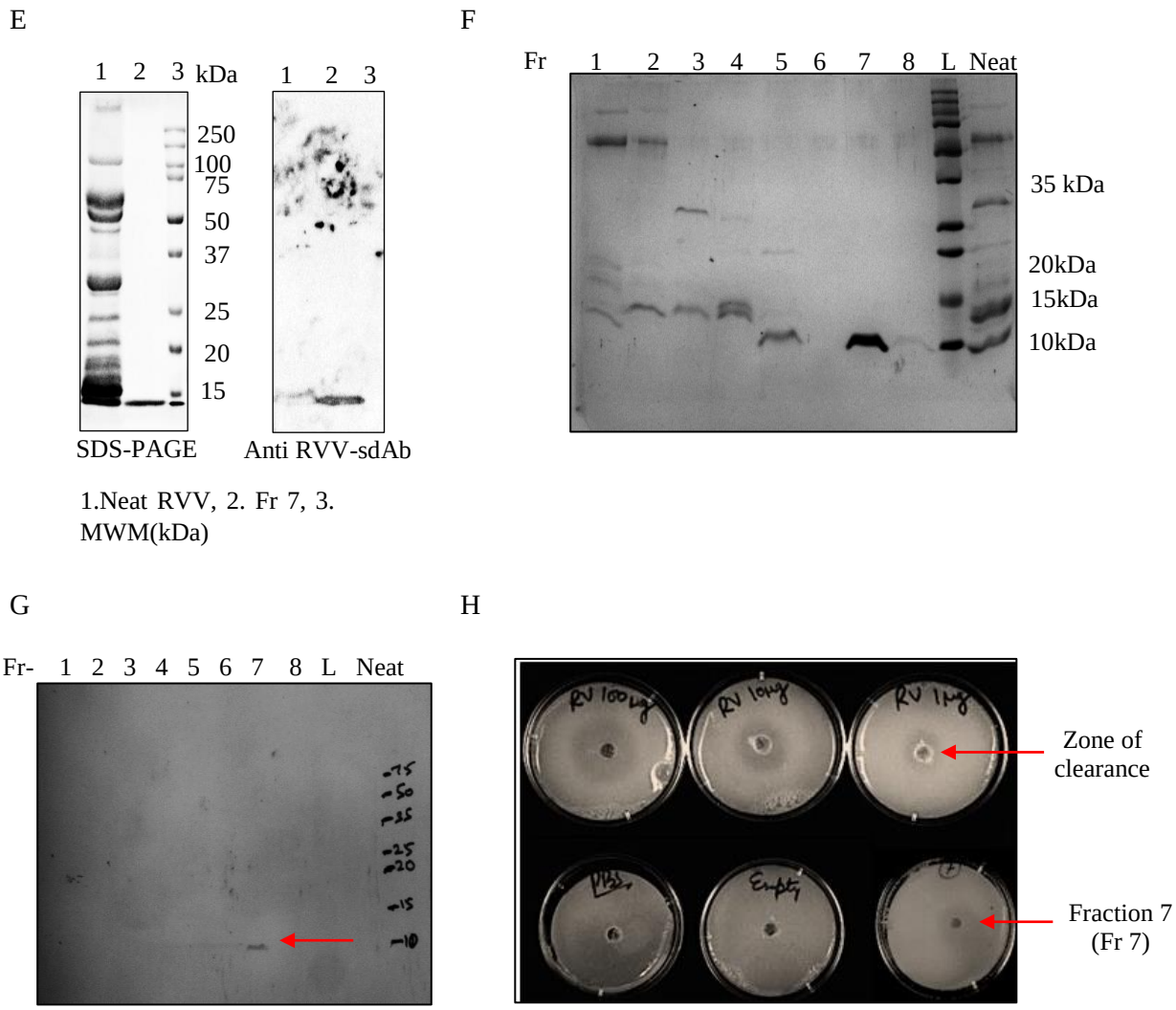

Figure no. 4.4. Expression, purification of sdAb (VHH) and identification of its ligand. A& B. SDS PAGE of purified VHH and after refolding, CD graph showing its secondary structure, C &D. Pull down by using neat RVV and Fr7 with sdAb Ni NTA magnetic beads, F &G. SDS PAGE and Immunoblotting of different fractions of RVV by biotinylated sdAb, H. Phospholipase A2 assay of different concentrations of RVV and 10µg of Fr7.

Binding kinetics of sdAb with neat RVV and Fr 7

The most critical characteristics of therapeutic or the diagnostic antibody is its affinity of interaction with the antigens as this would help decide the neutralizing dose. To measure its binding kinetics we performed biolayer interferometry (BLI). We used different concentrations of neat venom and observed strong association of VHH with RVV (Fig no. 4.5A&B). As the RVV has many proteins so the effective concentration of binding partner

cannot be determined unambiguously. Nonetheless the approximate affinity of interaction of the clone of sdAb against RVV was found to be $4x10^{-7}$. Similar experiment was performed where RVV was treated with Ni-NTA agarose beads for 1 hr and then residual RVV components were used for binding assay. We observed similar pattern pattern of binding and Kd was $2*10^{-7}$. We also performed ELISA as a supportive assay where fixed concentration of Fr 7 was coated in the ELISA plate (i.e.10µg/well) followed by addition of increasing molar ratios of sdAb to each wells. The plates were probed with anti $(HIS)_6$ tagged antibody. We observed a 50% binding at the molar ratio of 1:1.25 and at 1:10 molar ratio 93% binding was observed (Fig no. 4.5C).

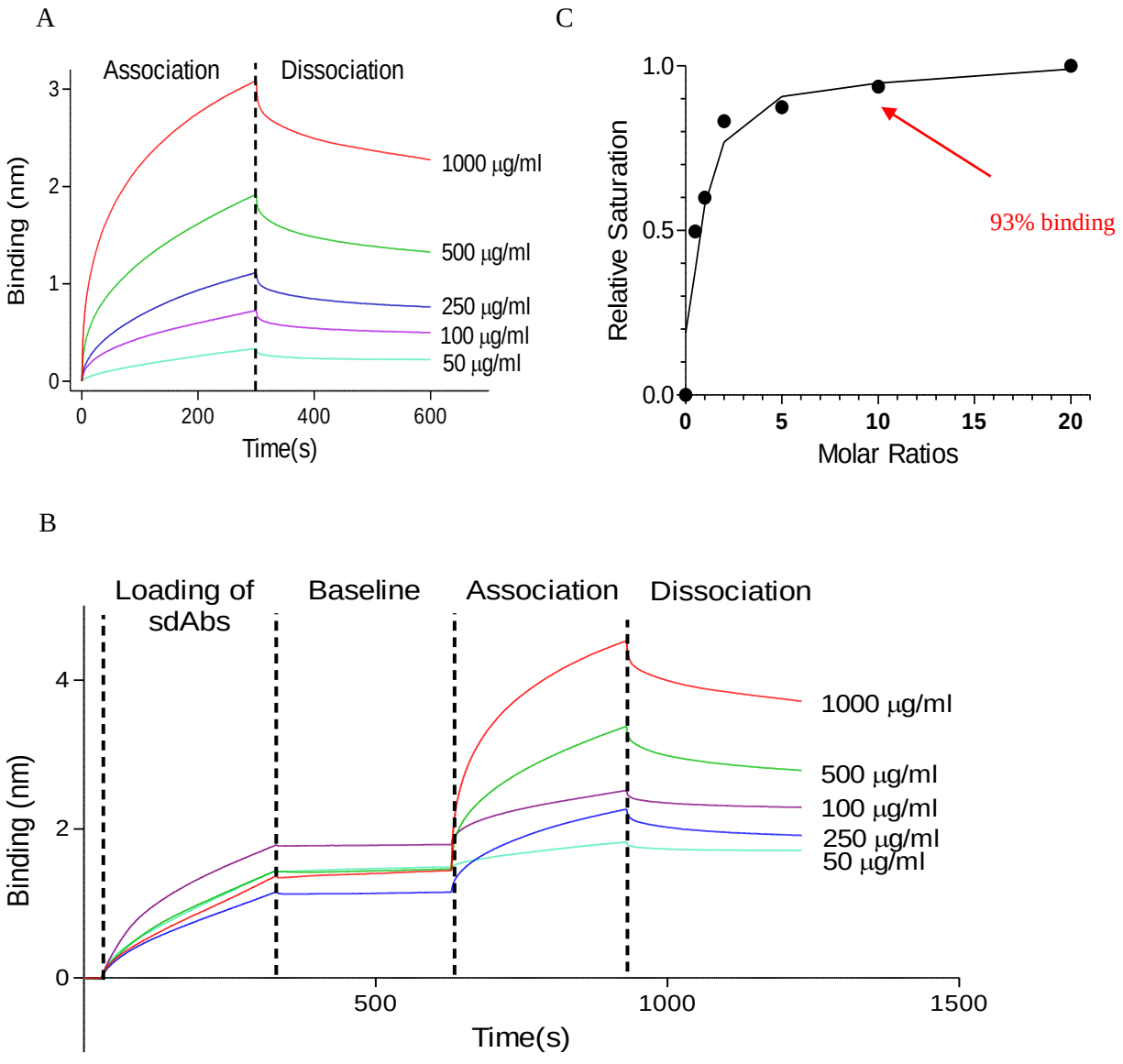

Figure no. 4.5. Binding kinetics of sdAb with its ligand. A. BLI graph with different concentrations of neat RVV are shown, B. The saturation curve of Fr7 with increasing molar ratio of sdAb.

Biophysical and biochemical properties of sdAb

Some studies have shown an enhanced thermal stability of sdAbs, we therefore measured the influence of different temperatures on the structural integrity of RVV specific sdAb. The RVV specific sdAbs did not loose their secondary structure upon incubating for 10 min upto a temperature of 65°C but a further increase in the temperature resulted in the loss of structural integrity as revealed by random coils in the CD spectral profile (Fig no. 4.6A). However, the calculated T_m value for RVV specific sdAbs was > 62.9°C (Fig no. 4.6B). Its thermal stability can be further enhanced by doing mutations in some regions (35) but it might affect its binding capabilities (36). We compared the CD spectra of sdAbs before heating to 90 °C and then gradually bringing them to 20 °C. After cooling, sdAbs regained its structure (Fig no 4.6C) and then we calculated the percentage of different secondary structures by using CDNN (Circular Dichroism analysis using Neural Networks) software (Fig no.4.6D). We also observed RVV specific sdAbs structural stability for prolonged incubations at different temperatures. At 4°C and 37°C, the secondary structures were retained by sdAbs upto a month, the last time point investigated. An increased temperature of 51°C could by resisted for 90 min., the last time point investigated (Fig no. 4.6E-G). Our results measuring the thermal stability of RVV specific sdAbs demonstrated their high thermal stability. These antibodies therefore can be handled at room temperature for extended durations and can also withstand temperature fluctuations during their transportation. In addition to measuring thermal stability we also investigated the influence of a pH range from 2 to 13 on the structural features of sdAbs. Upon exposure to different pH ranges, the sdAbs maintained their structure between 2 to 10 (Fig no. 4.6H). The

resistance of anti-RVV sdAbs would suggest that if required such antibodies can be administered orally for managing snakebites or in the cases of malicious poisonings. Thus, the gastric pH could range from 1.5 to 3.5 and is resisted by the RVV specific antibodies.

A

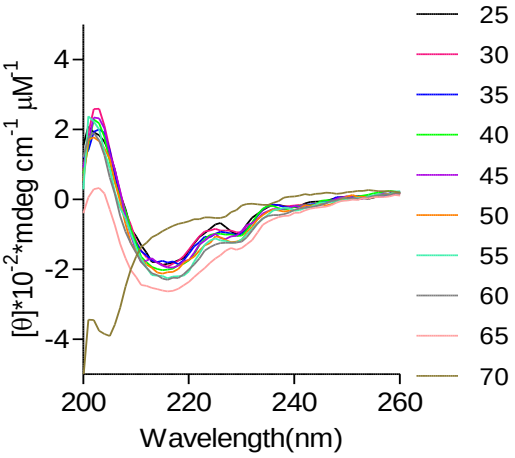

B

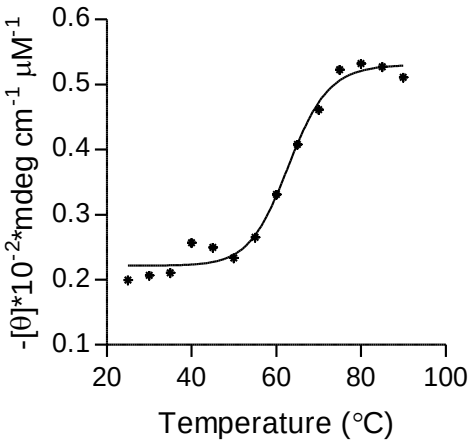

C

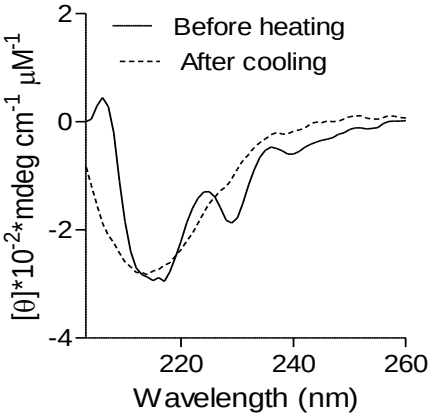

D

	Before Heating	After Cooling
Helix	11.31	12.46
Antiparallel	12.53	12.21
Parallel	15.7	15.2
Beta-Turn	17.17	17.28
Random Coil	43.21	42.77

E

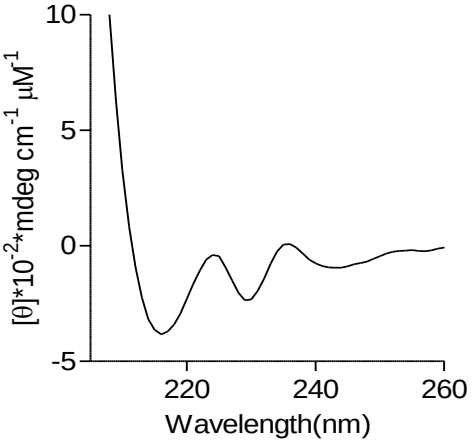

F

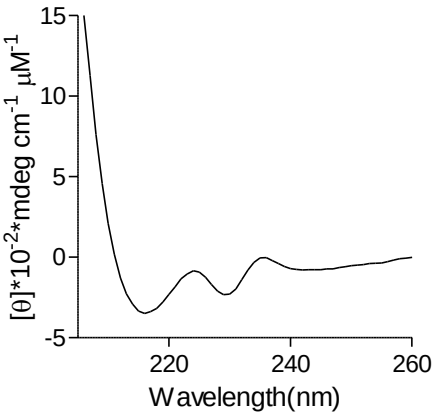

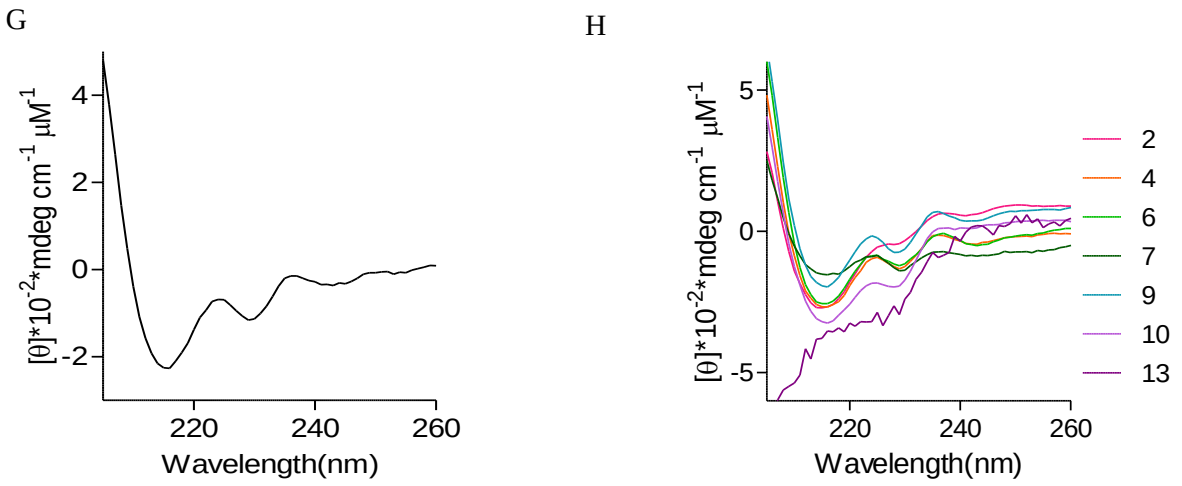

Figure no. 4.6 Biophysical and biochemical characterisations of sdAb. A Thermal stability of sdAb, B. Melting temperature curve of sdAb, C &D. CD graph showing secondary structure before heating and then after cooling till 25° C and percentage of different structural components respectively, E-G. Stability after keeping sdAb at 4,37 and 51 degrees C, H.Effect of different pH conditions at the secondary structure of sdAb.

Molecular docking

Whether or not the sPLA2 activity is blocked by the sdAbs by binding in the catalytic sites and thereby directly blocking the binding of the substrate, we performed molecular docking studies. We also predicted the residues of sPLA2 gp 12B interacting with sdAbs (Fig. no. 4.7). sPLA2 (1I, 43E, 44L, 45G, 46F, 47V, 48S, 89E and 90E) forms two protruding structures which fits into the pockets of sdAbs formed by (CDR1- 32S, 33K, CDR2- 54N, 56G, 57G, 59T, 60T, 61L, and CDR3- 105W, 106I, 107A, 108D, and 109C). Among these residues, following pairs of sPLA2-sdAbs formed H bonds: 89E-33K, 90E-105W, 46F-54N, 45G-59T and 48S-59T. The active site of snake phospholipase contains following amino acids, one residue of Histidine, two residues of Aspartic acid, one residue of Tyrosine and two residues of Glycine (37). This sdAbs interacts with two aspartic acid residues and one glycine hence interfering with the activity of phospholipase A2.

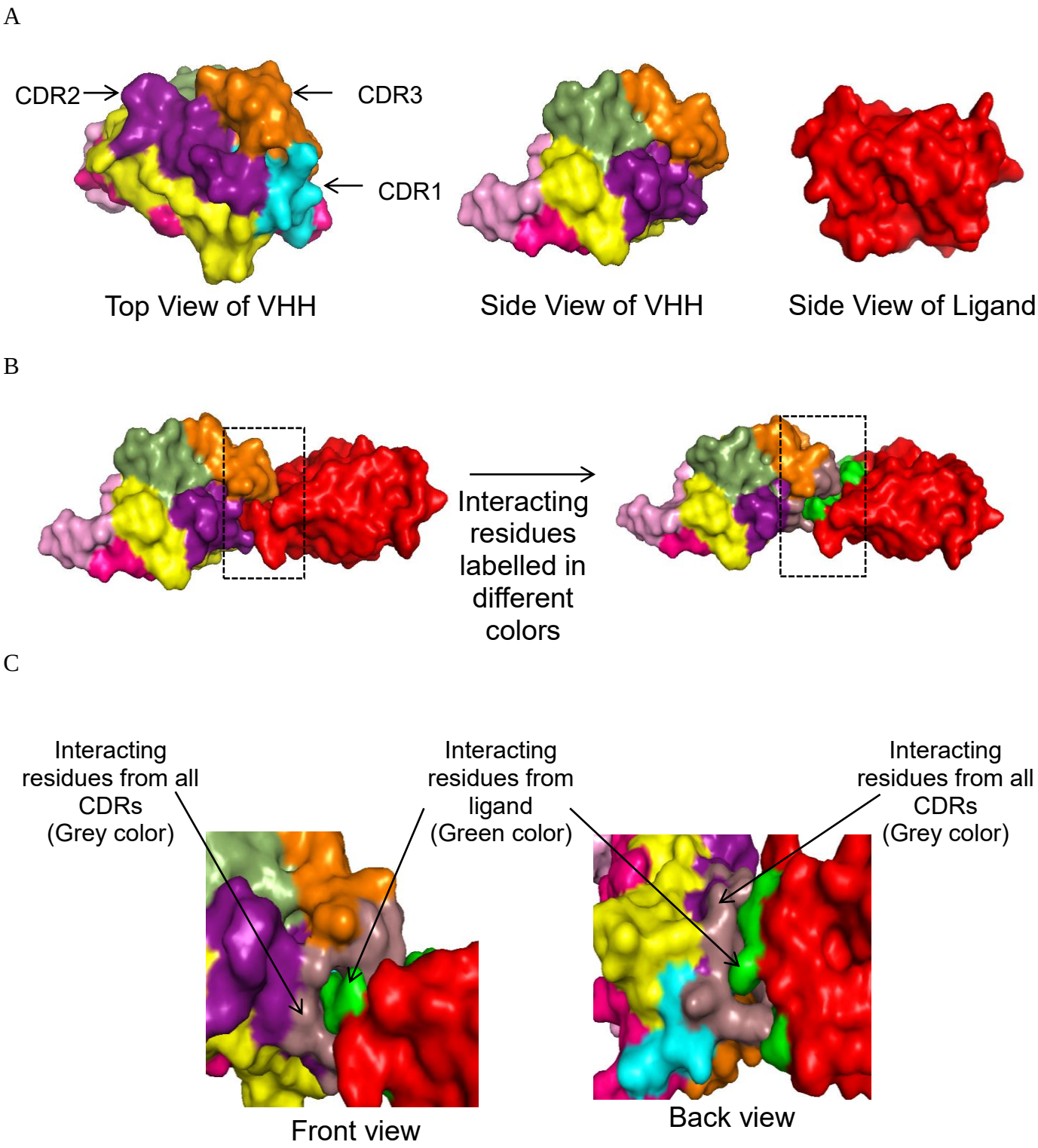

Figure no. 4.7 Molecular docking showing the interacting residues of sPLA2-sdAbs. A. Top and side view of sdAbs and sPLA2 respectively, B. Interacting residues of docked structures of sdAbs and 2PLA2, C. Protruding ends of sPLA2 fits into the pockets formed by CDR's of sdAbs.

Anti-RVV sdAbs efficiently neutralize the enzymatic activity of phospholipases in RVV

We demonstrated that the clone of sdAbs specifically reacted to phospholipase A2, we tested whether the enzymatic activity can be blocked by this antibody. Graded doses of sdAbs were pre-incubated with either the neat RVV or the fraction 7 for 30 min and the mix was then added in the wells of egg yolk gel plates. While the RVV and the fraction 7 exhibited the activity, RVV specific sdAbs inhibited the activity of phospholipase A2 in a dose dependent manner (Fig no. 4.8A). With 20µM of sdAbs, 20% phospholipase A2 activity was reduced and the extent of inhibition remained same with higher dose of sdAbs i.e. upto 75µM. When the fraction 7 was used for measuring the phospholipase A2 activity

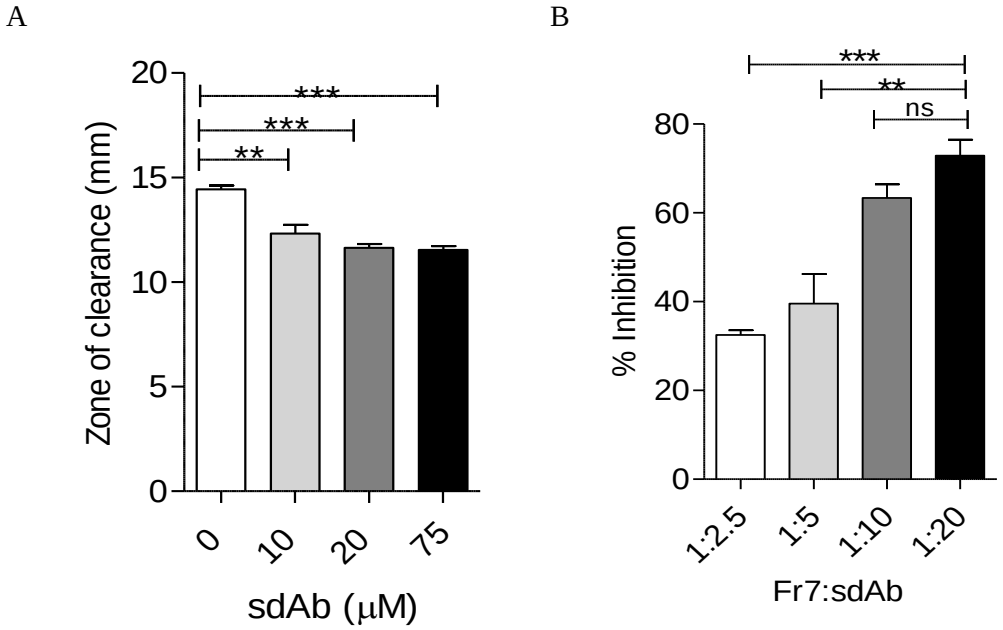

Figure no. 4.8. Inhibition of phospholipase A2 activity by sdAbs. A&B. Egg yolk assay for inhibition of phospholipase A2 activity of neat venom and Fr 7 with sdAb respectively.

and its neutralization by sdAbs, we obtained upto 75% inhibition of the activity (Fig no. 4.8B).

Cellular toxicity of RVV

To measure the cellular toxicity of venom, both primary cells and established cell lines were used. We analyzed immune cells such as $CD4^+$ and $CD8^+$ T cells as targets for measuring venom induced cytotoxicity because these cells are critical for controlling herpesvirus reactivation from the latency (38). Some evidence indicate that patients envenomed by snakebites tend to reactivate latent herpesvirus that cause herpes labilis (39). Therefore, we reasoned that the snake venom acting either directly or by inducing host factors could kill T cells to trigger HSV1 reactivation. Graded doses of RVV were added to the MACS sorted cells. A time dependent analysis was done for the cellular death markers using flow cytometry. One of the major pathways of cytotoxicity is apoptosis wherein the inner leaflet of lipid bilayer membrane is flipped and exposes the phosphatidyl serine to the exterior of cell. The exposed phosphatidyl serine can be detected by fluorescent annexin V. $CD4^+$ and $CD8^+$ T cells were lysed when exposed to RVV and the effect occurred in a dose and time dependent. At lower doses of RVV, the proportion of dying cells was surprisingly reduced for both $CD4^+$ and $CD8^+$ T cells. As the dose was increased the cytotoxicity became apparent for both $CD4^+$ (Fig no. 4.9A&B) and $CD8^+$ T cells (Fig no. 4.9C&D). These results therefore suggest the T cells cytotoxicity caused directly by RVV could possibly contribute to the reactivation of latent herpesviruses. We do not currently have any

explanation why at lower doses of exposure, the cells were showing more proportions of double negative (Annexin V and PI) cells. This could be because of the presence of some of the components in the venom that could either promote cell survival or the results could suggest for the intrinsic problems with the assays used for analysis. However this remains the part of ongoing activities in the laboratory. Similar experiments were performed to measure the cytotoxicity of different fractions. For this we used Jurkat cells, a lymphocyte cell line from humans. We found a lesser degree of toxicity in Jurkat cells as compared to that in the primary immune cells but the overall patterns of cytotoxicity were similar (Fig 4.9E&F). The observed effects could be explained either by intrinsic variations in their biological properties or some extrinsic factors such the aberration induced as a result of purification processes. RVV treated and control Jurkat cells were also stained with acridine orange/EtBr mixture and observed under fluorescent microscope. RVV killed Jurkat cells in a dose dependent manner (Fig 4.9G). As RVV is composed of multiple polypeptides so we analyzed the effect of each fraction (collected from gel filtration chromatography) on Jurkat to identify the toxicological components in RVV. The treated Jurkat cells were analyzed after staining with annexin V and PI staining followed by flow cytometric analysis. Out of all the fractions, there was no significant difference in the cytotoxicity caused by fraction 3 to 7 and the neat RVV as measured by annexin V positivity but for PI staining, neat RVV and fraction 5 showed similar pattern (Fig no. 4.9H&I). Additionally, semi-adherent HEK cells exposed to RVV fractions were analyzed microscopically. Similar results were

obtained when toxicological effects were HEK cells observed under the microscope (Fig no. 4.9J). Apart from cellular cytotoxicity, we have also addressed the issue whether RVV exposure could interfere with cell cycle phases. For that Jurkat cells were grown in serum free RPMI medium overnight for synchronization. Thereafter the cells were incubated in serum-enriched media with or without RVV for 4 hrs. After washing, the cells were fixed with ethanol followed by staining with PI. We did not observe any significant difference in the proportion of cells between control and treated groups in different stages of cell cycle as measured by DNA staining. (Fig no. 4.9K&L).

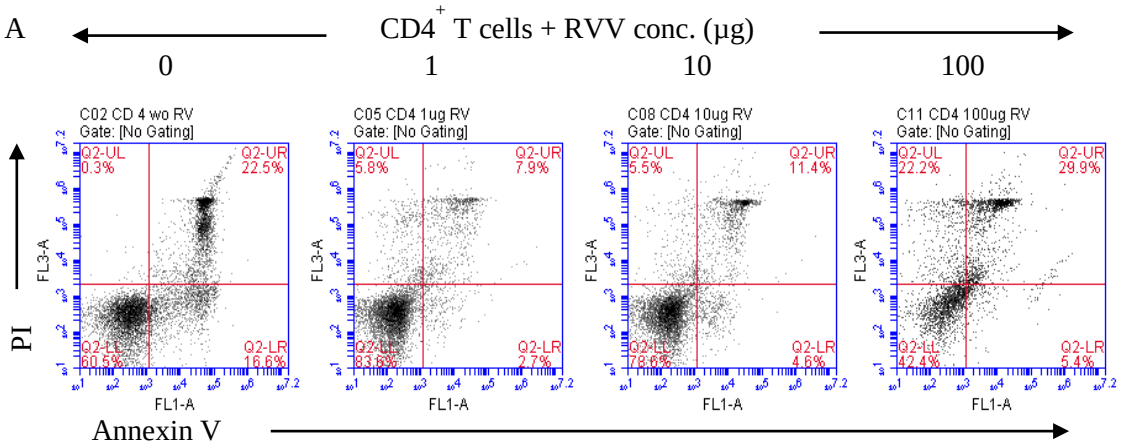
A
CD4+ T cells + RVV conc. (µg)
0
1
10
100
C02 CD 4 wo RV
Gate: [No Gating]
Q2-UL 0.3%
Q2-UR 22.5%
Q2-LL 60.5%
Q2-LR 16.6%
C05 CD4 1ug RV
Gate: [No Gating]
Q2-UL 5.8%
Q2-UR 7.9%
Q2-LL 83.6%
Q2-LR 2.7%
C08 CD4 10ug RV
Gate: [No Gating]
Q2-UL 5.5%
Q2-UR 11.4%
Q2-LL 78.6%
Q2-LR 4.6%
C11 CD4 100ug RV
Gate: [No Gating]
Q2-UL 22.2%
Q2-UR 29.9%
Q2-LL 42.4%
Q2-LR 5.4%
FL3-A
FL1-A
PI
Annexin V

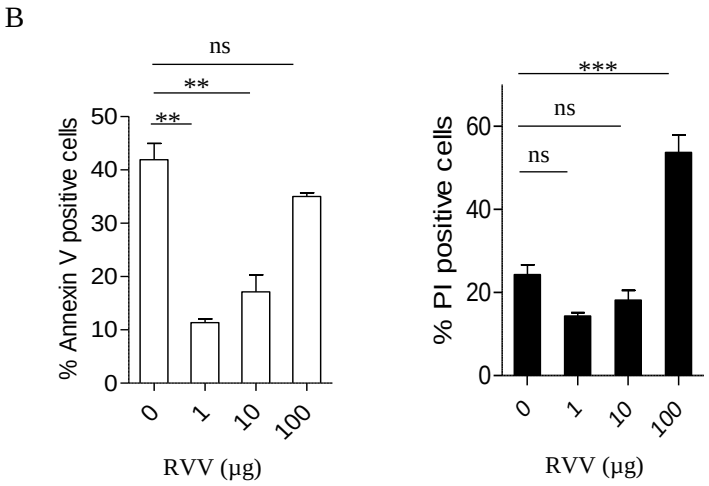
B
ns
**
**
% Annexin V positive cells
50
40
30
20
10
0
0
1
10
100
RVV (µg)
***
ns
ns
% PI positive cells
60
40
20
0
0
1
10
100
RVV (µg)

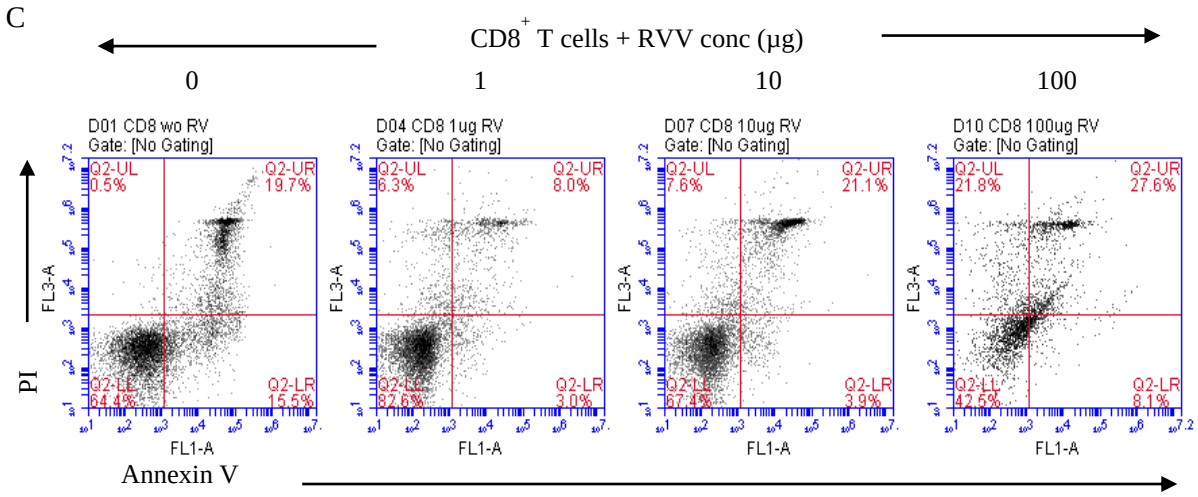
C
CD8+ T cells + RVV conc (µg)
0
1
10
100
D01 CD8 wo RV
Gate: [No Gating]
Q2-UL 0.5%
Q2-UR 19.7%
Q2-LL 64.4%
Q2-LR 15.5%
D04 CD8 1ug RV
Gate: [No Gating]
Q2-UL 6.3%
Q2-UR 8.0%
Q2-LL 82.6%
Q2-LR 3.0%
D07 CD8 10ug RV
Gate: [No Gating]
Q2-UL 7.6%
Q2-UR 21.1%
Q2-LL 67.4%
Q2-LR 3.9%
D10 CD8 100ug RV
Gate: [No Gating]
Q2-UL 21.8%
Q2-UR 27.6%
Q2-LL 42.5%
Q2-LR 8.1%
FL3-A
FL1-A
PI
Annexin V

D

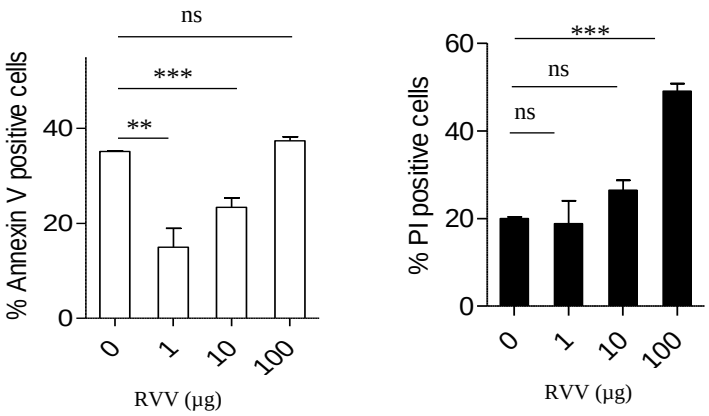
ns
***
**
% Annexin V positive cells
40
20
0
0
1
10
100
RVV (µg)
***
ns
ns
% PI positive cells
60
40
20
0
0
1
10
100
RVV (µg)

E

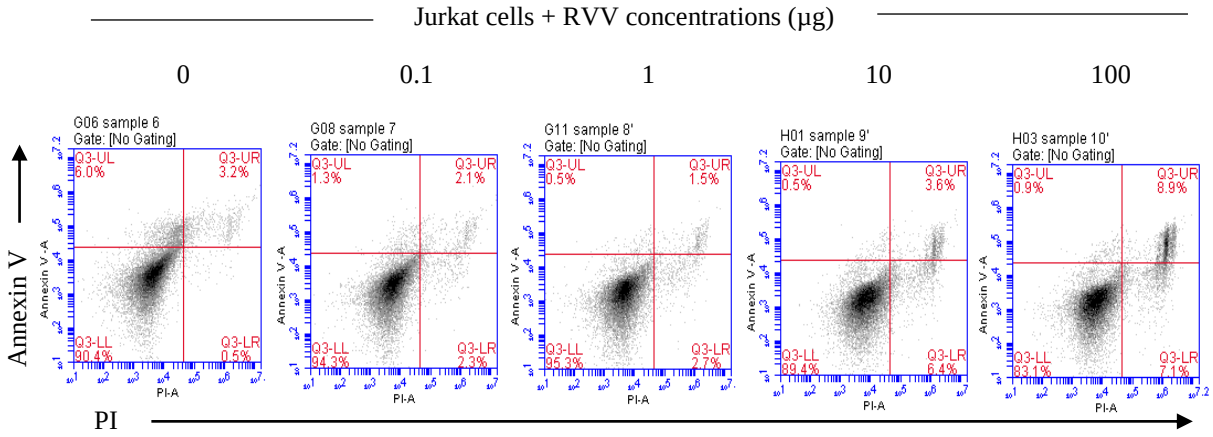
Jurkat cells + RVV concentrations (µg)
0
0.1
1
10
100
Annexin V
PI
G06 sample 6
Gate: [No Gating]
Q3-UL 6.0%
Q3-UR 3.2%
Q3-LL 90.4%
Q3-LR 0.5%
G08 sample 7
Gate: [No Gating]
Q3-UL 1.3%
Q3-UR 2.1%
Q3-LL 94.3%
Q3-LR 2.3%
G11 sample 8'
Gate: [No Gating]
Q3-UL 0.5%
Q3-UR 1.5%
Q3-LL 95.3%
Q3-LR 2.7%
H01 sample 9'
Gate: [No Gating]
Q3-UL 0.5%
Q3-UR 3.6%
Q3-LL 89.4%
Q3-LR 6.4%
H03 sample 10'
Gate: [No Gating]
Q3-UL 0.9%
Q3-UR 8.9%
Q3-LL 83.1%
Q3-LR 7.1%
Annexin V-A
PI-A

F

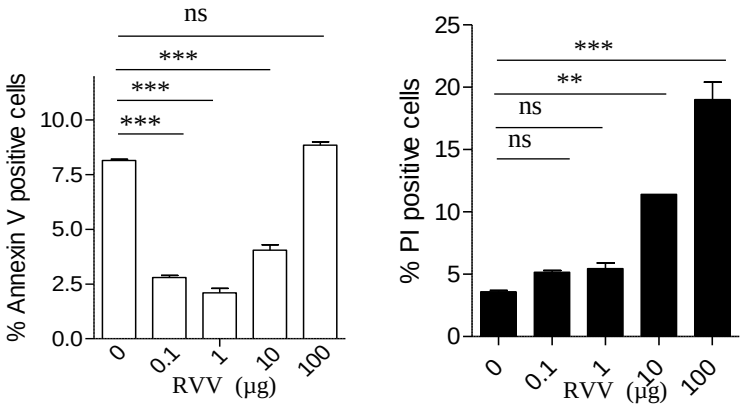
ns
***
***
***
% Annexin V positive cells
10.0
7.5
5.0
2.5
0.0
0
0.1
1
10
100
RVV (µg)
***
**
ns
ns
% PI positive cells
25
20
15
10
5
0
0
0.1
1
10
100
RVV (µg)

G

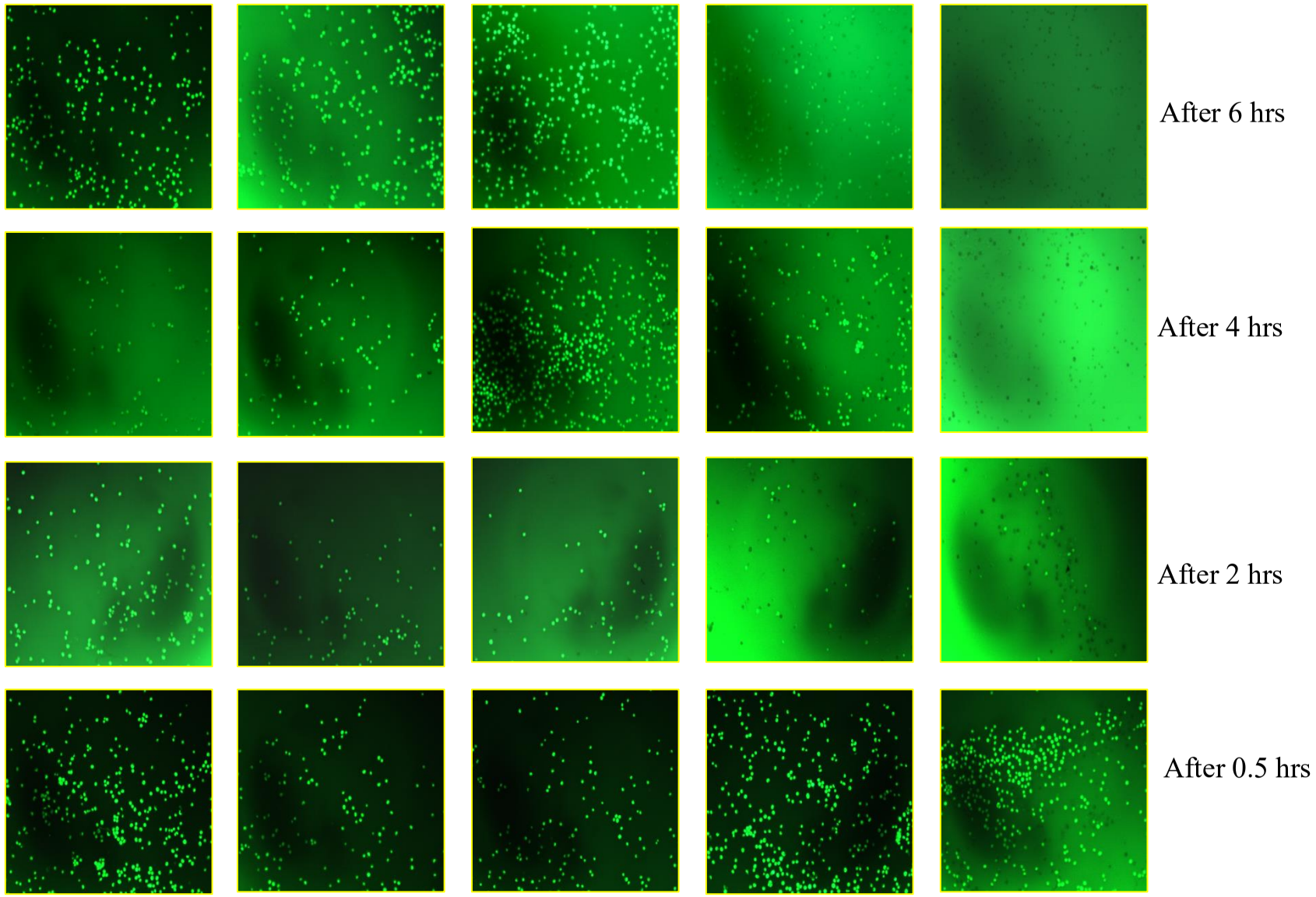
After 6 hrs
After 4 hrs
After 2 hrs
After 0.5 hrs
Without RVV
0.1 µg RVV
1 µg RVV
10 µg RVV
100 µg RVV

H

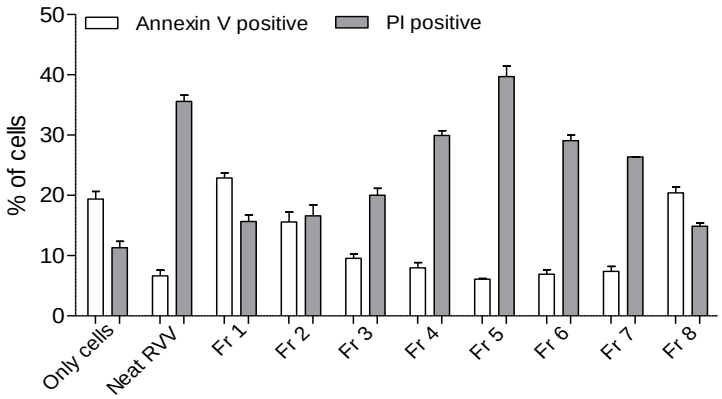

I

	Annexin V	PI
Neat RVV vs Fr 1	***	***
Neat RVV vs Fr 2	***	***
Neat RVV vs Fr 3	ns	***
Neat RVV vs Fr 4	ns	*
Neat RVV vs Fr 5	ns	ns
Neat RVV vs Fr 6	ns	*
Neat RVV vs Fr 7	ns	***
Neat RVV vs Fr 8	***	***

J

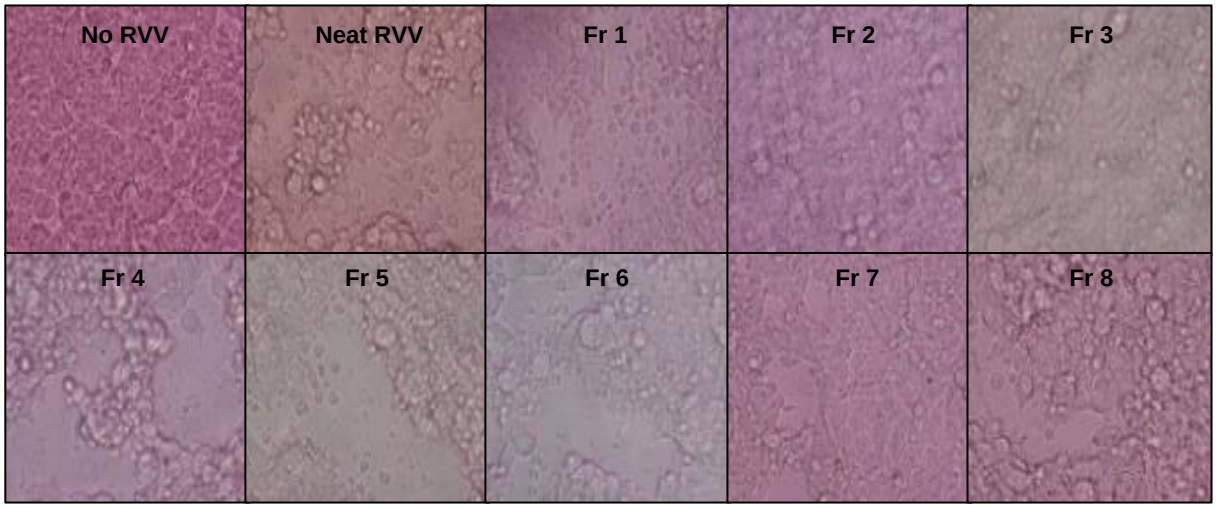

K

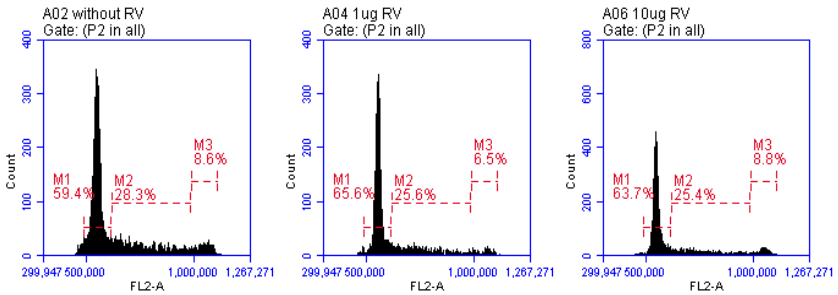

Without RVV 1 µg RVV 10 µg RVV

L

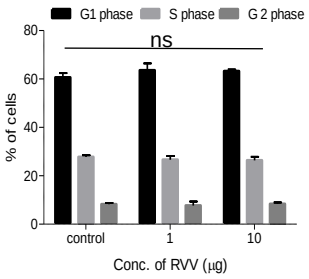

Figure no. 4.9. Cellular cytotoxicity of RVV. A, C&E. Dose dependent effect of RVV on $CD4^+$,$CD8^+$ and Jurkat cells respectively, B, D&F. Accumulative data of annexin V and PI staining of $CD4^+$, $CD8^+$ and Jurkat cells respectively, G. Dose dependent effect of RVV at different time intervals and stained by EtBr/Acridine orange, H&J . Cellular cytotoxicity of RVV fractions on Jurkat cells and HEK293T cells, I. Comparative analysis of neat RVV with different fractions, K&L. FACS plots showing effect of neat RVV on cell cycle and its accumulative data respectively.

RVV specific sdAbs neutralize RVV induced cellular toxicity

Having established the *in vitro* toxicity of RVV against target suspension cells $CD4^+$, $CD8^+$, Jurkat cells as well as adherent cells, first we first performed *in vitro* neutralization assays first using purified HCAbs and then those with selected sdAbs. We used two different concentrations of purified HCAbs from control and immune sera to get an idea whether or not the neutralizing activity if present in such antibodies. We found that with increasing concentrations of HCAbs, the PI staining reduced from 78% in case only RVV to 70% with 200mg of HCAbs. This provided us with a clue that the neutralization offered by selected sdAbs. (Fig no. 4.10A). We then exposed Jurkat cells to a fixed concentration of fraction 7 and pre incubated it with the increasing molar ratios of sdAb and then added the mix to the cells. After two hrs post incubation, the cells were analyzed for their phenotype after staining with annexin V and PI followed by flow cytometric analysis. While the exposure with Fraction 7 increased the frequencies of PI positive cells and decreased the frequencies of double negative cells, increasing the concentration of sdAbs reversed the observed effects (Fig 4B). Thus, ~50% reduction of PI positive cells occurred upon neutralization of Fraction 7 (10 μ g) by the sdAbs (Fig 4C-D). At a 10 fold lower dose of Fraction 7, similar results were also obtained for Annexin V positive cells. Thus, the results showed that sdAbs neutralized the cytotoxicity caused by Fraction 7 (phospholipase A2).

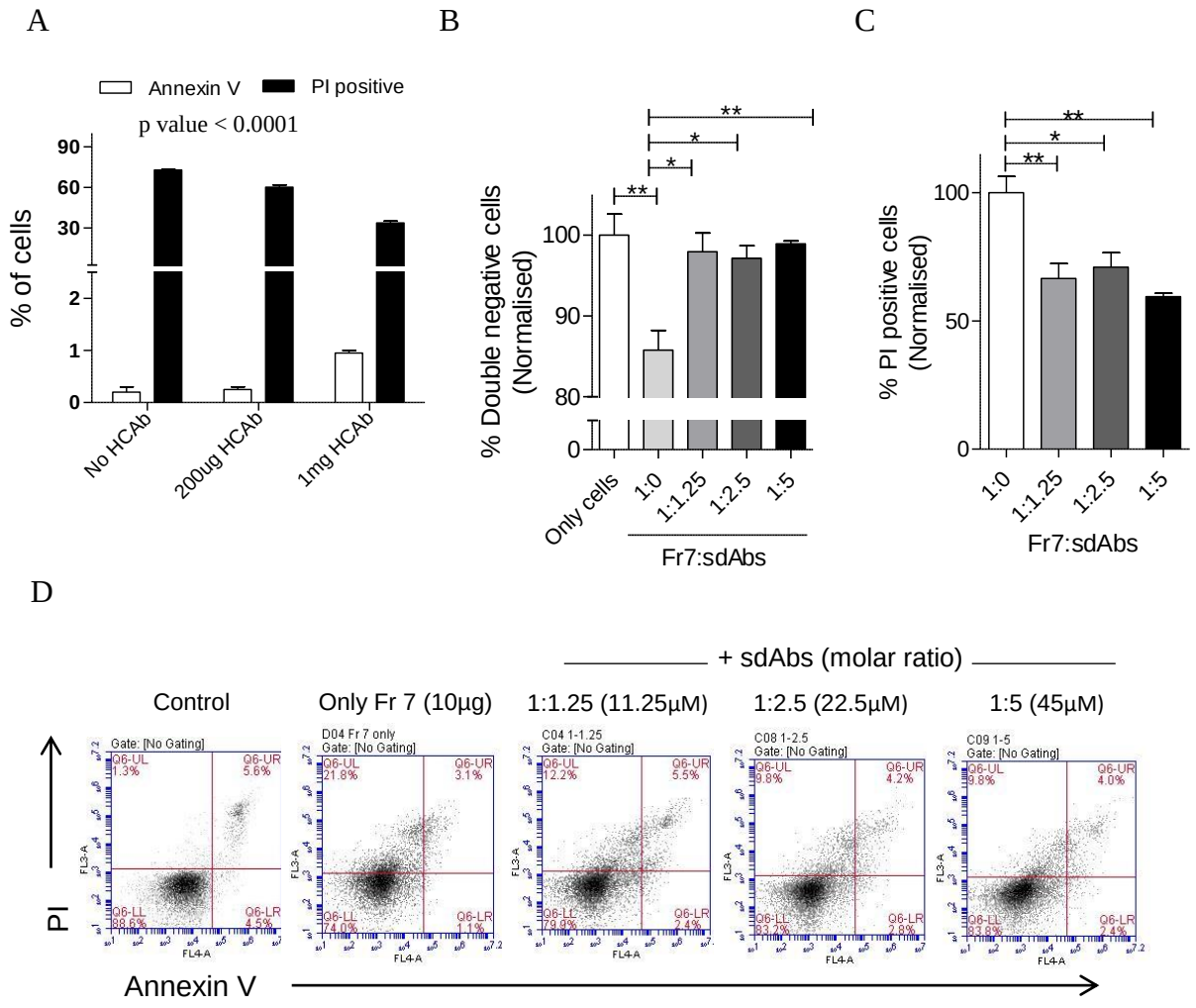

Figure no. 4.10. ***In vitro*** **neutralization of neat RVV and Fr7 by using HCAbs and sdAbs.** A. Neat RVV was neutralised in a dose dependent manner by purified HCAbs from camel hyperimmune serum. B&C. Bar graph showing *in vitro* neutralization of Fr7 with different molar ratios of sdAb. D. Representative FACS plots showing *in vitro* neutralization of Fraction 7.

RVV specific sdAbs prolong the survival of experimentally intoxicated zebrafishes

For measuring the intoxication caused by RVV, we first aimed to develop a vertebrate animal model to test the toxicological effects and their neutralization by sdAbs. As was done for in vitro neutralization assays, first we purified HCAb's sera samples and injected intoxicated zebrafishes with a sequential injection of HCAbs for three times. Control

animals were similarly injected with HCAbs from unexposed sera (p-HCAbs). The latter preparation although extended survival of zebrafishes but all animals eventually died. However HCAb isolated from immune sera (h-HCAbs) samples significantly enhanced protection (Fig no. 4.11A). These results led us to believe that sdAbs could also protect intoxicated zebrafishes and serve as a potent anti-toxin. In intoxicated fishes further to analyze the toxic effect of RVV, we dissected the fishes and observed blood clots with large patches all over their ventral side of the body. Snake venom metalloproteinases are known to cause hemorrhage so these patches might be due to these enzymes in RVV. We also isolated intestines of fishes from all groups of animals and prepared 10mm cryosections (as mentioned in materials and methods) and stained with hematoxylin and eosin stains. Under 100X magnification, we observed that the outer intestinal layer plus villi were completely damaged in case of RVV (Fig no. 4.11B) and the disruption might be due to the action of collagenase and other proteases (40). However, we did observe significantly reduced tissue toxicity in antibody treated animals. Then we did *in vivo* neutralization assay with this sdAb. The single domain antibody binds to only one component of the RVV nonetheless we measured whether or not it could provide protection. Thus, how different components of RVV work to cause toxicity is not clearly defined. We found out that repeated doses of sdAb significantly delayed the onset of mortality (Fig no. 4.11C). As the sdAbs neutralized the effect of only one of the components it is obvious that such antibodies against multiple components could provide complete protection

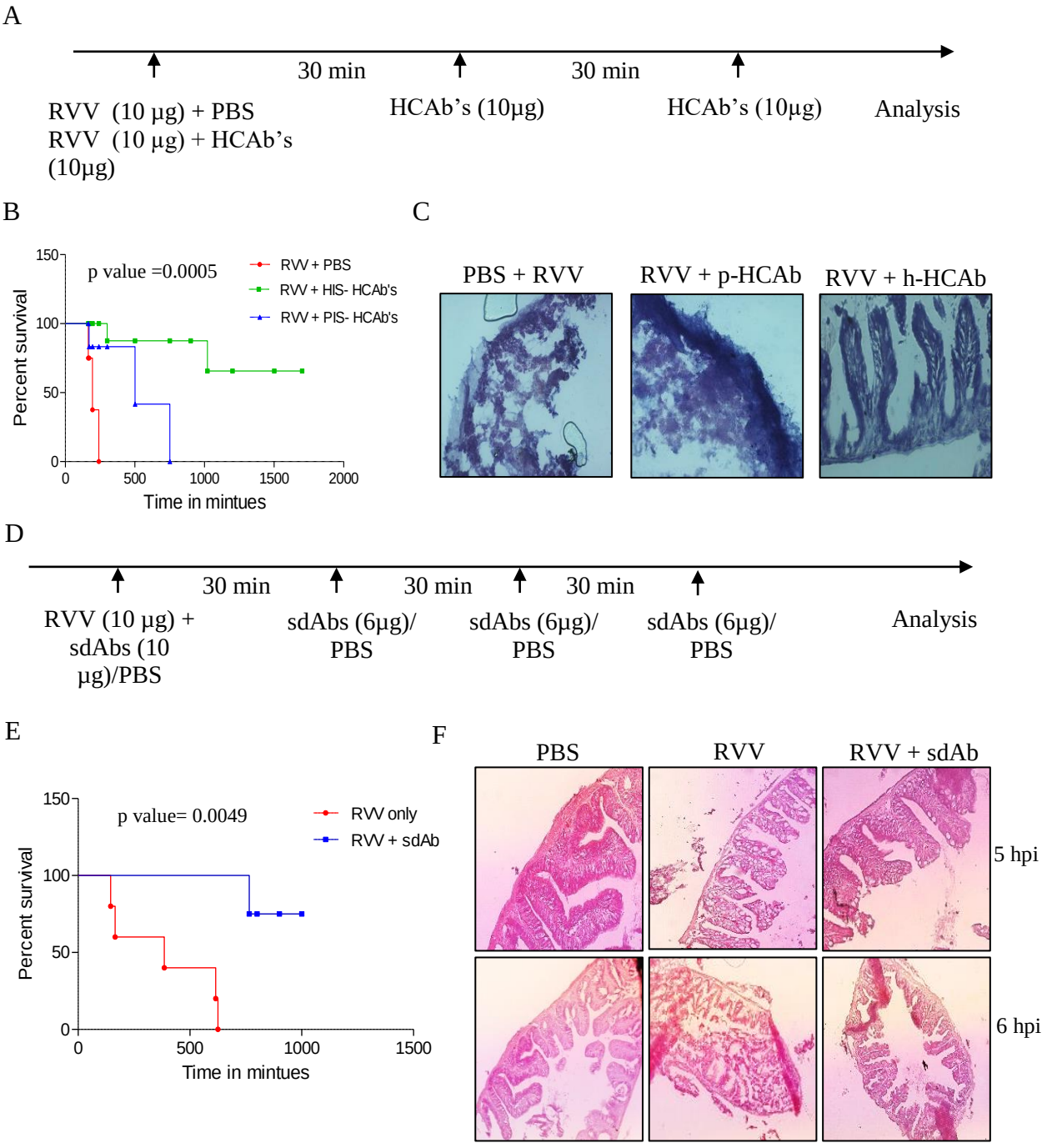

Figure no. 4.11. In vivo neutralization of neat RVV 7 by using HCAbs and sdAbs. A&D. The schematic of the experiments, B& E. Survival curve showing the percentage of survivors among the different groups after neat RVV neutralisation with HCAbs (preimmune serum /Hyperimmune serum) and sdAbs respectively, C&F. Histological sections of intestine of fishes from different groups of RVV neutralisation with HCAbs and sdAbs respectively.

.

Discussion

Recently WHO has declared the snake envenoming as a “neglected tropical disease” (disease of poor) as it majorly affects the residents in tropical countries especially rural areas. The most challenging thing in the development of a suitable antivenom is the diversity of snake venoms as it varies from species to species as well as with geographical areas (41). The current antivenom therapy includes polyclonal sera and mixture of monoclonal antibodies but as these are conventional antibodies i.e. full length antibodies so there are certain issues with them such as serum sickness. We tried to address the above issue by using phage display technology where we explored the potential use of single domain antibodies (sdAbs) against toxic components of Russell viper venom (RVV). We immunized the camel and used its immune sera to blot the different components of RVV and observed that not all the polypeptides are toxic, infact proteins in the range of 10-15, 25, 35 and 65kDa are immunogenic (on reducing SDS PAGE). These polypeptides corresponds to phospholipases A2 (10-15kDa range), serine proteases (25kDa), metalloproteases and acetylcholinesterase (65kDa). As it contains phospholipases A2 as a major component so we targeted phospholipases and selected sdAbs against RVV which binds to PLA2 group12B protein. We showed the PLA2 group12B binding and its neutralization by sdAbs in different functional assays. We used zebrafishes as an accessible model to show *in vivo* toxicity of RVV and its neutralization by sdAbs. We observed that neutralization of only one component i.e. PLA2 group 12B, significantly reduced the mortality of RVV intoxicated zebrafishes. This suggests that the use of sdAbs to treat snake envenoming is a more promising way as compared to current therapeutics. It can be done by selecting sdAbs against other immunogenic components and then use as multispecific tetramers.

In order to evaluate the therapeutic potential of anti-toxins during preclinical stages, rodents have been extensively used. Given the utility of zebrafises in preclinical studies, we used experimentally intoxicated zebrafishes with RVV. We also tested whether RVV specific monoclonal sdAbs (anti-sPLA2, gp12B sdAbs) selected from phage display libraries could provide beneficial effects in either delaying the symptoms of toxicity or prevent toxicological effects when admixed with the RVV followed by its administration. Owing to their smaller size and variability in the Fab region, such antibodies could alleviate or minimize the risk associated with xenogenic reactions such as hypersensitivities and anaphylaxis. Furthermore their ability to neutralize cytotoxicity and well as delaying organismal toxicity could also suggest that binders against multiple components could actually serve as potential therapy as an alternative to the existing complete serum or the polyspecific antibodies. The additional attributes associated with such binders include their enhanced stability and solubility, resistance to harsh physicochemical conditions such as pH and high temperature, extended shelf life and their ease of manipulation.

The sPLA2 specific neutralizing sdAbs could also be used for ameliorating inflammatory conditions caused by infections, damage or some cancers by virtue of their ability to block the activity of the enzyme. Thus, the sPLA2 independent of the enzymatic activity could either directly ligate the receptor on various cells to induce signaling or by generating some of the inflammatory mediators such as eicosanoids could contribute to inflammatory diseases. However this aspect we have not covered in the current communication and remain part of our ongoing studies.

References

1. Ahmed, S., A. Choudhary, J. Mahajan, J. Pal, A. Nadeem, and M. Ahmed. 2009. Emergency treatment of a snake bite: Pearls from literature. *J. Emergencies, Trauma Shock* 1: 97.

2. Kasturiratne, A., A. R. Wickremasinghe, N. De Silva, N. K. Gunawardena, A. Pathmeswaran, R. Premaratna, L. Savioli, D. G. Lalloo, and H. J. De Silva. 2008. The global burden of snakebite: A literature analysis and modelling based on regional estimates of envenoming and deaths. *PLoS Med.* 5: 1591–1604.

3. Harrison, R. A., A. Hargreaves, S. C. Wagstaff, B. Faragher, and D. G. Lalloo. 2009. Snake envenoming: A disease of poverty. *PLoS Negl. Trop. Dis.* 3.

4. Chippaux, J. P., V. Williams, and J. White. 1991. Snake venom variability: methods of study, results and interpretation. *Toxicon* 29: 1279–1303.

5. Alirol, E., S. K. Sharma, H. S. Bawaskar, U. Kuch, and F. Chappuis. 2010. Snake bite in south asia: A review. *PLoS Negl. Trop. Dis.* 4.

6. Campbell, C. H. 1975. The effects of snake venoms and their neurotoxins on the nervous system of man and animals. *Contemp.Neurol.Ser.* 12: 259–293.

7. Berling, I., S. G. A. Brown, F. Miteff, C. Levi, and G. K. Isbister. 2015. Intracranial haemorrhages associated with venom induced consumption coagulopathy in Australian snakebites (ASP-21). *Toxicon* 102: 8–13.

8. Warrell, D. A. 2010. Guidelines for the management of snake bites. *World Heal. Organ.* 30 Suppl 1: 1–85.

9. Jayawardana, S., A. Gnanathasan, C. Arambepola, and T. Chang. 2016. Chronic Musculoskeletal Disabilities following Snake Envenoming in Sri Lanka: A Population-Based

Study. *PLoS Negl. Trop. Dis.* 10.

10. Jayawardana, S., C. Arambepola, T. Chang, and A. Gnanathasan. 2018. Long-term health complications following snake envenoming. *J. Multidiscip. Healthc.* 11: 279–285.

11. Calvete, J. J., R. A. Harrison, N. R. Casewell, S. C. Wagstaff, F. M. S. Bolton, L. Sanz, W. Wuster, D. A. N. Cook, D. Pla, and S. I. King. 2014. Medically important differences in snake venom composition are dictated by distinct postgenomic mechanisms. *Proc. Natl. Acad. Sci.* 111: 9205–9210.

12. Geneviève, L. D., N. Ray, F. Chappuis, G. Alcoba, M. R. Mondardini, I. Bolon, and R. Ruiz de Castañeda. 2018. Participatory approaches and open data on venomous snakes: A neglected opportunity in the global snakebite crisis? *PLoS Negl. Trop. Dis.* 12.

13. Segura, Á., M. Villalta, M. Herrera, G. León, R. Harrison, N. Durfa, A. Nasidi, J. J. Calvete, R. D. G. Theakston, D. A. Warrell, and J. M. Gutiérrez. 2010. Preclinical assessment of the efficacy of a new antivenom (EchiTAb-Plus-ICP®) for the treatment of viper envenoming in sub-Saharan Africa. *Toxicon* 55: 369–374.

14. Tan, C. H., J. L. Liew, K. Y. Tan, and N. H. Tan. 2016. Assessing SABU (Serum Anti Bisa Ular), the sole Indonesian antivenom: A proteomic analysis and neutralization efficacy study. *Sci. Rep.* 6.

15. Casewell, N. R., D. A. N. Cook, S. C. Wagstaff, A. Nasidi, N. Durfa, W. Wüster, and R. A. Harrison. 2010. Pre-clinical assays predict Pan-African Echis viper efficacy for a species-specific antivenom. *PLoS Negl. Trop. Dis.* 4.

16. Evazalipour, M., B. S. Tehrani, M. Abolhassani, H. Morovvati, and K. Omidfar. 2012. Camel Heavy Chain Antibodies Against Prostate-Specific Membrane Antigen. *Hybridoma* 31: 424–429.

17. Hellman, U., C. Wernstedt, J. Gonez, and C. H. Heldin. 1995. Improvement of an "In-

Gel" Digestion Procedure for the Micropreparation of Internal Protein Fragments for Amino Acid Sequencing. *Anal. Biochem.* 224: 451–455.

18. Ribble, D., N. B. Goldstein, D. A. Norris, and Y. G. Shellman. 2005. A simple technique for quantifying apoptosis in 96-well plates. *BMC Biotechnol.* 5: 12.

19. Sehrawat, S., and A. Singh. 2006. Anti-erythrocyte natural antibody activity in the unconventional "heavy chain" immunoglobulins of Indian desert camel (Camelus dromedarius). *Vet. Immunol. Immunopathol.* 111: 139–147.

20. Maggi, M., and C. Scotti. 2017. Enhanced expression and purification of camelid single domain VHH antibodies from classical inclusion bodies. *Protein Expr. Purif.* 136: 39–44.

21. Yang, Z., L. Zhang, Y. Zhang, T. Zhang, Y. Feng, X. Lu, W. Lan, J. Wang, H. Wu, C. Cao, and X. Wang. 2011. Highly efficient production of soluble proteins from insoluble inclusion bodies by a Two-Step-Denaturing and refolding method. *PLoS One* 6.

22. Zhang, Y. 2008. I-TASSER server for protein 3D structure prediction. *BMC Bioinformatics* 9.

23. Roy, A., A. Kucukural, and Y. Zhang. 2010. I-TASSER: A unified platform for automated protein structure and function prediction. *Nat. Protoc.* 5: 725–738.

24. Yang, J., R. Yan, A. Roy, D. Xu, J. Poisson, and Y. Zhang. 2014. The I-TASSER suite: Protein structure and function prediction. *Nat. Methods* 12: 7–8.

25. Prado, N. D. R., S. S. Pereira, M. P. Da Silva, M. S. S. Morais, A. M. Kayano, L. S. Moreira-Dill, M. B. Luiz, F. B. Zanchi, A. L. Fuly, M. E. F. Huacca, C. F. Fernandes, L. A. Calderon, J. P. Zuliani, L. H. P. Da Silva, A. M. Soares, R. G. Stabeli, and C. F. C. Fernandes. 2016. Inhibition of the myotoxicity induced by Bothrops jararacussu venom and isolated phospholipases A 2 by specific camelid single-domain antibody fragments. *PLoS One* 11.

26. Wang, H., X. Chen, M. Zhou, L. Wang, T. Chen, and C. Shaw. 2016. Molecular characterization of three novel phospholipase A2proteins from the venom of Atheris chlorechis, Atheris nitschei and Atheris squamigera. *Toxins (Basel).* 8.

27. Greenfield, N. J. 2007. Using circular dichroism collected as a function of temperature to determine the thermodynamics of protein unfolding and binding interactions. *Nat. Protoc.* 1: 2527–2535.

28. Putt, F. a. 1954. *Histopathologic Technic and Practical Histochemistry*,.

29. Leenaars, M., and C. F. M. Hendriksen. 2005. Critical steps in the production of PAb and MAb: evaluation and recommendations. *Ilar J.* 46: 269–279.

30. Dumoulin, M., K. Conrath, A. Van Meirhaeghe, F. Meersman, K. Heremans, L. G. J. Frenken, S. Muyldermans, L. Wyns, and A. Matagne. 2002. Single-domain antibody fragments with high conformational stability. *Protein Sci.* 11: 500–515.

31. McIlwain, S., K. Tamura, A. Kertesz-Farkas, C. E. Grant, B. Diament, B. Frewen, J. J. Howbert, M. R. Hoopmann, L. Käll, J. K. Eng, M. J. MacCoss, and W. S. Noble. 2014. Crux: Rapid open source protein tandem mass spectrometry analysis. *J. Proteome Res.* 13: 4488–4491.

32. Chambers, M. C., B. Maclean, R. Burke, D. Amodei, D. L. Ruderman, S. Neumann, L. Gatto, B. Fischer, B. Pratt, J. Egertson, K. Hoff, D. Kessner, N. Tasman, N. Shulman, B. Frewen, T. A. Baker, M.-Y. Brusniak, C. Paulse, D. Creasy, L. Flashner, K. Kani, C. Moulding, S. L. Seymour, L. M. Nuwaysir, B. Lefebvre, F. Kuhlmann, J. Roark, P. Rainer, S. Detlev, T. Hemenway, A. Huhmer, J. Langridge, B. Connolly, T. Chadick, K. Holly, J. Eckels, E. W. Deutsch, R. L. Moritz, J. E. Katz, D. B. Agus, M. MacCoss, D. L. Tabb, and P. Mallick. 2012. A cross-platform toolkit for mass spectrometry and proteomics. *Nat. Biotechnol.* 30: 918–920.

33. Käll, L., J. D. Canterbury, J. Weston, W. S. Noble, and M. J. MacCoss. 2007. Semi-supervised learning for peptide identification from shotgun proteomics datasets. *Nat. Methods* 4: 923–925.

34. Schmitt, J., H. Hess, and H. G. Stunnenberg. 1993. Affinity purification of histidine-tagged proteins. *Mol. Biol. Rep.* 18: 223–230.

35. Fan, K., B. Jiang, Z. Guan, J. He, D. Yang, N. Xie, G. Nie, C. Xie, and X. Yan. 2018. Fenobody: A Ferritin-Displayed Nanobody with High Apparent Affinity and Half-Life Extension. *Anal. Chem.* 90: 5671–5677.

36. Hassanzadeh-Ghassabeh, G., N. Devoogdt, P. De Pauw, C. Vincke, and S. Muyldermans. 2013. Nanobodies and their potential applications. *Nanomedicine* 8: 1013–1026.

37. Kini., R. M. 1997. Venom phospholipase A2 enzymes : structure, function, and mechanism. In *Venom phospholipase A2 enzymes : structure, function, and mechanism* 1–511.

38. Nash, A. A. 2002. T Cells and the Regulation of Herpes Simplex Virus Latency and Reactivation. *J. Exp. Med.* 191: 1455–1458.

39. Waikhom, R., R. Sapam, K. Patil, J. P. Jadhav, D. Sircar, A. Roychowdhury, S. Dasgupta, and R. Pandey. 2011. Case report: Herpes labialis in patients with Russell's viper bite and acute kidney injury: A single center experience. *Am. J. Trop. Med. Hyg.* 84: 1016–1020.

40. Maruyama, M., M. Sugiki, E. Yoshida, K. Shimaya, and H. Mihara. 1992. Broad substrate specificity of snake venom fibrinolytic enzymes: Possible role in haemorrhage. *Toxicon* 30: 1387–1397.

41. Kalita, B., S. P. Mackessy, and A. K. Mukherjee. 2018. Proteomic analysis reveals geographic variation in venom composition of Russell's Viper in the Indian subcontinent: implications for clinical manifestations post-envenomation and antivenom treatment. *Expert*

Rev. Proteomics 15: 837–849.